An Investigation of Useful Fluid Flow in Grinding

Andrew Jackson

A thesis submitted in partial fulfilment of the requirements of Liverpool John Moores University for the degree of Doctor of Philosophy

April 2008

Abstract

The purpose of this project was to investigate the factors that affect the useful flow. In addition to this the effect of useful flow on differing output parameters was examined. The early work included the development of a novel system for the capture of useful flow and the subsequent use of this system in the testing of parameters affecting the useful flow. The useful flow device was created for use on two different surface grinding machines. Testing was carried out on a range of wheel speeds, with several grinding wheels and several supply flowrates and supply jet speeds. A Taguchi test was conducted to differentiate the factors that affect the useful flowrate from the ones which do not. Further testing was conducted on a range of wheel speed values focussed around the commonly accepted target of matching the jet speed. The results of these tests were used to draw out relationships between the useful flowrate and key input parameters.

The results of the Taguchi test showed the wheel speed and jet speed as having the a profound effect on the useful flowrate. It was also found for the first time that the combined effect of these two parameters had a significant influence on the useful flowrate, validating the speed ratio (v_j/v_s) as a key parameter. Testing of the wheel speed in full factorial testing showed that a speed ratio of between 0.5-0.9 will give the maximum useful flowrate. The jet speed was found to be the key to achieving a high percentage useful flow. As the wheel speed approaches the jet speed the useful flowrate was found to follow a roughly linear relationship, a situation where the air barrier surrounding the wheel is easily penetrated. Having the jet speed exceed the wheel speed did not force more fluid through the grinding contact zone. A maximum percentage useful flow was found to be 50 % of the applied flow for a 54 % porosity wheel and 30 % of the applied flow for a 45 % porosity wheel of similar grain/bond type. These values could not be exceeded without substantial extra effort and justification for this could not be found from the analysis of the output parameters. These values of achievable useful flowrate allowed guidance to be given on a maximum supply flowrate, exceeding this supply flowrate will serve only to decrease the percentage useful flow.

An equation has been derived based on fluid occupation of the pores, this is known as the achievable useful flowrate, which can be used to predict the supply flowrate

required for a given grind. It has been found that the supply flowrate should normally be at least two to three times the achievable useful flowrate. A general guideline of four times allows a margin to cover a wider range of conditions. It has also been found that for non-aggressive grinding situations the supply flowrate can be matched to the achievable useful flowrate.

Further work was carried out to analyse the surface topography of the grinding wheels under analysis and modelling of the surface was used to predict values of useful flowrate. These tests were conducted using surface replication techniques and optical scanning via the Uniscan and Wyko Vision® systems. Using these techniques it was also possible to test the dressing process and bedding-in process for their effects on a grinding wheel surface. Analysis of the wheel surface scans gave a value of useful flowrate based on filling the pores of the wheel surface. This value was compared to the measured useful flowrate taken from experiments showing that at no point do the pores of the grinding wheel become completely filled with fluid.

Acknowledgements

I would like to thank my director of studies, Dr Michael Morgan for his support and guidance during the course of this work.

Gratitude is also due to Professor Brian Rowe and Dr David Allanson whose invaluable assistance and boundless encouragement throughout the project has been vital to the author. Particular thanks go to Dr Andre Batako, whose efforts both in practical help and theoretical guidance were fundamental to the successful completion of the project.

Acknowledgements are extended to the EPSRC for the grant that supported this work and to the collaborating partners, Holroyd, Cinetic Landis Lund, Castrol, Wendt Boart, Dantec Dynamics and Ford Cosworth Racing for their financial support, advice and guidance.

Thanks are due to the people of the AMTReL and GERI, both the visiting scholars and the permanent members for their help and support during this project.

I would also like to thank the technical staff without whom none of this work could have been accomplished, particular thanks go to Mr Peter Moran, Mr Paul Wright, Mr John Carrier, Mr Thomas Scargill, Mr Mick Noord, Ms Helen Pottle and Mr Dave Windsor for their constant encouragement, endless enthusiasm and priceless support throughout my time at AMTReL.

Finally, I would like to thank my friends and family who have provided critical emotional support and guidance throughout the course of this endeavour.

Contents

Nomenclature

Symbol	Meaning	Units
a	Applied depth of cut	m
a_e	True depth of cut	m
a_d	Dressing depth	m
A	Cross-sectional area	m^2
b_d	Effective width of the dressing tool	m
b_s	Wheel width	m
b_w	Contact width	m
C_p	Specific heat capacity	kJ/kg·K
d_e	Equivalent wheel diameter	m
d_s	Wheel diameter	m
d_w	Workpiece diameter	m
E	Young's modulus	Pa
F_t	Tangential grinding force	N
F_n	Normal grinding force	N
h_{eq}	Equivalent chip thickness	m
h_t	Nozzle gap thickness	m
k	Thermal Conductivity	kW/m·K
l_c	Contact length	m
l_e	Real contact length	m
l_g	Geometric Contact length	m
m	Mass	kg
$\dot{m}_a$	Air mass flowrate	kg/s
$\dot{m}_j$	Jet mass flowrate	kg/s
$\dot{m}_n$	Nozzle mass flowrate	kg/s
$\dot{m}_u$	Useful mass flowrate	kg/s
n_d	Number of dressing passes	-
p_a	Absolute atmospheric pressure	bar
P	Grinding power	W
P_f	Spindle power due to fluid	W
P_j	Nozzle jet power	W
q_{ch}	Heat flux dissipated to grinding chips	W
q_f	Heat flux dissipated to grinding fluid	W
q_s	Heat flux dissipated to grinding wheel	W
q_t	Total heat flux generated in the grinding zone	W
q_w	Heat flux dissipated to the workpiece	W
Q_d	Supply flowrate	l/min
Q_w	Volumetric removal rate	m^3/s
Q'_w	Specific volumetric removal rate	m^3/s
$\dot{Q}_u$	Volumetric useful flowrate	m^3/s
r_s	Wheel radius	m
Re	Reynolds number	-
s	Dwell time	s
T	Absolute temperature	K
U_d	Dressing overlap ratio	-

v_a	Air velocity	m/s
v_{cr}	Critical wheel peripheral velocity	m/s
f_d	Dressing feedrate	mm/min
v_f	Infeed rate	mm/min
v_j	Fluid jet speed	m/s
v_n	Fluid speed at nozzle outlet	m/s
v_s	Wheel surface speed	m/s
v_w	Workpiece surface speed	m/s
ϕ	Wheel porosity	%
ϕ_s	Wheel surface porosity	%
κ	Thermal conductivity	Kw/m·K
μ	Dynamic viscosity	kg/m·s
ρ	Density	kg/m^3
υ	Kinematic viscosity	m^2/s
ω	Angular frequency	rad/s

CNC	Computer Numerical Control
EU	European Union
HEDG	High Efficiency Deep Grinding
MQL	Minimal Quantity Lubrication
MTA	Manufacturing Technology Association
UK	United Kingdom
VIPER	Very Impressive Performance Extreme/Efficient Removal

List of Figures

List of Tables

Chapter 1. Introduction

1.1 Genesis

Grinding as a process has existed from the earliest of times in some form or other. In its most basic form grinding involves a hard object rubbing and removing material from a softer object. It can be generally expected that the harder object be one order of magnitude harder than the softer material.

Grinding is a well established machining process that has been subject to substantial recent research and process development. The process is inherently complex due to the unpredictable nature of grain – workpiece interactions. As a result of this complexity, extensive research has been necessary to improve understanding and capability. Grinding as a manufacturing process is an essential part of nearly all metal cutting procedures; whenever a tight surface finish or geometric tolerance is needed grinding will be essential as the finishing process. As geometric tolerances become tighter in order to control complex design interactions grinding becomes increasingly important.

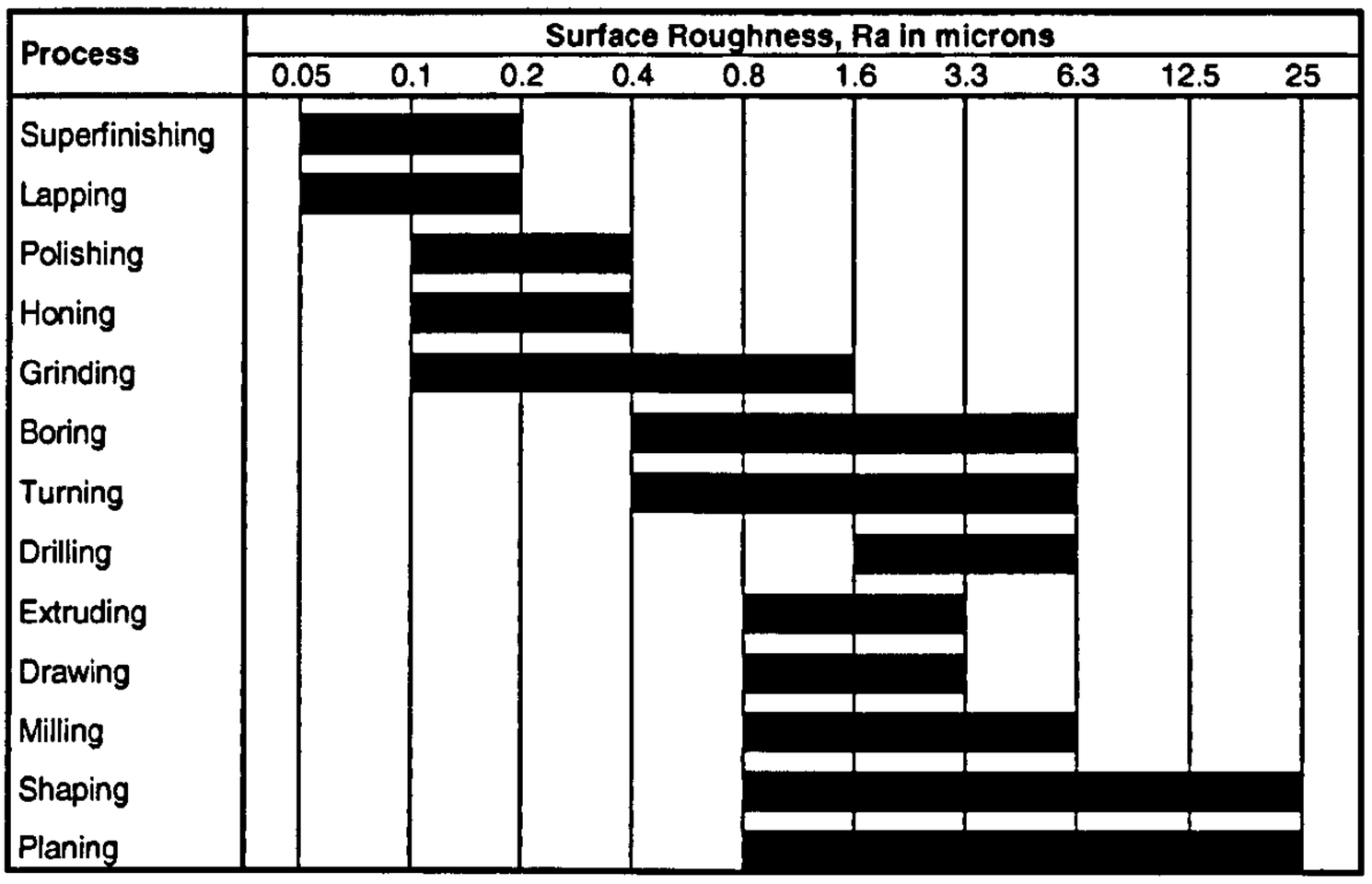

Table 1, Typical surface roughness values from different finishing processes (Dagnall, 1997).

As can be seen from Table 1 grinding typically achieves better surface finishes than most other processes and is predominantly the quickest way to remove material from a hard surface. Within the machine tool manufacturing industry as a whole grinding makes up 15% of a £438 million market (http://www.mta.org.uk, Basic Facts Brochure, 2006).

The supply, maintenance and disposal of grinding fluid is a significant expense, particularly when fluid is used in high volume. Approximately 7-17% of total

machining cost was estimated to be consumed by the use and disposal of the grinding fluid (Ramesh, Huang and Yin, 2004). Any advance in this area would be beneficial to manufacturers. Grinding is generally a finishing stage in a multi-stage manufacturing process. It is applied at the high-value end of manufacturing and hence carries a substantial significance to all manufacturers.

Currently, environmental legislation and concerns are disseminating down from a multinational level regarding the use and disposal of grinding fluids. The pressures for new methods take the form of EU initiatives, new parameter definitions and industry support groups. This will impact on UK business in the form of extra cost in purchase and disposal of grinding fluids and the cost of conforming to possible new quality standards. These factors lead to a need for nearly all machining companies to improve fluid delivery and disposal either for legal conformity reasons or to remain competitive in the increasingly aggressive European and Global manufacturing market. Despite common perception machine tool sales is a prosperous business for those willing to advance. The first six months of 2006 showed that for metal working machine tool manufacturers in the UK exports totalled £231.8 million, an increase of 12.4% on previous years (Professional Engineering, 2006). Further to this, analysis by product type showed that it was CNC grinding machines that had the largest trade surplus for the first 9 months of 2006, £13.7million (http://www.mta.org.uk, Dec 2006). The increase in exports is mainly due to development in Asia and Russia (Professional Engineering, 2006).

Brinksmeier *et al* (1999) stated 'Further investigations in the fields of fluid dynamics processes in supply nozzles and in the grinding zone are the key to optimization of cooling and lubrication during grinding', it is from this notion that the terms regarding flow within the grinding zone have gained importance. Previous work on fluid delivery has mainly focussed on how to deliver fluid to the grinding machine, the effects of using oil or emulsion as a coolant and the need to supply fluid at high speed and in sufficient quantity. More recent research has seen focus on the quantity of fluid that actually gains access into the grinding contact zone. This quantity that enters the grinding contact zone is termed 'Useful flow'. Useful flow is always less than the flow supplied through the nozzle by the coolant system. It is commonly known that a

significant quantity of the delivered flow fails to enter the grinding contact zone. It is this difference that justifies the need for, and analysis of, the term useful flow.

Previous researchers have based prediction of useful flow and nozzle flow, or recommendations on target values of useful flow and nozzle flow, on abstract terms that can only be obtained via specific additional testing. However, it would be much more valuable if useful flow could be estimated based on parameters that are readily available to any manufacturer. Furthermore there is a need to investigate how much useful flow can reasonably be achieved in a grinding operation. It is postulated in this project that physical limits may exist. Any guidelines for industry should account for these, there is little point in specifying a large target volume of useful flow if it cannot be achieved in practice or if there is no additional benefit in achieving it. There is a need then, to consider the nature of the guidance that should be given to industry on fluid delivery specification.

The basic hypothesis of this work is that the useful flow mainly relates to the volume that can be accommodated in the surface pores of the grinding wheel. It is this notion that drives the theories and approaches used within this thesis.

1.2 Aim

The aim of this research is to establish a system to define the application of fluid delivery in grinding, with special relevance to useful flow.

1.3 Objectives

The distinct objectives of this research are:

- To investigate and evaluate the term useful flow.
- To design and implement a reliable useful flow collector and establish design methodologies
- Correlate collected flow with grinding parameters to provide a basis for predicting useful flow.
- To develop a theoretical model for the estimation of useful flow and hence the optimal application of grinding fluid.

1.4 Layout

The first chapter gives an introduction to the subject and a description of the aims and objectives associated with this work. The introductory chapter defines both the problem being assessed within this work and the needs as defined within the overall project. This includes the theories covering the justification for the projects and other sources of support located independently by the author.

The second chapter reviews previous relevant research on the use of fluids in grinding. The review starts by covering the grinding process in general then focuses on the use of coolant in grinding and any work where fluid flow through the contact zone has been mentioned or measured. The chapter concludes with a review of the problems associated with how grinding fluid is applied in industry today.

Chapter 3 reviews relevant grinding theory. Specifically this chapter describes assessment techniques employed both in industry and in some previous research projects. The theories presented relate to grinding effectiveness evaluation, grinding wheel topography specification and grinding zone geometry definitions. The chapter finishes with a critical analysis of previous useful flow prediction techniques implemented by other authors.

Chapter 4 describes equipment used for the testing stages. All main and ancillary apparatus is described both in how it was used and if necessary the calibration procedure employed. This chapter includes all relevant information regarding the grinding wheels and workpiece materials.

Chapter 5 seeks to explain the experimental process used in this thesis. A full layout of all the experiments carried out during this project is shown, describing in detail the information relevant to each individual test.

Chapter 6 describes the development of the useful flow collection system. This began with the preliminary testing required to design, build and evaluate a reliable and repeatable useful flow measurement system. Several stages of testing are defined, described and reviewed for their usefulness to the main body of testing. The main body

of testing utilised a fully developed and reliable technique. The chapter concludes with a description of the fully developed useful flow collection system.

Chapter 7 describes the main body of testing; this work is carried out as a basis for achieving a useful flow prediction technique. This chapter also seeks to define values of useful flow that should be targeted by industry as being realistically achievable. The argument over fluid application speed is also addressed. The results from this chapter are utilised throughout the thesis.

Chapter 8 describes the tests carried out to investigate grinding wheel topography. The replication technique and the optical system employed along with the post-processing stages are detailed. Results from analysis into the effect of changes to dressing parameters are described along with results regarding the change of state of a grinding wheel surface after a dress has been performed.

Chapter 9 seeks to utilise the knowledge gained from the testing stages to formulate a strategy for predicting useful flow. It is proposed that the surface pores of the grinding wheel act as a pump and that surface pores can be approximately filled. This hypothesis is used within the two approaches described in this chapter. Both approaches are detailed, along with experimental verification of each method using tests performed within this project and tests performed during other works.

Chapter 10 presets a comprehensive discussion of all the work undertaken. The validity of the relationships proposed for useful flow are examined. All experimental and development work that was undertaken is discussed; with description of all major errors and obstacles found during the experimental process.

Chapter 11 summarises the main conclusions from the thesis. Conclusions are made to provide concise insight into the developments this work can offer.

Chapter 12 concludes the thesis by discussing future developments in this field and suggesting several projects for the continuation of the work started within this project.

1.5 Scope

The thesis reviews previous research on grinding and then focuses specifically on useful flow and any work where fluid flow through the contact zone has been mentioned or measured. Previous useful flow models are analysed to draw out the key factors such as permeability, pressure and wheel surface topography. The research then discusses the analytical tools that may be used to quantify both the grinding process and a grinding wheel.

A flow collector was designed to trap flow which had passed through the contact zone. This required all other grinding fluid to be diverted away from the collection apparatus. Experiments were carried out to establish the reliability of the flow collector on two surface grinding machines with a maximum wheel speed of 50 m/s on the first and 70 m/s on the second. The main body of testing took place at the higher speed range. Several stages of initial testing were needed to design, build and test a reliable and repeatable method of useful flow capture. Three levels of initial testing and development were required in order to fully design the useful flow system. These incorporated a basic test, an exploratory test and then a refining test. The final arrangement incorporated all necessary gauging.

Before confidence was established in the system from the tests, it was possible to formulate a basic strategy for predicting useful flow. It was proposed that the surface pores of the grinding wheel act as a pump. The surface pores can be approximately filled. After this, it becomes difficult to increase useful flow. This hypothesis becomes the basis for the remaining investigation. In order to validate this proposal tests were planned to measure the surface topography of several grinding wheels at various dressing stages. The use of a non-contact optical method of measurement allowed several accepted surface parameters to be defined both for verification and further analysis. The results are displayed and analysed along with examination of the effectiveness of dressing in opening up fluid carrying cavities within the wheel surface.

The research shows that useful flow is mainly related to the volume of the surface pores of the grinding wheel. For an extremely porous and open wheel the surface pumping capacity of the grinding wheel allows a linear relationship between the useful flowrate and wheel speed up to where the wheel speed equals the jet speed. For a less

accommodating wheel, low porosity and closed surface structure, the linear proportionality breaks down and the relationship becomes more complicated becoming far more dependant on the ratio of the wheel speed to the jet speed. However, for both wheels the guidance for nozzle delivery speed suggests the jet speed should be 50-90 % of the wheel speed, this range allows the highest percentage of fluid to pass through the contact zone. Certain provisos exist for non-aggressive grinding situations, such as low depth of cut or very well suited wheels and fast workpiece speeds, in these scenarios the percentage can be much lower.

For a well positioned nozzle, it was found that wheel speed, jet speed, wheel porosity and nozzle flowrate are the most significant parameters affecting useful flowrate. It is recommended that when setting up a grinding process for the first time the achievable useful flowrate should be used as guidance for the setup delivery conditions. The value of achievable useful flowrate was found to depend on the wheel speed, wheel width, bulk wheel porosity and grain diameter. These parameters were then related using knowledge developed during the experimental section of this project. Good agreement was found with experiments performed both within this project and from work described by other authors.

Chapter 2. Literature Review

2.1 History of Grinding

Grinding, as a modern manufacturing process, has only developed over the last 150 years and analysis of the process over the last 100 years (Alden, 1914) (Guest, 1914). In spite of substantial research, elements of the process are still not fully understood. Grinding requires a high energy input per unit volume of material removed with virtually all of this energy converted into heat and concentrated within what is known as 'the grinding contact zone'. It is due to this heat generation within the grinding contact zone that a coolant is usually required. Grinding fluids (or coolant) are needed to reduce frictional losses, prevent rapid wheel wear, reduce specific energy, and maintain good product quality in terms of surface texture and integrity. Even with these requirements receiving common acceptance the actual volume of fluid flow required is unknown. Currently there is significant discussion on the best way to deliver fluid to the grinding zone. A better understanding of the science could lead to significant advances in more than just process efficiency, significant steps would be possible in reducing process and capital costs along with a reduction of negative environmental effects.

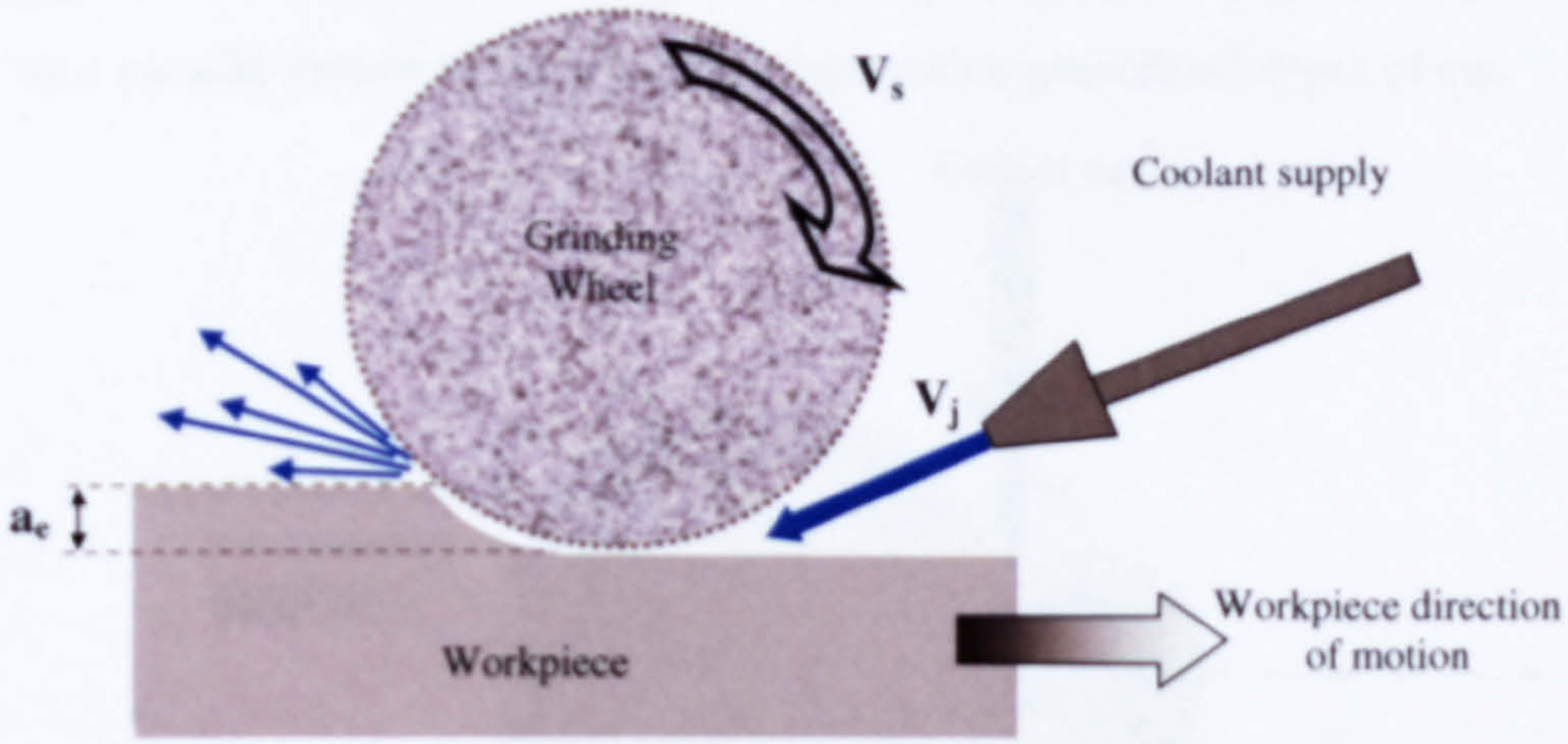

Figure 1, Typical surface grinding system schematic.

Grinding is often regarded as a finishing process and consequently carries a high value in a manufacturing system. The most common grinding operations are surface and cylindrical and these are therefore the most researched. The grinding process with its high-energy input converts nearly all of this energy into heat that is concentrated within the grinding zone. The region known as the grinding zone or contact zone refers to the area where contact is possible between the abrasive wheel and the workpiece. The contact zone region is defined by the product of the actual contact length l_c and the wheel width, b_s. However, there will only be physical contact between the wheel and

the workpiece for a portion of this possible area at any one time. When considering wear flats there was found to be contact over only 5% of this possible region (Malkin, 1989). This low value is due to the stochastic nature of the layout of the abrasive grains in the three dimensional bond of the grinding wheel.

2.1.1 Surface Grinding

Surface grinding is a reciprocating process where the wheel passes over a surface that may be larger or smaller in width than the grinding wheel employed. This geometry difference is overcome with a step progression so several passes are required to cover a complete surface. A plunge in-feed can be added at the end of the stroke when the wheel is in air and has passed fully over the entire surface once. Most surface grinding is performed to gain a flat, parallel and smooth surface. Traverse surface grinding is represented in Figure 1.

2.1.2 Cylindrical Grinding

Cylindrical grinding exists in two modes, traverse and plunge. Plunge mode is a straight in-feed towards the workpiece and traverse mode involves the wheel axis having a parallel motion to the workpiece axis with a predefined depth of cut.

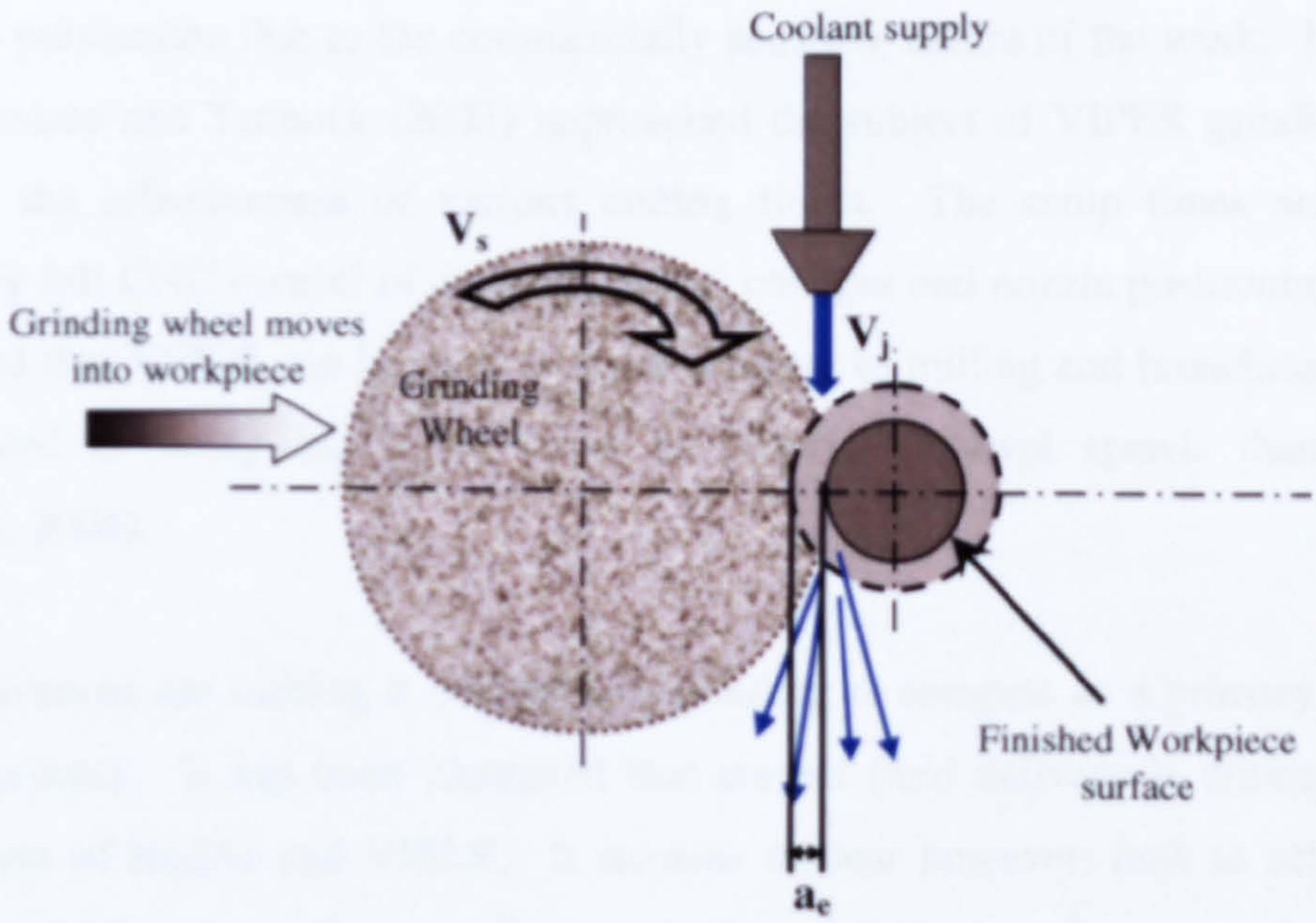

Figure 2, Diagram of a typical external cylindrical grinding process.

Cylindrical grinding machines can either produce external or internal diameters. The two types of machine require a different layout and present different challenges for fluid delivery. External grinding is simpler for nozzle positioning than internal grinding. A

cylindrical process is used to gain high levels of surface finish and geometrical accuracy on a rotationally symmetrical part. A typical external cylindrical grinding process can be seen in Figure 2.

2.1.3 Cutting Edge Developments

The view that grinding is a finishing process is being challenged by advances in the process such as: High Efficiency Deep Grinding (HEDG) (Rowe *et al*, 2005) and Very Impressive Performance Extreme Removal (VIPER) (Venables, 2006) grinding techniques. HEDG is defined as deep grinding at high work speeds and very high removal rates. It has the advantage of being able to achieve low specific grinding energy, approximately 10 J/mm^3 (Jin, Stephenson & Corbett, 2002) (Rowe & Jin, 2001).

VIPER cell grinding is a new technology developed by Rolls-Royce in collaboration with Japanese machine tool builder Makino and Austrian grinding wheel producer, Tyrolit. The principle is to use alumina grinding wheels mounted to a horizontal machining centre, this is then supplied with high pressure coolant and is currently mostly used when machining tough nickel based aero-alloys. VIPER techniques have seen little publication due to the commercially sensitive nature of the work. However, Axinte, Axinte and Tannock (2003) approached the subject of VIPER grinding when analysing the effectiveness of various cutting fluids. The setup times are greatly reduced by full CNC control of dressing, wheel changes and nozzle positioning. It has been stated that VIPER can be used as a replacement to milling and broaching and has been quoted as being ten times faster in material removal speeds than milling (Venables, 2006).

These advances are making it possible for grinding to compete as a primary material removal process. It has been identified that correct fluid delivery is critical for the achievement of HEDG and VIPER. It remains unclear however, how to achieve the optimal fluid delivery conditions in these and other process operations.

2.2 Lubrication

The importance of lubrication in grinding is a well established fact (Brinksmeier, Heinzel and Wittmann, 1999). Lubricants used in grinding are commonly referred to as grinding fluids. A grinding fluid is used primarily for two purposes, to minimise

thermal energy build-up by convective cooling and minimise friction generated heat by lubricating the interacting faces. Grinding fluid is also used to reduce grinding wheel wear and improve process efficiency. The use and delivery of grinding fluid has attracted significant research, however conflicting advice is reported. In some situations a lubricant can be a hindrance, such as mirror grinding where the thermal shock of the workpiece hinders achievement of target tolerances; but in general it provides a much needed function. Although the needs of coolant are commonly accepted it has been found that lubrication when machining at very high wheel speeds can appreciably increase the capital cost of a machine and also negatively affect power demands and cutting forces in process (Brinksmeier and Minke, 1993). The key differences in current advice relate to fluid delivery speed, direction and flowrate. These aspects of fluid delivery have significant implications for system costs, fluid costs and process efficiency. Brinksmeier, Heinzel and Wittman, (1999) report on the fact that 'reliable data on the essential requirements for efficient coolant systems are simply not generally available'. The difficulties presented by the grinding process such as the large contacting areas, high friction and coolant supply are illustrated within this review paper.

Kim and Guo (1997) showed how important correct lubrication can be. In their work about the heat generated by a creep-feed 'down' type grind, only 2-4 % of the heat energy generated during material removal passes to the workpiece, therefore the rest must either stay in the tool, pass to the chips or be removed by the coolant. This energy partitioning is displayed in Figure 3. In their experiment it is found that the low speeds and vitrified wheel allowed enough cooling to avoid burn, so this can generically be termed an efficient cooling situation. Rowe *et al* (2003) stated that advances in grinding technologies such as HEDG techniques rely greatly on efficient application of coolant to the grinding contact zone. Effects such as fluid film boiling may result in excessive temperature zones and this can only be counteracted during HEDG by sufficient fluid being applied correctly to the grinding contact zone. Rowe *et al* (2003) reported for a particular HEDG test with a removal rate of 288 mm^2/s and a wheel speed of 55 m/s that 21 % of the heat flux can be convected by the fluid and only 2 % will pass to the workpiece or wheel. Again, this situation describes efficient coolant delivery, and shows how coolant delivery if insufficient can adversely change the energy partitioning

in a process, possible allowing 20 % of the heat energy of the process to pass in to the workpiece.

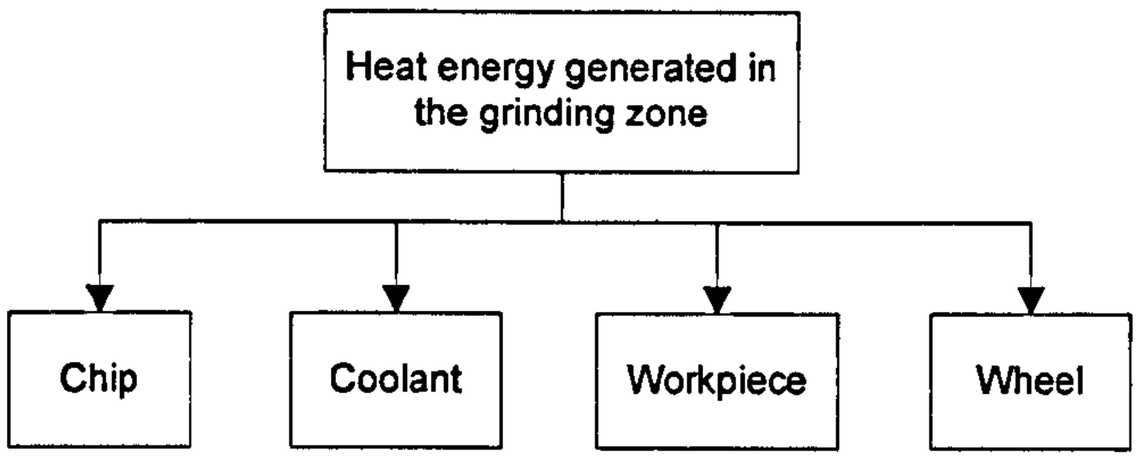

Figure 3, Grinding zone energy partition.

2.2.1 Types of Coolant

Grinding fluid can be split into two broad categories, oil based and water based. These can be further subdivided into water based emulsions and straight or neat oils. A neat/straight oil is pure mineral oil, including trace levels of additives if any are used at all. Water based emulsions consist of an oil in water mixture in the region of 1 part oil to 5-20 parts water. The type of oil used is further subdivided based on the composition of pure mineral oil and additives. A soluble oil fluid is 50-80% mineral oil, a semi-synthetic is 5-30% mineral oil and a semi-synthetic is less than 5% mineral oil (Howes, 1990).

Oil has the benefits of good lubricity, enhanced wheel life and a stronger fluid film than an emulsion. A neat oil has better lubricity than an oil based emulsion, thereby making friction less of an issue. These advantages however are offset by the fact that a large volume of neat oil is more costly than an emulsion. Oil is highly flammable and hence very dangerous, and when in an evaporated state the oil vapour is easily inhaled making it hazardous to an operator's health. Oil has a poor specific heat capacity, typically around 1.9 kJ/kgK when compared with water, the specific heat capacity of liquid water being roughly 4.2 kJ/kgK (Rogers and Mayhew, 2001). This means that water can absorb more heat energy per unit temperature than oil. This makes water a better conduit of energy from the contact zone. Water also has a good thermal conductivity of 600 W/mK in comparison to a mineral oil with a typical value of 130 W/mk. A large thermal conductivity can reduce grinding zone temperature by removing the heat promptly after it has been generated. In contrast oil works better at

lubricating the faces that would otherwise generate large volumes of thermal energy, thus preventing the heat from being generated in the first place.

Typically a water-based coolant is far cheaper to purchase than an equivalent amount of oil-based coolant and is generally cheaper than oil in terms of maintenance and cleanliness. A water based coolant (typically an emulsion with a 10% concentration in water) can also benefit from enhanced physical properties with the inclusion of additives. These additives could be: pour point depressants to aid fluid flow, extreme pressure additives to allow the fluid to operate effectively at high pressures or a fatty oil agent to aid lubricity of the fluid. Other additives are necessary to prevent bio-degradation due to bacteria and additives to prevent corrosion of the machinery and workpiece.

The following is a list of coolant types along with their important characteristics (Irani, Bauer, & Warkentin, 2005)

	Synthetics	**Semi-synthetics**	**Soluble oil**	**Straight oil**
Heat removal/ Cooling	4	3	2	1
Lubricity/ Film strength	1	2	3	4
Maintenance	3	2	1	4
Filterability	4	3	2	1
Environmental	4	3	2	1
Cost	4	3	2	1
Wheel life	1	2	3	4
G-Ratios	2.5-7.5	2.5-6.5	4-12	60-120

Table 2, Grinding fluid types and properties (5 denotes good performance and 1 denotes poor performance).

When considering a coolant it is important to understand the modes of effectiveness, this draws attention to the importance of the coolant and its constituent parts to the grinding process. As an emulsion is a mixture of oil and water (and maybe other additives) it can be expected that the constituent parts will burn out at different rates. Typically oil also has a higher boiling point than water and hence will last longer in a grinding zone where the temperature exceeds the reported boiling point of an emulsion-

type grinding fluid, this is in excess of 100°C as established by Howes (1987). As the thermal conductivity of a mineral oil is typically a quarter of the value for water (Klocke, Baus & Beck, 2000) it is the water within the grinding fluid that accounts for the majority of thermal energy transfer that takes place within the contact zone. At that point where convective cooling no longer takes place the temperature of the workpiece interface will rise faster, the only limiting factor to rising temperature is the lubrication the oil can provide to the grain rake face. At around 300°C the oil will eventually burn out and may cause the specific grinding energy to increase and wheel wear to rapidly increase. Hence efficiency will drop and the surface roughness of the finished surface will increase. It is at this point where the coolant burns out and the lubrication fails that the process becomes inefficient. This may cause the part, depending on the material, to become thermally damaged and scrapped.

2.2.2 Industrial Implementation and Legislation

A focus within industry is currently on environmental effects of grinding fluids due to increasing legislation at a multinational level. These concerns most recently take the form of EU initiatives (EU Council Directive 75/439/EEC, June 1975) (Directive 2000/76/EC of the European Parliament and of the Council of 4 December 2000) and parameter definitions (Council Directive on the disposal of waste oils 75/439/EEC, Article 1.) designed to help implement regulations and new directives. These guidelines have lead to industry support groups such as the Hazardous Waste Reduction Group, HAZRED (*http://www.hazred.org.uk/*) and the Waste Exchange (*http://www.wasteexchangeuk.com/*), both groups sole purpose is to minimise the disposal of waste materials.

Recent research by the UK government (*http://www.envirowise.gov.uk/home.aspx*) has shown that the purchase, management and disposal of metal working fluids (including processes other than grinding) is worth approximately 15 % of overall manufacturing costs to the engineering industry. This statistic shows that the efficient use of coolant can be an effective cost savings tool. Further to this 10 % of the UK total oil sales for 1999 (approximately 1,000,000 tonnes a year) can be attributed to metalworking as an industry. If metalworking alone could lower fluid usage by just 5 % a year this would relate to a 5000 tonnes reduction and would have a significant environmental impact. This in turn would have a considerable effect on the amount of grinding fluids that would need to be disposed of. Cutting fluid at this time costs approximately £2.30 a

litre and disposal costs are in the region of £20 for a 200 litre barrel, excluding transportation costs. These costs should equate to a significant financial and environmental saving for any company willing to invest in improved efficiency of coolant application.

Within manufacturing, certain niche sectors have arisen to accommodate the demands of minimal fluid usage. Minimum Quantity Lubrication (MQL) is a prime example of the attempts to advance coolant delivery, consumption and efficacy. Both dry machining and MQL are specialised fields falling outside the scope of this investigation. MQL currently focuses on using millilitres of oil per hour. This significantly lowers the purchase cost of coolant; however the exact benefits and areas of usage for MQL are still to be determined and verified.

It is between MQL and conventional coolant delivery where the relevance of useful flow is most significant. The goal is to create a bridge between the specialist area of absolute minimal fluid application and the common industrial approach of 'more is better'. This should allow some of the benefits of MQL to be applied in a more generalised manner. In order to achieve this kind of advance the entire grinding process needs to be considered. The most important grinding process parameters, such as wheel speed, workpiece speed, fluid delivery pressure, fluid delivery method, fluid delivery rate and depth of cut must be allied to any attempt at advancing grinding fluid application. But in reference to a useful flow definition it is expected that these will be of paramount significance.

2.3 Grinding Zone Flow

Within the following reviews a distinction is drawn between useful flow research and research on general delivery rates; specifically for any attempt at modelling, predicting or dictating what the useful flow could be. Most researchers have not attempted to optimise useful flowrate, as this would require a significant volume of grinding trials. However, some attempts are made at guidance to what the supply flowrate should be for a particular purpose. Such attempts are not specifically aimed at stating what the useful flowrate is but rather what the flow is required to be, given certain criteria, such as limiting a particular temperature rise. When giving a value of target grinding zone flowrate most times it is ignored exactly how that target can be achieved. As stated

previously the nozzle flow will always be greater than the grinding zone flow or useful flow. The principal outcomes of previous research concerned with fluid delivery, fluid application, and the effects of fluid on grinding performance are reported below.

Schumack *et al* (1991) analysed fluid flow in the contact zone from first principles using a perturbation technique, incorporating at its most complicated the 2-dimensional Navier-Stokes equation including inertial effects. Schumack *et al* used a smooth wheel that was in the spark-out position (equivalent to an infinitesimally small gap). This method of analysis meant that there must be a gap left between the smooth wheel and the workpiece for the theory to be valid. The value of Reynolds number used was based on a characteristic length defined by the grinding wheel radius, and a speed value governed by the circumferential speed of the grinding wheel. The use of grinding wheel radius as a characteristic length seems unusual for a case involving a gap between the grinding wheel and the workpiece.

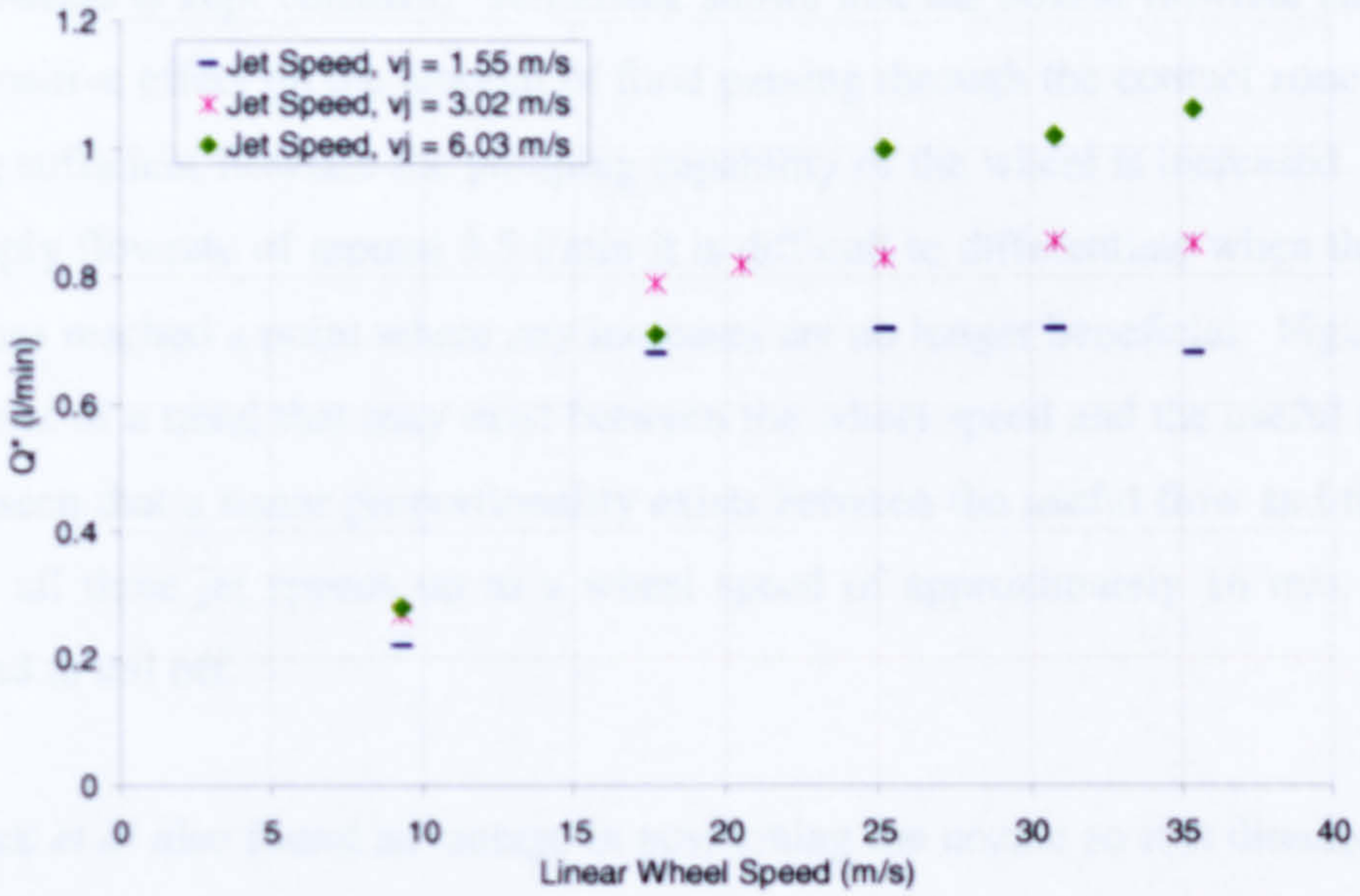

Figure 4, Collected flow, Q^* against wheel speed at varying jet speeds and supply flowrates, Schumack *et al* (1991).

This model was found to be useful at what was termed a low Reynolds number, approximately 7800. At higher Reynolds number, typically 6.45×10^5, reasonable analysis was possible, however it failed when the Reynolds number got too high, typically 3.9×10^6. At conventional wheel speeds (typically in the region of 30 m/s) and jet speeds (typically above 15 m/s) the Reynolds number will exceed the limit for laminar flow between two plates, thereby nullifying the model. Schumack *et al* states that the contact region pressure is small in grinding. The assumption of low pressure

may only be true at low jet speeds and low wheel speeds. As there is no contact between the wheel and workpiece any thermally generated property changes must also be neglected.

Schumack *et al* suggests that an emulsion at a low jet speed of 1.55 m/s will give a useful flow curve that has an upper limit at 700 ml/min, approximately 20 % of the applied flow. This upper limit occurs when the wheel speed is 25 m/s. Figure 4 shows these results in graphical form. However increasing the speed of the jet to 6 m/s will give a maximum useful flow of approximately 30 % of the applied flow, with an undefined upper limit occurring when the linear wheel speed is in excess of 35 m/s.

Schumack does not make a clear distinction between the nozzle flowrate, nozzle outlet size and the jet speed. Schumack appears to be using a round nozzle which must have significant geometry change in order to change the speed by a factor of 4, assuming the nozzle flowrate is kept constant. Schumack shows that the nozzle flowrate can have a directly positive effect on the amount of fluid passing through the contact zone and that by having sufficient flowrate the pumping capability of the wheel is increased. At such a low supply flowrate of around 3.5 l/min it is difficult to differentiate when the supply flowrate has reached a point where any increases are no longer beneficial. Figure 4 also shows a hint of a trend that may exist between the wheel speed and the useful flowrate. It can be seen that a linear proportionality exists between the useful flow and the wheel speed for all three jet speeds up to a wheel speed of approximately 16 m/s, then the results tend to tail off.

Schumack *et al* also found advantage in positioning the nozzle so it is directed toward the wheel rather than the gap or the workpiece. The results suggest a possible difference of 50 % in measured flowrate in varying the position and hence direction of the nozzle, with the maximum useful flow being when the nozzle is directed at the wheel above the contact zone. Schumack *et al* concludes that only a three dimensional model incorporating complex end effects could accurately predict true grinding flows.

Guo and Malkin (1992) stated that the most important factors affecting the useful flowrate are nozzle position, jet speed and effective wheel porosity. The effective porosity relates directly to the bulk porosity of the wheel. All testing was conducted at low wheel speeds and jet speeds, and does not address the commonly held notion that

the jet speed needs to match the wheel speed. Predictions of useful flow were attempted based on the model developed by Chang (1994) from within the same group. Experimental comparison was made to the work of Engineer, Guo and Malkin (1992). It was also stated that creep feed wheels provided better flowrate due to their increased effective porosity and the impact that parameter has on the ability of the wheel to pump fluid through the grinding zone. Guo and Malkin (1992) postulated that film boiling may give rise to the failure of convective cooling thereby inducing a temperature rise in the surface of the workpiece.

The work by Engineer, Guo and Malkin (1992) was conducted on a reciprocating grinding machine and used mechanical flow isolation to collect the flow that had passed through the grinding contact zone. Engineer chose to use the term 'Percentage Utilisation' for useful flow. The collected flow was compared to applied flow, bulk wheel porosity, nozzle position, dressing and flowrate. Engineer *at al* found that the percent utilisation was in the region of 5-20% of the applied flow. These values were obtained during a test where the flowrate was varied by changing the pressure at the pump. However, this will invariably change the jet speed as well as the flowrate. Jet speed is considered to have its own influence, mainly regarding the air barrier effects discussed later in this thesis. The results from Engineer *et al* can be seen in Figure 5.

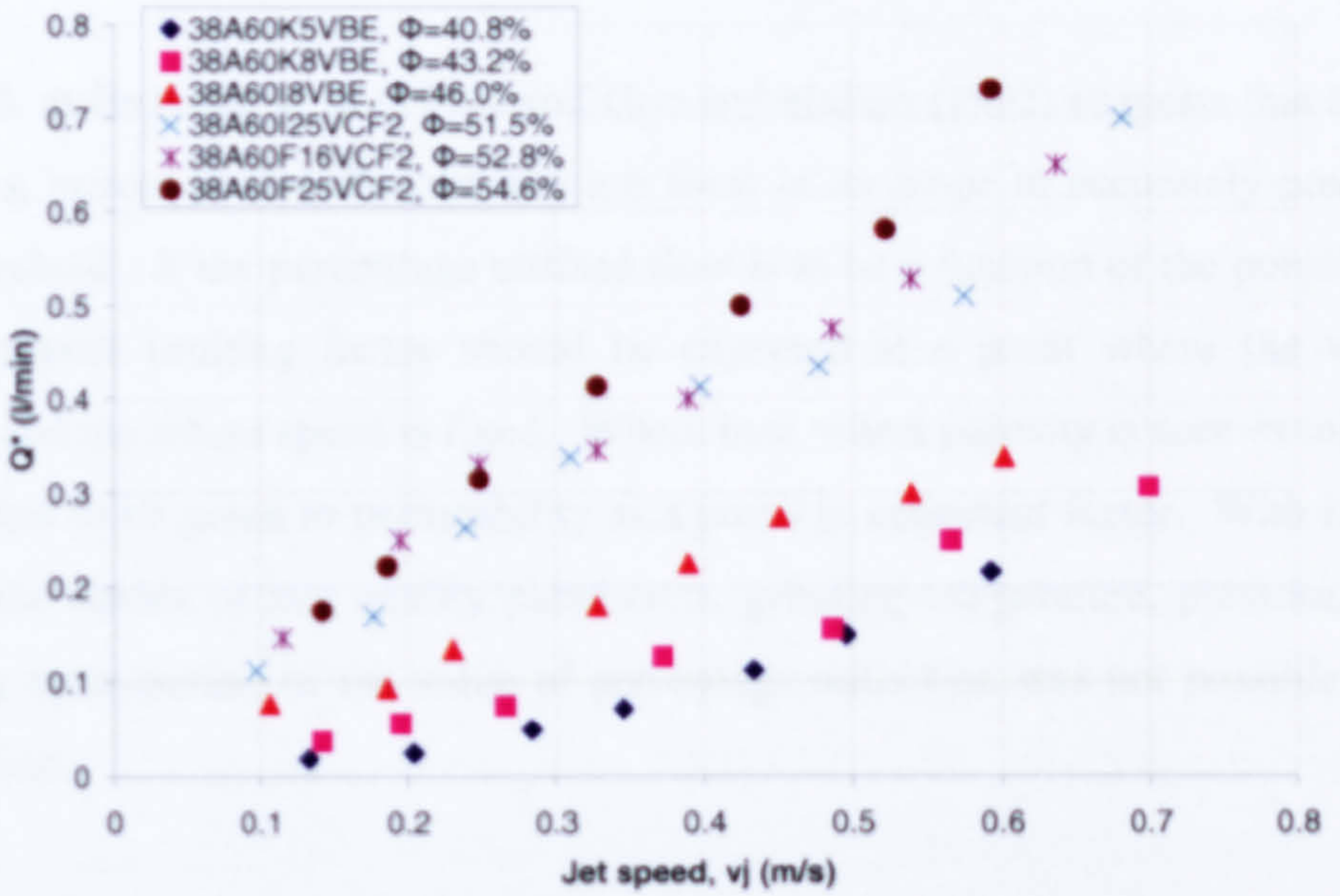

Figure 5, Percentage utilisation versus nozzle exit speed for grinding wheels of various bulk porosities Φ, when v_s=30m/s, a=12micron, s_d=160μm, v_w=0.09m/s, b_w=19mm and d_s=250mm. (Engineer *et al*, 1992).

This value of 5-20 % was in reasonable agreement to Akiyama *et al* (1984), who found useful flow in the region of 20-40 % of the applied flow. The results of Engineer *et al* lead towards the conclusion that depth of cut, dressing parameters and workpiece speed are of no significance. The findings also suggested wheel dressing has a minor input due to the controlling function the dressing has over the more influential factor of wheel porosity at the surface. The most influential factors found were the bulk porosity of the wheel and nozzle position (Engineer, Guo, Malkin, 1992). Engineer *et al* showed a linear relationship between the useful flowrate and the applied flowrate (shown as nozzle exit speed in Figure 5) for the relatively low values of 30 m/s wheel speed and a supply flowrate of up to 3.6 l/min (0.0036 m^3/min).

The methods used to capture flow by Engineer although acceptable for the lower jet speeds would fail when using the more aggressive jet speeds and flowrates that are targeted in order to match the wheel speed. As in Figure 4, it appears there is a linear proportionality between the useful flowrate and jet speed. In Figure 5, the slope of the linear portion depends on the wheel porosity. The highest porosity gives the steepest slope. According to these results an increase in bulk wheel porosity from 41 % to 55 % can increases useful flowrate by a factor of 5 times. This is a very large difference and more than likely is compounded by the increase in supply flowrate that is accompanied by an increase in nozzle exit speed.

The work of Engineer *et al* (1992) and Guo and Malkin (1992) suggests that there are no limiting factors or that the test was too short in its scope to accurately predict any upper threshold. If the percentage utilized flow is to be a function of the porosity, then a topographical limiting factor should be expected at a point where the wheel is saturated and the wheel speed is fixed. Where bulk wheel porosity is seen as influential attention has to be given to permeability as a possibly important factor. With no report made of the values of key quality parameters, grinding temperature, pressure, power, force; any optimisation of the value of percentage utilisation was not possible for this investigation.

Chang (1994) used a theoretical model to describe several relationships some of which were verified against experimental data from Yasui and Tsukuda (1983) in a creep feed process. Chang's model described that an increase in wheel speed will decrease the

depth of fluid penetration into a porous wheel, this is due to the centripetal acceleration required by the fluid being stronger than the pressure effect the fluid will experience in the contact zone. The penetration depth appears to follow a decrease proportional to a 'Power' trend. When the wheel speed is 20 m/s the fluid can penetrate 60 μm radially into the wheel, and when the wheel speed is 70 m/s the trend shows the penetration would be approximately 15 μm (see Appendix C). It was described that the depth of penetration could be increased by increasing the supplied flowrate, this relationship appears to follow a linear trend. Chang predicted that when the flowrate is 4.2 l/min the penetration depth is 40 μm and at 18 l/min the penetration depth is 100 μm, if a linear trend is assumed. Chang also states that the useful flowrate can be increased by increasing the porosity of the wheel, in some instances the useful flowrate can be at least doubled when the porosity is doubled for a given jet speed. A larger useful flowrate can be achieved by increasing the jet speed, and that a higher porosity wheel will allow the nozzle exit speed to have a more pronounced effect. Therefore it was stated that permeability may be important when the wheel is highly porous.

Krishnan *et al (1995)* used a novel method of capturing the flow using unique physical boundaries surrounding the wheel. It was found that a percentage useful flow up to 55 % could be measured when using a highly porous wheel at workpiece speeds equivalent to creep feed and using low wheel speeds. Krishnan observed that the grit size, wheel porosity, wheel speed and nozzle position were the key influences to useful flowrate. Agreement was found with Guo and Malkin (1992) in that dressing had a secondary influence, and more specifically the dressing depth being the factor with any control at all. This brought to attention the surface condition of the wheel as possibly being a key factor to the ability of the wheel to transmit fluid. The wheel speeds employed for testing by Krishnan were limited to 30 m/s, slow by modern standards. No attention was drawn to the influence of the jet speed even though applied nozzle flowrates were varied and labelled as key. Increasing the flowrate was most likely achieved by increasing the pressure at the supply pump; this would undoubtedly lead to an increase in jet speed if the same nozzle was used. This would make separating the two factors difficult and drawing conclusion on either impossible. The effects of the air boundary layer that is generated around a rotating wheel and hence the needs for an increased jet speed were not addressed. Krishnan also introduced an approach similar to Marinescu *et al* (2004) that utilised a value of useful flowrate to estimate the thickness of a fluid

layer that is equivalent in volume to the useful flow. This approach involved creating a theoretical fluid layer thickness based on a comparison to the grain diameter. All the wheels tested were vitrified alumina wheel with grain sizes of between 108-184 μm. Krishnan's results pointed to a value of h_{uf} equivalent to 10-16 times the average grain diameter when using applied flowrates of approximately 135 l/min and grinding wheel porosities ranging from 45-55%. These are extremely high values for h_{uf} and are most likely a result of the very high supply flowrate and very high jet speed. The situation employed could easily be considered inefficient due to the large amounts of energy required to accelerate the fluid to such high speeds.

In the review paper by Brinksmeier, Heinzel and Wittman (1999), a discussion of the grinding zone flowrate led to an acknowledgement that any increase in coolant jet speed could lead to lower cooling efficiency (Brinksmeier *et al*, 1999). This finding was linked to a geometric limitation to the flow through the grinding arc (Vits, 1989 from Brinksmeier *et al*, 1999). Brinksmeier also drew attention to an optimal value of grinding wheel wear and residual stresses found by Tawakoli *et al* (1990) when a nozzle flowrate of 60 l/min was applied at a pressure of 15 to 20 bar. The paper by Kovacevic and Mohan (1995) describes the use of a nozzle flowrate of 3.6 l/min as giving a decrease in process forces of 25 % and surface roughness of 50 % in comparison to a flood fluid application system.

In the work by Gviniashvili *et al* (2004) a simulated grinding situation was implemented, this was a 'zero gap' scenario achieved using a gap elimination technique, similar to Schumack (1991). Gviniashvili's results showed that to achieve a sufficient useful flowrate the nozzle should be positioned as close as possible to the contact zone. It showed that at high wheel speed, the difference in measured useful flow could be up to 100 %. Particular attention was paid to the spindle power requirements to overcome the fluid resistance to motion. It remained undetermined whether a true contact would add to the power needed for fluid traction. This power value is a combination of coolant jet drag from the need to accelerate the applied coolant and the hydrodynamic drag effect present due to viscous shear of the fluid. Gviniashvili *et al* (2004) concluded that matching wheel speed and jet speed allows useful flowrate per unit power to be approximately maximised and prevents total power from becoming excessive. The use of experimentally determined correction factors limit the extent to

which the model developed within this work can be applied without additional calibration. Further to this was a tentative suggestion that when the wheel speed matches the jet speed, the spindle power to accelerate the fluid will be equal to the jet power.

Gviniashvili *et al* (2004) also showed the effect of an air barrier, as was previously demonstrated by Ebbrell *et al* (2000). At high speed, the air boundary layer around the wheel tends to deflect the grinding fluid making it more difficult for coolant to get close to the wheel surface. Also shown was the effect of the disruption of the air barrier by a nozzle and scraper arrangement. This creates a pocket directly after the scraper where a fluid can be entrained by the wheel as a new air barrier is formed. This aids the coolant in passing into the contact zone.

As has been stated in this chapter and shown by mentioned authors the flow expected to pass through the contact region is strongly dependant on the bulk porosity of the wheel, the wheel speed, nozzle position and the jet speed. Exact relationships have yet to be fully established.

2.4 Issues of Coolant Application

When specifying or analysing a coolant system several factors need to be addressed. These are nozzle design, nozzle position, nozzle angle and supply flowrate.

Nozzle design characterises the type of nozzle being used and the specific geometry it employs. There are three categories of nozzle employed today; jet nozzles, slot nozzles and shoe nozzles. Although the shoe nozzle can be an extremely effective method of utilising fluid without waste, it has some significant drawbacks. A shoe nozzle relies on being able to apply a fluid pressure directly to the wheel periphery thereby forcing fluid into its pores by virtue of its permeability. A shoe nozzle uses pressure to force grinding fluid far enough into the wheel in order that it may be retained until that segment of the wheel reaches the contact zone. Typically the difference between the shoe nozzle position and the grinding zone is at least 45° on the wheel periphery. Powell (1979) observed that a shoe nozzle can force fluid through the periphery of a wheel up to a radial depth of 10mm when a highly porous wheel is used, this value was later theoretically corroborated by Chang (1994). The usefulness of grinding fluid

forced up to and beyond 10mm is questionable and is yet to be verified. The outlet of the nozzle must be in intimate contact with the wheel surface at all times, this forms the seal that allows a pressure to build up and force fluid into the wheel. However, the wheel will decrease in diameter as a grinding process is performed or as a dress is performed thus creating a gap between the wheel and the nozzle once again. It is this need for a pressurised fluid volume to be in contact with the wheel surface that is its major disadvantage. No system exists that at a reasonable cost can maintain this intimate contact between the nozzle and the wheel as the wheel diameter decreases.

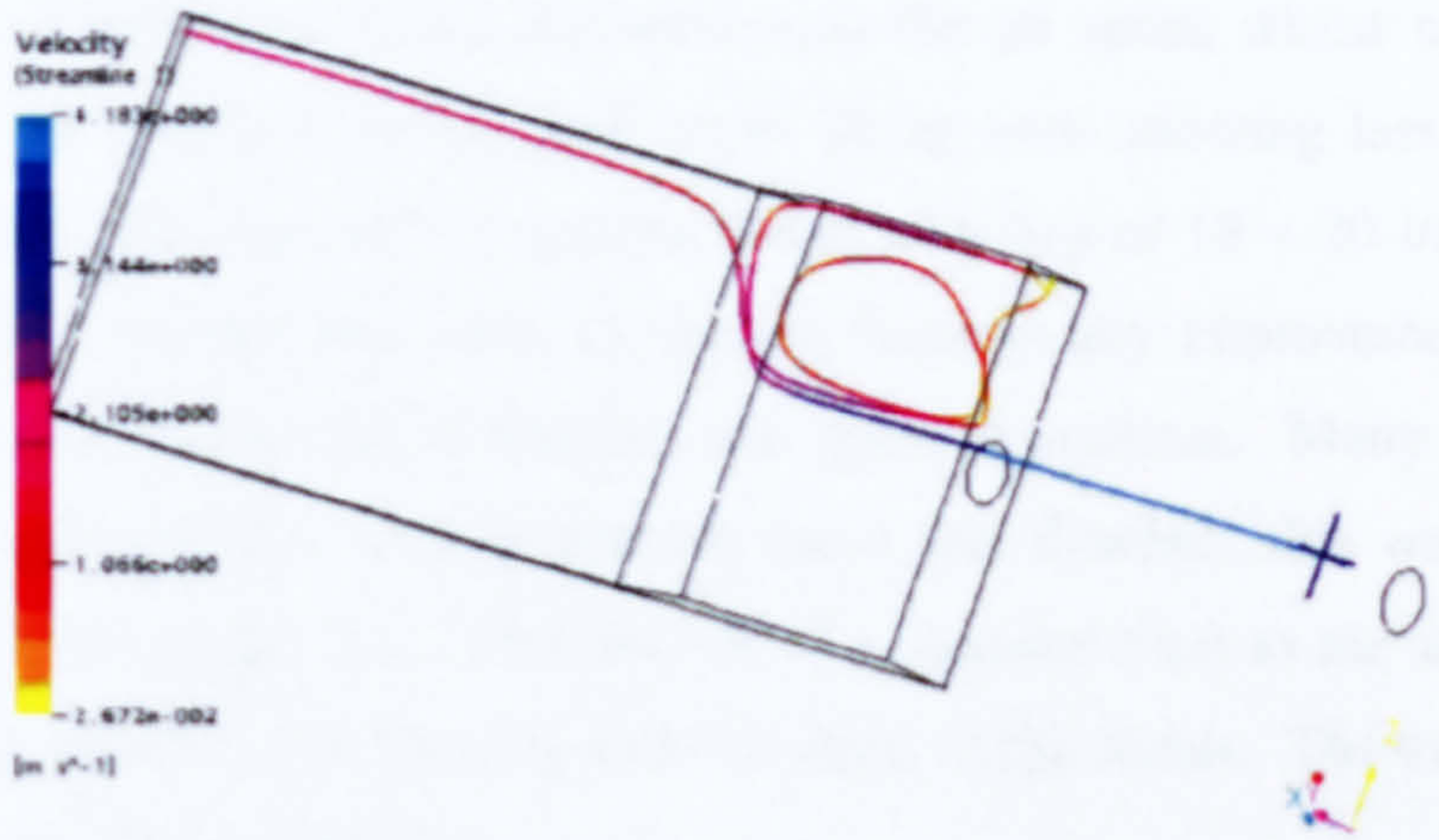

Figure 6, Flow trace of a massless particle passing through a slot nozzle, showing a flow recirculation area indicating poor nozzle design (Baines-Jones, 2005).

The most common type of nozzle in use today is the jet nozzle. This type comes in many forms, with the most common being the click-lock plastic variety. These plastic nozzles are available in various outlet geometries with the most common being round and slot, however others do exist. The round jet type creates a cylindrical stream of fluid that can be readily directed into an area of interest, in this case the grinding contact inlet zone, and can have a wide possibility of speeds. This type has benefit found in its simplicity, they are generally easy to manufacture and always easy to use. However, this ease of use is its downfall. As the nozzle is easily positioned it is also easily moved out of position. There is a tendency by operators to move an awkward nozzle and this can negate many of the advantages this type of nozzle can provide. A suitable jet nozzle can allow the user the ability to reach high nozzle emission speeds, Kovacevic and Mohan (1995) reached speeds of 365 m/s with a 380 MPa supply pressure through a jet nozzle. This is considered very high pressure and therefore costly to attain, and in order to reach the high nozzle emission speeds the outlet of the nozzle would need to have a very small diameter. Kovacevic *et al* showed the benefit of large jet speeds in

low grinding zone temperature, reduced wheel wear and loading and an improved surface finish on the part. The authors also referenced a paper by Ganesan, Guo and Malkin (2001) stating that increased coolant pressure could lead to a reduction in process total force at higher cutting speeds.

A paper by Ramesh, Huang and Yin (2004) found that a water based coolant will help to avoid thermal damage and achieve better surface integrity as well as a higher grinding ratio. Although at no point did Ramesh measure or quantify useful flow. Ramesh *et al* (2004) also found that increasing the jet speed whilst maintaining the flowrate can be beneficial to grinding forces along with allowing less coolant to be used. Further to this the authors suggested that a ceiling of 18 – 20 l/min for nozzle flowrate exists. Beyond this value of applied flowrate any improvement in grinding force, power flux and surface roughness was deemed minimal. Many grinding trials were performed explicitly varying coolant speed and flowrate, this was achieved by varying the nozzle outlet size. The concept of a physical limit to the amount of fluid that should be supplied is in keeping with the ethos of this thesis. The transferability of this value needs to be scrutinized.

It is also important to position and direct the jet nozzle correctly as a high emission speed will generally imply a small cross-sectional area for the stream of fluid. Precise nozzle positioning has seen little concerted research effort as it is intrinsically difficult to separate nozzle flowrate, speed, position and type for complete analysis. Engineer, Guo and Malkin (1992) showed the benefit of close positioning in the amount of fluid forced through the contact zone. Engineer *et al* also brought to attention the need to have good positioning in combination with sufficient supply flowrate. Furthermore, a nozzle angle which is tangential to the wheel and at a position 10° - 25° before the contact zone was seen as the optimal angle and position for free jet fluid delivery (Vits 1985 and Ot, 1991 from Brinksmeier *et al*, 1999), this result was independently verified by Brücher (1996 from Brinksmeier *et al*, 1999). Of course, if the jet speed matches the wheel speed, a tangentially directed water or oil jet can easily displace air because the momentum of the liquid is much greater than the momentum of the air. However, if the jet speed is much lower than the wheel speed, the jet may be required to point slightly more directly towards the wheel surface to avoid being diverted by the boundary layer.

This means that conclusions reached by previous workers for the optimum angle may only be relevant for a particular combination of jet speed and wheel speed.

In conjunction with nozzle position and direction is the concept of a coherent jet design. Coherency in terms of fluid dynamics describes the tendency of a stream of fluid leaving an orifice to break up after a given distance. It is this break up of the fluid that means that a nozzle must be placed near to the grinding contact zone. A non-coherent nozzle jet breaks up quickly, not allowing jet speed to be maintained over a significant area of impact. If jet coherency is maintained then the nozzle can be positioned further from the grinding contact zone. This would allow significant flexibility in coolant application system design. Jet break-up distances are estimated in the PhD thesis by Cui (1995) and the paper by Baines Jones (2006) and the need for jet coherency is emphasised by Webster, Mindek and Cui (1995). Indeed the work by Baines-Jones highlights a newly relevant factor of peak velocity length, defining the distance that the jet stream will take to lose a significant area of fluid velocity from a given cross-section.

2.4.1 Air Barrier

Ebbrell *et al* (1999) showed the negative effect of flow reversal when a flood application method is used (see Figure 8). The air barrier created by a high speed grinding wheel causes a reversal of flow just before the grinding zone inlet area, thereby opposing any flow directed towards the contact zone. This is due to the non-slip effect inherent to any fluid flow over a real wall such as the grinding wheel surface. The fluid directly in contact with the wall will have a similar velocity to the wall, in this case the air in contact with the wheel will move at v_s. The fluid away from the wall will have a mean bulk speed, which in this case is zero as it can be considered stationary air. A gradient will exist between the air at the wheel and the bulk air, the thickness of this layer where there is a gradient is known as the air boundary layer. The exact nature of this boundary layer in regards to a grinding wheel has yet to be fully defined. The effect of the roughness of the wheel surface will tend to induce a turbulent boundary layer earlier than an equivalent smooth wheel. Essentially a rougher surface makes the critical Reynolds number for transition lower; thereby change from laminar to transitional to turbulent boundary layer happens at lower wheel speeds. It is unlikely that a laminar boundary layer will predominate with any grinding wheel due to the high wheel speeds and inherently rough surface. However, whether the boundary layer is in

a transitional state or fully turbulent will depend on the combination of specific wheel surface speed and possibly the roughness. At low wheel speeds and low grinding wheel surface roughness's the boundary layer may hold within the transition region longer than a rougher wheel. Simple calculations of the Reynolds number for a flow over a flat plate for comparisons is shown below. This can be used for rough comparison to a grinding wheel of diameter 250mm.

$$\mathrm{Re} = \frac{Ux}{\nu} \tag{1}$$

When U is free stream velocity, x is the distance along the surface from point of zero boundary layer thickness, in this case the grinding wheel circumference, ν is the kinematic viscosity.

$$\mathrm{Re} = \frac{30 \cdot 0.75}{1.6 \times 10^{-5}} = 1.4 \times 10^{6}$$

A Reynolds number of 1.4×10^{6} means the boundary layer will be in a transitional phase. A transitional phase means there would be a reasonable thickness of laminar sub-layer but with some turbulence properties such as eddy formations. The Reynolds number would need to be below approximately 5×10^{5} to be laminar and above approximately 5×10^{6} to be turbulent. As mentioned previously these values could be expected to decrease with increasing roughness. A larger Reynolds number generally means a larger boundary layer thickness. Hence it would present a more substantial resistance to penetration.

Ebbrell *et al* also recommend firing the jet slightly above the area of flow reversal, the nature of this reverse flow can be seen as fluid velocity vectors in Figure 7 and Figure 8 and also as a photograph of a real setup in Figure 8.

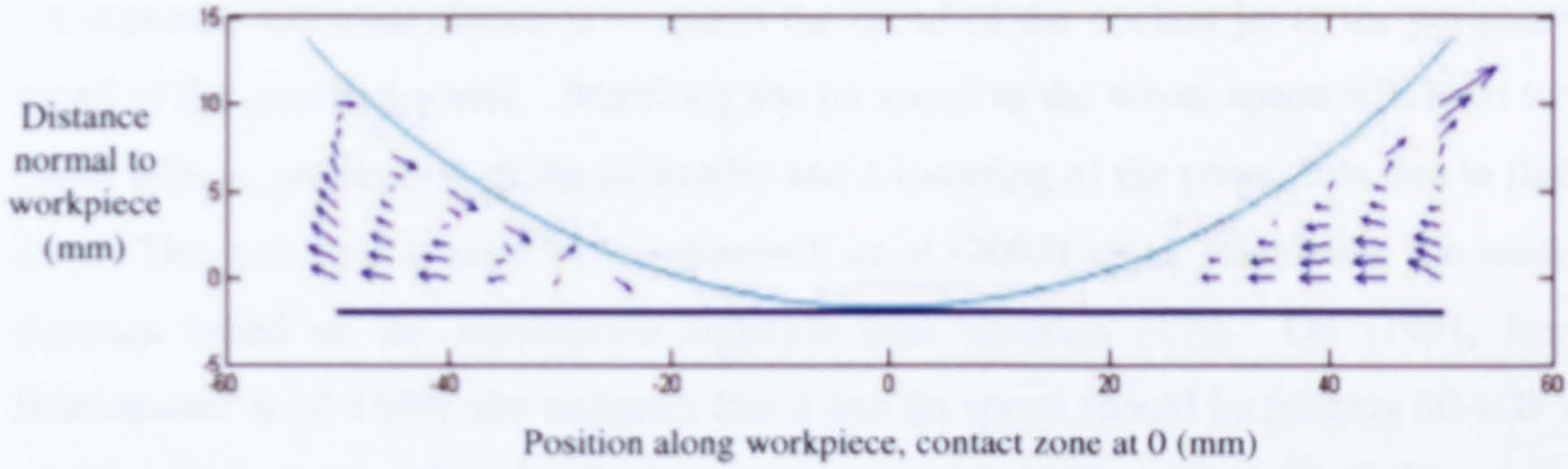

Figure 7, LDA diagram showing fluid flow vectors around an anti-clockwise rotating wheel in a spark out position (Wu, 2005).

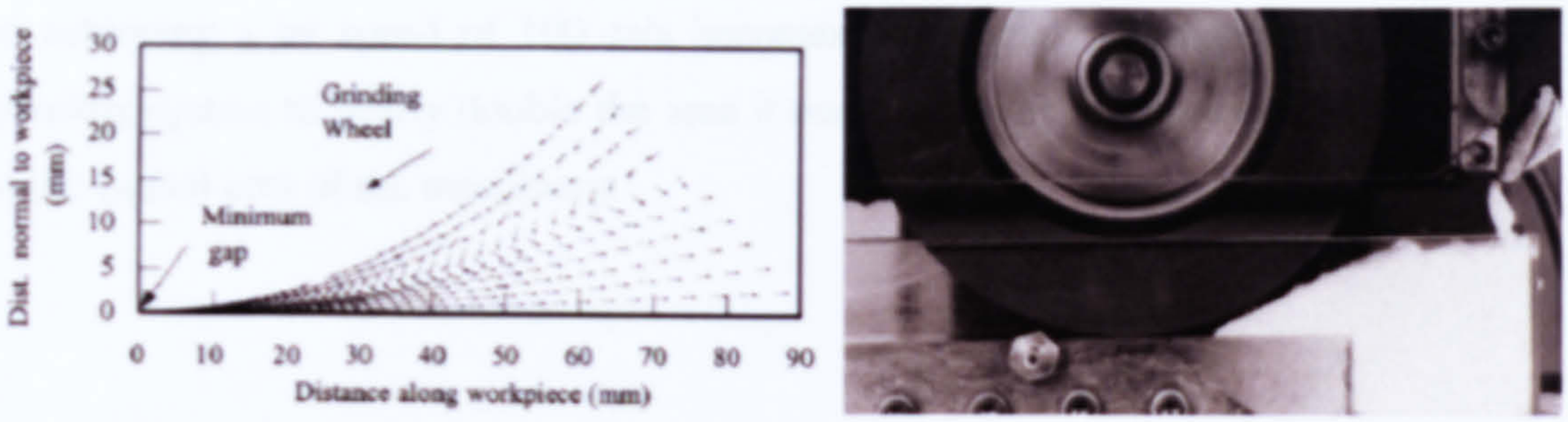

Figure 8, Diagram showing predicted air flow patterns around a clockwise rotating grinding wheel, left. Picture showing fluid backing up at the contact zone due to a flow reversal caused by the boundary layer, right (Ebbrell, 2000).

Marinescu *et al* (2004) stated that in order to penetrate the air barrier the rate of momentum per unit width of the wheel of the incoming fluid must be at least equal to the momentum of the air barrier. The rate of momentum of the fluid is given by

$$M'_f = \rho_f . h_{jet} . v_{jet}^2 \qquad (2)$$

Where ρ_f = Fluid density, h_{jet} = Jet thickness and v_{jet} = Jet speed

The rate of momentum of an air boundary layer of thickness h_{air}, generated by the wheel is given by

$$M'_{air} = \rho_{air} . h_{air} . v_s^2 \qquad (3)$$

Where ρ_{air} = Air density, h_{air} = Air boundary layer thickness and v_s = Wheel speed

These two equations allow an approximation of the minimum jet speed that will be required to penetrate the air barrier, as shown in equation (4). This is assuming the jet profile used will supply the entire length of the grinding zone contact inlet.

$$v_{jet} = v_s . \sqrt{\frac{\rho_{air} . h_{air}}{\rho_f . h_{jet}}} \qquad (4)$$

A common recommendation is to match the speed of the coolant jet to the peripheral speed of the grinding wheel. Matching the jet speed to the wheel speed will have two major effects, penetration of the air barrier and a lowering of the power loss due to fluid drag. This principle is used by Gviniashvili *et al* (2003) when calculating the useful flowrate based on the momentum equation (see equation (27)). Ott (1991, from Brinksmeier *et al*, 1999) also suggests that a free jet speed should be roughly 60-100 % of the wheel speed. Wheel speeds at the time were in the region of 30-60 m/s, so matching the jet speed to the wheel speed was possible with a convenient value of pressure and flowrate. However, modern wheel speeds can be up to or exceed 100 m/s

so achieving a jet speed of 100 m/s becomes more costly; sometimes requiring the grinding system to nearly double the area it needs to occupy, in turn adding up to 40% to the capital cost of the machinery.

Chapter 3. Theory

3.1 Modelling in Grinding

This chapter presents some general grinding theory and the mathematical relationships necessary for understanding the grinding process and the work presented within this thesis.

3.1.1 Specific Grinding Energy

The evaluation of a grinding process will normally include several key factors. Specific Grinding Energy, e_c is one of the most important factors when assessing the efficiency of a grinding process. Specific grinding energy is the ratio of the machining power to the rate of material removal and is related to the efficiency of the process. A higher value than might be expected for a given process means the machining power is increasing for no extra material removal, an inefficient state.

$$e_c = \frac{P}{Q_w} = \frac{F_t\left(v_s \pm v_w\right)}{b_w a_e v_w} \tag{5}$$

Where P = Grinding power, Q_w = Material removal rate, F_t = Tangential force, v_s = Grinding wheel speed, v_w = Workpiece speed, b_w = Contact width, a_e = Actual depth of cut and ± designates either up-grinding or down-grinding for surface grinding operations; or internal or external for cylindrical grinding.

When considering this value in relation to grinding fluid effectiveness, it is worth noting that F_t, is lowered by the correct use of coolant. This is obvious when you consider the force interactions occurring during a simple surface grind. At any point there are 3 components of force resulting from the interaction of wheel on workpiece; F_t, F_n and F_a, as shown schematically in Figure 9 (F_a not shown). In a single grinding pass during a traverse process the axial force component, F_a can be treated as insignificant in comparison to the much larger normal force, F_n and tangential force, F_t components.

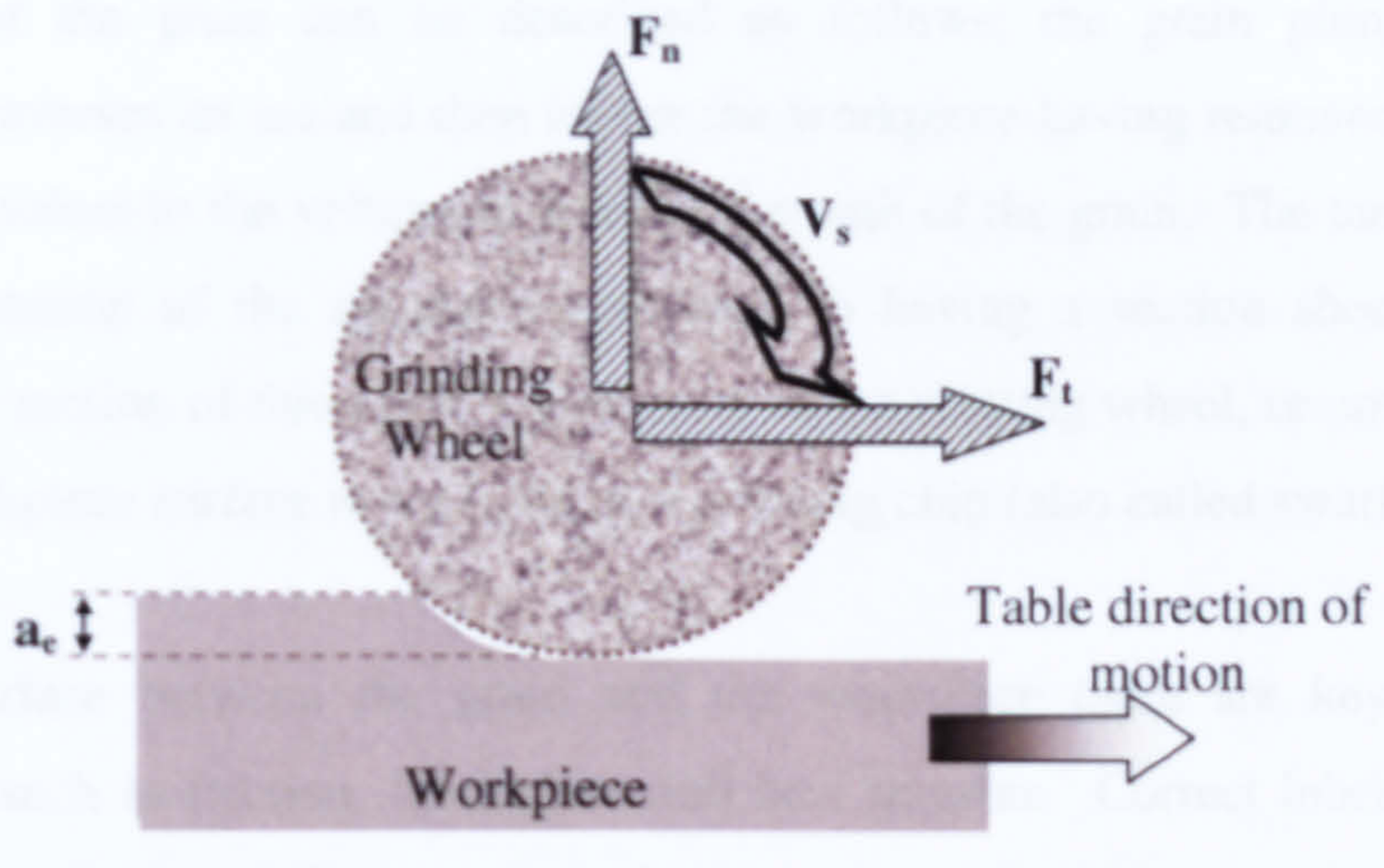

Figure 9, Grinding wheel schematic showing forces.

The normal force is larger than the tangential force. It can also be considered that the normal force is the reaction of the abrasive as the grains attempt to plunge into the workpiece. The normal force is a function of the stiffness of the machine, the wheel surface integrity and type of workpiece. It is the tangential force that drives any material removal; this is why F_t is a factor in the specific grinding energy and why the specific grinding energy is an important measure when assessing a grinding scenario. The relevance becomes clear when you consider a single grain.

Figure 10 shows the path of a single grain of an abrasive as it passes through a workpiece during the process of removing material from a planar surface. The abrasive grain is passing through the material with a speed equivalent to $v_s - v_w$.

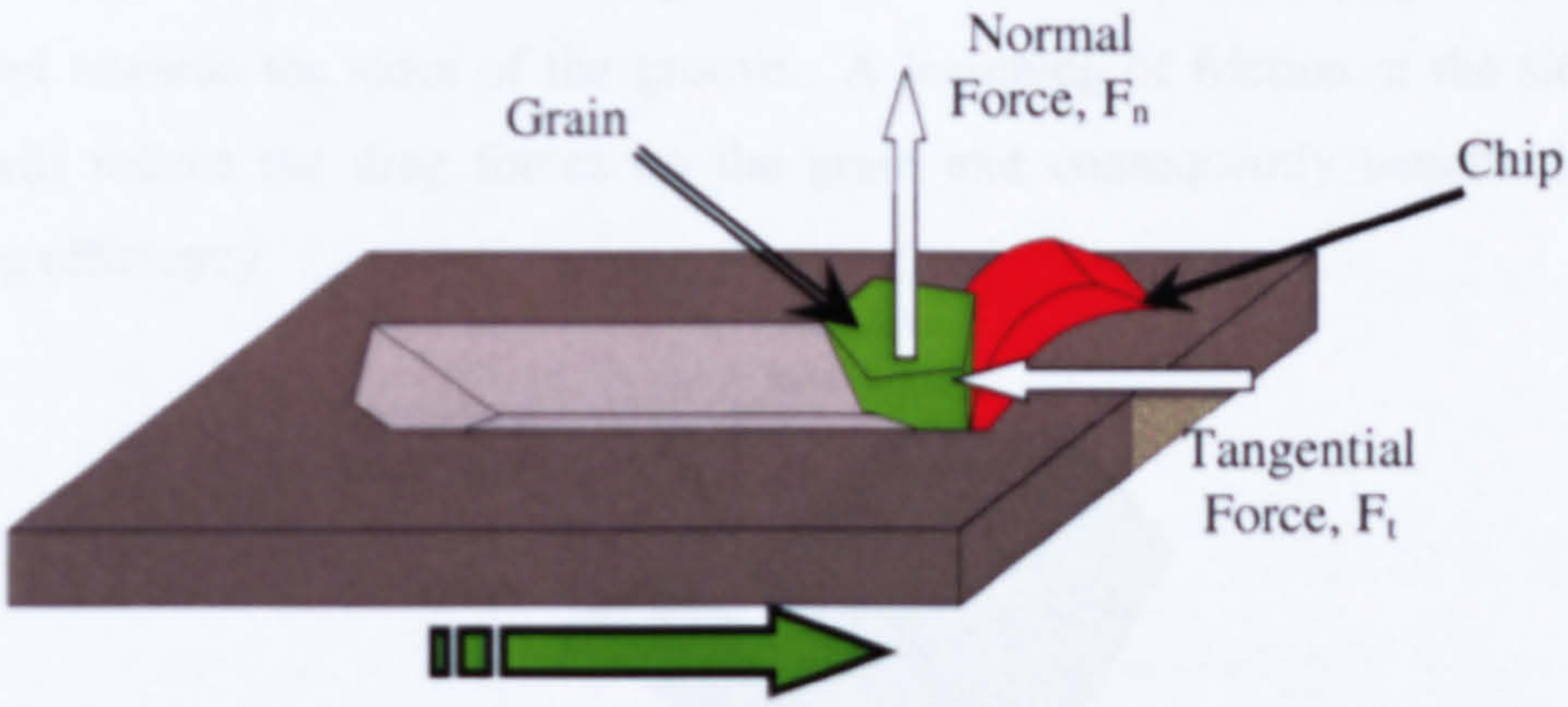

Figure 10, Single grain schematic, (N.B wheel direction of motion opposite to Figure 9.)

The path of the grain can be described as follows; the grain plunges into the workpiece, traverses an arc and then leaves the workpiece having removed a section of material equivalent to the volume in front of the path of the grain. The tangential force is a representation of the materials resistance to having a section sheared from its surface. The motion of this force is tangential to the rotating wheel, removing material from the workpiece surface in the form of a grinding chip (also called swarf).

At the interface between the grain and the workpiece there are key tribological interactions, such as friction, lubrication and heat transfer. Correct lubrication of the abrasive grain rake face will decrease both the cutting and sliding energies (Osman and Malkin, 1972) and reduce the grinding power by lowering tangential force. However, at shallow depths of cut with high wheel speeds any coolant can be a hindrance as it increases the power demands of the process (Werner and Tawakoli, 1988). A lower tangential force will in turn reduce the specific grinding energy. Marinescu *et al* (2004) explains how there are three key areas of material change where shearing of workpiece material takes place. An area of compression ahead of the negative rake angle of the chip causes the material to compact in front of the grain and be forced up the leading face of the grain. This is the first stage of chip formation. This compression induces a shear zone at the base of the forming chip, it is this and the coupled effect of the arced path of the grain as it is being pulled from the material that induces the chip to separate from the workpiece. As the grain is ploughing through the material it will carve a groove, this is due to material being removed in the form of a chip and also being displaced towards the sides of the groove. A lessening of friction at the sides of the grain will reduce the drag forces on the grain and consequently benefit the overall grinding efficiency.

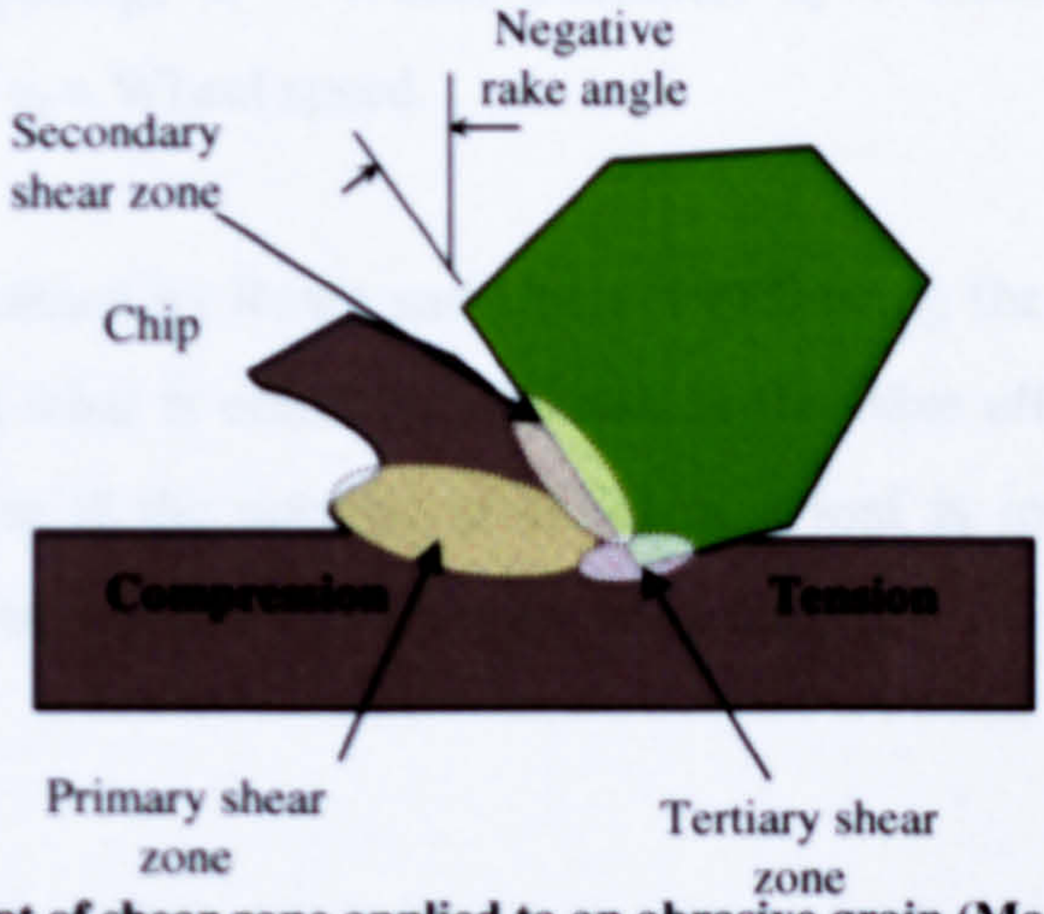

Figure 11, Concept of shear zone applied to an abrasive grain (Marinescu *et al* 2004).

3.1.2 Equivalent Chip Thickness

The Equivalent Chip Thickness, h_{eq} is considered another good general measure of overall process efficiency. This value gives the thickness of an equivalent material layer for a volumetric removal rate per unit width; it does not actually represent the thickness one might expect to measure on a machined chip. Accepting the relevance of chip thickness as an indicator of process performance it is relevant to note that it is inversely proportional to the wheel speed.

$$h_{eq} = a_e . \frac{v_w}{v_s} \tag{6}$$

When v_w = Workpiece speed, v_s = Linear wheel speed and a_e = Actual depth of cut.

The equivalent chip thickness is known to compare well with other performance characteristics, but cannot differentiate between wheel types and topographies. Grain spacing for example can have a large effect on surface finish but is not recognised by the equivalent chip thickness. Reducing the chip thickness or increasing the wheel speed is known to reduce the workpiece roughness and cutting forces and increase the wheel life. It is worth noting that Shaw (1996) found that in general, the specific energy varies exponentially with the uncut chip thickness, h_m.

$$e_c = \frac{1}{h_m^x} \tag{7}$$

Where x is a function of the volume of material removal attempted, 0.3 for stock grinding and nearly 1 for finish grinding and h_m is given by equation (8).

$$h_m = 2L . \frac{v_w}{v_s} . \sqrt{\frac{a_e}{d_s}} \tag{8}$$

Where L = Grain spacing, d_s = Wheel diameter, a_e = Actual depth of cut, v_w = Workpiece speed and v_s = Wheel speed.

This concept is explained by Rowe and Chen (1997) using the 'sliced bread analogy' and is an advance on what is commonly known as the 'size effect'. The sliced bread analogy describes how if the number of slices of a loaf is increased the amount of energy expended slicing the loaf will increase accordingly.

3.1.3 Thermal Damage Threshold

One of the most important variables when considering whether a grind has been successful is grinding zone temperature. Should the temperature get too high the part may burn. This can result in one or more of the following phenomena: visual damage, phase transformations, size errors, material softening, chemical reactions, tensile residual stresses (possibly with cracks) and will generally cause the part to be scrapped. A temperature of 300°C can be considered an approximate boundary to thermally damaging effects for grinding most steels. This will obviously vary depending on material type. A fine line exists between the positive effects of grinding, inducing compressive stresses to the surface thus pre-loading the material; and the negative effects of inducing excessive tensile stresses into the surface that occur when the large heat source is removed.

Several models have been developed for predicting the grinding zone temperature. Variations tend to be on the method of definition of the theoretical heat flux used, such as; a triangular source (Rowe *et al*, 1997), a circular arc source (Rowe *et al*, 2003) or a uniform source (Rowe *et al*, 2004). As an example of the methodology employed for these predictive models the circular arc source as described by Rowe *et al* (2003) is shown in equation (9).

$$T = \frac{1}{\pi \cdot k} \int_0^c q \cdot e^{\frac{v_w}{2\cdot\alpha}(x - l_i \cos\phi_i)} \cdot K_0 \left[\frac{v_w \cdot r_i}{2 \cdot \alpha} \right] dl_i \qquad (9)$$

Where $r_i = \sqrt{(x - l_i \cos\phi_i)^2 + (z - l_i \cos\phi_i)^2}$, K_0 is the Bessel function of second kind, order zero, α is thermal diffusivity, k is thermal conductivity, l_i is the arc length, ϕ is the angle of the coordinate under analysis and x and z represent coordinates along the circular arc

Firstly, the assumption is made that the total heat flux from the grinding contact is shared between the workpiece (subscript *w*), grinding wheel (subscript *s*), grinding fluid (subscript *f*) and the grinding chips (subscript *ch*). The heat flux, q_t is defined by the power used during the grind divided by the area of the grinding contact. This can be seen in equation (10),

$$q_t = \frac{P}{A_c} = \frac{P_w + P_s + P_f + P_{ch}}{b_c . l_c} \tag{10}$$

Where q_t = Heat energy, A_c = Contact area, l_c = Contact length and P = Power

When assuming the power that is passed through these four conduits is dissipated as heat it becomes necessary to consider the basic heat transfer mechanisms used. This equation is then developed to include convection factors to approximate the heat transfer rate at the different interfaces, as shown in equation (11),

$$q_t = q_w + q_s + q_f + q_{ch} = h_w . T_{\max} + h_s . T_{\max} + h_f . T_{\max} + h_{ch} . T_{ch} \tag{11}$$

Where T = Temperature and h = Heat transfer coefficient

This equation then uses values from Carslaw (1959), Hahn (1966), Morgan *et al* (1998), Rowe (2001) and Rowe *et al* (2003), to approximate the values of heat transfer for the workpiece, wheel, fluid and chips respectively. A value of chip temperature is also approximated at this stage. This then leads to equation (12), which defines the maximum temperature expected within the grinding zone when using a workpiece-wheel partition ratio, R_{ws} that defines the dispersion of the heat flux between the workpiece and the grinding wheel.

$$\theta_m = 0.8 \frac{R_{ws}\left(e_c - e_{cc} - e_{cf}\right) a_e}{\sqrt{(\kappa \rho c)_w}} \left(\frac{v_w}{l_e}\right)^{1/2} + \theta_a \tag{12}$$

Where e_c = total specific energy due to grinding, e_{cc} = specific energy convected by the grinding chips, e_{cf} = specific energy convected by the fluid, l_e = Real contact length and θ_a = Workpiece ambient temperature and where R_{ws} is given by

$$\frac{1}{R_{ws}} = 1 + \frac{\kappa_g}{\sqrt{(r_0 . v_s)} . \sqrt{(\kappa \rho c)_w}} \tag{13}$$

Where r_o = Wear flat contact radius, κ_g = Coefficient of thermal conductivity for the abrasive, κ = Coefficient of thermal conductivity for the workpiece, ρ = Workpiece density and c = Workpiece specific heat capacity

Ebbrell (2003) reported typical values of R_{ws} for various wheel speeds using the values of thermal conductivity reported by Morgan *et al* (1998) and Rowe *et al* (1997) for Alumina and cBN.

3.1.4 Contact Zone Length

When considering any measurement that is a function of the grinding contact zone it is necessary to analyse the geometry of the contact zone. The contact zone area is the product of the contact width, b_w and the geometric contact length, l_g. The contact width is commonly the wheel width and as such is specific to a machine setup and will remain constant unless the wheel is changed. However, the contact length is highly dependant on the type of grind being attempted, the material being ground and the grinding wheel being used.

When viewing the scaled schematic of a grind an estimate can be attempted of the expected contact length based on stiff object geometry as shown in Figure 12. However, Qi (1995) showed that the geometrical contact length is always an underestimate of the actual contact length achieved when grinding, sometimes by a factor of 3. A 'real' contact length, l_e according to Qi *et al* (1997) is dependant on the roughness of the wheel, the normal force, the depth of cut and the mechanical properties of the wheel. The deformation of both the wheel and the workpiece causes a lengthening effect of the contact zone. So when considering the length of any grinding contact zone it is important that the more realistic value of real contact length is used. This becomes apparent in the analysis of the thermal model for the calculation of grinding zone temperature (Morgan *et al*, 1998).

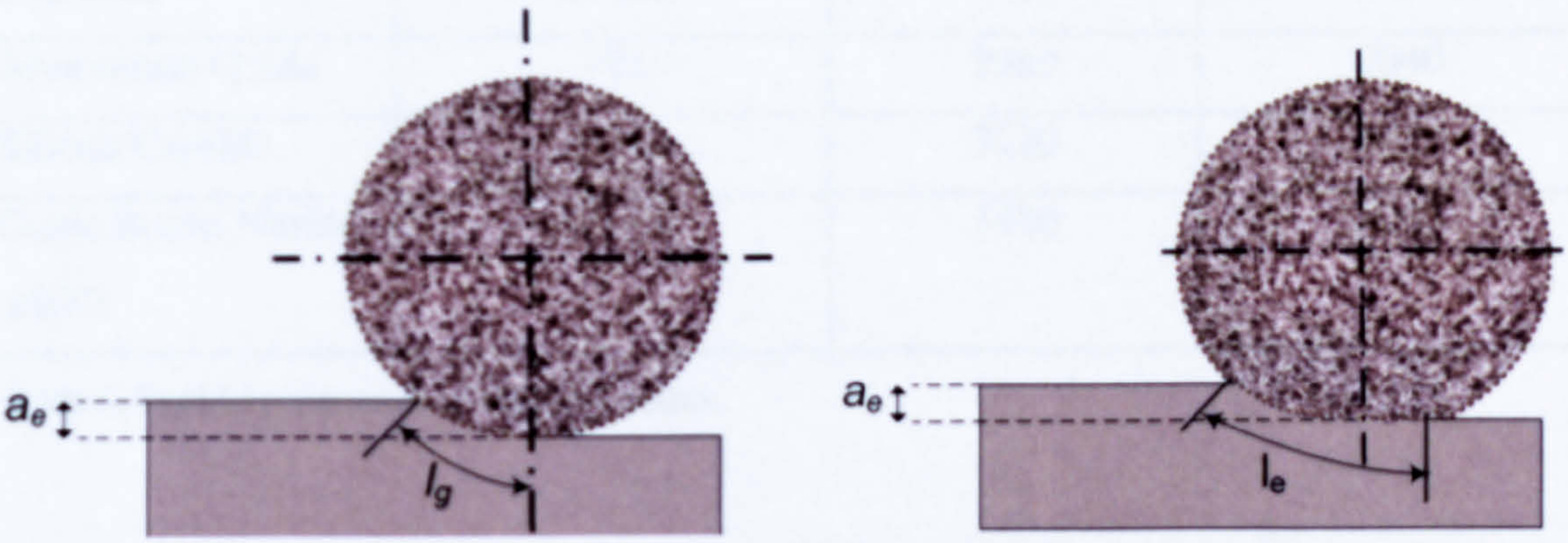

Figure 12, Geometrical contact length (left) and 'Real' contact length (right) schematic.

These considerations lead Qi to the following equations defining the real contact length based on roughness parameters, equation (14) and a second equation utilising a contact area approach, equation (15).

$$l_e = \left[R_r.8.F_n \left(K_s + K_w \right) d_s + a.d_s \right]^{0.5} \tag{14}$$

And

$$l_e = \left[R_A \cdot \left(\frac{R_p}{c} \right)^2 \cdot \left(\frac{F_n'}{H_v} \right) + a.d_s \right]^{0.5} \tag{15}$$

Where $R_r = a^*/a_o$ = Roughness Factor, a^* = The effective 'contact radius' of a rough surface defined by Greenwood and Tripp (1967) and a_o = The contact radius for smooth surfaces given by Hertz theory

3.2 Grinding Wheels

A grinding wheel is a bonded structure containing many abrasive grains. It is these grains that remove material from the workpiece. The most common abrasive is Aluminium Oxide, otherwise known as Alumina or Corundum. These Alumina grains are generally suspended in a vitrified or resinoid bond. A vitrified bond is a high temperature sintering of powdered glass, frits, clays and chemical fluxes. Grinding wheels can also be made from many other types of abrasives see Table 3. Each grinding wheel is tested and given a maximum rpm and surface speed which it should not exceed, this is a safety factor designed to stop a wheel from fracturing due to internal stresses caused by its own centrifugal force.

Abrasive type	**Hardness (GPa)**	**Density (kg/m^3)**	**Melting Point (°C)**
Diamond	56-102	3520	3700
Aluminium Oxide	~21	3980	2040
Silicon Carbide	~24	3220	2830
Cubic Boron Nitride (cBN)	42-46	3480	3200

Table 3, Typical properties of abrasive grains.

These grains can be suspended in many types of bonds, see Table 4

Bond Type	Hardness (GPa)	Elastic Modulus (GPa)
Resin	2.4	1.2
Vitrified	3.7	4.1
Metallic	2.7	5.5

Table 4, Typical properties of wheel bond types.

3.2.1 Structure

Grinding wheels can be made up of many types of bond and grain. This makes it necessary to have a specification system in place to define exactly what type of wheel is being used for an individual grinding scenario. This comes in the form of a grinding wheel standard marking system, an example of such can be found in Figure 13. The marking system can give a large amount of detail, and is helpful to both the user and manufacturer.

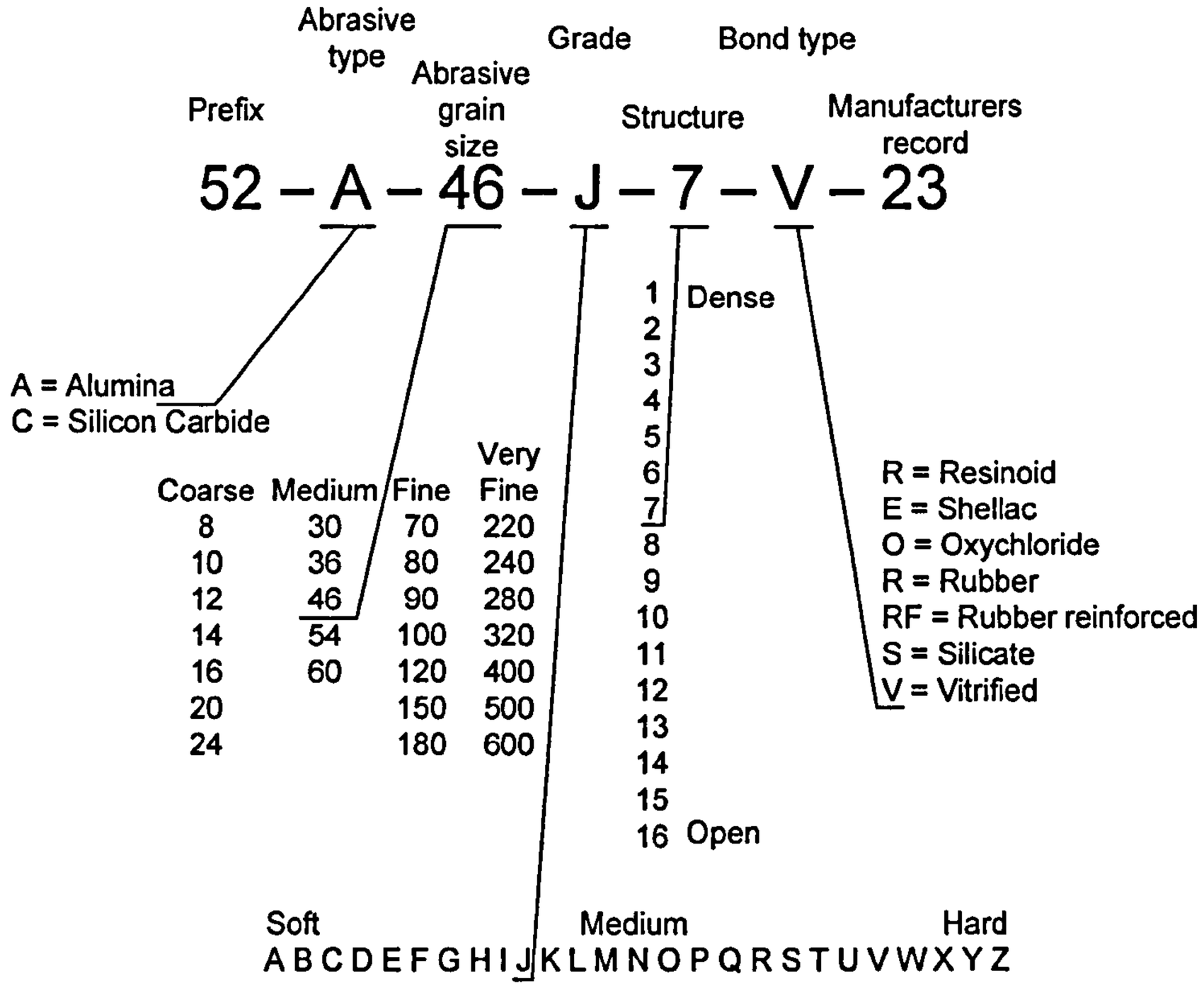

Figure 13, Example of grinding wheel standard marking system for Alumina and Silicon wheels with explanation of terms.

The grain size value relates to the sieves used to sort the grains before they are formed into a wheel. Using the 'grain size' value allows an estimation of the grain diameter to be found. The average value of grain diameter can be found using an empirical relationship such as equation (16), or by using a table of Grit Classification (Rowe *at al* p400, 2004);

$$d_g = \frac{15.2}{M}[mm] \tag{16}$$

Where M = Abrasive grain size from wheel specification (Malkin, 1989)

For example, the wheel with the specification shown in Figure 13 shows an abrasive grain size of 46. Using the tables, an abrasive grain size of 46 relates to a grain diameter of 350 μm. Using the formula in equation (16), an abrasive grain of 46 gives an average grain diameter of 330μm, as shown below.

$$d_g = \frac{15.2}{46} = 0.33mm \text{ or } 330\mu m$$

A useful visualisation of the composition of a grinding wheel structure was created by Peters, Snoeys and Decnaut (1968), illustrated in Figure 14.

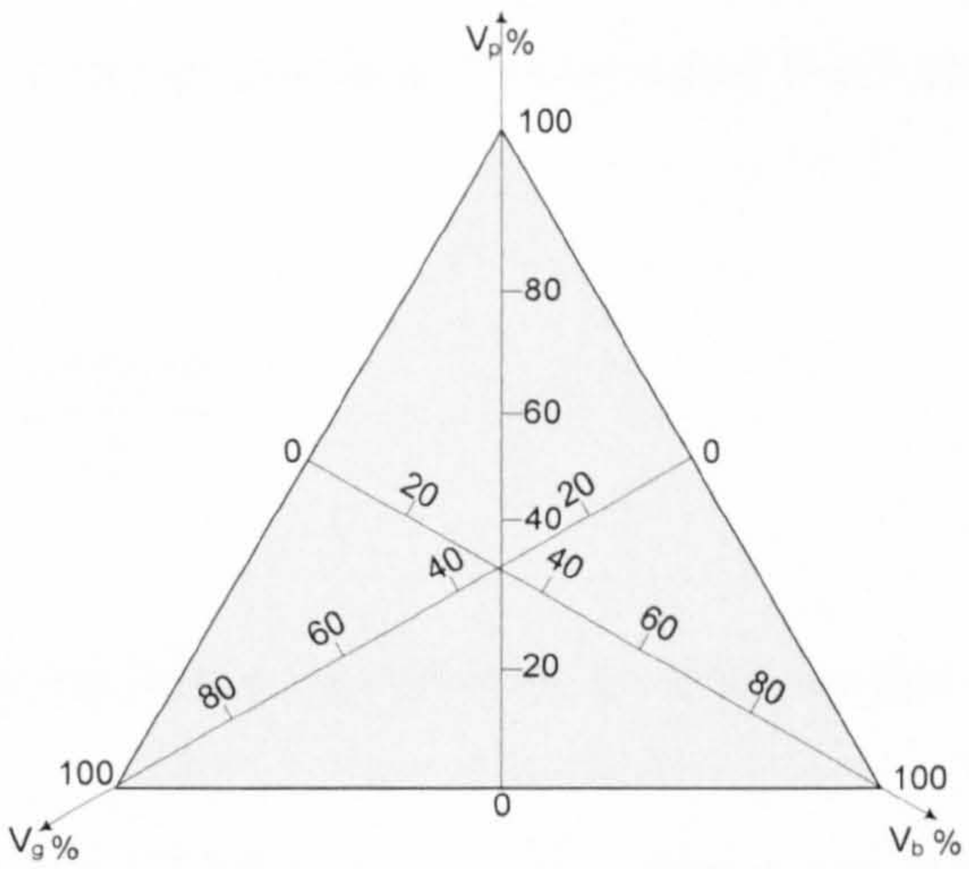

Figure 14, Grinding Wheel phase diagram, Peters, Snoeys and Decnaut (1968).

This system defines the wheel make-up based on its three constituent parts; bonding material, abrasive grain and porous space. Each apex of the triangle represents a 100 % concentration of one element, a technical impossibility. A line that connects the apex of the triangle to the mid-point of the opposing side will trace a decrease in the percentage

concentration from 100 % to zero. This means that at any point in the triangle the following statement of volume percentage is true;

$$V_g + V_b + V_p = 100 \tag{17}$$

Where V_g = Percentage volume of grain, V_b = Percentage volume of bond, V_p = Percentage volume of porosity

Another feature of this diagram is the iso-lines that represent contours of constant porosity, bond volume and grain volume. By using Figure 14 it is possible to describe the porosity of the wheel based on some predefined empirical relationships. If the structure number, S of the grinding wheel is known, equation (18) can be used to define an approximated value of bulk wheel porosity.

$$V_p(\%) = 45 + \frac{S - 2n}{1.5} \tag{18}$$

Where n is an integer correlating to the letter grade of the wheel, (for example, when the letter grade is A; n is 1, when the letter grade is B; n is 2, etc.). So for the wheel described in Figure 13, equation (18) is as follows when S = 7 and n = 10 (Grade J gives a value of 10).

$$V_p(\%) = 45 + \frac{7 - (2 \times 10)}{1.5}$$

$$V_p(\%) = 36\%$$

It can be expected that the bulk wheel porosity is ~36% for this wheel.

It is known that a porous wheel is a necessity when creep feed grinding with a shoe nozzle. It was shown by Powell that fluid penetration is dependant on bulk wheel porosity (Powell, 1979) and is more of an issue when considering use of a shoe nozzle. Powell also draws reference to the permeability of a wheel as having particular relevance to the fluid flow in his work. This value defines the volume of flow that can move within the wheel through the interstitial channels connecting the internal pores of a wheel. As previously stated, Powell found this value useful as he was expecting penetration to a depth of 10mm, thus the permeability or the ability of the wheel to

transport fluid to its interior was stated as a key factor. For work with jets of coolant from standard nozzles rather than shoe nozzles it is believed permeability will be of lesser significance in terms of useful flow. However, there will undoubtedly be some fluid forced into the wheel during any grinding process. This is shown by the commonly understood need to leave the wheel spinning after any wet grind. Further to this the permeability of the wheel is a difficult parameter to obtain, and as such is of limited use in deriving guidelines for industrial use.

3.2.2 Wheel Wear

When considering the life span of a grinding wheel the mechanisms of transient wear must be considered; the most common of these is categorised as attritious wear. This is represented in Figure 15a by a single point dressing tool performing the wear in the abrasive grain. Attritious wear in this instance is caused by the many cuts an abrasive grain performs chipping away and rounding off its leading edge. Wheel wear is best described by the material volume removal rate from the wheel, this is generally used in conjunction with the workpiece material removal rate in the form of the Grinding Ratio or G-ratio of the process.

The radial volume of material removed from the wheel is given by

$$V_s = \pi d_e \Delta r_e b_s \tag{19}$$

Where d_e = Mean diameter of wheel before and after grinding, Δr_e = Measured decrease in wheel radius.

The G-Ratio, G is given by

$$G = \frac{V_w}{V_s} \tag{20}$$

Where V_w = Volume of material removed from the workpiece = $b_w a_e l$.

The grinding ratio is a useful measure of the appropriateness of the wheel/process to the task required. A high grinding ratio (~1000) may sometimes imply the wheel is too hard for the task. A low grinding ratio (~1) means the wheel is not hard enough for the material being machined (Marinescu *et al*, 2003).

3.2.3 Dressing

During a grinding process a wheel can expect to become blunt and clogged with workpiece debris. The sharp cutting faces that are necessary to remove material from the workpiece will dull and instead of inducing ploughing and cutting will merely promote a rubbing action that does not remove material. A dull wheel will tend to have an increased wear flat area, this is a region where the wheel rubs and does not cut. Wear flats are the result of attritious wear to the grains leading edge. In this situation it has been shown that the normal and tangential forces increase significantly (Malkin, 1989). This increase of forces lowers the efficiency of the process and raises the likelihood of thermal damage. Thus the dressing process is necessary for the operator in order to refresh the wheel surface.

The effect of dulling over time (or artificially introduced by poor dressing parameters) is true of all grinding wheels and justifies the need to dress a wheel to re-introduce sharpness. The dressing process can sometimes be accompanied by a truing process. Both processes involve using a material harder than that of the wheel grain, generally diamond. The purpose of the dressing process is to produce new cutting faces on the wheel surface by cutting through the wheel. The truing process has the purpose of removing material from the wheel to prevent significant run-out of the wheel from its spindle.

Figure 15a, Attritious wear of the grain due to dressing with a single point diamond.

Figure 15b, Grain fracture due to dressing with a single point diamond

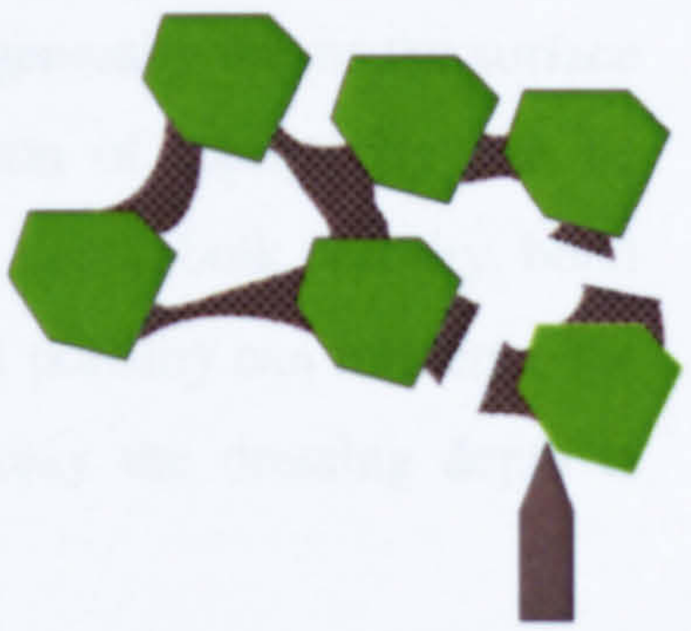

Figure 15c, Bond fracture due to dressing with a single point diamond

The dressing process takes advantage of the friable nature of a wheel. When the diamond passes through the wheel surface one of two processes can take place; grain fracture or bond fracture. Grain fracture is represented in Figure 15b and involves the grain breaking across a fracture plane induced by the dressing tool, thus exposing in the

wheel surface a new profile with a new sharp edge. Bond fracture is when the bond holding the abrasive grain fractures thus exposing a new grain or exposing a pore, displayed in Figure 15c. It has been shown that this process does not necessarily fracture the grain along the exact profile of the dressing tools helical path. Malkin and Anderson (1972) showed the size of the dressing debris could be larger than dressing depth but smaller than grain size, it was concluded that the process was two-stage. Firstly grain fracture occurs, and then once the grain has been significantly eroded the bond holding the grain in place will fracture releasing the grain.

The dressing parameters used are dressing depth, a_d and dressing federate, f_d. The dressing process is most succinctly defined by the Overlap ratio given below. This value defines how many times a single point diamond can be expected to pass through a length equivalent to its own diameter. A high overlap ratio will leave a shallower pattern in the wheel and tends to mean a closed wheel surface.

The Overlap ratio is defined below,

$$U_d = \frac{b_d}{f_d} \tag{21}$$

Where b_d = Dressing tool engagement length and f_d = Dressing feed rate.

3.2.4 Topography

When referring to the topography of a grinding wheel one generally means the surface topography on the periphery of the wheel. The definition of topography can be influenced by many factors: grit size, dressing lead, dressing depth, bulk porosity, bond type etc. Some researchers have observed that only the bulk porosity can influence the useful flow significantly and of the dressing parameters only the dressing depth is suspected to have any influence at all (Krishnan, 1995).

It is widely accepted that the porosity of the wheel can have a significant effect on process outputs. When using a creep feed process a highly porous wheel is normally advised. The effect of porosity on the surface topography of the wheel has been somewhat overlooked. Krishnan (1995) postulated that a varying surface porosity could affect the ability of the wheel to pass fluid through the grinding zone, whereas Cui (1995) seemed to show that the surface topography was barely a secondary influence. It is known that the effect of a change in the surface topography of the wheel over time

can be detrimental to the surface finish and power requirements of a process. This transient effect is overcome by dressing the wheel thereby removing swarf from the pores and exposing or creating new cutting faces. This proves the effect of dressing on surface topography and therefore the ability of the wheel to transport fluid through the grinding zone. The measurement of the small changes to topography and useful flow created by differing dressing depths of cut would be very difficult to quantify. It is likely that the effect of dressing to remove swarf and therefore re-expose pore space is the only way the dressing could affect the useful flow.

In preceding analyses of grinding wheel topography some interesting parameters have been developed. Cai (2002) presented a comprehensive study of topography for cBN grinding wheels, defining several useful parameters and their relevance to process outputs. Specifically the term Effective Volume Porosity ratio, V_{pw}, was presented as a definition of the effective volume of the pores to the volume of the wheel.

$$V_{pw} = \frac{V_p\big|_{z \geq z_i}}{V_w\big|_{z \geq z_i}} \tag{22}$$

Where V_p = Percentage volume of pores, V_w = Volume of wheel, z = Radial depth into the wheel, z_i = The active radial depth into the wheel below which the cutting edges are active.

Cai tested two internal cBN grinding wheels. One had a high porosity but small grain size, this gave an effective volume porosity ratio of 0.45. The other had a medium porosity with a large grain size giving an effective volume porosity ratio of 0.35. Testing using two external wheels both of vitrified cBN, the higher porosity wheel showed an effective volume porosity ratio of 0.5 and the lower porosity wheel showed an effective volume porosity ratio of 0.35. It was also noticed that during grinding tests the porosity volume ratio of the wheel dropped 14 % when nearing the end of the dressing cycle.

The use of this parameter is dependant on verification by manual analysis of the height of a reference plane in the grinding wheel surface. This reference plane defines the position of the workpiece when it is truly in contact with the wheel. Any grain below this reference plane would be considered not in contact with the workpiece surface and

therefore not active in the cutting process. This is a very useful parameter but is difficult to obtain, requiring analysis through a combination of optical systems and manual interpretation. The effective volume porosity ratio used an understanding developed around the value of Active Cutting Edge Density, C_a. This value gives an approximation of the amount of cutting edges that will be employed during a grinding pass. This is further developed by the understanding that the number of active cutting edges are dependant upon the dynamic effect of the wheel deflection during a cut, and hence is known as the Dynamice Cutting Edge Density, C_{dyn} and is given by.

$$C_{dyn} = C_{stat}\left(\frac{v_w}{v_s}\right)^c(\theta')^c \tag{23}$$

Where C_{stat} = Static cutting edge density, θ' = Wheel rotation angle during contact length and superscript c is a constant for a particular wheel and dressing conditions, values range from 0.4 – 0.8.

Further to this is the influence of the theory of irregular grain spacing and depth, which is also summarised by the value of dynamic cutting edge density. The values obtained by Cai (2002) are approximately 10-60 cutting edges per mm^2 for a cBN vitrified wheel with grain diameters of 90 μm. These values show that at least 90 % of the grinding contact area does not experience direct contact between the wheel and the workpiece.

3.3 Coolant Flow through the Grinding Zone

The definition of useful flow is based solely on the volume of fluid passing through the grinding contact zone. The useful flowrate is known to depend on the flowrate delivered from the nozzle but it is also dependant on other factors, such as nozzle jet speed, nozzle position and wheel speed. The purpose of this work is to advance this definition and to focus on a further adaptation of the term useful flow.

It is at this point the author would choose to add some clarifications to the use of the term 'useful flow'. The term useful has the following meanings in the English language.

> **Useful,** *Adjective* 1, able to be used for a practical purpose or in several ways. 2, informal very able or competent (Oxford English Dictionary, 2007)

When using this word it is necessary to define 'usefulness'. For this investigation usefulness could be assumed when any flow that passes through the grinding zone performs the functions described in previous chapters, such as reducing grinding wheel wear, reducing forces between the contacting surfaces, providing cooling and improving process efficiency. Previously useful flow has been defined as being fluid that has passed through the grinding contact zone only and although the author would not dispute this definition the application of 'useful' in this context makes several assumptions. Most of these characteristics are assessed using standard grinding output parameters, so in order to term any flow passing through the contact zone as 'useful' it must be defined as such by the use of these established grinding assessment criteria. Since only flowrate that passes through the grinding contact zone can provide lubrication or cooling benefits, the term useful flow in the context of this thesis is restricted to the existing definition of flow through the grinding contact. However, the author proposes that useful flow can be further related to several definable contributory concepts. The first is termed the 'Convenient Flow' and refers to the amount of fluid which will fill any gaps between the wheel/grains and workpiece due solely to surface geometry. This definition allows a close comparison to the mechanics of a displacement style pump. Therefore convenient flow is defined as stated below.

> *Convenient flow is the flow that passes through the grinding zone based solely on the topography of the interface.*

What can be termed convenient will be a function of surface porosity, wheel speed and wheel width only, as defined by Rowe in equation (24). It could be considered for the convenient flow that beyond a single grain depth the wheel is an impervious solid. The ability to fill the pores may not be a physically possibility, it may be true that only a percentage of the available space can be utilised. It may also be true for more porous wheels that fluid penetrates deeper than the surface pores.

The secondary concept incorporates any and all unknown or intangible factors. These could include pressurised flow, permeated flow or any thermally induced physical state changes. These parameters are difficult if not impossible to manually assess during a grinding trial and have in the past been subject to either offline analysis or simplified

predictive modelling. This clarification surrounding useful flow leads to the following definition proposed by the author.

> *Useful flow is defined as the amount of fluid that passes through the grinding contact zone.*

The useful flowrate is always less than the nozzle flowrate, and can be represented as a percentage of supply flowrate and termed the percentage useful flow. Depending on process and supply conditions the useful flow could be a range of values; a useful flowrate of 10 l/min may perform as effectively to the part specification as a useful flowrate of 20 l/min. In this scenario it would be beneficial to the process as a whole to use the least amount of coolant. With this in mind a further definition is necessary. This advancement of the definition considers that there will be a maximum value of useful flowrate that may be achieved but which may be excessively costly in terms of plant specification and power consumption. This value may provide the most benefit and the highest value of flowrate through the grinding zone but at too high a cost. However, as no manufacturing process can be considered independent of its overheads there will also be a value that is capable of fulfilling the process requirements whilst minimising plant and power costs. This has been termed the Optimal Useful flow and refers to the most efficient value of useful flow; the definition is given below,

> *The optimal useful flow is the minimum amount of fluid that passes through the grinding contact zone functioning as an effective lubricant and providing sufficient local cooling*

The optimal useful flow is the true target of any grinding operation. It is this value of optimal useful flow that will allow the grinding process to proceed at its highest efficiently. It is expected that optimisation of applied flow will have a three-fold benefit.

- Reducing the cost to the manufacturer.
- Lessening the environmental impact of the process waste.
- Delivering process improvements.

Using the optimal useful flow will mean there will be no thermal damage, size holding will be achieved, tolerances will be held and efficient power usage will be possible. It will also have minimised the amount of fluid required to do the job thereby allowing cost savings in fluid usage, purchasing and disposal. A truly optimised value of useful flow would require complete knowledge of the requirements of each individual process. Thus optimisation as a term is difficult to utilise when discussing a grinding process in general terms.

It is important to quantify a term that has relevance to the processes being analysed within this thesis. Although the optimised useful flow value is the overall goal of any process setup it is not something that is a worthwhile target within this work. Any guidance in terms of an optimised useful flowrate will be inherently very process/system specific and thus non-transferable. As the optimised useful flow is a modification of the idea of useful flow we also now choose to add a further modification. So far we have described the optimal useful flow as being the ideal target to aim for; achievable and identifiable only for individual processes. More than likely this is not the case and in this situation we define a further parameter as the achievable useful flow.

The achievable useful flowrate can be considered a target value, one that a user may hope to realistically achieve without the meticulous analysis required of a truly optimised useful flow. It can be said that this value takes no account of needs and defines only the possible useful flow a setup may achieve without explicit knowledge of process requirements. The achievable useful flow is a more realistic target and will in most cases be a percentage of the convenient flow that takes account of known limitations found during exploratory experiments.

3.3.1 Current Theory

Rowe *et al* (2004) estimated useful flow by two methods, both based on the assumption of making a comparison to average thickness of the fluid layer. The governing equation containing the equivalent fluid layer is shown in equation (24).

$$\dot{Q}_u = h_{uf} \times v_s \times b_s \tag{24}$$

Where h_{wf} = Equivalent fluid layer, v_s = Wheel speed, b_s = Wheel width (when $b_s \geq b_w$ workpiece width) and $\dot{Q}_u$ = Useful volumetric flowrate

Although simple in nature equation (24) remains the basis of all models to date, with advances existing in the estimation of the equivalent fluid layer and the interpretation of the speed term. The average thickness of the fluid layer was defined by Rowe in two separate ways, the first method is topographical. This method defines a porosity value and the surface pore depth of the wheel to give the thickness of the fluid layer. The thickness of the fluid layer in equation (25), is based on the pores of the surface of the wheel being filled with fluid. Rowe assumes fluid carried through the grinding contact by the pores of the wheel is considered to be the maximum useful flow that can be achieved without further pressurising fluid beyond the surface of the wheel. In light of the terms just introduced this method can be considered to give a value of maximum convenient flowrate. This definition benefits from its simplicity in implementation, however the thickness of the fluid layer is very difficult to predict and will be dependant on many other variables. The surface pore depth is an unknown and has no method of prediction that does not involve a value acquired from preceding direct measurement. Hence up to this time the value of h_{pores} has been compared to the average grain diameter, d_g and some other factors.

$$h_{uf} = \phi \times h_{pores} \tag{25}$$

Where h_{pores} = Mean depth of pores and ϕ = Bulk wheel porosity.

The second approach explored by Rowe *et al* (2004) was to define how thick a fluid layer would need to be for enough heat conduction to take place to make the temperature at the surface of the fluid boundary layer ambient. This thickness layer was termed the thermal boundary layer and is given in equation (26). This equation assumes a solid stationary layer of fluid exhibiting constant heat transfer due to its thermal diffusivity, thus it can be defined using standard material thermal properties.

$$h_{uf} = 2 \times \sqrt{\frac{\alpha . l_c}{v_s}} \tag{26}$$

Where α = Thermal diffusivity = $\frac{k}{\rho c_p}$, k = Thermal conductivity, c_p = Specific heat capacity, ρ = Density and l_c = Real contact length.

Gviniashvili *et al* (2004) used an equation that is based on the conservation of momentum equation. Equation (27) shows the power required to cause a rate of change of fluid momentum of the grinding fluid through the contact zone related to the delivery nozzle parameters. Equation (27) shows the volumetric useful flowrate in relation to the spindle power, wheel speed, jet speed, a frictional power loss coefficient and a jet speed loss coefficient.

$$\dot{Q}_u = \frac{1}{\rho_f}\left(\frac{K_f \times P_f}{v_s^{\,2} - \left(K_j \times v_j\right) v_s}\right) \tag{27}$$

Where P_f= Spindle power due to fluid, v_j = Jet speed, K_j = Jet speed loss coefficient and K_f = Spindle power loss coefficient.

Gviniashvili's (2003) second approach is based on the conservation of energy equations and is shown in Equation (28). This is a derivation relating the kinetic energy of the flow from the jet to the kinetic energy of the useful flowrate passing through the contact zone plus the pressure energy deriving from the rejected flowrate and other losses. The pressure energy in the contact zone is a function of the useful flow and yields the contact pressure. The values of K_j, K_f, K_g and p_c are all determined experimentally.

$$\dot{Q}_u = \frac{\dot{m}_j}{\rho_f}\left(\frac{\rho_f \left(K_g \times v_s\right)^2 - 2p_c}{\left(\rho_f \times v_s^{\,2}\right) - 2p_c}\right) \tag{28}$$

Where ρ_f = Density of grinding fluid, p_c = Contact pressure and K_g = Fluid velocity loss coefficient.

Gviniashvili's use of experimentally determined parameters makes use and verification of the validity of the model very difficult. With four experimental parameters existing within a single definition of the useful flow the accuracy and robustness of the equation to predict useful flowrates is questionable. However the use of momentum equations to define the ability to penetrate the air barrier proves an interesting step and is an approach that has proved useful to authors in the past.

Metzger (1986) chose a different approach in defining a minimum required flowrate $\dot{Q}_r$, that is then related to the value of useful flow. This minimum flowrate is a target to

aim for governed by the change in spindle power during a grind. This power difference is assumed to relate the contact friction between the wheel and the workpiece, in turn this friction becomes heat and has to be removed by the coolant. Thus the minimum flowrate is the smallest flowrate that could remove the friction-generated heat from the contact zone. Metzger's equation is shown equation (29). Metzger's equation is an interesting aside in the analysis of useful flow, giving a target that should be achieved with no regard as to how this may be done. The use of a target based on a predetermined value of spindle power presumably in dry conditions seems limiting.

$$\dot{Q}_t = \frac{60 \times P_s}{4.184 \times C \times \rho \times \eta \times \Delta\theta} \tag{29}$$

Where P_s = Grinding power, C = Specific heat capacity of the fluid, ρ = Fluid density, η = Nozzle efficiency, $\Delta\theta$ = Friction generated temperature rise.

The next approach presented is by Cui (1995). This method assumes the flowrate is governed by the topography and the pressure gradient through the contact zone. A simplified version assuming a linear speed gradient is presented in equation (30). It can be seen that equation (30) is equivalent to the Couette flow between two parallel plates that have a relative speed v_s and separation h. There is a more complex version that equates a non-linear pressure gradient between the wheel and the workpiece seen in equation (31).

$$\dot{Q}_u = \bar{h} \times b_s \times \frac{1}{2} v_s \tag{30}$$

Where $\bar{h}$ = Mesh parameter (grit size in mm)

$$\dot{Q}_u = b\bar{h} \times \frac{1}{h} \int_0^{\bar{h}} v_s \frac{y}{\bar{h}} + \frac{\bar{h}^2}{2\mu} \frac{dp}{dx} \left[\left(\frac{y}{\bar{h}} \right)^2 - \frac{y}{\bar{h}} \right] dy \tag{31}$$

Where μ = Dynamic Viscosity, p = Pressure and y = Position across the grinding zone.

Cui also defined a value called relative ram pressure that can be used to describe a constant pressure value across the grinding contact zone inlet area. This is shown in equation (32);

$$P_{RR} = \frac{1}{2} \rho v^2 \tag{32}$$

When ρ = density and v = fluid speed.

The inclusion of pressure as a key part of the analysis is a valuable progression in the discussion of useful flow. However, merely using it to define variations in speed across the contact thickness seems not to be confronting the main effect a pressure build up would have. A significant increase in pressure within the contact zone could be expected to have two key consequences; the first would be to increase the pressure required of the fluid to enter the contact zone. The second impact would be in forcing fluid into a porous wheel. Only with a completely non-porous wheel will there be no radial fluid penetration into the wheel. An assumption of no porosity seems to be counter-intuitive, at the very least an approximation based on expected penetration depth should be used or even a factor allowing for some penetration. Cui's use of a ram pressure allows a degree of flexibility in the definition of the boundary conditions one might associate with a volume analysis of the contact zone. A ram pressure value is a plausible means of assessing the efficacy of nozzle positioning and type. This may however need some provisos attaching due to the losses a free-stream jet will have between the nozzle outlet and the grinding inlet zone. A linear ram pressure profile across the contact zone is an elegant way of representing the inlet but would be inherently difficult to replicate in real-life.

Cui also ventured a methodology similar to Metzger in attempting to predict the requirement of a flowrate based on knowing the amount of heat energy generated by the grinding wheel spindle. Knowing this generated energy level allows a prediction of the required volume of fluid necessary to dissipate this energy. This was achieved by constructing a rig that measured the fluid temperature directly before and after passing through the contact zone. Cui predicts the amount of coolant a process will require using equation (33). This equation defines the volume of fluid required based solely on the term Q_c, which is the amount of fluid required for convection of the generated heat energy.

$$Q_c = \frac{16.2\left(\frac{\dot{W}_m}{\Delta T}\right)^{1.94}}{1.5^{1.44\ln\frac{v_s}{32.2}}} \tag{33}$$

Where $\dot{W}_m$=Spindle power, ΔT = Change in fluid temperature.

Then using a relationship taken from external cylindrical plunge grinding the useful flowrate is predicted using equation (34) based on a value of corrected delivery flowrate, Q_d. The corrected delivery flowrate value is a summation of the needs of the system including the convection and various other factors.

$$Q_u = 0.26 Q_d^{0.58} \tag{34}$$

This relationship was approximated from Cui's results and no attempt was made to robustly verify the validity of the equation. This method is found to have limited scope for execution.

Finally the work of Chang (1994) is addressed. Chang used an analytical approach to attempt to predict various grinding performance parameters. The method for calculating useful flow involved taking a control volume D-C-G-H, and balancing the forces the fluid experiences across it. The control volume, shown in Figure 16, defines an area equal to an internal section of the wheel, with no distinction made between the wheel surface and the wheel internal volume. It is a reasonable assumption that there will be a distinction between the method of fluid transport at the surface of the wheel and the method of fluid transport inside the wheel. Chang goes into great detail concerning the forces acting on the control volume, defining the fluid pressure force at the inlet (side H-C), the permeability force within the wheel, the centripetal force required by the fluid for the rotational motion of the wheel and the pressure force the fluid feels from the geometry of the contact zone (side D-C). Chang also brings in further advances in the use of a modified Reynolds equation to equate pressure to the determination of fluid penetration into the wheel.

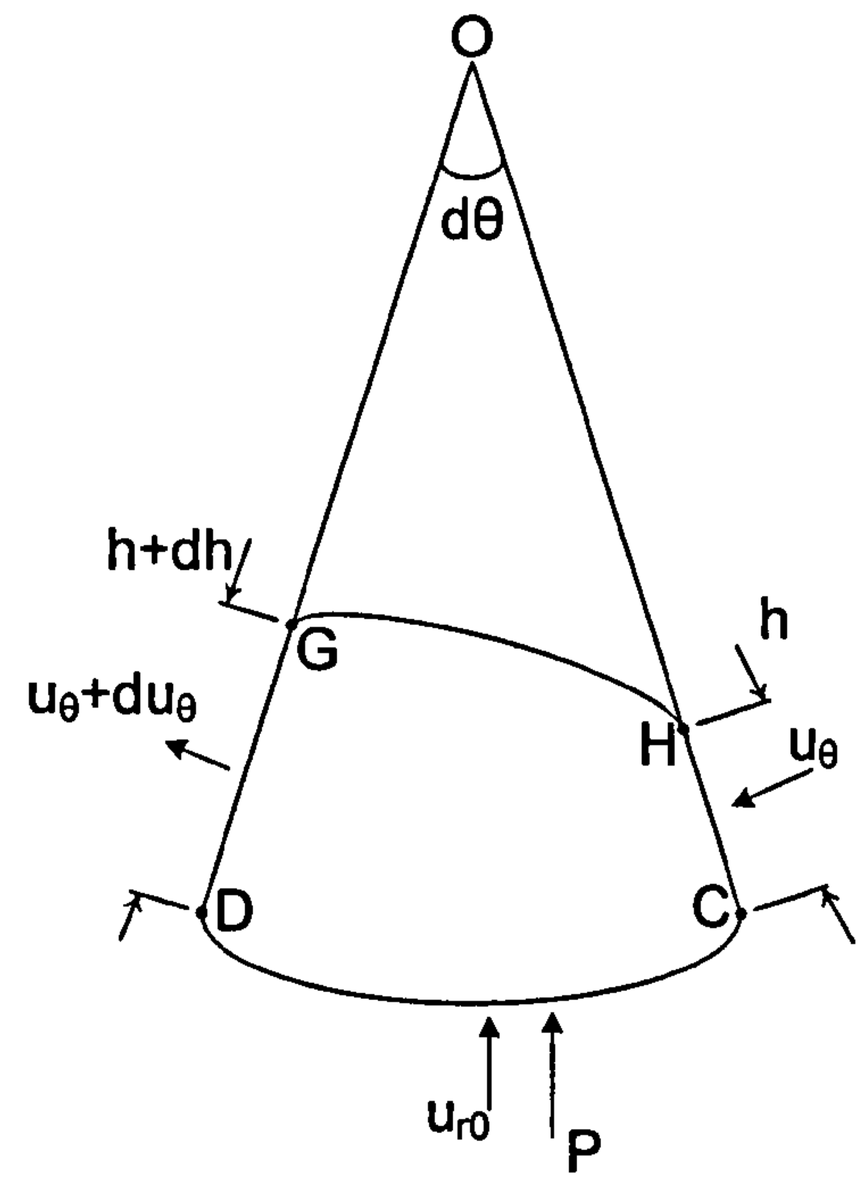

Figure 16, Diagram of the control volume used by Chang (1994).

At the crux of his work Chang utilises the concept of permeability. Permeability can be considered a measure of the ability of a material to transmit fluid. Chang's work uses equations that assume the porosity within a grinding wheel to be both uniform and independent of orientation. Chang draws on the idea of wheel permeability as being a major factor controlling the volume of useful fluid flow. It is postulated that the permeability becomes important when the wheel is of a vitrified composition or is highly porous. If the permeability is a controlling factor and no distinction is drawn between the internal fluid flow and surface flow then the surface porosity will need to be similar to the bulk wheel porosity.

Defined within the work is the penetration depth of the fluid into the wheel, there is however no distinction drawn between the fluid penetration into the wheel and the fluid that has been 'used' either for conduction or lubrication in the grinding contact zone. It is self-evident that for a contact length measured in millimetres any fluid penetrating 10mm into the wheel, as can be achieved with a shoe nozzle, will have no positive effect on the specifics of the grinding zone. Although the governing equation is similar in nature to the definition used by Rowe in equation (24) much complexity exists within the concept of permeability. Due to the use of permeability, the terms defining the fluid speed and the fluid layer thickness require further specific definition. At its most simplistic level Chang's useful flow predictive model can be seen in equation (35).

$$\dot{Q}_u = h \times b_s \times \phi \times u_\theta \tag{35}$$

Where h= Depth of fluid penetration into the wheel, u_θ= Tangential fluid velocity through porous media and $\dot{Q}_u$ = Useful volumetric flowrate.

This equation can only be solved when a further three equations (36), (37) and (38) are solved simultaneously using a set of boundary conditions that describe the following initial form.

1. At the inlet the tangential velocity of the fluid through the porous media is zero.

   $$\text{At } \theta_0, u_\theta = 0$$

2. The variation of the depth of fluid penetration is linear and governed by a function of the angle of interest and the wheel radius.

   $$dh/d\theta = \cot\theta_0 R$$

3. The pressure at the inlet is given by a ram pressure that is governed by the workpiece speed, nozzle jet speed and fluid density.

   $$P = P_0 = \rho(v_0 + V_w)^2/2$$

4. That the change in pressure across the grinding zone is zero.

   $$\frac{dP}{dx} = 0$$

The following two equations, equation (36) and equation (37), relate the flow of momentum across the boundaries of the control volume, shown in Figure 16, in the tangential direction and the radial direction respectively. Equation (38) is a modification of the Reynolds equation for lubrication for a two dimensional analysis and accounting for the permeability of the grinding wheel.

$$u_\theta \frac{du_\theta}{d\theta} - \frac{\mu R\phi}{k_\theta \rho}(V_s - u_\theta) = 0 \tag{36}$$

$$\frac{1}{2}\frac{u_\theta^2 h}{R}\frac{d^2h}{d\theta^2} - \frac{h^2}{R}\left(\frac{du_\theta}{d\theta}\right)^2 + \frac{2u_\theta h}{R}\frac{du_\theta}{d\theta}\frac{dh}{d\theta} + \frac{1}{2}\left(\frac{1}{k_r} - \frac{1}{k_\theta}\right)\frac{\mu h^2\phi}{\rho}\frac{du_\theta}{d\theta} + \frac{1}{2}\frac{\mu\phi u_\theta h}{k_r\rho}\frac{dh}{d\theta} + \frac{1}{2}\frac{\mu h^2\phi}{\rho}(V_s - u_\theta)\frac{d}{d\theta}\left(\frac{1}{k_\theta}\right) + u_\theta^2 h - \frac{PR}{\rho} = 0 \tag{37}$$

$$\frac{d}{dx}\left(H^3\frac{dp}{dx}\right)=6\mu(V_s+V_w)\frac{dH}{dx}+\frac{24k_r}{\phi}\left(\frac{P}{h}-\frac{\rho u_\theta^2}{R}\right) \tag{38}$$

Where b_s = Wheel width, ϕ = Porosity of wheel, k_r = Radial permeability, k_θ = Tangential permeability, R = Grinding wheel radius, θ = Angular position, v_s = Peripheral velocity of porous wheel, v_w = Speed of workpiece, h = Depth of fluid penetration into the wheel, H = Hydrodynamic film thickness, μ = Dynamic viscosity, ρ = Fluid density and P = Hydrodynamic pressure (see Figure 16).

The need for such complex equations limits the applicability of this model and prevents solutions being found without major simplifying assumptions. Although it is undeniably thorough, accounting for so many variables introduces a level of complication that could be avoidable by eliminating the secondary effect variables through preliminary testing.

The use of theory so far in regards to useful flowrate prediction has been somewhat varied and confused. This has manifested itself in either complex equations that are difficult to replicate and therefore verify; or simplifications of what can be considered essential parts of the useful flow analysis. The only accessible and verifiable equations are what are termed within this document the convenient flow analyses. Predictions based on topographies should be easily transferable between processes, independent of process type, wheel type or other physical limitations. It should also be possible to compare experimental values of measured useful flowrate directly with predictions of convenient flowrate.

The experimental nature of this project led the author to favour a more practical and exploitable way of defining the useful flow theoretically. As such equation (24) has been preferred for adaptation from the results of this work. This equation was deemed the most likely to allow the use of commonly held input parameters to predict a value of useful flowrate. The practical nature of the term h_{uf} has also been deemed important to the experimental analysis of useful flowrate.

Chapter 4. Equipment

4.1 Introduction

During the course of the testing several pieces of equipment were common to many of the testing stages. Therefore a section has been devoted to concise description of the equipment used throughout the preliminary and main stage testing. The equipment used for the tests can be subdivided into the grinding trials equipment and the topography testing equipment. After these sections the equipment integral to all the tests or of minor significance is described as the ancillary equipment.

4.2 Grinding Trials

Below is described all the equipment required for the grinding trials. This includes the grinding machines, coolant supply systems, data acquisition system and all sensing equipment.

4.2.1 Grinding Machines

Two grinding machines were used for the testing conducted throughout this project. All developmental testing was conducted on an Abwood Series 5020 grinding machines described in detail below. The Abwood grinding machine allowed complete access to all parts of the system, giving the flexibility required when developing the useful flow collector. The main testing was conducted on a Jones and Shipman Dominator surface grinding machine. This machine tool had full CNC control of all axes leading to a far greater accuracy in the control of key variables. The Dominator was not available from the start of this project so was not used for the development stages. This was in some ways fortuitous as the Dominator did not allow the necessary access due to it being a closed-guard system.

4.2.1.1 Abwood Series 5020 Surface Grinding Machine

Developmental experimentation was carried out on the Abwood Series 5020 grinding machine as it was the most accessible and flexible of grinding machines available. The Abwood was capable of conventional wheel speeds and had analogue pneumatic controls for the automatic traverse cycles, this restricted accuracy in programmed traverse speed. The power of the spindle motor power was 2.2 kW at a continuous rate, this allowed a maximum speed of approximately 50 m/s using a 190 mm diameter wheel running at 5000 rpm. The machine specification can be seen in Table 5. The Darenth coolant unit was attached to the Abwood so high fluid pressures could be applied to the worktable area.

Parameter	Value
Spindle motor power	2.2 kW continuous power 8 kW instantaneous power
Spindle speed	Variable up to 6000 rpm
Longitudinal travel, via worktable - Resolution	530 mm 10 µm
Cross traverse of head, via headstock - Resolution	260 mm 10 µm
Vertical traverse of head, via head stock - Resolution	350 mm 1µm
Maximum wheel size	400 mm x 25 mm
Automatic feed	Pneumatic control in X, Y and Z axis.
Other information	Cantilever headstock, mechanical magnetic chuck,

Table 5, Specification for Abwood Series 5020 Surface grinding machine.

The wheel speed was controlled through an AC servo motor fitted during a previous experiment giving variable control up to 6000 rpm. An accuracy of approximately 20 rpm was achievable when programming in set-up mode using the analogue controller. During a grind cycle a 'constant power' feedback system meant the wheel speed could be maintained within an accuracy of approximately ±50 rpm, this was verified before full trials began using a portable tachometer attached to the wheel spindle.

4.2.1.2 Jones and Shipman Dominator 624 Surface Grinding Machine

The main body of the testing was carried out on a newly acquired Jones and Shipman 'Dominator' 624 surface-grinding machine. The Dominator was equipped with full CNC control using the 'Easy' software package, this allowed fully automated grinding and dressing. Testing at higher speed ranges was possible as the machine came equipped with a high-speed spindle and an upgraded motor. The machine also came fitted with a custom built acoustic emission system courtesy of Balance Systems, Italy. This extra package allowed semi-automated wheel balancing, along with acoustic emission measurement from the wheel and the worktable, and also spindle power readings. The Darenth coolant unit was attached to the Dominator so high fluid

pressures could be applied to the machine tool coolant delivery system. The specification of the Dominator can be seen in Table 6.

Parameter	**Value**
Spindle motor power	11 kW continuous power
Spindle speed	Variable up to 4386 rpm
Longitudinal travel, via worktable Resolution Max traverse speed	640 mm 0.1 μm 24 m/min
Cross traverse of head, via headstock Resolution Max traverse speed	200 mm 0.1μm 6 m/min
Vertical traverse of head, via head stock Resolution Max traverse speed	440 mm 1μm 6 m/min
Maximum wheel size	300 mm x 70 mm (76.2 mm bore)
Automatic feed	Digital servo motor driven ball-screw mechanism on all axis.
Other information	Full load electrical power consumption 24 kVA, mechanical magnetic chuck.

Table 6, Specification for Dominator 624 surface grinding machine.

Full CNC control of wheel speed was possible with secondary readings from the attached acoustic emission system. The Easy software allows automation of most simple processes, however the single pass required for the main test had to be simulated in a creep feed cycle.

4.2.2 Integrated Sensors

The sensor array courtesy of Balance Systems, Italy, was integrated into the Dominator and used to monitor the acoustic emission and the spindle power of the grinding machine. As part of the custom array several other sensors were available but were not used directly for measurement. All acoustic emission and power systems were integrated into the hardware of the Dominator controller and as such had been pre-

calibrated at the factory. However for the power and acoustic emission readings to be utilised successfully an analogue output was configured on the control board. The Balance Systems equipment came with 9-pin analogue output that can be used to feed continuous instantaneous data into a Data Acquisition System. The control board allowed two outputs, in this case attached to the power and the worktable acoustic emissions. Both of these sensors were configured at the control board using a digital volt meter, this allowed verification of the analogue readings. The acoustic emission is a relative value and as such merely required that performance be checked and confirmed. The power meter could be configured to output a series of readings depending on the accuracy required and the range necessary.

4.2.2.1 Acoustic Emission system

There were four sensors attached through the Balance Systems controller, only two of which were relevant to testing during this project. A power sensor was attached to each phase of the three-phases of the motor powering the spindle. With these direct power measurements values of grinding force can be calculated. An acoustic emission sensor was attached to the worktable to obtain readings from the workpiece. The acoustic emission from the worktable sensor afforded the author the ability to monitor the grinding positions during a grinding pass.

4.2.2.2 Power Meter

A measure of power from the grinding wheel motor spindle was possible using the Balance Systems sensors integrated to the Dominator machine. The balance systems sensors were fitted to all three phases of the motor thereby obtaining an instantaneous value of voltage on all three phases. These readings are then averaged using a Root Mean Square equation, thus getting an accurate running value of the power required by the grinding wheel. The value of grinding power is calculated by obtaining a value of no-load power for when the wheel is spinning and the coolant is on and then subtracting the total power value obtained during the test.

4.2.3 Coolant Supply Systems

In order to conduct testing at high pressure a high pressure coolant supply system was used, this is described further below. This system was attached using high pressure hydraulic hose to the grinding machine. For both machines a flowmeter was fitted as close to the nozzle as physically possible in order to accurately measure the flowrate of

the coolant and thus obtain the jet speed using simple continuity equations. A system for limited nozzle positioning was available for connecting the coolant supply system to each grinding machine.

4.2.3.1 Arboga Darenth High Pressure Coolant System

The coolant system used was an Arboga Darenth type 2210/3057. It supplied coolant up to 35 bar at a flowrate of up to 100 l/min. The Darenth is equipped with two filtering mechanisms; a cartridge type and a centrifuge type. Control of the Darenth was carried out using a digital display of the motor power; pressure readings were available at the outlet of the pump and at the outlet of the system. Further flow control is possible via a restriction valve at the outlet of the pump. The Darenth unit can be seen in Appendix C.

4.2.3.2 Flowmeter

A flowmeter was installed in the pipe system connecting the Darenth coolant supply unit to the grinding machine in order to accurately gauge the flowrate coming from the supply pump. An Omega FTB-791L unit was used which allowed accuracy of ±0.05 l/min using an inline flow-turbine system incorporating a digital display. A flowmeter was also present at the Darenth outlet pipe, however this was an analogue unit and allowed a reading accuracy of only ±0.5 l/min. Field calibration of the Omega unit was possible in order to calibrate for different fluids. The unit was supplied pre-calibrated for water at ambient temperatures and testing proved that this was an accurate calibration for use with the Hysol XF emulsion in a ~90% water mix. The FTB-791L unit can be seen in Figure 17.

Figure 17, Flowmeter showing straight lead inlet section.

The flowmeter selected had a working range of 1.9-37.9 l/min. It could operate in temperatures of -10 up to 60°C and was rated up to a pressure of 103 bar. The unit was also capable of having the digital display located remotely from the main turbine unit. This allowed the unit to be located as close to the inlet of the Dominator coolant system

as possible. It was recommended that there be a straight pipe of at least 20 cm in length before the inlet to the flowmeter, this recommendation is based around the flowmeter working when it is measuring a fully developed flow. This was accommodated as much as our unique space requirements would allow.

The flowmeter was required to measure the flow of a two-phase (dirty) liquid. This was outside of its standard operating conditions. With this in mind the system was calibrated to ensure accuracy and was regularly stripped apart and cleaned to ensure any particulate build up would not affect the readings. Even with the three filtering systems employed to clean the fluid, removing all the debris that had been carried from the grinding zone could not be guaranteed. However, the flowmeter dealt well with the particulate-contaminated fluid passing through it. No significant loss of accuracy was recorded.

4.2.4 External Sensors

In order to conduct the tests satisfactorily both grinding machines were equipped with several extra pieces of equipment; some allowing additional measurements and others as essential extras to the successful completion of a grinding experiment.

4.2.4.1 Dynamometer

In order to measure the grinding forces on the Abwood grinding machine a Kistler dynamometer type 9257A was used. This is a three axis system that allows measurement up to 5000 N in conventional X, Y, and Z for the system developed around it. It allowed measurement to a resolution of <0.01% of designated full scale, however calibration was only carried out up to 500 N, so linearity beyond that scale for this specific experimental rig was never verified and accounted for. The Kistler 9257A is a piezoelectric transducer. This type of transducer gives each component of force a proportional electric charge. This charge, once fed through the charge amplifier, will be readable as a voltage that is proportional in value to the force impinging upon the dynamometer. This voltage is then fed into the analogue input of a Data Acquisition system (DAQ) and using values obtained from calibration can be post-processed to give a value of the force being experienced by the dynamometer and hence the experimental rig.

The dynamometer required a base to secure it both to the workpiece and table. This base had to electrically insulate the dynamometer and all other components mounted above the dynamometer from the magnetic worktable. The insulation prevented noise from the grinding machine being picked up in the thermocouple sensor. This was done using an ABS plastic block machined to roughly an inch thick with two metallic feet attached with screws to its base. The metallic feet were used so the system could be held in place by the magnetic chuck of the Abwood grinding machine. ABS was chosen as it is an effective electrical insulator and was also capable of being machined to size with strong threads.

The dynamometer was calibrated using a simple pulley system attaching known weights at a given angle to the measuring plane of the dynamometer. This can be seen schematically in

Figure 18. Calibration took place using a random distribution of masses; this was done in both loading and un-loading modes as recommended by the manufacturer. The dynamometer also had the workpiece attached so any effect the workpiece arrangement might have could be accounted for during calibration. The calibration took place at an ambient temperature of ~20°C. The charge amplifier was set at 'long' reading scale during calibration and testing. The cable connecting the dynamometer and the weights had a high modulus of elasticity and as such will have not significantly change dimension due to the strain exerted during the calibration process.

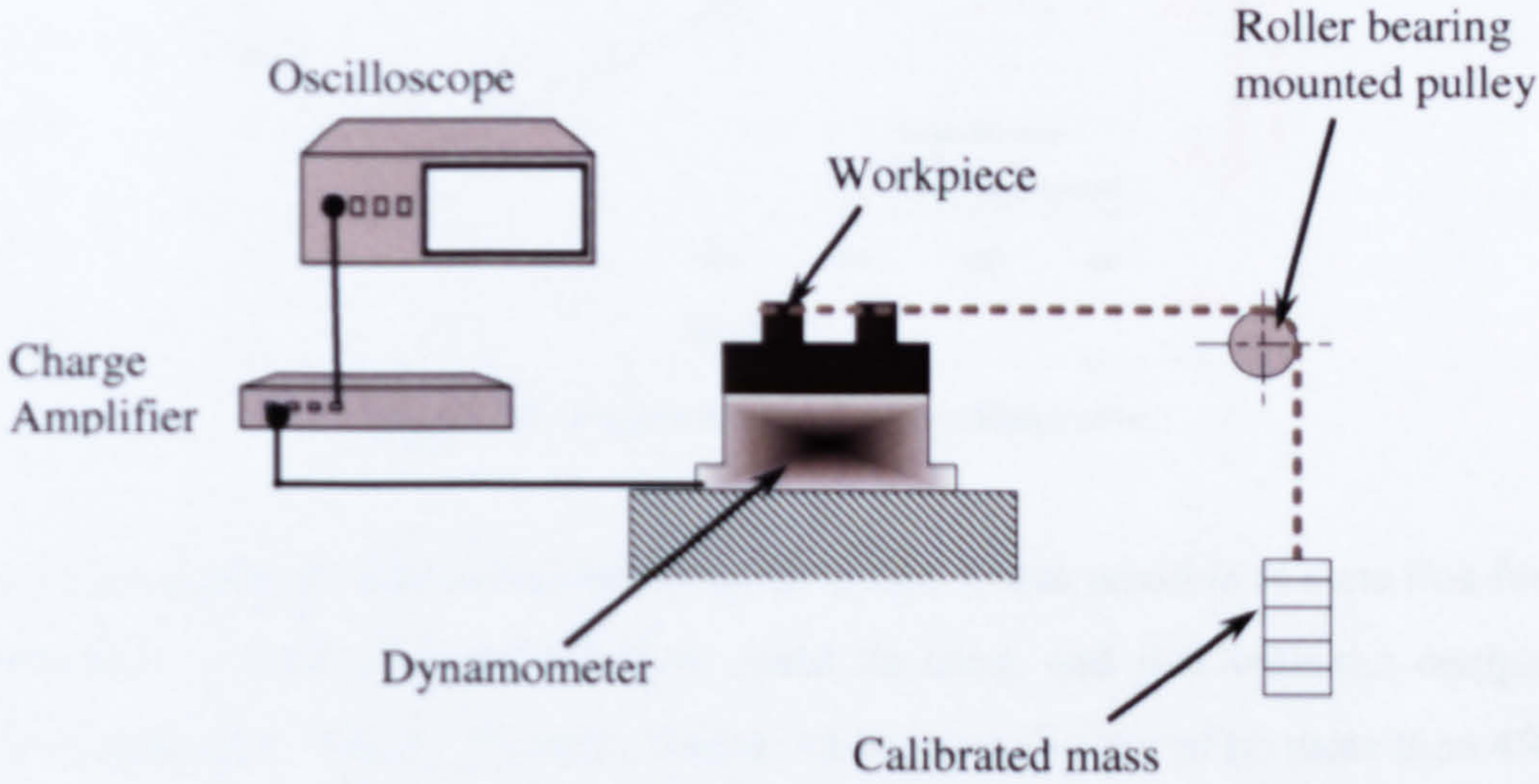

Figure 18, Experimental rig for calibration of the dynamometer.

For the normal component of force the charge amplifier was set at a sensitivity of 8.04 pC/N and the scale was set at 1000 units per volt. For the tangential force component the charge amplifier was set with a sensitivity of 3.75 pC/N and the scale was set at 500 units per volt. Both of these values were taken from the calibration certificate issued to the dynamometer/charge amplifier system and worked well across the range required for calibration.

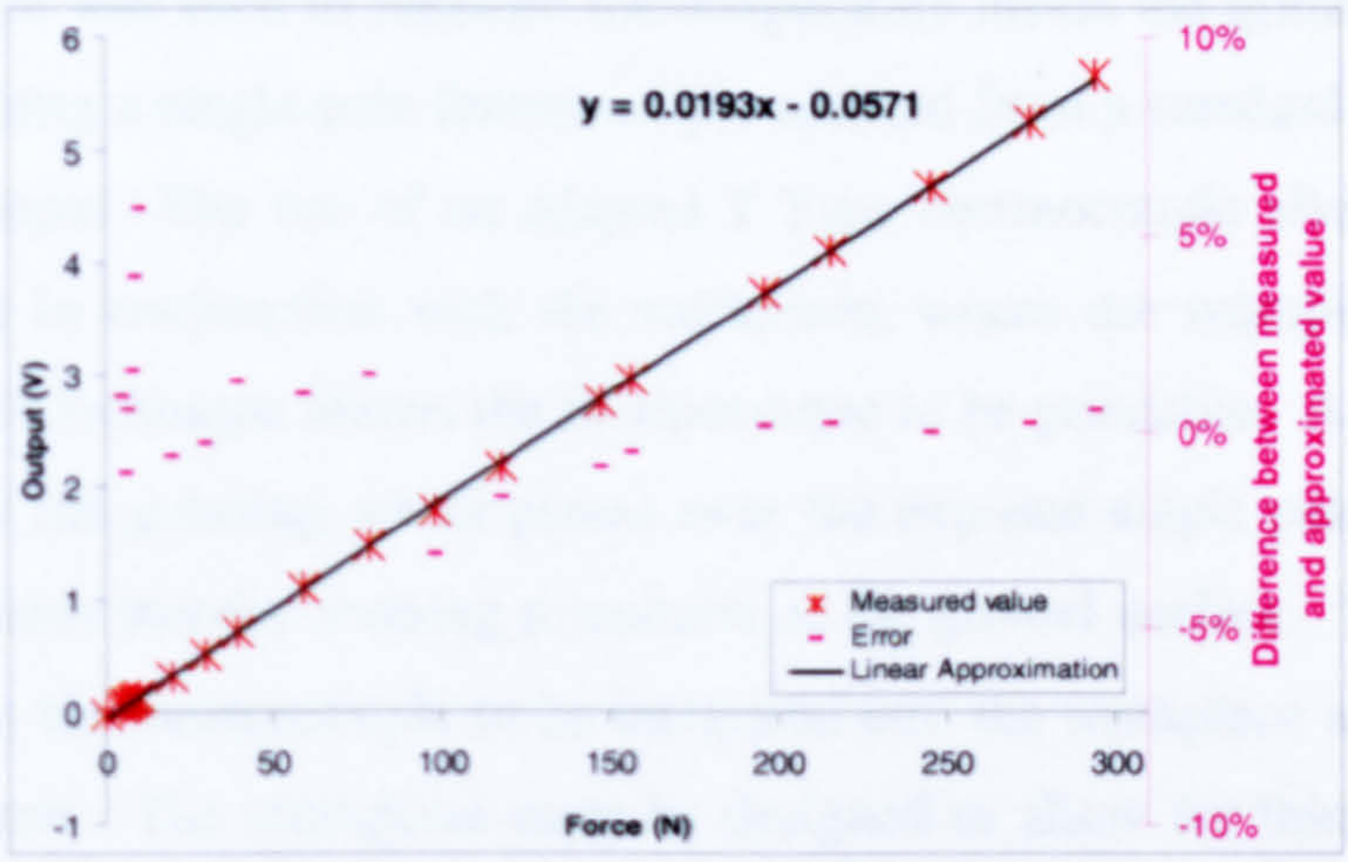

Figure 19, Normal force calibration results.

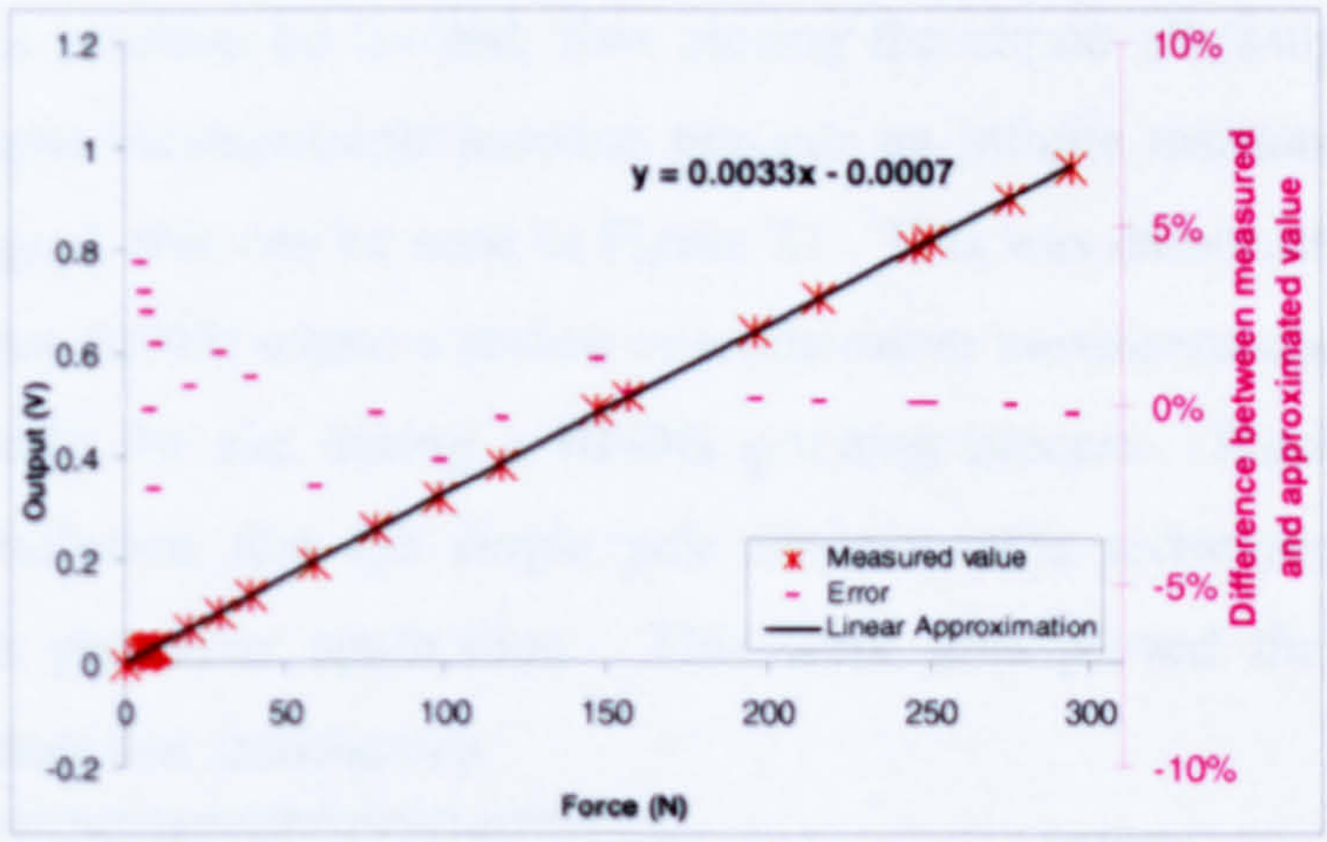

Figure 20, Tangential force calibration curve.

Using the calibration lines extracted from the graph it was possible to state that for the normal force a scale of 1.93×10^{-3} V/N could be used, and that with the equipment attached the 0 value was at -57.1mV. These values give an error of no more than 4%, as can be seen from Figure 19 where the error is worked out by calculating the difference between the measured value and the value obtained via the factor shown above. For the tangential force a factor of 3.28×10^{-3} V/N and an offset of -0.7mV were found, this

value of offset was considered negligible and was considered to be 0 for post-processing of the data. It was also noticed that the system suffered from a considerable transient drift problem. This problem occurred over periods of hours rather than minutes so this issue was easily overcome during testing by resetting the 'Zero' of the system prior to each test.

4.2.4.2 Temperature Sensor

A thermocouple was used to measure the temperature inside the grinding zone. This was achieved using a single pole thermocouple adapted from a standard double pole T-Type thermocouple. The use of an adapted T-Type thermocouple allows use of only one of the legs in conjunction with the workpiece, where the workpiece acts as the second leg. This technique allows the thermocouple to be grindable. A J-type junction is formed when the grinding wheel passes over the exposed single pole and smears it over the workpiece thereby forming a junction at the ground surface. The single pole method requires the thermocouple to be integrated into the workpiece at an early stage in its manufacture. The workpiece must be designed to allow for this. The signal is then fed through a thermocouple amplifier to a Data Acquisition system (DAQ) for post-processing. Not until the grinding wheel has smeared the thermocouple over the workpiece will a junction be formed, thus closing the circuit allowing a signal to be retrieved. An open thermocouple junction presents an infinite resistance to the circuit and hence no signal, this can be seen in Figure 21. This was demonstrated by Batako, Rowe and Morgan (2005) where a review of temperature measurements techniques was shown, specifically for use during a HEDG grinding process. Batako *et al* (2005) reached the conclusion that the single pole thermocouple technique was the most reliable for that particular application. This work also proved the latency of the thermocouple setup was satisfactory.

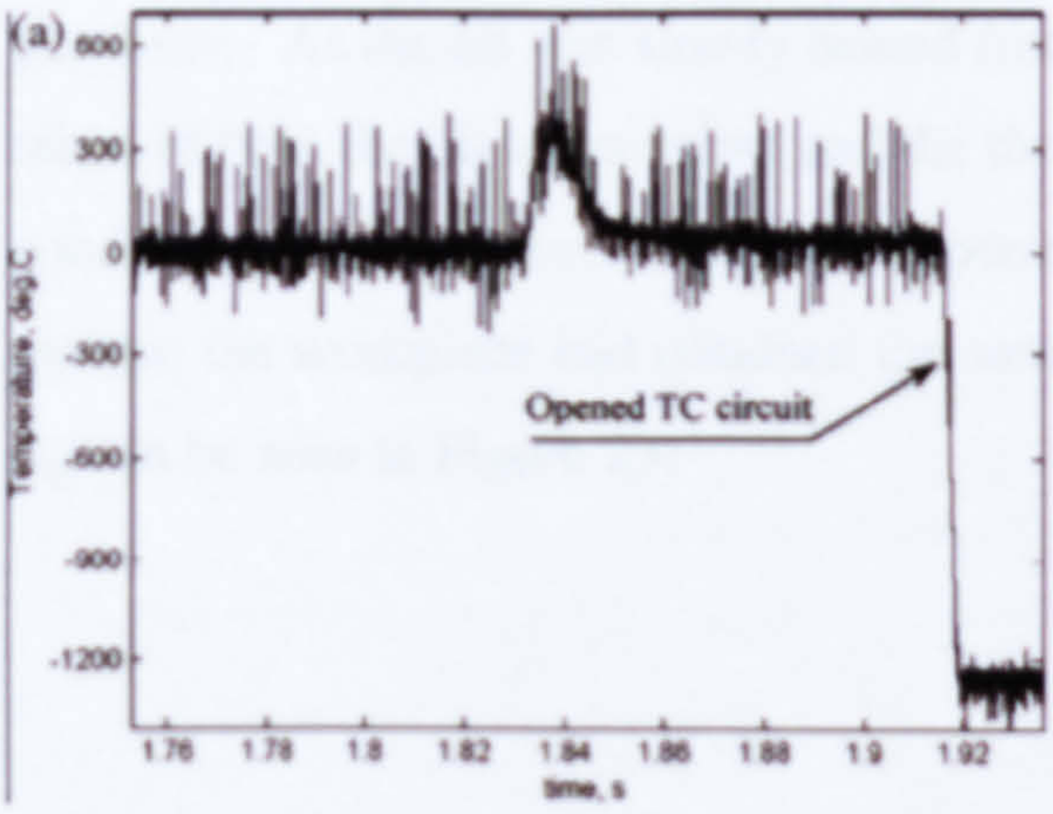

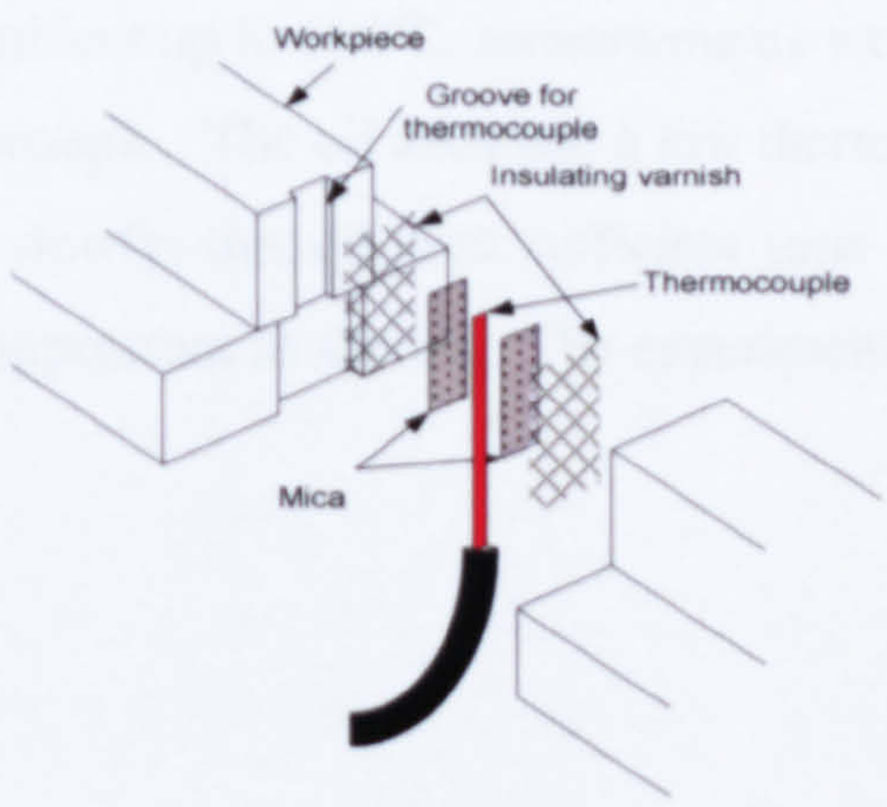

Figure 21, Graph showing an open thermocouple junction (Batako *et al* 2005).

Figure 22, Schematic of thermocouple junction build.

For the measurement of temperature in these experiments a J-Type thermocouple was formed by embedding a Constantin strip in a mild steel workpiece. The Constantin strip was sandwiched into a split workpiece and electrically insulated from the workpiece using a combination of thin Mica strips (approximately 20μm thick), insulating varnish and electrical wire sheath. This can be seen in Figure 22. With one end exposed at the workpiece surface, the other was connected to a female J-type socket mounted in the wall of the workpiece. The remaining junction of the female J-type socket was connected using electrical wire to the workpiece in close proximity to the socket.

Once the thermocouple was mounted inside the workpiece a continuity test was performed to guarantee electrical isolation of the thermocouple leg. Proving electrical isolation at this stage guaranteed that during a grinding pass the junction would only be formed at the workpiece surface. A J-type electrical wire was then used to connect the socket of the workpiece to the amplifier. The amplifier was then plugged into the DAQ system, this data then needed to be offset using calibration data to get a true value of temperature. A calibration procedure was devised to analyse the complete thermocouple system used during this test.

Calibration took place using an oil bath, a digital thermometer, a hot plate and a ventilation chamber. Firstly the workpiece surface was ground so that a junction was formed. The workpiece was then lowered into the bath of oil until the ground surface was about 10mm deep into the oil. With the workpiece immersed in the oil the hot plate was used to heat the oil, everything was kept within a ventilation chamber for safety purposes. As the oil was slowly heated from ambient up to 150°C, measurements were taken of both the oil temperature and the thermocouple. The oil used had a low thermal conductivity and as such changed temperature slowly, this allowed sufficient time to assume the workpiece had obtained the same temperature as the oil. The experimental rig can be seen in Figure 23.

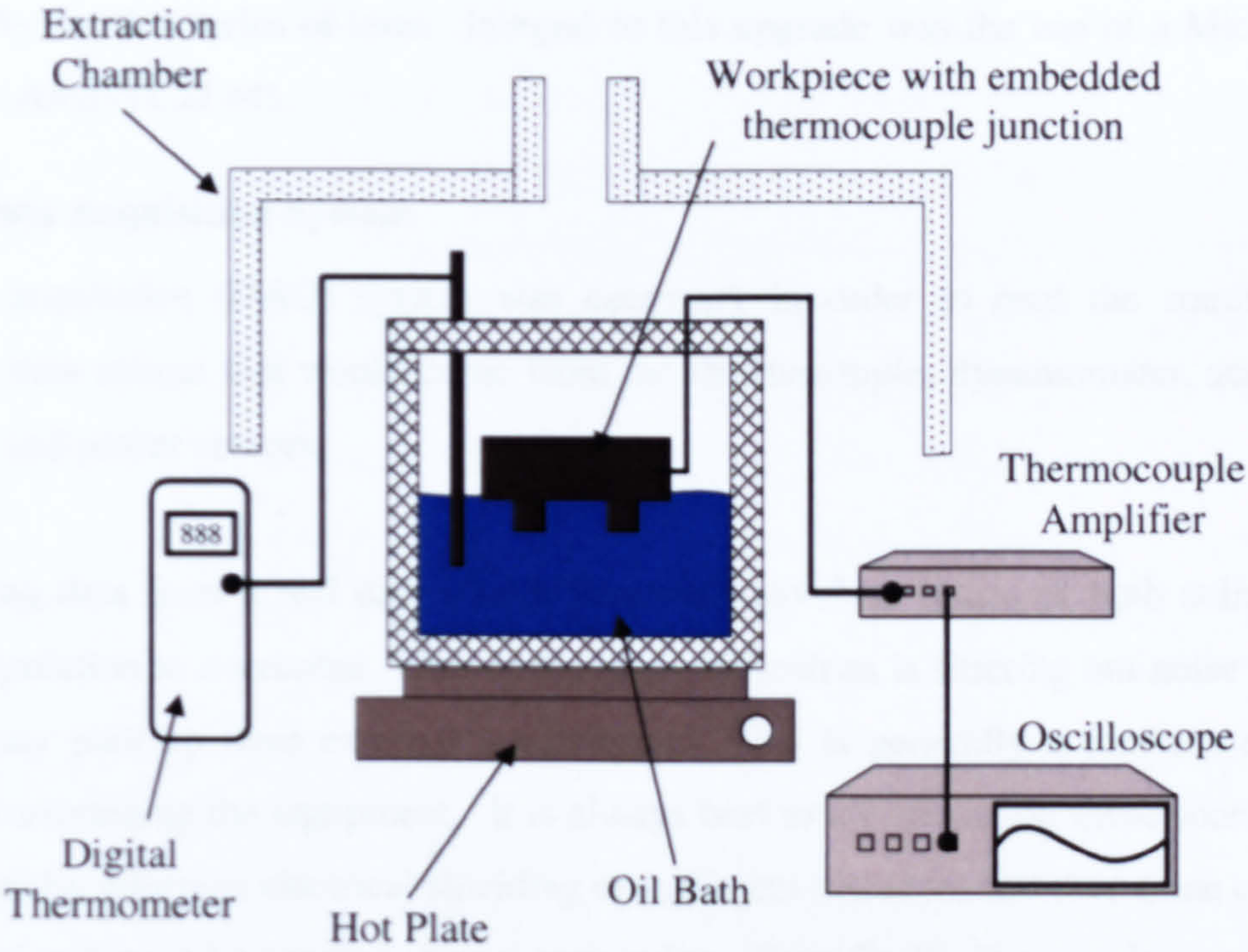

Figure 23, Thermocouple calibration arrangement.

By comparing the voltage output to the temperature measured by the digital thermometer a graph was created to calibrate the particular setup in use for this experiment. The calibration graph can be seen in Figure 24. The results showed that over a range of 20 up to 110°C in cooling and heating phases a linear approximation can be made that will be accurate to within 2%.

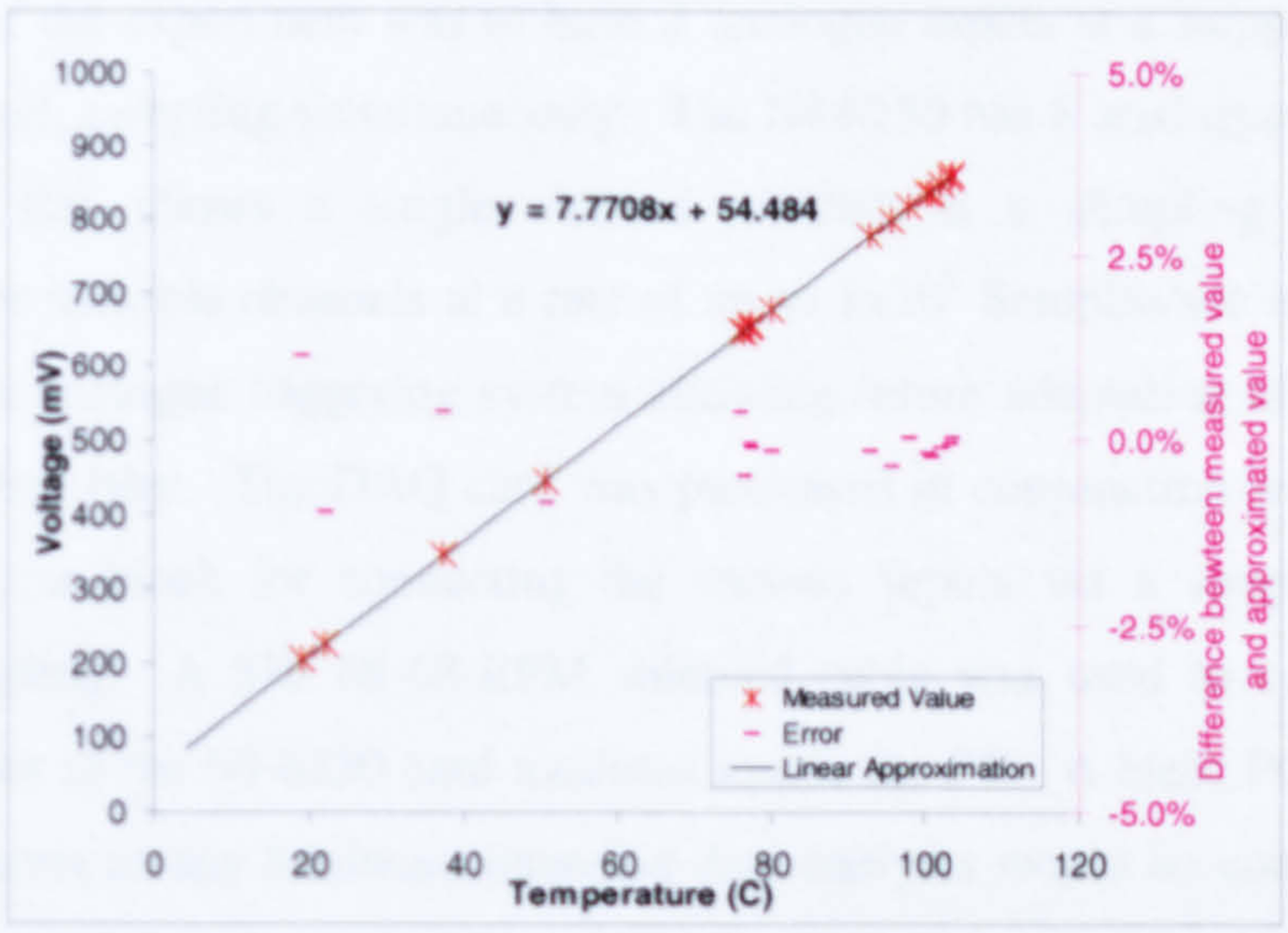

Figure 24, Thermocouple calibration chart.

Once calibrated, the system was used for testing on the Abwood. However, before the main testing the equipment was updated to include a dedicated amplifier devised

specifically for this series of tests. Integral to this upgrade was the use of a Michigan Scientific AMP-TC2J-M1.

4.2.5 Data Acquisition System

A data acquisition (DAQ) system was necessary in order to read the continuous analogue data stream that would come from the thermocouple, dynamometer, acoustic emission and power sensors.

Extracting data from a real data source invariably involves issues of both collection and manipulation to overcome. One of the main difficulties is filtering out noise that a system may pick up from external interference. This is generally a function of the systems surrounding the equipment. It is always best to try and avoid these sources of error either by adequate electrical shielding or sufficient distance, however some cannot be ignored and must be handled in post-processing. Specifically in an analysis relating to grinding it is generally found that the motor driving the grinding wheel will induce a signal in the DAQ equipment, again it is only viable to approach removal of this type of noise in post-processing.

The DAQ system is used to acquire data received from the sensors. A National Instruments NI-6250 data acquisition card was chosen to fulfil these needs. The requirement of the experiment was to have 3 analogue inputs at a sampling rate of 10 kHz per channel, sampling simultaneously. The NI-6250 has 8 analogue inputs using a 16-bit ADC, this allows a single channel of data at a sampling rate 1.25×10^6 Samples/sec or multiple channels at a rate of up to 1×10^6 Samples/sec in total. It also comes with an analogue triggering system allowing future adaptation of the collection system described later. The DAQ card was purchased in conjunction with a CB-68LP 68-pin connector block for connecting the various inputs via a simple grub screw electrical coupling. A SHC68-68-EPM shielded cable was used to connect the pin connector block to the NI-6250 card mounted inside the PC. A basic PC was used for these experiments as any hardware intensive data analysis would be conducted on one of the more powerful workstation PC's within the laboratory.

The hardware was controlled using LabView 7.1. A program was written for the tests in the Labview 7.1 'Virtual Instrument' (VI) environment so that continuous analogue data was sampled from all sensors at a frequency of 10 kHz. This data was then

manipulated in binary file format to form a 3 column matrix. The inputs required for Abwood testing were temperature, tangential force and normal force. For the main body of testing the inputs were temperature, acoustic emission and spindle power. For both systems the software was designed to give a visual display of the current values in a graphical and a numerical way. It also allowed front end control of sampling rates, input of values for control of the internal data buffering and the ability to write the data to a binary file with 3 columns of data. The data stream was written continuously into a file that can be saved and then post processed. The program can be seen in Appendix D. The front end of the program used for the main body of testing can be seen in Figure 25.

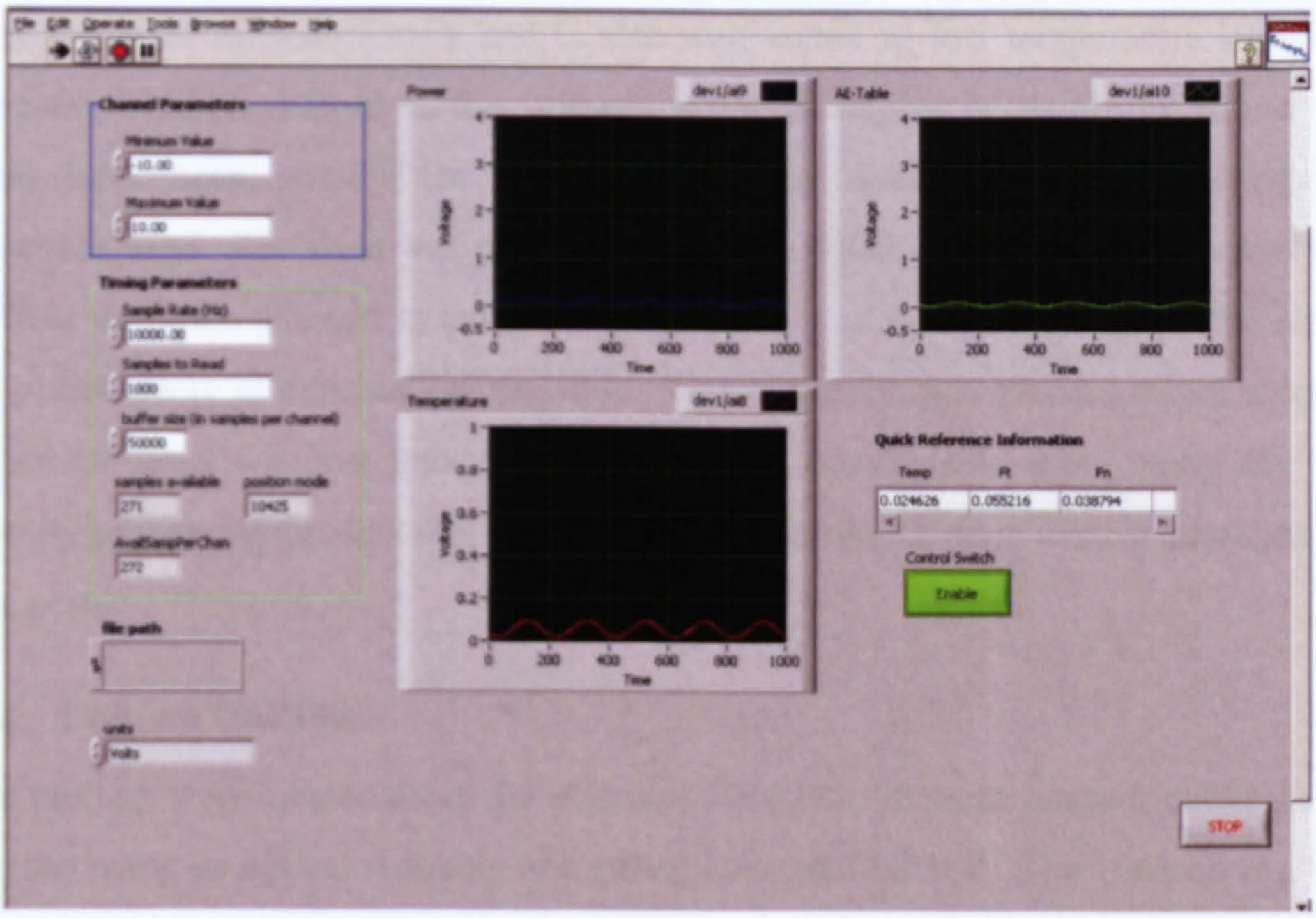

Figure 25, DAQ program used for the main tests.

The post-processing took place in the MATLAB programming environment. The program performing the post-processing involved; using the sampling frequency to establish a time domain for reference, separating and tagging the individual inputs and then using a low-pass Butterworth filter to extract the noise from each signal then plotting the data in a logical manner. The MATLAB code used for the main test can be found in Appendix D.

4.3 Topography

A previous project within the AMTReL group (Cai, 2002) had defined the best methods of taking an impression of a grinding wheel and thus measuring a profile. These methods, described in detail later, involve equipment still available within the group and have been shown to give accurate and reliable results. Below is described all the equipment required for the grinding wheel topography tests.

4.3.1 Microset 101RF

The impression of the wheel surface was created using a polymer compound called Microset 101RF, this type of replication product allows fast cure times, excellent reproduction of microstructures and is also well suited to low temperature situations. Microset 101RF is a fluid so this allowed a greater degree of flexibility in use than would have been possible in comparison to the thixotropic type of compound sometimes used. The fluid was pumped into a bath which the wheel was lowered into; the fluid was then allowed to cure for approximately an hour. Once cured the replica was pealed away as delicately as possible. Unfortunately, this process meant a certain amount of detail was lost into the wheel. This is unavoidable when using any low-viscosity replicating product that is designed to penetrate through narrow passages into large pores.

4.3.2 Uniscan OSP100

The replicas were created using the Microset 101RF fluid, these samples could then be analysed using an optical scanning unit called Uniscan OSP100. The Uniscan is a laser triangulation type system, capable of a resolution of 0.5 μm over a scale of 100 mm^2 and a depth of 35 mm. Using a 5 mm by 5 mm sampling area each scanning line was separated by approximately 10 μm. Although the Wyko RST Plus system offers more accuracy on topography, the need to have the option of a larger sample area and deep pores led to the use of the Uniscan laser triangulation approach. The depth measurement also made the use of the Uniscan system preferable. As Cai (2002) reported, the Wyko RST system has a higher resolution but it is only suitable with a small sample size and could not measure height differences of more than 500 μm.

4.3.3 WYKO Vision® Software Tool

Once the scan was made with the Uniscan system the data could be transferred to a desktop computer for analysis in the Wyko Vision® software package. Although the

Uniscan system had a limited analysis package, the Vision® software package from the Wyko RST plus system offered far more flexibility in both visualising the scanned area and also in topographical analysis.

4.4 Ancillary Equipment

In order to conduct the tests satisfactorily both grinding machines were equipped with several extra pieces of equipment; some allowing measurement of various parameters and others as essential extras to the grinding experiments.

4.4.1 Workpiece Materials

During the tests three types of workpiece material were used; a general purpose Mild Steel, EN 3B bearing steel and B01 tool steel. The general purpose mild steel was used for ease of manufacture during the early stages of collector development, the exact specification was unknown. During the main body of testing an EN3B / 070M20 (from BS 970-3:1991) bearing steel was used, this represented an easier to grind material. A B01 tool steel was used to represent a harder to grind material, this material was further through hardened to a hardness of approximately 53 HRc.

4.4.2 Grinding Wheels

All testing was conducted using alumina wheels with vitrified bonding. Initial testing was conducted using a custom made alumina wheel (otherwise known as the Altos wheel) The grains within the Altos wheel were of a particular long aspect ratio, in the region of 10:1. Visual methods found the grains have an average characteristic length at the widest point of 850 μm. A typical grain can be seen in Figure 26. The exact wheel specification was not known as this particular wheel was custom made for a previous project many years ago. However, previous testing within the laboratory had found the porosity to be between 50-55%, this was verified using the volume displacement method as used by Krishnan, Malkin and Guo (1995), where the wheel was found to be 54% porous in bulk structure. The Altos wheel was initially 200 mm in diameter but at the start of testing was actually measured at 188 mm using a vernier calliper. The Altos wheel was approximately 25 mm wide with no supporting solid annulus.

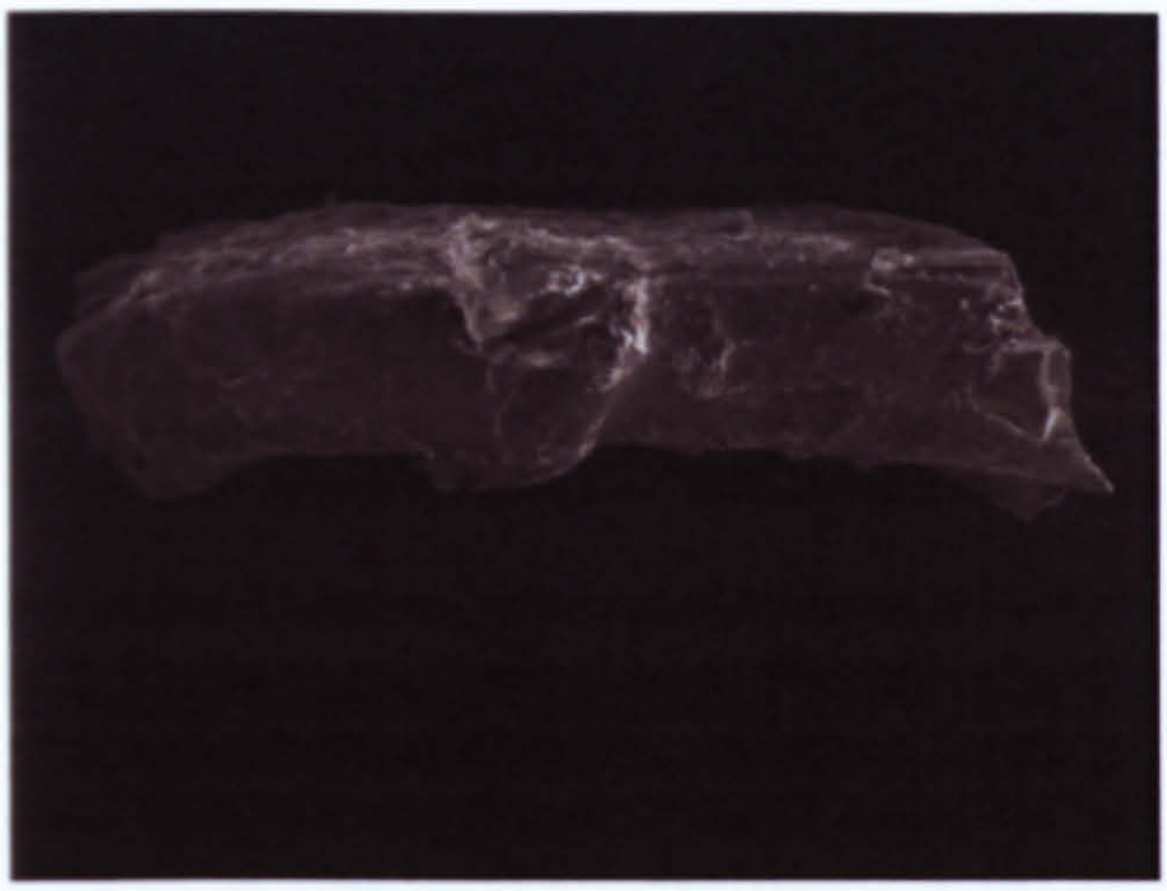

Figure 26, SEM image of an individual alumina grain from the Altos Wheel.

The grinding trials that did not use the Altos wheel were performed with another alumina grinding wheel with a O1W-A-60-K-/-V-L specification, this was known as the Flexovit wheel and was supplied by Saint Gobain Abrasives. All wheel specifications are stated to conform to EN 12413. The Flexovit wheel had an initial diameter of 310 mm with a width of 25 mm. This wheel was rated for use at up to 70 m/s linear wheel speed. Using the same principle as described in verifying the Altos wheel, the Flexovit wheel was found to have a porosity of 44 %, this was verified by the manufacturer. According to equation (16) this wheel should have abrasive grains averaging a diameter of 250 μm. Testing using visual aids showed that the grains within this particular wheel had a profile that could be approximated to a circle i.e. an aspect ratio of approximately 1:1. Visual measurement showed that the grains had an average diameter of 340 μm at the widest point.

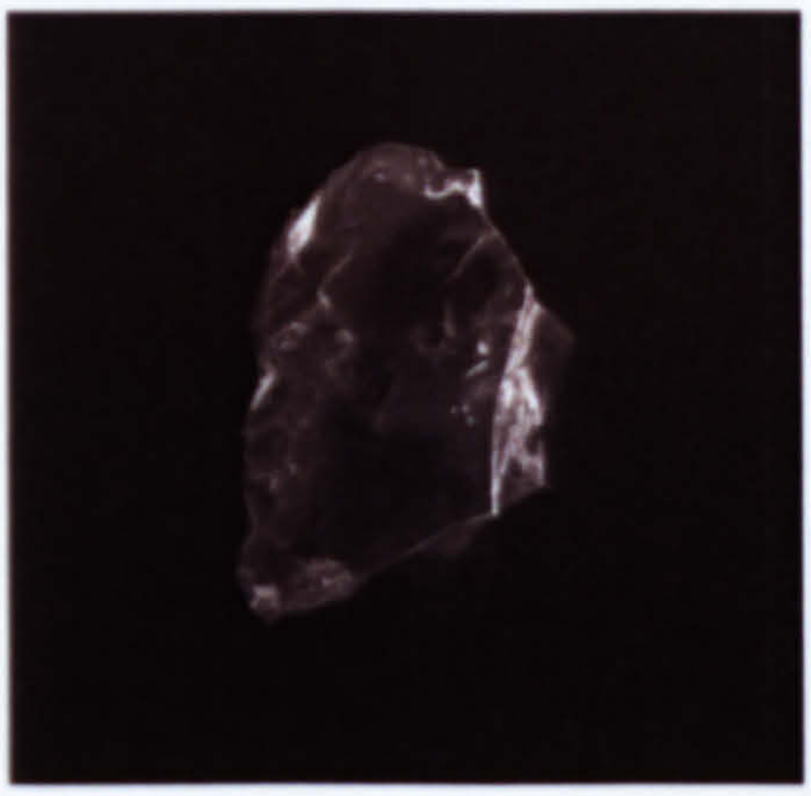

Figure 27, SEM image of an individual alumina grain from the Flexovit Wheel.

A further wheel was used during the topography tests, this was again an alumina vitrified wheel described for the purposes of this thesis as the 'Universal' grinding

wheel, the specification is 52-A-46(1)-J-7-V-L. Using the same visual technique the Universal wheel was found to have an aspect ratio of approximately 1:1, with a diameter of 440 μm. Equation (16) stated that the grains within this wheel should have an approximate diameter of 330 μm.

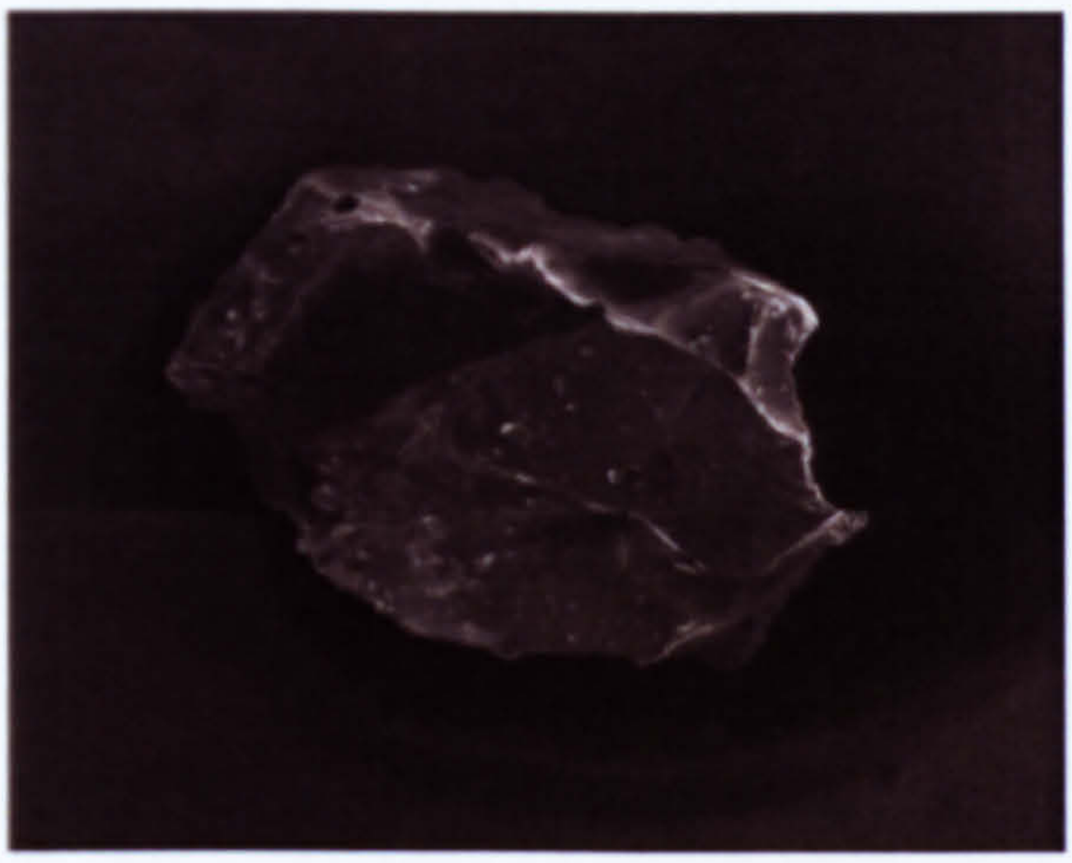

Figure 28, SEM image of an individual alumina grain from the Universal Wheel.

The sample sizes for all of the visual measurements were limited, thereby restricting the ability of the sample to reflect the overall true value of the average grain size. However, given the large amount of grains contained within the wheel and the limited capacity to remove grains from a wheel that is needed for grinding tests (without adversely affecting the balance), the sample size of approximately thirty from a population of nearly 200 extracted grains was deemed sufficiently representative.

Chapter 5. Experimental Procedure

5.1 Introduction

The experimentation required for the project can be split into 3 distinct sections

1. Useful flow collector development trials
2. Grinding trials
3. Topography trials

Some of the testing for these distinct sections overlaps; so at this point it is worth describing the procedure that is common for each stage of the testing. The specific results and exact nature of each test is discussed later in this document.

The layout of the experimental portion of this work was designed with specific goals in mind. Firstly the development of the useful flow collector. Then followed the analysis of the useful flowrate using a (Taguchi) fractional factorial approach; this gave qualitative results that were expanded on using full factorial testing. The experimental part of the project was then concluded with a wheel analysis section to aid the topographical analysis of the work.

The purpose of the preliminary testing was to develop the useful flow collection system. However, at a certain point of maturity the collector was proved reliable, therefore some the results in this section could be trusted for further analysis. Several developmental stages are not shown in detail as they were used for verification of parts that were later superseded or had no merit in terms of analysis of useful flow. The Surface Grinding Trials and Taguchi trials all used a fully developed useful flow collector and as such are complete trials where the results are repeatable and reproducible. The Topography trials also draw reference to some of the useful flow collection testing results. Where this has happened the relevant test from the grinding trials has been referenced using the notation described above.

5.2 Trials Layout

All experiments were conducted using the equipment described in Chapter 4, the combinations of which vary. The layout of the trials can be described as follows with the needs for each test in regards to the sections previously listed shown after.

- Preliminary testing
    - Test 1
    - Test 2
    - Test 3
- Surface Grinding Trials
    - Abwood speed ratio test
    - Dominator speed ratio test
    - Jet flowrate/speed test
- Taguchi Trial
- Topography Trials
    - Bedding-in test
    - Dressing test

5.2.1 Preliminary Test Stages

All testing at the developmental stage was conducted on the Abwood grinding machine using the Altos grinding wheel at conventional wheel speeds. Beyond these parameters the following differences were considered key.

- **Test 1** varied the wheel speed v_s and was unique in using a preliminary useful flow collection system that had side scrapers that extended beyond the contact zone. This situation can be seen in detail in Figure 29 and is described fully in the following chapter. This first test used the plunge cycle grinding operation. This was done to ease the initial requirements placed on the first generation of the useful flow capture system.

Grinding Machine	Abwood
Grinding wheel	Altos
Type of Process	Plunge
Useful flow collector version	Development stage 1
Workpiece material	Mild steel
Depth of cut	10 µm plunge
Traverse speed	n/a
Wheel speed	7-17 m/s
Supply flowrate	7.2 l/min

Jet speed	12 m/s
Coolant type	8-10% Hysol X solution
Variables measured	Useful flow
Variables to be tested	v_s

Table 7, Summary specification for preliminary test 1.

- **Test 2** varied the wheel speed v_s and jet speed v_j (by varying the supply flowrate q_d) and used the next stage of the useful flow collection system but also with extended sides, this can be seen in detail in Figure 30 in the following chapter.

Grinding Machine	Abwood
Grinding wheel	Altos
Type of Process	Traverse
Useful flow collector version	Development stage 2
Workpiece material	EN3B
Depth of cut	20 μm
Traverse speed	2 mm/s
Wheel speed	25-45 m/s
Supply flowrate	11-33 l/min
Jet speed	19-54 m/s
Coolant type	8-10% Hysol X solution
Variables measured	Useful flow
Variables to be tested	v_s, $v_j(q_d)$

Table 8, Summary specification for preliminary test 2.

- **Test 3** varied the wheel speed v_s and jet speed v_j. This test used the fully developed flow collection system that covers the sides only up to the contact zone.

Grinding Machine	Abwood
Grinding wheel	Altos
Type of Process	Traverse
Useful flow collector version	Fully Developed for the Abwood
Workpiece material	Mild steel
Depth of cut	20 μm
Traverse speed	2 mm/s

Wheel speed	11-51 m/s
Supply flowrate	18.9 l/min
Jet speed	35-45 m/s
Coolant type	8-10% Hysol X solution
Variables measured	Useful flow
Variables to be tested	v_s, v_j

Table 9, Summary specification for preliminary test 3.

Test 1 and 2 were predominantly used for developing the useful flow collector. Test 3 was the final stage of developing the useful flow collector and as such some of the results have been referenced in the discussion of the surface grinding trials.

5.2.2 Surface Grinding Trials

Only trials with a fully developed useful flow collector were allocated to the surface grinding trials section. All of these results were considered reliable for their accuracy. The surface grinding trials were conducted on both the Abwood and the Dominator grinding machine. The useful flow collection system used on both machines was essentially identical; the only changes between the two were either aesthetic or machine specific in nature. The key differences of each test were as follows.

- **Abwood speed ratio test** was designed to test the effect of wheel speed on useful flow, therefore only the wheel speed, v_s was varied. This test used the Altos grinding wheel and the fully developed useful flow collector with side scraping up to but not beyond the contact zone.

Grinding Machine	Abwood
Grinding wheel	Altos
Type of Process	Traverse
Useful flow collector version	Fully Developed for the Abwood
Workpiece material	Mild steel
Depth of cut	25 μm
Traverse speed	6 mm/s
Wheel speed	11-51 m/s
Supply flowrate	18.9 l/min
Jet speed	24 m/s

Coolant type	8-10% Hysol X solution
Variables measured	Useful flow, Grinding zone temperature, tangential force, normal force,
Variables to be tested	v_s,

Table 10, Summary specification for the Abwood speed ratio test.

- **Dominator speed ratio test** was designed to take the previous Abwood test a stage further in terms of wheel speed and also to use a different wheel; with this in mind only the wheel speed, v_s was varied. The test was conducted using the Flexovit grinding wheel and the fully developed useful flow collector adapted for the different machine.

Grinding Machine	Dominator
Grinding wheel	Flexovit
Type of Process	Traverse
Useful flow collector version	Fully developed and adapted for the Dominator
Workpiece material	Mild steel
Depth of cut	35 μm
Traverse speed	10 mm/s
Wheel speed	14-69 m/s
Supply flowrate	18.9 l/min
Jet speed	24 m/s
Coolant type	8-10% Hysol X solution
Variables measured	Useful flow, Grinding zone temperature, spindle power.
Variables to be tested	v_s,

Table 11, Summary specification for Dominator speed ratio test.

- **Jet flowrate/speed test** was conducted on the Dominator grinding machine and was designed to test the effects of varying the jet flowrate independent of the jet speed, with a fixed wheel speed. Consequently only the jet speed v_j and the supply flowrate q_d were varied for this trial. This test was also conducted using the Flexovit grinding wheel and the fully developed useful flow collector.

Grinding Machine	Dominator
Grinding wheel	Flexovit
Type of Process	Traverse
Useful flow collector version	Fully Developed and adapted for the Dominator
Workpiece material	Mild steel
Depth of cut	35 μm
Traverse speed	10 mm/s
Wheel speed	30 m/s
Supply flowrate	6-24 l/min
Jet speed	10-40 m/s
Coolant type	8-10% Hysol X solution
Variables measured	Useful flow, Grinding zone temperature, spindle power.
Variables to be tested	v_j, q_d.

Table 12, Summary specification for Jet flowrate/speed test.

All three of these tests were used for the analysis of the useful flowrate. During all of the tests the temperature was measured. For the Abwood speed ratio test the force was measured, but for the Dominator speed ratio test and the Jet flowrate/speed test the power was measured. This change was to remove the dynamometer as an issue for testing (due to its inability to cope with fluid ingress) and because the Dominator had a wider scope of integrated sensors.

5.2.3 Taguchi Trials

Part of the grinding trials was a fractional factorial test following a Taguchi methodology. The Taguchi trials and the experimental method are described in detail in Chapter 7.5.

5.2.4 Topography Trials

The majority of the topography trials are purely measurement of the surface topography of grinding wheels in different states. These tests were conducted on the Abwood and Dominator grinding machines using the Altos and Flexovit grinding wheels. Some stages of system testing are mentioned during discussions later in the

thesis, however these are not used for analysis so are not summarised below. The key tests of each of the topography trials are as follows

- **Dressing tests** were conducted to discover how the dressing affects the surface topography and therefore the fluid carrying capability, of the grinding wheel. Testing was conducted on the Universal grinding wheel. The purpose of the test was to vary the key dressing parameters of feed rate f_d and dressing depth a_d.

Grinding Machine	Dominator
Grinding wheel	Universal
Variables to be tested	a_d, f_d.

Table 13, Summary specification for Dressing test.

- **Bedding-in tests** are designed to test the wear effect of the bedding-in process on the surface topography of the wheel. Testing was carried out using the Flexovit grinding wheel. During this test the bedding-in process was analysed by taking samples at various stages of wheel wear post dressing.

Grinding Machine	Dominator
Grinding wheel	Flexovit
Variables to be tested	n/a

Table 14, Summary specification for Bedding-in test.

- Several further samples were made on both the Altos and Flexovit grinding wheels, with samples taken from a steady state grinding wheel. The purpose of this test was to allow the author to compare the surface topography of the grinding wheel to a measured value of useful flow.

For every topography sample an impression is taken of the wheel surface using the Microset replicating fluid. Before each sample is created the wheel must be cleaned of swarf and fluid, this was done with a combination of high speed spinning and an air gun directed at the surface. The sample was then created by filling a dipping bath with Microset fluid and lowering the wheel into the bath up to a depth of at least 3 mm. The sample was then allowed to set for approximately 30 minutes. Once the sample had set it was removed from the wheel surface, this process invariably resulted in some of the fluid being left within the surface. Although regrettable this cannot be helped, as the fluid penetrates deep into the wheel it passes through small passages filling larger pores

beyond. Once the sample is peeled away these features were lost as the semi-solid fluid broke. Finer detail is still clear within the sample and significant pores could still be seen, represented by the semi-solid peaks of the Microset fluid.

The sample was then taken to the Uniscan system to be optically scanned. The resulting data was then exported to the Wyko Vision® software for post-processing. The post-processing was performed in several stages. Firstly the data is inverted so that the data represents the wheel surface rather than the surface of the negative replica. Secondly the data is passed through the 'cylinder and tilt' filter, this allows the curvature of the wheel to be accounted for and also any tilting of the sample that may be caused by an uneven surface on the face opposing the wheel impression. This data is then filtered using a level 3 window pass filter, this allows a lot of the fluctuations that occur at the grain surface to be removed, thus cleaning the image slightly. This also tended to even out the extremes of the sample that are due to bad reflections or gaps in the replica material. At this point the surface analysis techniques of the Wyko Vision® software could be employed to pick out standard values such as *Ra*, *Rt* or *Rp*. The Wyko Vision® software then allowed the processed data to be exported as cloud point data in an ASCII file type for further analysis in MATLAB. The MATLAB program was then used to analyse the surface further by line-scanning the data and building more detailed datasets. The techniques in MATLAB allowed nearly limitless control of how the sample could be analysed.

Chapter 6. Useful Flow Collector Development

6.1 Introduction

Following the review of previous approaches to flow capture and grinding analysis a series of tests were planned in order to begin development of a novel approach to useful flow capture. These preliminary experiments were designed to test the effectiveness of the devised flow capture methods throughout development. The key flow capture ideas were identified and used in the design of the final version of the useful flow capture device.

6.2 Aims

The aim for the preliminary testing stage was solely to measure useful flow. This was the most significant and necessary advance for this project. In order to complete the investigation it was essential to find a way to capture and measure the amount of fluid that passes through the contact zone in a way that is both functional and repeatable. One further requirement of the fluid collection system was that it be capable of housing or attaching to the necessary extra gauging; temperature sensor, power/force sensors.

6.3 Collector Development stage 1

To begin the design process an initial investigatory test was planned. This stage of testing is summarised earlier as preliminary test 1. The purpose was to establish some fundamentals before the testing and design process could progress into novel design development. Therefore, the goals of preliminary test 1 were as follows;

- To prove a volume of flow through the contact region was collectable with the machinery available.
- Assess approximate volumes of fluid.
- To analyse a method of capture.
- Compare results to the work of previous authors.

Testing was carried out on the Abwood surface grinding machine using a flow collection device that was adapted from a previously used experimental rig. As stated in the goals, the testing was to prove flow passes through the contact zone in a significant enough volume to be collected and to also approximate the volume of flow so a suitable collector and channelling system could be developed. Previous works had shown that collectable flow could be approximately 40 % of the applied flow (Engineer *et al*, 1992) or up to 90 % in certain situations (Gviniashvili, 2003). Further

to this, should the collection methods prove instantly viable, direct comparison could be made with work by other authors in the field.

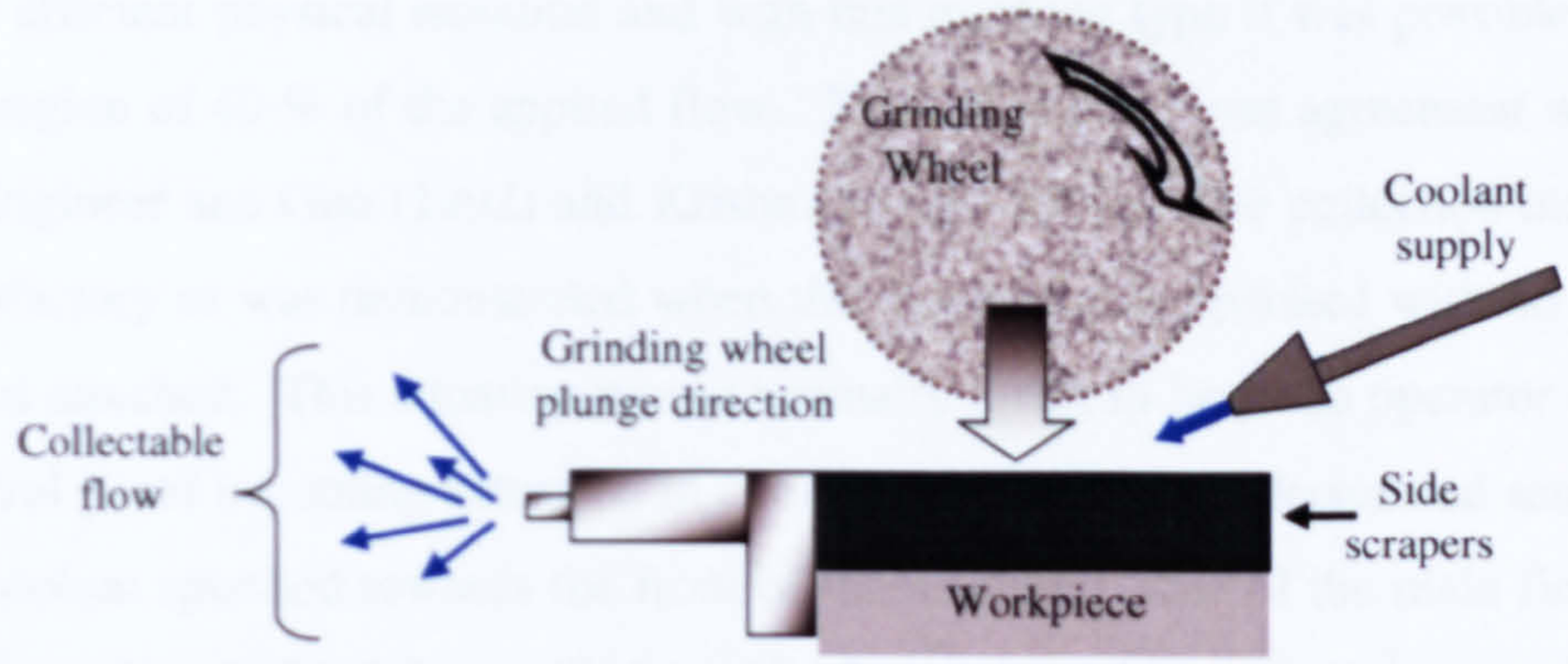

Figure 29, Schematic of Plunge grind process used in collector development stage 1.

The methodology for capture of the flow was to physically isolate the fluid that had passed through the grinding contact zone. This required using side scrapers, a workpiece the same width as the wheel and a post-contact zone scraper. The physical barriers needed to be in contact with the wheel, this meant it was necessary to attempt to minimise the drag effects that physical contact would have on the grinding outputs. The side scraper consisted of a foam glued to an aluminium plate that was spring mounted to the workpiece; this would allow the side scrapers to 'hug' the wheel and workpiece thus creating a physical barrier to the fluid along the sides of the wheel. The post contact zone scraper had to be held rigidly in position so contact could be maintained with the wheel periphery at all times. However, this contacting area needed to be as minimal as possible so as not to induce a force which could distort later results. Aluminium was used for this scraper as this is considered an easy-to-grind material and would provide minimal resistance to the wheel when contact is made.

Preliminary test 1 showed some promising results but also highlighted the need to conduct testing using a traverse grinding operation rather than a plunge type. The Abwood grinding machine has a cantilevered headstock resulting in a lack of machine stiffness. When the wheel was lowered into position and the cut applied, a tendency for the wheel to 'bounce' was observed. This meant that a constant contact between the wheel and the workpiece could not be guaranteed during a test. Therefore, any flow

collected may have passed through what was essentially an open passage rather than a true grinding contact zone.

By efficient physical isolation and with this machine type it was possible to collect in the region of 40 % of the applied flow. This value had close agreement with the work of Engineer and Guo (1992) and Krishnan *et al* (1995). The collection method proved satisfactory as was demonstrated when the machine was operated with no front splash-guard attached. This situation would normally result in both the operator and the front control panel becoming saturated in coolant, but with the collector and scraper in place no coolant splashed towards the front of the machine. One of the main findings of this test was that 40% of the applied supply flowrate could be passed through the contact zone and subsequently collected with suitable physical isolation systems. Another key finding was that a continuous cut could not be guaranteed with a plunge-type grinding process thus a traverse grind process was needed for future tests. This made it necessary to convert the successful methodology shown within this test to a traverse grinding situation.

6.4 Collector Development Stage 2

Having established some key design characteristics for the useful flow capture device from the first preliminary test, the next test was planned to verify that these methods were also viable for a traverse grind. This stage of testing was summarised previously as preliminary test 2.

The second stage of design for the useful flow collection system involved splitting the main components in two so that they could move relative to each other. The primary parts included the flow director and side scrapers; this formed the system that directed the isolated flow away from the surrounding/rejected fluid. The secondary part was the post contact zone scraper and was designed to attach to the head-stock of the machine so that the scraper could be located in a fixed position relative to the wheel. These changes made the system more complex and meant some adaptations had to be made to the Abwood wheel guard, but it did allow isolation and extraction of the contact zone fluid whilst maintaining a cut on the Abwood using a traverse grind. The system in Figure 30 illustrates the wheel, collector and scrapers.

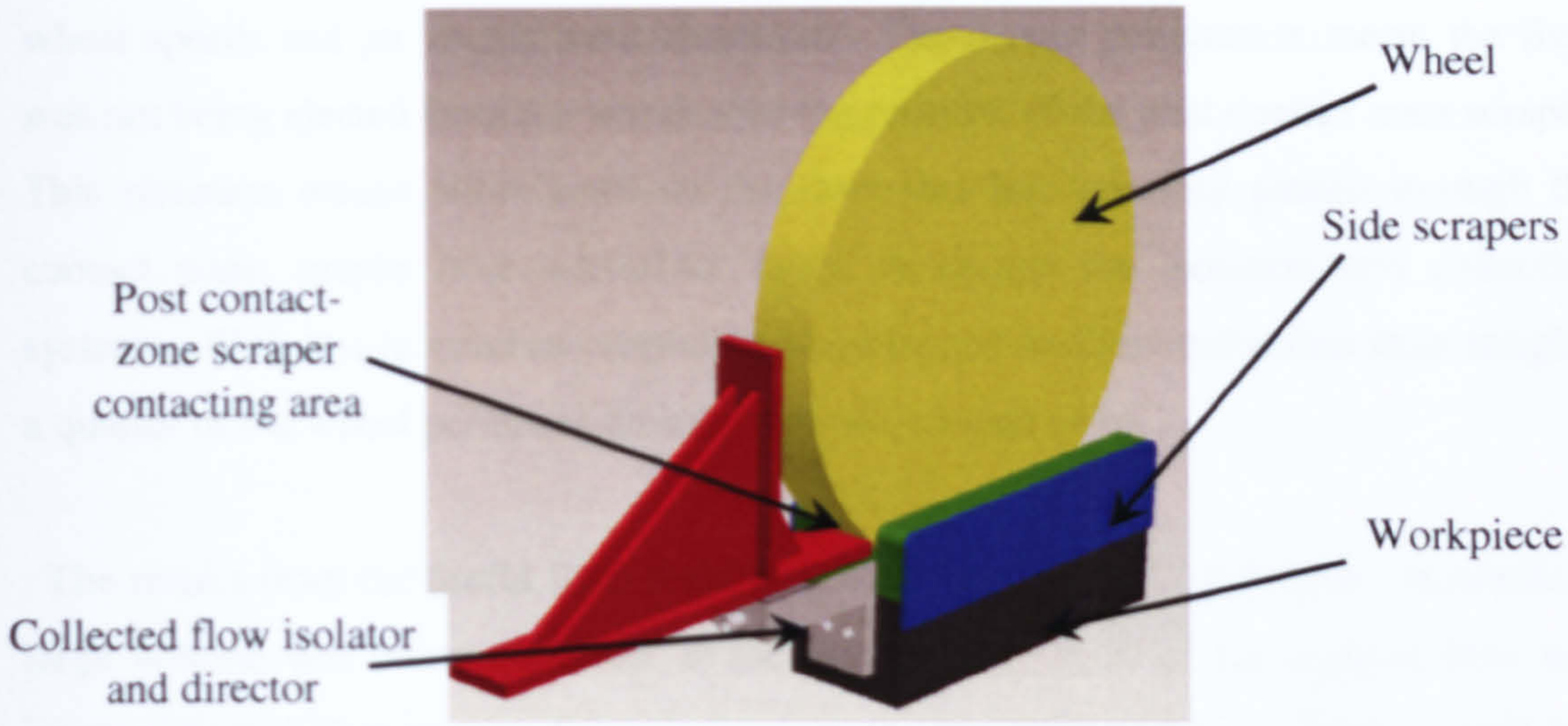

Figure 30, CAD representation of traverse grinding system for collector development Stage 2.

These design adaptations meant the wheel was capable of moving laterally relative to the side scrapers thereby allowing a basic traverse grind to be performed. The resulting system isolated the flow in such a way that it follows the path shown in Figure 31.

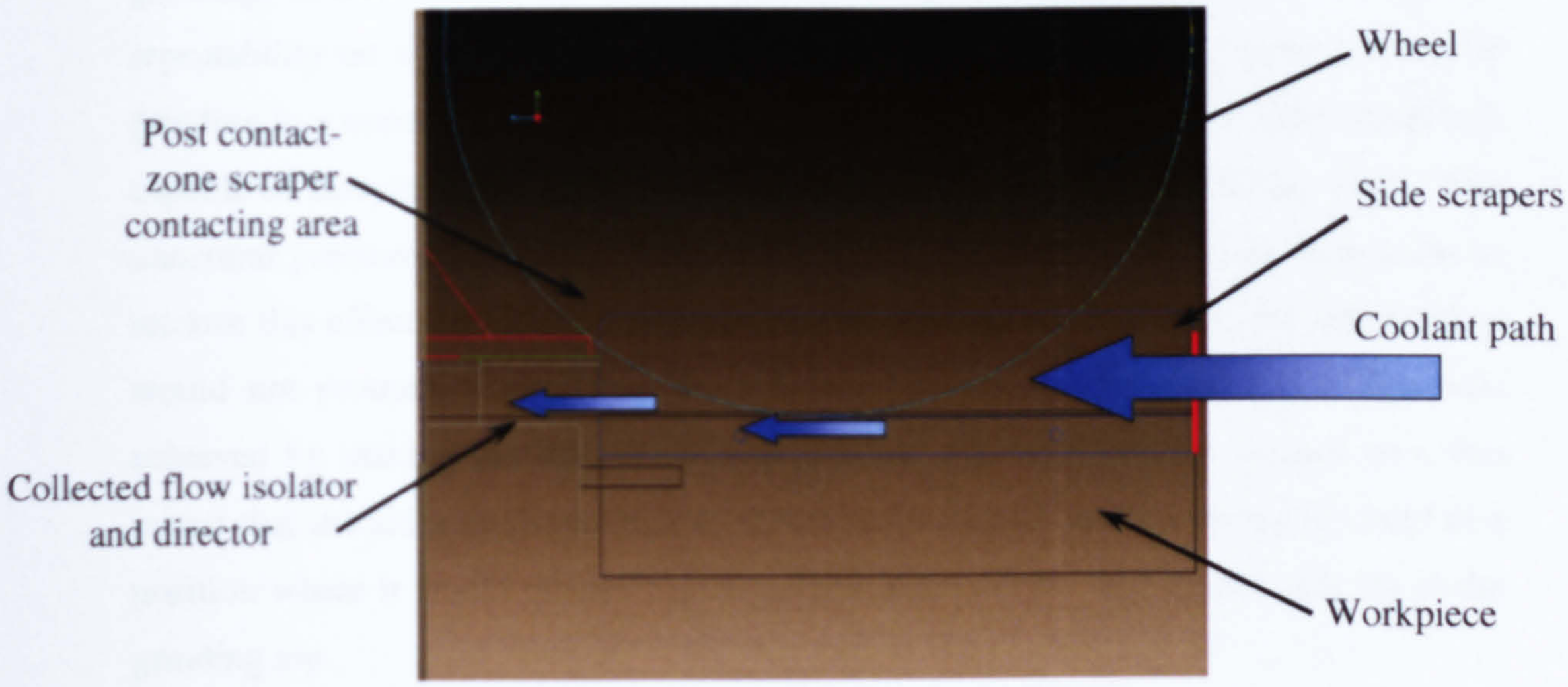

Figure 31, Path of fluid through collection system used in Development stage 2.

These tests provided some expected and unexpected results, these are discussed in full in regards to the useful flow in Chapter 7.4. The coolant was again extremely well directed as was expected, the use of the side scrapers and post-contact zone scraper worked well. It was visible that at faster wheel speeds the coolant was being ejected from the wheel further after the contact zone than previously suspected. It seemed that the grinding fluid had managed to penetrate further into the wheel when the higher

wheel speeds and jet speeds were employed. The deeper penetration meant the fluid was not being ejected from the wheel after the position of the post contact zone scraper. This situation would allow some of the flow that had possibly passed through the contact zone, maybe in a subsurface layer, to escape the isolation and collection systems. With this in mind an adaptation was planned to allow collection from roughly a quarter of the wheel periphery directly after the contact zone.

The results from the useful flow collection were satisfactory in principle. However, a large volume was being collected, at the highest over 80% of the applied flow was being collected after passing through the contact zone during the cut. It was found that with a high speed/high flowrate coolant jet aimed directly at the grinding nip, a significant ram pressure was being created at the inlet to the contact zone. This pressure was in part due to the side scrapers completely encompassing the area before and after the contact zone. This situation allowed a pressurised reservoir of fluid to form at the entrance to the grinding contact zone. Although this is a very useful occurrence when grinding, indeed almost an ideal situation, it was entirely unrealistic in terms of repeatability on a day-to-day industrial basis and would provide no understanding of grinding in a normal factory situation. However, the principle that the Altos wheel was capable of carrying such volumes of fluid proved extremely useful to the work. The unnatural pressure zone was not wanted in the actual grinding trials and so in order to remove this effect the isolation and scraping system was redesigned so the side barriers would not protrude further than the grinding contact zone at any time. This was achieved by making the side barriers part of the post contact zone scraper arm, this meant that the sides no longer had relative motion to the wheel, it would be fixed in a position where it would always hug the wheel and provide side barrier only up to the grinding nip.

The practicality of collecting for a fixed period was also an issue raised during this test. It proved awkward guaranteeing that collection of fluid only took place when a cut was being performed. This was because the isolator and scraping system were always attached and working to isolate and direct all flow passing through the contact zone. It was necessary during this test to start a grinding pass but wait approximately two seconds before collecting the fluid from the end of the system. This delay guaranteed that collection was taking place of only the flow that had passed through when a cut was

being performed and not of flow that was passing through the system before complete isolation had been achieved. This situation proved quite wasteful in terms of resources. A system was designed to automate the collection period thus overcoming this issue. This system utilised an optical sensor, a pneumatic valve, a rotary actuator, a control circuit and some design variations to the flow director. The optical sensor was mounted to trigger a pneumatic valve that changed an input to the actuator altering its state, this then mechanically redirected the flow to where it could be collected. This system allowed complete control of the timing of collection.

6.5 Collector Development Stage 3

It was at this stage that all the remaining systems were installed, tested and verified. This involved testing and proving the temperature sensing equipment, the dynamometer and the data acquisition apparatus.

The testing took place on the Abwood grinding machine using the Altos wheel which had a diameter of 186mm at the time. The Abwood had the facility to automatically traverse in the x-axis, this was controlled by a rather loose hydraulic valve. The valve required trial and error measurement in order to set it to run at a constant speed of 2 mm/s. Although quite slow it was necessary to run at this speed so sufficient flow could be collected for measurement. At this stage no formal testing took place of the collector system, although the developments were verified for its functionality by running grinding passes no testing was conducted in regards to a larger experimental design.

Fluid collection and measurement was undertaken using a channelling system and a collection chamber. The mass of the chamber was pre-measured so measurement of the collected fluid was by mass rather than volume. This removed the issue of frothing that is normally associated with a high speed wheel and coolant jet that would affect any measurement by volume. In order to guarantee this method the density of the coolant was established prior to testing. Although the coolant is nearly 90% water it was necessary to verify a true value of density for the mixture. The density of the grinding fluid mixture at the ambient temperature was found to be 991 kg/m^3.

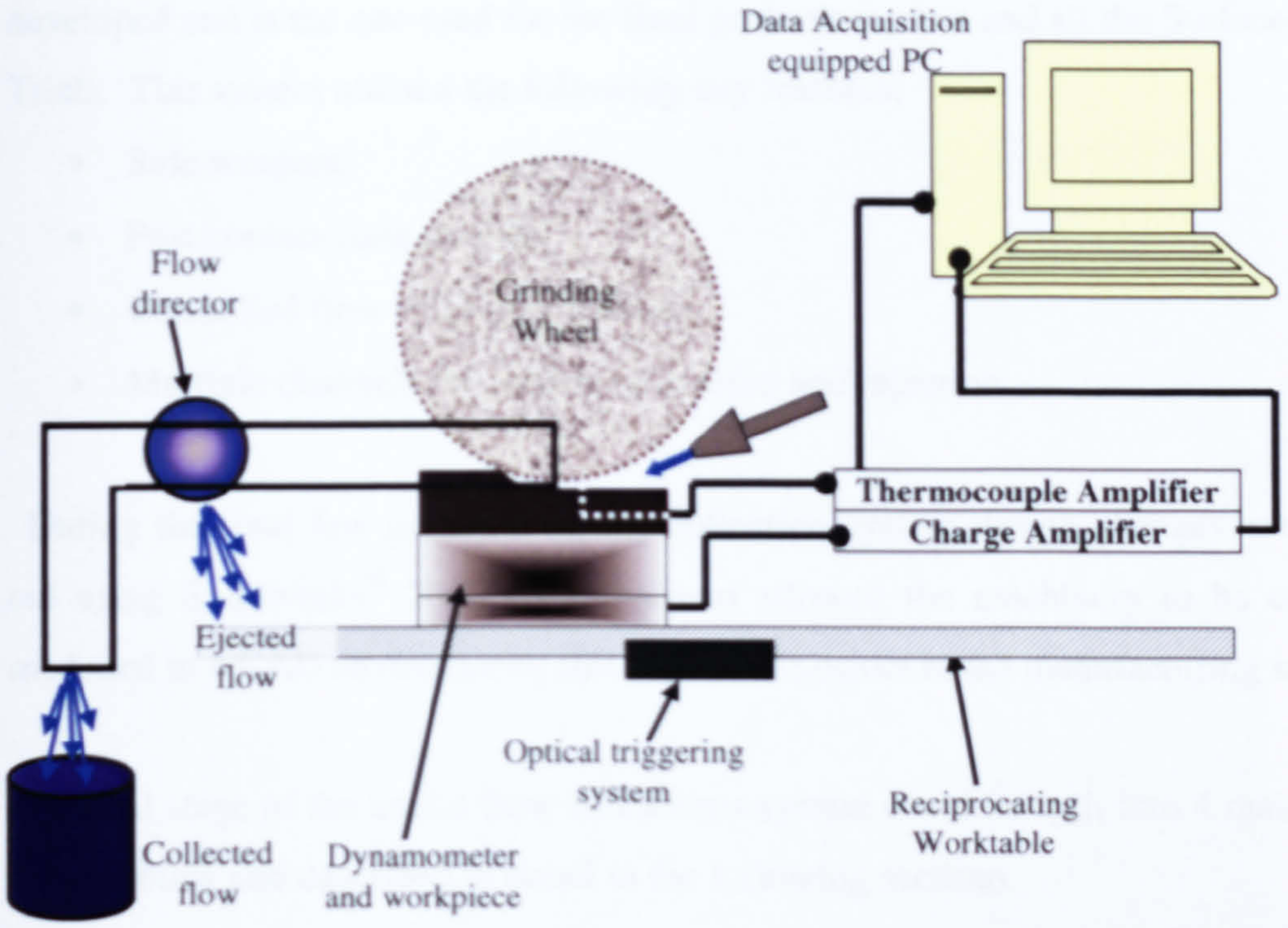

Figure 32, Schematic of experimental rig.

In terms of assessing the equipment nearly all sections were assessed and found to be at least satisfactory. Some cosmetic changes were decided upon for the final design and are listed below.

1. An expansion of the fluid channel through the director.
2. Tighter tolerances on the scraper system to improve alignment to the wheel.
3. Location from a machined face of the wheel guard.
4. A more controllable optical interrupter would be preferable.

It was decided that it was desirable to test over a wider speed range than possible with the Abwood machine. Therefore the decision was made to transfer the project to the new Jones and Shipman Dominator surface grinding machine. In transferring to the new machine most parts had to go through minor design alterations. No new methodologies were necessary in transferring the collector to the new machine.

6.6 Collector Final Design

In line with the developments of the preliminary tests a final design was achieved during the fifth generation of the useful flow device. This iteration was considered fully

developed and is the one used for the final preliminary test and all the Surface Grinding Trials. This system utilised the following key features;

- Side scrapers.
- Post contact zone scraper.
- Controlled flow collection period.
- Multiple channels for collection of fluid and rejection.

During the final few iterations of the collection system design changes were carried out using Solidworks© 2006. This system allowed the machinery to be completely modelled in a CAD environment; this limited the errors in the manufacturing stages.

The final stage of the useful flow collections system could be split into 4 main sections defined blow and described in detail in the following sections.

- Flow isolating system
- Collected flow director with actuator
- Optical trigger with circuit
- Channelling system

6.6.1 Flow Isolating System

The scraping system included the use of side scrapers, post contact zone scrapers and location geometry features. The side scrapers and post contact zone scraper used the same principles developed for the design used in Preliminary test 2. This involved forming a sealed channel for all flow that passes through the grinding contact zone (see Figure 33). The side scrapers covered the sides of the wheel and the side of the workpiece, they were designed to cover roughly 5 mm below the workpiece face. The sides were made from aluminium so there was some flexure possible in the fit. The insides of the scrapers were covered with a sponge so that there was no metal-on-metal contact to add to the power requirements of the system. The first stages of testing had utilised a black foam that had proven useful in previous tests, this material was highly flexible and easily adhered to the aluminium. However, this substance had a tendency to tear at wheel speeds above 35 m/s. For the higher wheel speeds of the main body of testing this was not satisfactory. For these tests a silicon sponge was used that allowed minimal contact friction and did not tear under when exposed to large shearing forces. The used of this sponge required pre-treatment to increase the surface energy of the

metallic surfaces. A post contact zone scraper was used at a position of 90° passed the grinding contact zone. This post contact zone scraper used the foam as a barrier.

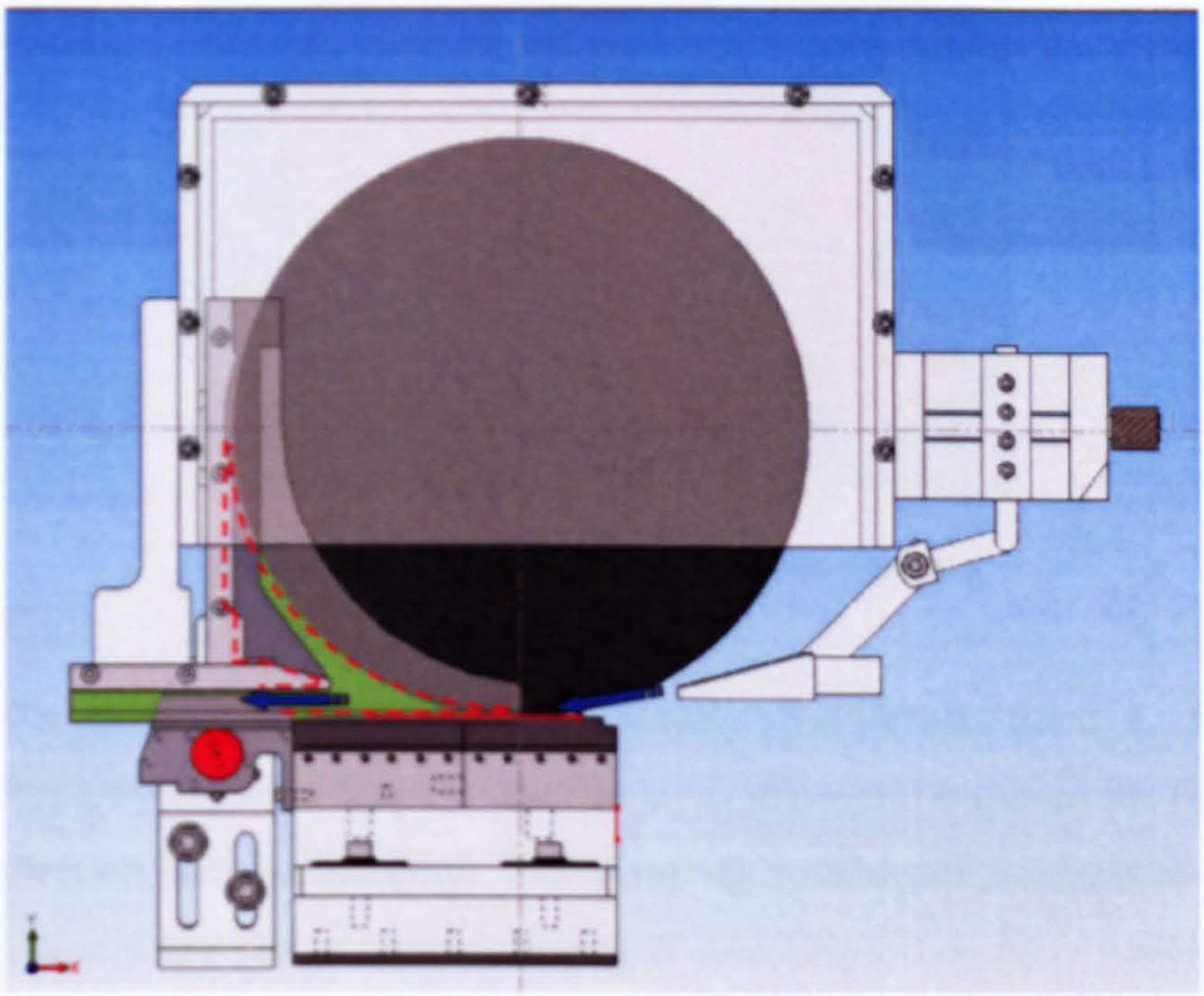

Figure 33, CAD drawing showing scraper positioning, fluid flow direction and the physical boundaries employed to isolate the grinding contact zone flow.

The fluid scrapers for this system required accurate positioning relative to the wheel. To do this a wheel guard was manufactured to replace the original. The new guard had several ground faces each with a flatness tolerance of 20 μm, further to this a squareness tolerance of 20 μm was necessary between the wheel front face and the guard end face. The scraper was mounted to the left face and thus the two ground surfaces were held together.

6.6.2 Flow Director Control Valve

With the scraping system isolating the grinding zone flow from the rejected flow, a flow director was required to control the start and the duration of the collection period. A device was designed and manufactured that was attached to the end of the workpiece that would direct the flow away from the workpiece. This flow was forced into a channel with two exits, one that expels fluid back into the machine coolant handling systems and one that directs fluid into a channelling system for collection and analysis. The control of the flow direction was achieved using a rotating valve similar in concept to the Thames Barrier employed in London, UK. This valve can be seen in Figure 34.

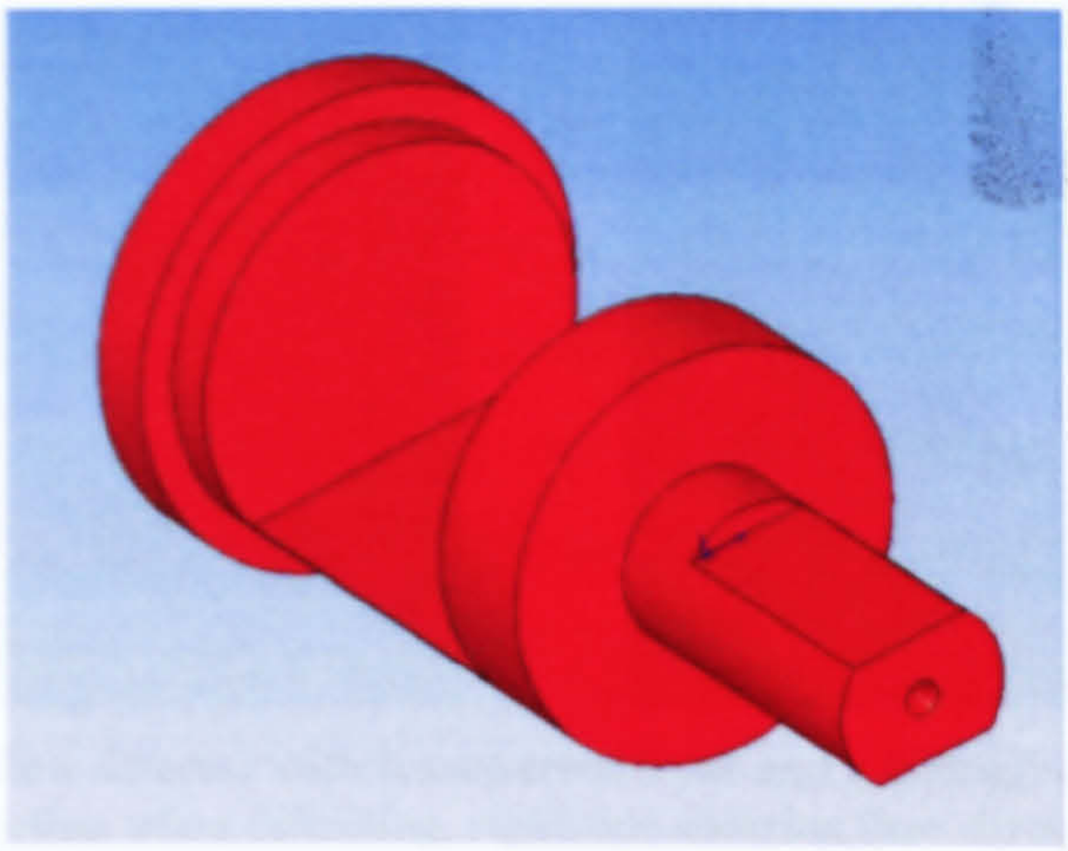

Figure 34, Representation of flow control valve.

The need for a device like this was noticed early in preliminary test 1. However, it was only after Development Stage 2 that the level of control required for the timing of the flow collection became essential. The scraping system was transient in its abilities to isolate flow regimes and at certain times and positions it was not a sealed system; at these times any flow passing through the valve could not be guaranteed as having passed only through the grinding contact zone. Accounting for these errors in real time meant designing both a controlling sensor mechanism and a form of valve to control the flow direction. The flow director is depicted in Figure 35. The open and close positions can be seen in Figure 36. The director was made from mild steel as the material composition was not of great importance, there are minimal loads on this part and any contact mechanics require the director to remain un-deformed. The valve was made from a self-lubricating bronze, which was machined to a tight fit within the director but would wear in relation to the steel director to form the required seal.

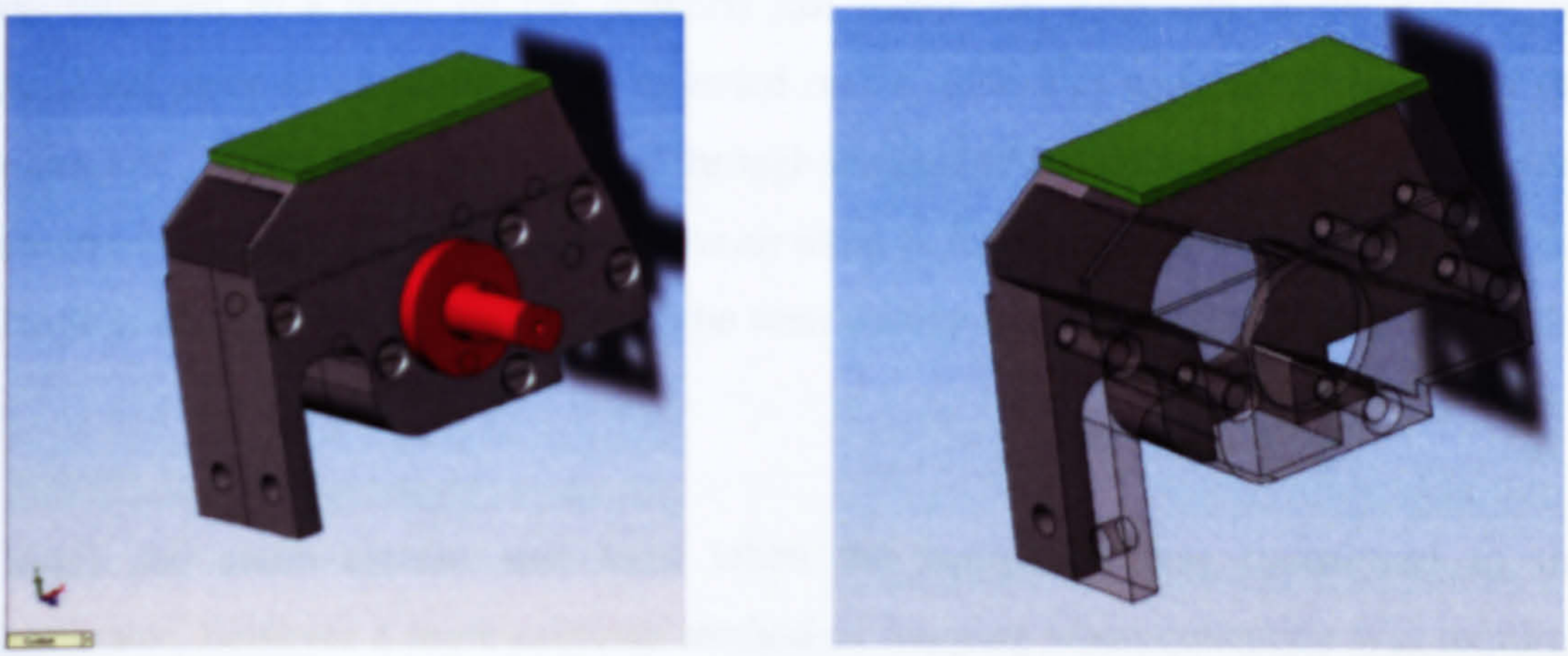

Figure 35, CAD drawing of flow director; left showing solid with valve, right showing only the director with a transparent front face to show the internal structure.

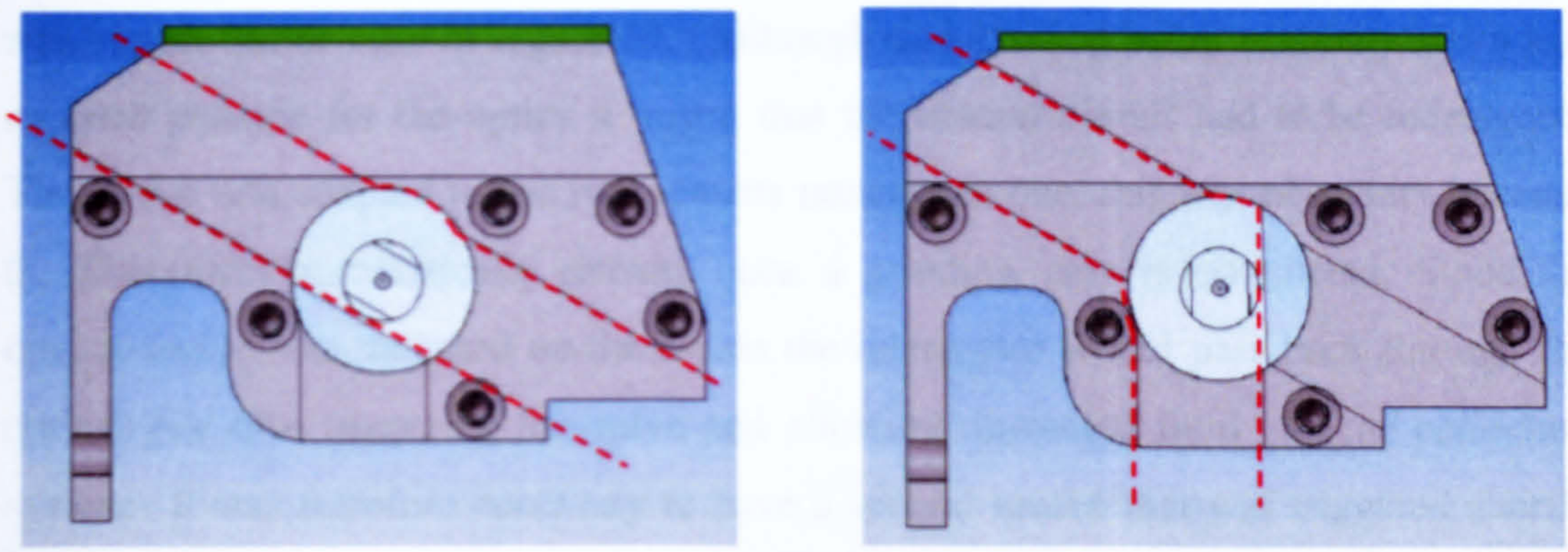

Figure 36, Side view of flow director with transparent front and a highlighted fluid path, left image showing flow direction when collecting, right side showing flow direction for rejection.

As the valve was essentially a rotating pivot, a device was required to rotate the barrier into the open and close positions. This was achieved using an SMC rotary actuator (type CDRB1BWU30-180S-R73L) mounted onto a stand with a coupling between the actuator and the barrier. This single vane system used two pneumatic inputs to allow up to a 180° rotation on the output shaft. With the use of two mechanical stoppers the actuator could be set to move between the two required positions. The shaft was coupled to the valve, housed within the director, thereby controlling the direction of flow out of the director. In order to control the rotary actuator some form of triggering system with a control circuit was required.

6.6.3 Optical Trigger and Control Circuit

The control of when the actuator collected and rejected the flow required some sort of logical triggering. This was firstly achieved using a simple optical switch in conjunction with a basic control circuit. The optical switch was fixed on a bracket that was mounted to a point on the Abwood just below the slide-way of the x-axis. A machined piece of aluminium was mounted on the slide-way and thus moved with the workpiece. As the aluminium passed through the gate of the optical switch a signal was sent to a pneumatic valve that altered the air input to the rotary actuator and changed the direction of fluid flow. The logic can be seen clearly in the flow diagram in Appendix C.

Much the same system was used when the equipment was transferred to the Dominator, however a more accurate method of flagging when collection was required was developed. This adaptation involved the use of an interrupter blade mounted to a rig at the back of the machine that was attached to the x-axis. The upgraded locating

mechanism can be seen in Figure 37. Although this allowed better accuracy and a less exposed position for the optics it meant that the control circuit had to be redesigned. The circuit was adapted to use two sensors rather than one, this was necessary because the Dominator automatically retracts once a grinding pass is completed. Since the optical sensors are mounted on the x-axis the interrupter would pass back through the optical gate thus triggering the valve and allowing unwanted fluid into the collection system. It was therefore necessary to have a second sensor that was triggered shortly after the grinding pass was finished. The sensor trips the circuit and locks the valve in its default 'rejecting flow' position.

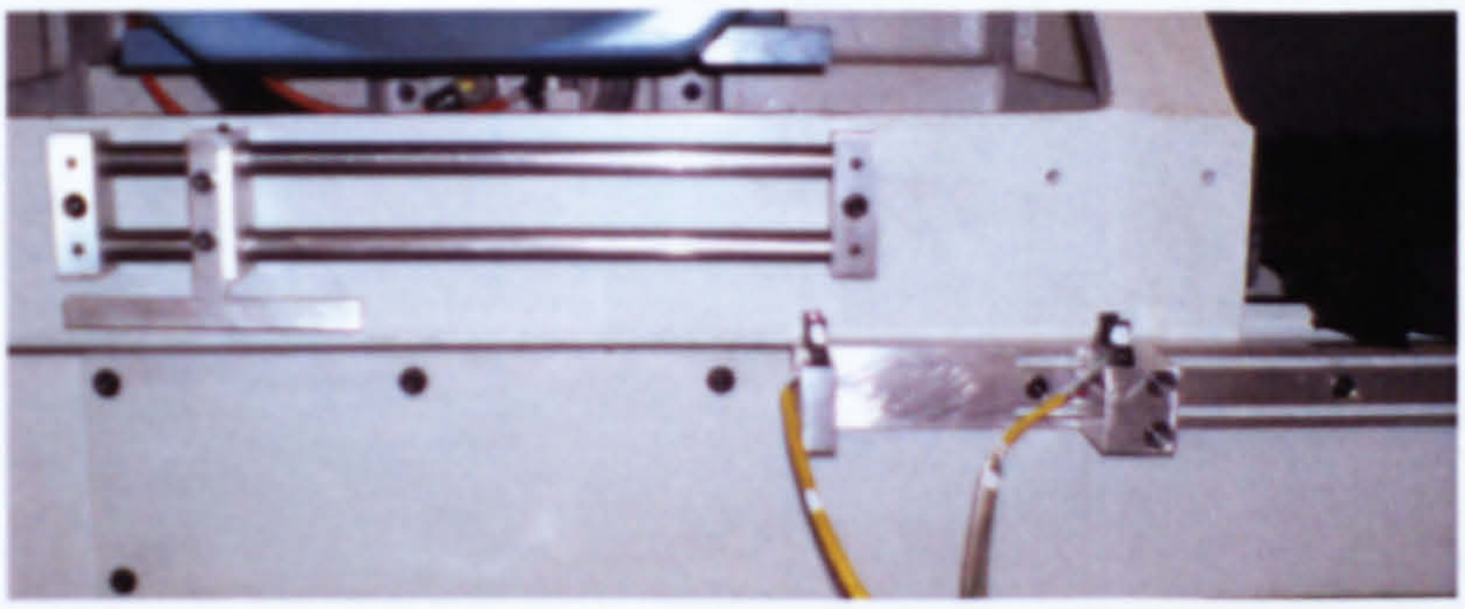

Figure 37, Optical triggering system for the flow director.

6.6.4 Channelling System

Once the grinding zone flow was separated from the rejected flow it was necessary to channel it away to a point where it was contained. This was done with a channel of plastic pipes connected to a container. On the Abwood this system took the flow outside of the machine housing. On the Dominator the flow system and collection was kept inside the housing. This was unavoidable as the Dominator employed a closed guard system where grinding could not take place without the machine guard closed and locked in place. The collection container was separated from the pipe network by a quick-lock junction, this allowed easy access and water-tight connections. Several junctions existed between the interconnected parts; flow director to pipe, pipe to container, these were all sealed using an instant gasket mixture. The use of this material allowed the system a certain amount of flexibility that was beneficial as grinding passes accumulated. Once a pass had been performed and fluid collected the flow container could be detached and taken away for measurement.

As can be seen in Figure 38, the final system employed several methodologies developed from the preliminary testing and some adapted from previous work. The

amalgamation proved highly effective when coupled with a sophisticated sensor array and a suitable grinding rig.

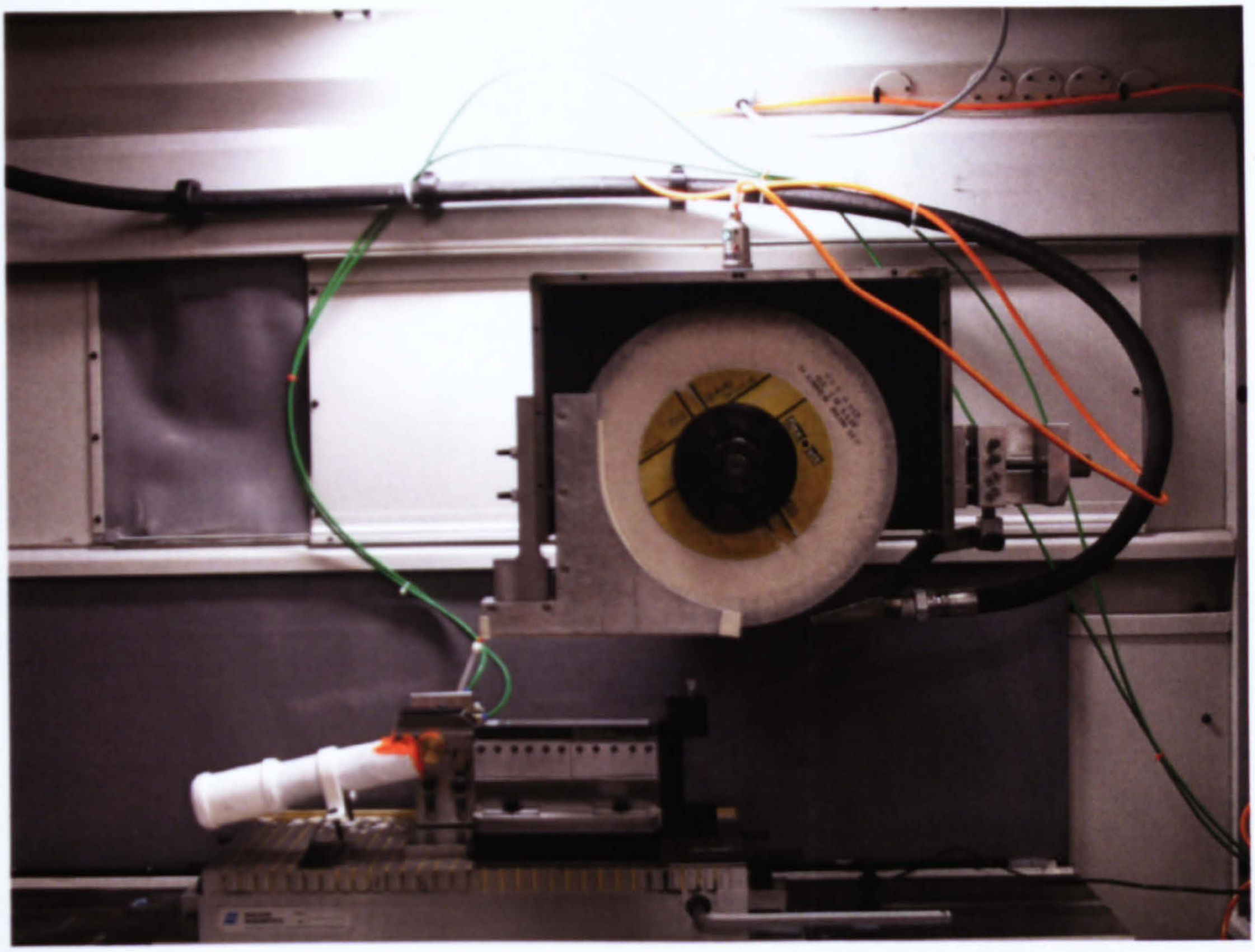

Figure 38, Picture of useful flow collection system in-situ on the Jones and Shipman Dominator surface grinding machine.

The fully developed useful flow system has also seen some adaptation for use in external cylindrical plunge grinding processes. Although this thesis does not involve cylindrical processes the project this work was part of has a vested interest in the development to cylindrical processes.

Chapter 7. Surface Grinding Trials

7.1 Introduction

The main body of testing was conducted to analyse the effects of useful and to verify and assist in the development of a method of useful flow prediction. This section of the project was split into several parts. The chapter begins with a discussion of useful flow and how it is affected by various parameters. These tests were only possible due to the development of the collection device described in Chapter 6. Discussion then moves on to how the amount of useful flow affects the performance of certain process characteristics. Grinding trials were conducted using standard full factorial methods along with a fractional factorial test using Taguchi methodology. The tests discussed within this chapter were previously summarised in Chapter 5 under the headings Preliminary Test 2, Preliminary Test 3, Abwood speed ratio test, Dominator speed ratio test, Jet flowrate/speed test and the Taguchi Trial. It is worth noting that Preliminary Test 2 is separated from the main body of discussion within this chapter. Although some interesting results were found the issue of the side scrapers clouds the ability to compare and analyse results.

The work then moves towards analysing the volume of collected flow and how this can be predicted in order to reduce applied flow volumes and improve the effectiveness of fluid application.

7.2 Aim

The aim of the main body of testing within this chapter was to both validate theory and to develop further understanding of the effect certain parameters have on useful flow and how these values can be manipulated to increase or decrease useful flow values.

7.3 Specific Objectives

During the grinding trials the objectives were as follows:

- Measure useful flow.
- Analyse how the useful flow is affected by the programmed parameters.
    - Programme parameters are defined as wheel speed, jet speed, jet flowrate and workpiece type.
- Analyse how the useful flow affects the process outcomes.
    - Measure and record power, acoustic emission, actual depth of cut and temperature.

7.4 Preliminary Test 2

Several of the development stages of testing involved fluid capture in various situations. Once the capture device had reached the level of maturity where it was capable of providing reliable and repeatable results the findings could be addressed completely. However, just prior to this stage the collector had the design characteristic of providing too much cover to the area before the contact zone. This situation pushed the useful flowrate above what could be sensibly expected. The reason for these large values of useful flow could not be replicated in production and as such provided only theoretical insight rather than true guidance to industry. Although not useful for the longer term interests of this project, the effects of this situation have proved interesting and are therefore discussed within this chapter.

Preliminary Test 2 was planned to allow various ratios of wheel speed to jet speed to be tested. As mentioned previously there is an expectation that a relationship exists but as yet this correlation is unproven. This experiment was designed so that a total of 20 tests were performed, a broad range of values were selected. Five wheel speeds were chosen for analysis based on the known limits for both the Abwood grinding machine and the Altos grinding wheel. The experimental plan is shown in Table 15.

Prior to each experiment the workpiece was machined so a constant starting surface was assured. This was done by performing two cuts with a programmed depth of cut of 5 μm each with full coolant at a wheel speed of 2000 rpm. Where a clean constant surface was not visibly achieved this step was repeated. The coolant delivery flowrate was varied at the pump to give four variations of jet speed at given wheel speeds. Dressing was performed to give an open wheel structure. A full experimental specification can be seen in Table 15.

Wheel speed, v_s (m/s)		Jet speed, v_j (m/s)		Supply flowrate, Q_d (l/min)	Ratio (v_j/v_s)
1	24.6	1	18.9	11.4	*0.77*
1	24.6	2	28.4	17.0	*1.15*
1	24.6	3	35.3	21.2	*1.44*
1	24.6	4	40.4	24.2	*1.64*
2	29.5	1	18.9	11.4	*0.64*
2	29.5	2	28.4	17.0	*0.96*
2	29.5	3	35.3	21.2	*1.20*
2	29.5	4	40.4	24.2	*1.37*
3	34.5	1	18.9	11.4	*0.55*
3	34.5	2	28.4	17.0	*0.82*
3	34.5	3	35.3	21.2	*1.03*
3	34.5	4	40.4	24.2	*1.17*
4	39.4	2	28.4	17.0	*0.72*
4	39.4	3	35.3	21.2	*0.90*
4	39.4	4	40.4	24.2	*1.03*
4	39.4	5	45.4	27.3	*1.15*
5	45.3	3	35.3	21.2	*0.78*
5	45.3	4	40.4	24.2	*0.89*
5	45.3	5	45.4	27.3	*1.00*
5	45.3	7	53.6	32.2	*1.18*

Table 15, Experimental plan for Preliminary Test 2, conducted on the Abwood grinding machine using the Altos grinding wheel.

Figure 39 showed that the collected flowrate (or useful flowrate) increased with jet speed. The increasing useful flowrate tended to level off at higher jet speed, this is likely to be due to the fluid being increasingly rejected from the entry zone when the jet speed is in excess of wheel speed. It was argued by Gviniashvili (2003) that under these conditions jet momentum is being used to drive the wheel. There is an exchange of momentum associated with the change in direction of the rejected flow.

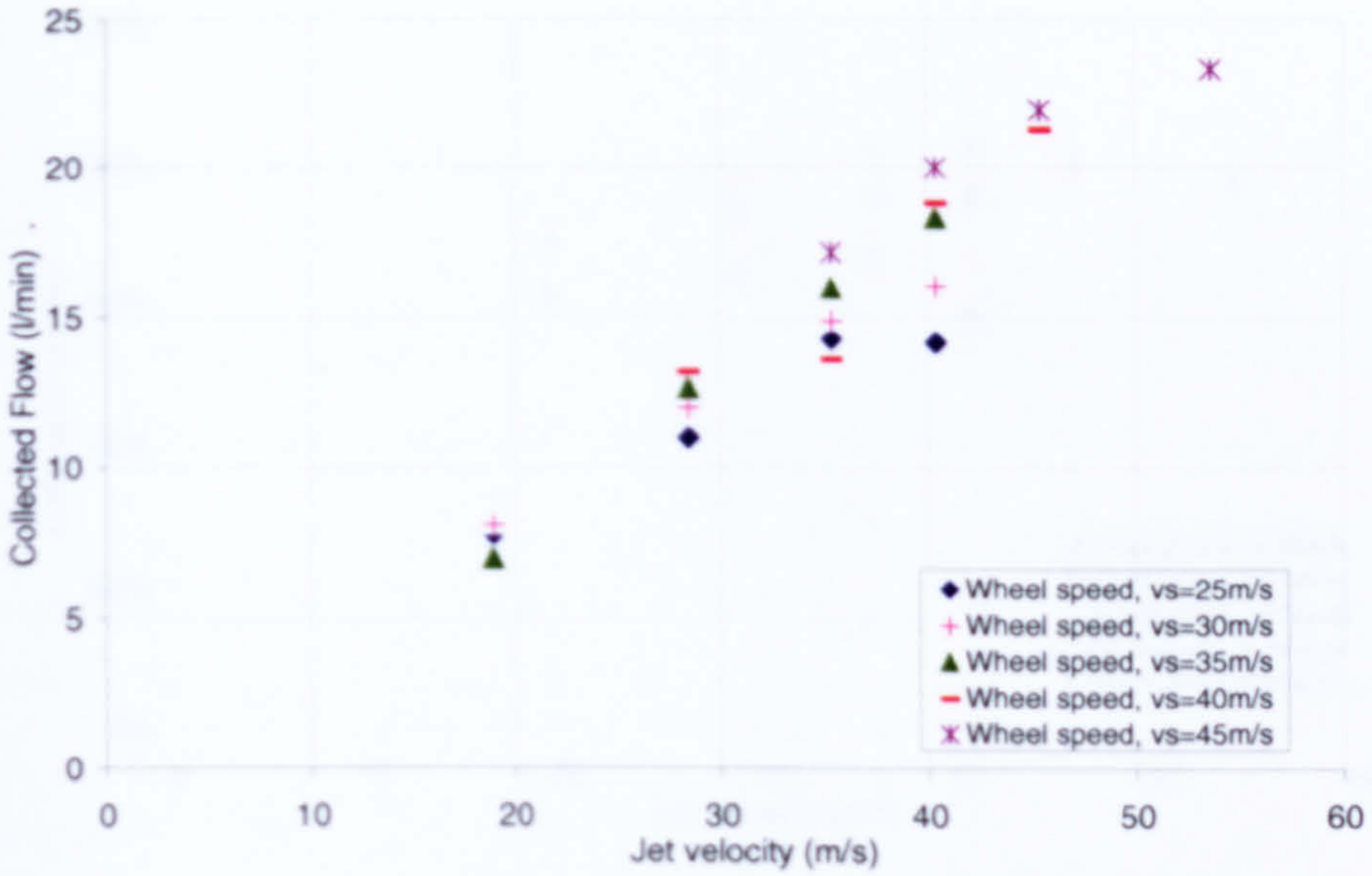

Figure 39, Collected flowrate versus jet speed at various wheel speeds for Preliminary Test 2.

Figure 40 shows the useful flow as a percentage of the applied flow. Percentage useful flow is a rather more abstract parameter than useful flowrate. Useful flow or percentage useful flow is a function of the applied flow and as such gives a good indicator of the amount of rejected flow from a system. It can be stated that the percentage useful flow has a higher dependency on parameters such as wheel speed, jet speed, nozzle flowrate and nozzle position. The interpretation of percentage useful flow is therefore more difficult than the interpretation of actual useful flowrate. The applicability of percentage useful flow as indicative of the effectiveness of fluid delivery or of the usefulness for grinding performance is also more difficult. It is possible to maximise percentage useful flow and find that actual useful flowrate is less than could be achieved with a higher nozzle flowrate, a higher jet speed or with a higher wheel speed. The interpretation of percentage useful flow remains ambiguous except where nozzle flowrate remains constant. It appears to measure effectiveness of fluid delivery but does not measure actual useful flow which differs for different supply flowrates. The true effectiveness of a system would be dependant on both the percentage useful flow and the useful flowrate. For a truly efficient system the percentage useful flow would need to be maximised and the useful flow would need to be optimised.

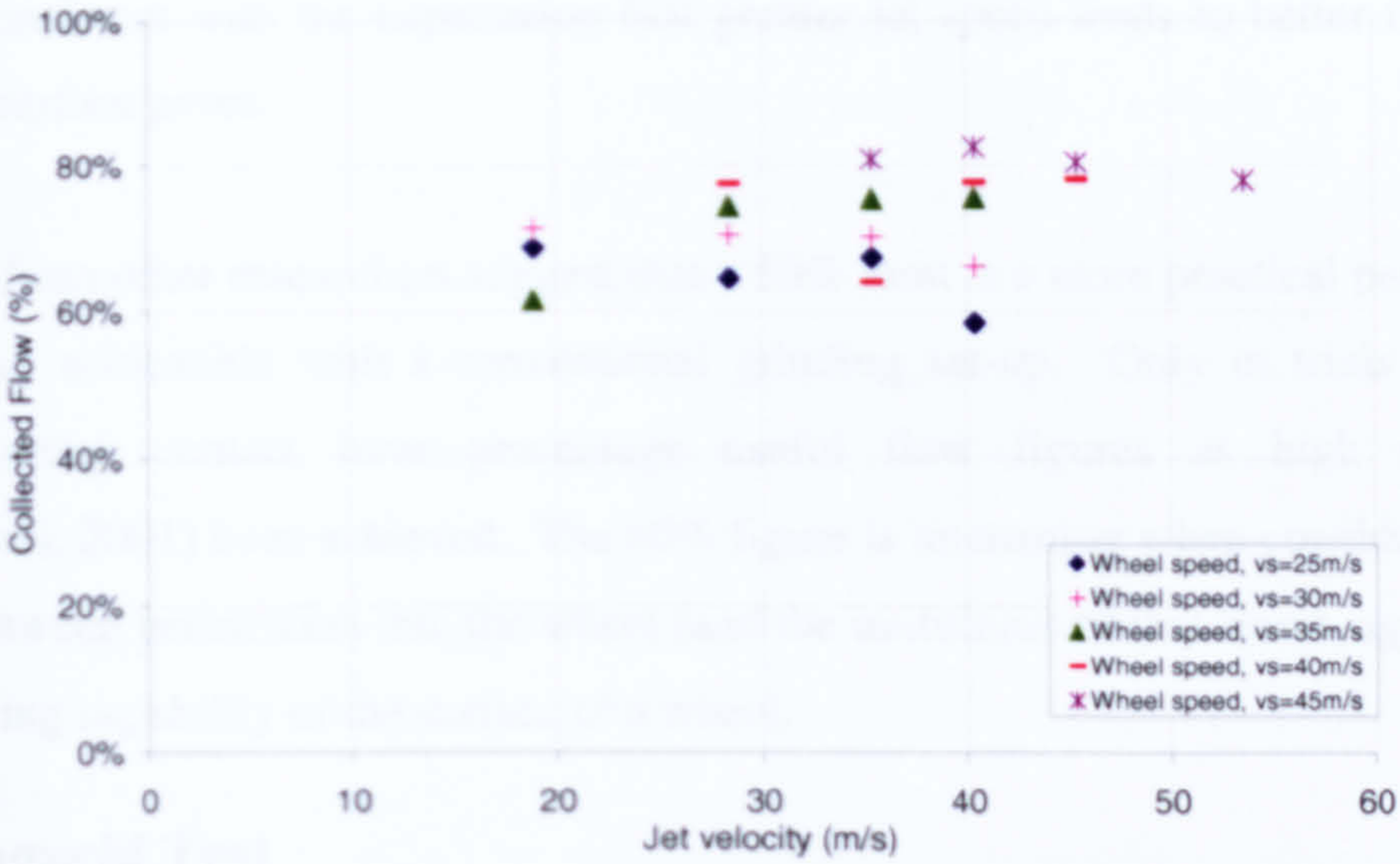

Figure 40, Percentage collected flow versus jet speed at various wheel speeds for Preliminary Test 2.

The results in Figure 40 showed collection of up to 80% of the applied flow. It was reasoned that this high percentage useful flow occurred because the side plates restricted the sideways escape of fluid from the grinding nip. In other words the volume of fluid rejected was reduced, as indicated by the high percentage useful flow. This might well be an advantage for fluid delivery but the use of side plates that extend alongside the entry region is considered to be impracticable in general grinding practice. There has been no precedent for this level of collection in a real grinding process without side plates of this geometry surrounding the entry region. The isolation system was known to be functioning adequately, and although this was not the final design it had most of the major principles employed and was capable of isolating and collecting the useful flow. The Altos wheel employed in this test had been designed to be extremely porous and allow vast quantities of fluid to be transmitted. This result has not been used for direct comparison to the other jet speed/wheel speed tests as the method of varying the jet speed does not provide sufficient isolation between the two influential factors of supply flowrate and jet speed. This does not detract from the relevance of the volume of the fluid that was transmitted through the grinding zone.

There is an approximately linear portion at lower jet speeds. The slopes of the linear portions increase with wheel speed. These results are consistent with measurements by Gviniashvili and are also consistent with the hypothesis that useful flow depends on the wheel surface flow pumped by the wheel pores. This follows since the surface flow is expected to increase with wheel speed. The fact that useful flow increases with jet

speed is consistent with the expectation that greater jet speed leads to better filling of the wheel surface pores.

Findings from other researchers suggest that a 50% limit is a more practical percentage useful flow, achievable with a conventional grinding set-up. Only in trials without actual grinding contact have percentage useful flow figures as high as 80% (Gviniashvili, 2001) been achieved. The 80% figure is interesting when considering the balance between penetration into the wheel (and the usefulness of that flow), against the fluid carrying capability of the surface of a wheel.

7.5 Taguchi Test

In analysing the effects of the input parameters it was necessary to conduct tests that account for as many variables as possible. The intention of this type of test was to eliminate the need to fully test parameters that were found to be ineffectual on useful flowrate. As grinding is such a complex process ten parameters were identified as possibly influential on the volume of flow that passes through the grinding zone. To do a full factorial test on ten parameters at only two levels would take 2^{10} tests = 1024 tests. With this in mind a fractional factorial approach was utilised in order to include as many parameters as feasible in a test designed to see which had the most significant influence. A fractional factorial approach allows qualitative results only. Analysis, research and discussion led to the identification of seven key parameters that could be assessed using the resources available. These can be seen in Table 16 below.

	Parameter	Level		
		1		2
A	Material Type	O1	------	Mild Steel
B	Nozzle position	Near	------	Far
C	Jet Velocity	50 m/s	------	10 m/s
D	Dressing condition	Coarse	------	Fine
E	Work piece surface speed	2 mm/s	------	10 mm/s
F	Wheel surface speed	35 m/s	------	65 m/s
G	Engagement, Actual depth of cut	6 µm	------	40 µm

Table 16, Parameters and level designations for the Taguchi test.

An L^2_{16} orthogonal array was identified as being suitable as it allowed enough space to measure all seven parameters along with several interactions between the parameters with some remaining columns for error estimation (columns 5, 10 and 14). Each parameter is tested at two levels, 'High' and 'Low'. These values should represent the extreme ends of the range of values a parameter can be, at each extreme it should be

expected that the measured parameter will be affected. Unfortunately this also has to take into account what is feasible with the equipment available. It can be seen from the array in **Error! Reference source not found.** that columns 3, 6, 9, 12 and 15 have been assigned interactions, these interactions have been assessed as relevant to the testing and analysis of either the useful flow directly or the other process outputs. One of the key interactions is represented in column 15, this is the interaction between the wheel speed and the jet speed, this has been discussed previously by this author and others but no proof beyond personal knowledge and experience has been forwarded regarding this issue. By including the interaction effect this should prove that the combined effect of the two parameters does directly influence the useful flow.

	Grinding Experiment															
	A	B	ExF	C	n	BxC	D	E	CxG	n	F	DxF	G	n	CxF	
	Column No.															Test Run
Trial No.	1	2	3	4	5	6	7	8	9	10	11	12	13	14	15	i ii
1	1	1	1	1	1	1	1	1	1	1	1	1	1	1	1	1
2	1	1	1	1	1	1	1	2	2	2	2	2	2	2	2	2
3	1	1	1	2	2	2	2	1	1	1	1	2	2	2	2	3
4	1	1	1	2	2	2	2	2	2	2	2	1	1	1	1	4
5	1	2	2	1	1	2	2	1	1	2	2	1	1	2	2	5
6	1	2	2	1	1	2	2	2	2	1	1	2	2	1	1	6
7	1	2	2	2	2	1	1	1	1	2	2	2	2	1	1	7
8	1	2	2	2	2	1	1	2	2	1	1	1	1	2	2	8
9	2	1	2	1	2	1	2	1	2	1	2	1	2	1	2	9
10	2	1	2	1	2	1	2	2	1	2	1	2	1	2	1	10
11	2	1	2	2	1	2	1	1	2	1	2	2	1	2	1	11
12	2	1	2	2	1	2	1	2	1	2	1	1	2	1	2	12
13	2	2	1	1	2	2	1	1	2	2	1	1	2	2	1	13
14	2	2	1	1	2	2	1	2	1	1	2	2	1	1	2	14
15	2	2	1	2	1	1	2	1	2	2	1	2	1	1	2	15
16	2	2	1	2	1	1	2	2	1	1	2	1	2	2	1	16

Table 17, Table showing the experimental layout for a '2' level 16 factor orthogonal array.

Finally some post-testing analysis is performed to analyse the validity of the results, this is in the form of a confidence test. This type of test allows the user to allocate a level of confidence to a result, where this value represents an estimate of the strength that an effect has on the analysed output.

7.5.1 Results

Analysis of a test such as this can be most easily viewed via direct effects charts. This type of chart is designed to show visually which parameter has the strongest effect on what is being measuring, this is shown by the longest line/steepest gradient. Further to this the signal to noise ratio can be plotted to show the clarity of the indicator.

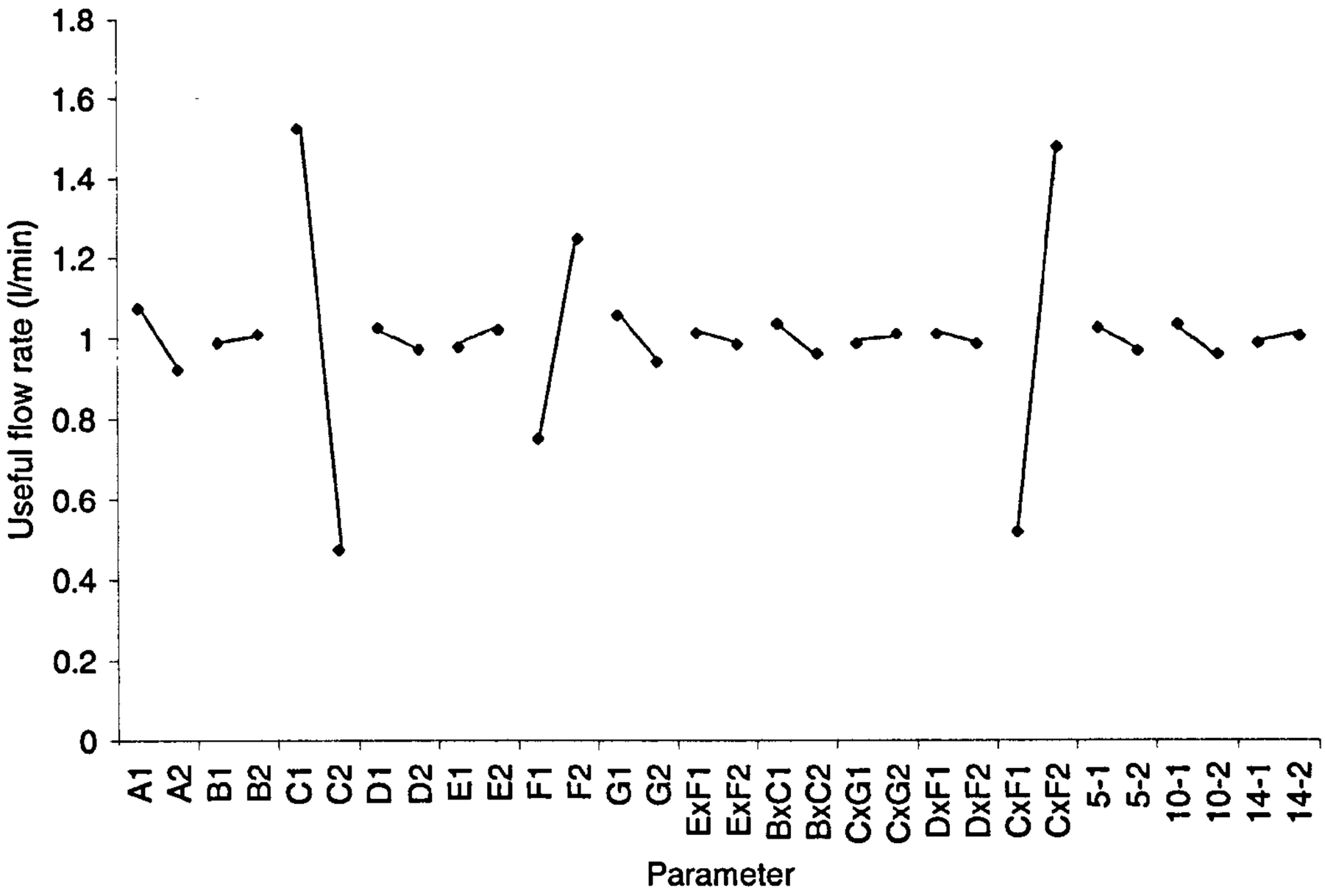

Figure 41, Direct effect chart for useful flowrate. A = Material Type, B = Nozzle position, C = Jet Speed, D = Dressing condition, E = Work piece surface speed, F = Wheel surface speed and G = Engagement, Actual depth of cut.

What can be seen clearly from Figure 41 is the strong effect, signified by the long line, corresponding to the C parameter, jet speed, and another strong effect in the F parameter column, wheel speed. What can also be clearly seen is that the interaction between these two parameters has an equally strong effect. It can also be seen from Figure 41 that columns 5, 10 and 14 that were assigned no parameters show minimal variation, these columns can be used for error checking and the small lines/shallow gradients prove the residual effects within the analysis are small. By examining the results it can be seen that the highest volume of useful flow was passed through the contact zone when the jet speed was high (C1) and the wheel speed was high (F2). It can also be said that neither the material type, nozzle position, dressing condition, workpiece surface speed or depth of cut had a strong effect on the useful flowrate. It is worth noting that the range of nozzle position was somewhat limited by the internal mechanisms within the Dominator grinding machine. With this in mind the conclusions on the effect of the nozzle position come with a proviso that when the nozzle is within 10 cm of the wheel surface any variation will have little effect at jet speeds greater than 10 m/s and supply flowrates greater than 4 l/min. This assumption of minimal effect may not be true when the nozzle is moved appreciably further away. Indeed it has been shown by Baines-Jones (2007) within AMTReL on a related project that large nozzle distances from the

grinding contact are detrimental. Therefore distances much larger than 10 cm need to be accompanied by a suitably optimised 'coherent' nozzle arrangement.

Using these results an ANOVA table was constructed, this allowed the author to run a confidence check using an F-ratio test, the results of which can be seen in Table 18. For a 95 % confidence level the F-ratio needs to be above 10.1, it can be seen that for parameters C, F and CxF the confidence levels are adequate. Another possibly notable effect appears to be visible in column A, the material type. This however shows only a slight effect and when combined with only a 90 % confidence interval it can be viewed as possibly anomalous.

Source	SS	v	V	F
A	0.18262	1	0.182623	7.35
B	0.00364	1	0.003638	0.15
C	8.79309	1	8.793088	353.74
D	0.02267	1	0.022673	0.91
E	0.01625	1	0.01625	0.65
F	1.95429	1	1.954287	78.62
G	0.10765	1	0.10765	4.33
EF	0.00710	1	0.007102	0.29
BC	0.04611	1	0.046114	1.86
CG	0.00445	1	0.004453	0.18
DF	0.00451	1	0.00451	0.18
CF	7.36230	1	7.362304	296.18
e	0.07457	3	0.024858	
T	18.57927	15		

Table 18, ANOVA table for the useful flowrate results, where SS is the Sum of the Squares for each variable, *v* is the degrees of freedom, V is the variance, represents errors as a factor and F is the value from the F-test.

Examining the interaction CxF further in Figure 42 shows the non-parallel lines that signify a definite relationship between the two parameters. A cross-over of the lines provides definitive proof but the sharp gradients are enough to validate the trend. It can also be more clearly seen that the highest useful flowrate is indeed at C1F2, high jet speed and high wheel speed.

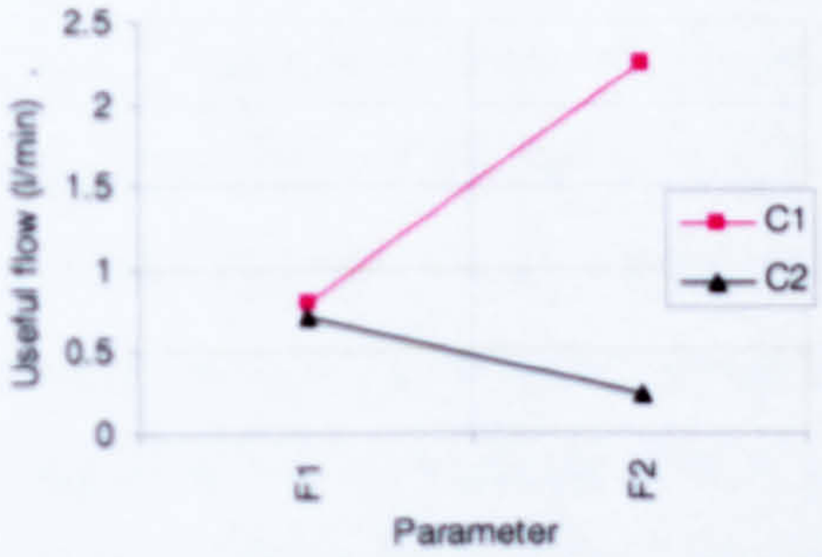

Figure 42, Interaction chart of the useful flowrate showing Jet speed, C and wheel speed, F.

A direct effects chart can also be plotted for the percentage useful flow as in Figure 43. This chart should be expected to show roughly the same effects as Figure 41, and

although the jet speed, parameter C, shows as a factor with considerable effect, the wheel speed, parameter F, does not. The interaction of the two parameters is again highlighted as significant. The F-ratio for jet speed and the interaction between the jet speed and the wheel speed puts them both in the 95% confidence interval bracket. The ANOVA table for the percentage useful flow results can be seen in Appendix However wheel speed falls into the 90% confidence bracket, possibly too low to draw a definite conclusion.

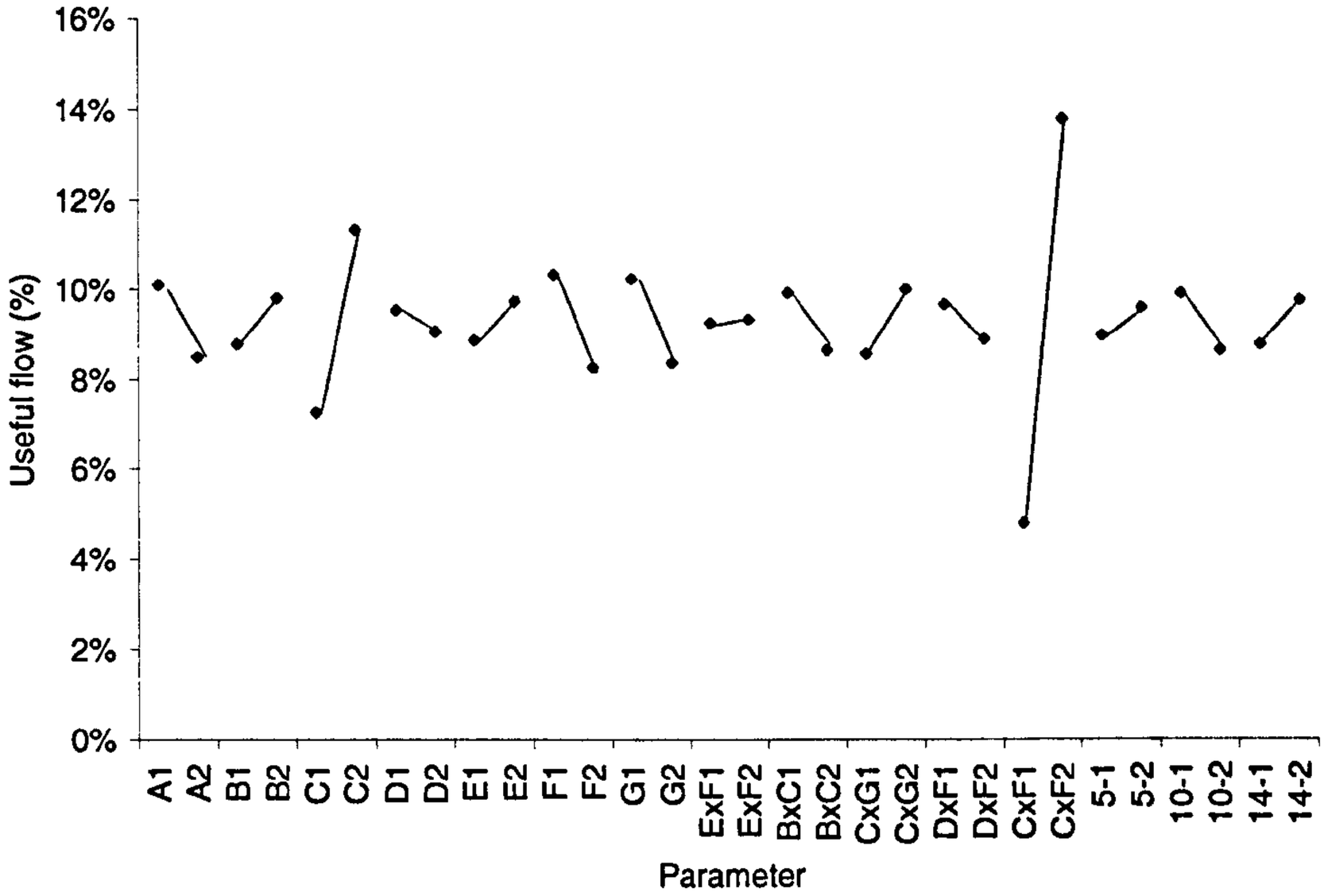

Figure 43, Direct effect chart for useful flow. A = Material Type, B = Nozzle position, C = Jet Speed, D = Dressing condition, E = Work piece surface speed, F = Wheel surface speed and G = Engagement, Actual depth of cut.

It can also be seen from Figure 43, that the best situation for utilising large amounts of the applied flow is to have a low supply flowrate (C2), low wheel speed (F1) and low depth of cut (G1). However, this condition results in a low useful flowrate and a condition where the wheel contact is starved of grinding fluid. This demonstrates the limited applicability of results presented in terms of percentage useful flow. The low confidence interval shows the true effect of the depth of cut, G1 may not be significant, this could be due to the film boiling experienced during some of the more demanding tests. This effect could have lowered the amount of useful flow that could be collected after the contact zone, thus lowering the percentage of flow collected within the system. The most noticeable effect within this analysis is the interaction between wheel speed and jet speed on the amount of useful flow utilised. This parameter has a confidence ratio above 99%. This leads to the need for an analysis of the individual interaction chart for the percentage useful flow.

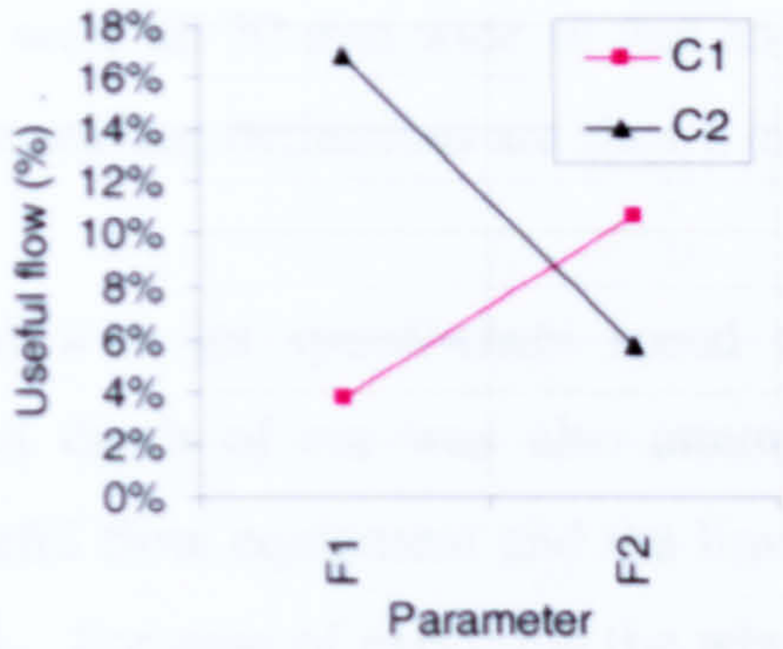

Figure 44, Interaction chart the useful flow showing jet speed, C and wheel speed, F.

What can be clearly seen is that the best percentage useful flow's are achieved for the combination of parameters C2 F1 and C1 F2. Both of these combinations correlate to when the jet speeds and the wheel speeds are at their most similar i.e. when the speed ratios are nearest 1.

7.6 Jet Speed /Wheel speed

As discussed earlier the perceived need to match coolant jet speed to grinding wheel speed leads to demands for larger and more expensive equipment in new high speed grinding machines. The following second stages of testing were designed to analyse the effect of the process parameters of supply flowrate, jet speed and wheel speed.

7.6.1 Preliminary Test 3

The first stage of this analysis took place on the Abwood grinding machine using the Altos grinding wheel. The testing has been summarised previously as Preliminary Test 3. The samples were made to give a 'grindable' length of 60 mm. An existing nozzle positioning system was used which allowed the nozzle to be moved closer to the wheel and move higher up the wheel. The nozzle was aimed so the fluid jet hit horizontally just above the grinding zone, parallel to the workpiece.

Nozzle Exit Height, h_n, (mm)	Nozzle exit Area, m^2	Nozzle exit speed, v_j, m/s
0.45	$9x10^{-6}$	35.1 m/s
0.40	$8x10^{-6}$	39.4 m/s
0.35	$7x10^{-6}$	45.1 m/s

Table 19, Nozzle exit dimension table for Preliminary Test 3.

The test was conducted with 3 separate nozzles with differing outlet areas, this allowed 3 jet speeds to be achieved whilst keeping the supply flowrate constant at 18.9 l/min.

The nozzle fluid exit areas were all 20 mm wide so that coverage of the grinding zone was roughly constant, the remaining definitions are shown in Table 19.

24 trials were conducted with jet speed/wheel speed ratios of 0.8 - 1.6 (v_j/v_s). Measurement of the actual depth of cut was also attempted, however this proved difficult with the novel useful flow equipment and the limitations of the control drive positioning of the Abwood. For ease of execution the wheel speeds were varied for a given jet speed, then the nozzle was changed and the wheel speeds were varied again. This test was conducted over a range of wheel speeds and jet speeds so trends could be observed for both parameters. The experimental plan can be seen in Table 20.

Test No,	Jet speed, v_j (m/s)	Wheel speed, v_s (m/s)	Ratio (v_j/v_s)
1	45	29	1.55
2	45	32	1.41
3	45	35	1.29
4	45	38	1.19
5	45	41	1.10
6	45	44	1.02
7	45	47	0.96
8	45	51	0.89
9	39	26	1.52
10	39	29	1.36
11	39	32	1.23
12	39	35	1.12
13	39	38	1.04
14	39	41	0.96
15	39	44	0.90
16	39	47	0.84
17	35	23	1.52
18	35	26	1.35
19	35	29	1.21
20	35	32	1.10
21	35	35	1.00
22	35	38	0.92
23	35	41	0.85
24	35	44	0.80

Table 20, Experimantal plan for Preliminary Test 3 on the Abwood grinding machine using the Altos grinding wheel.

A dress was performed every time the nozzle was changed or an unexpected event such as an impact of the wheel on the workpiece occurred, this was followed by several grinding passes to gain wheel stability. Dressing was also performed whenever the wheel started to blunt. A single point diamond was used with a dressing depth of 10 μm and a feed rate of approximately 200 mm/min.

7.6.1.1 Results

The results showed that the useful flowrate could be increased with a greater wheel speed, this can be seen in Figure 45. The results proved difficult to interpret conclusively as to whether a predictable trend existed between wheel speed and useful flowrate, and jet speed and useful flowrate.

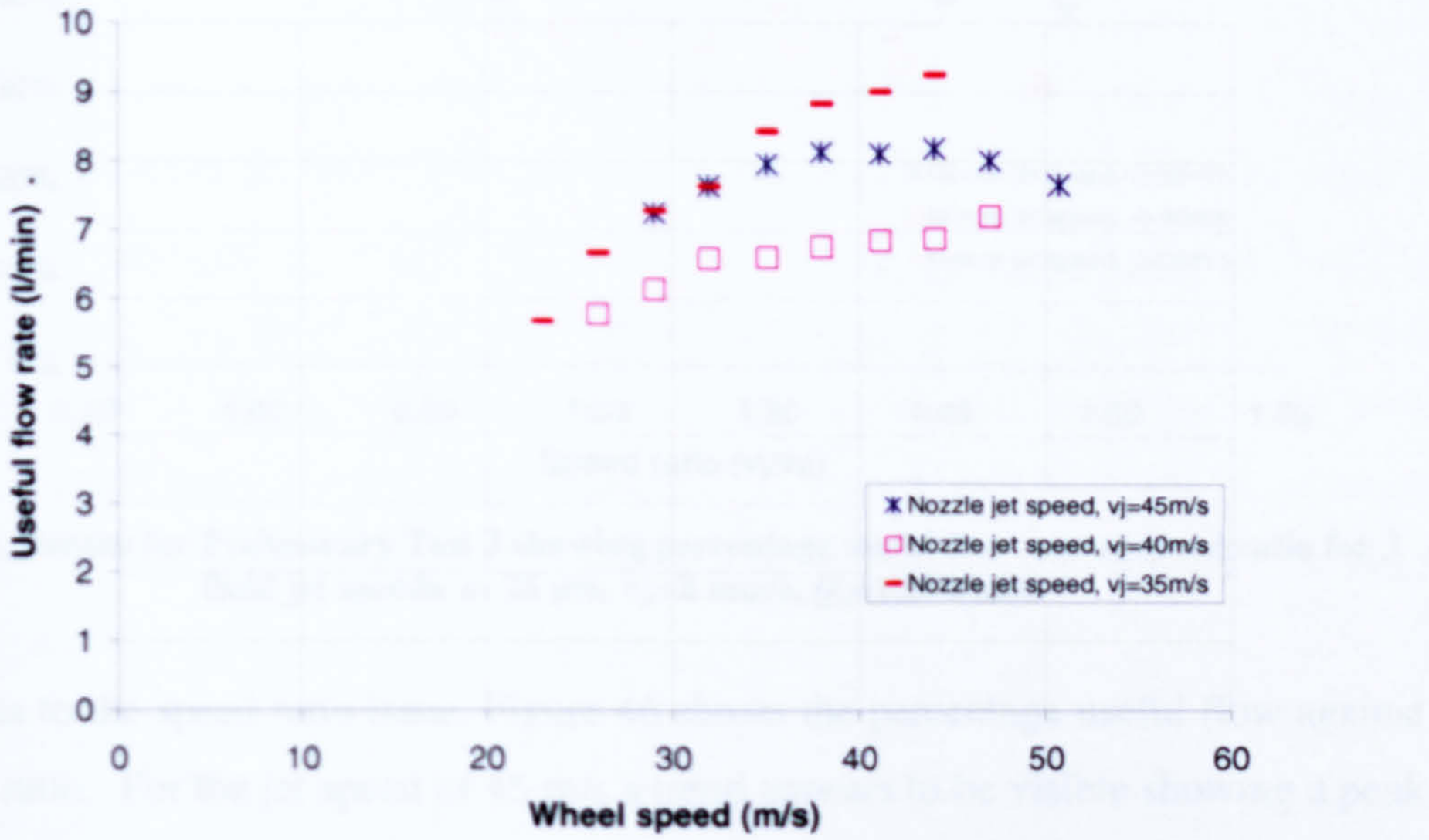

Figure 45, Results for preliminary test 3 showing useful flowrate versus wheel speed for 3 fluid jet speeds, a=25 µm, v_w=2 mm/s, Q_d=18.9 l/min.

Figure 45 appears to show that increasing the jet speed increases useful flowrate, however the results do not follow a consistent trend. This may be because the range of jet speeds is small and experimental errors were reasonable in these early tests. It is worth noting that the equipment suffered a transient deterioration as testing took place and that the 35 m/s test took place last. Although this might have affected the exact values of the useful flow and grinding force results somewhat, it is expected that the trends identified from this early test are still valid.

When considering these tests involved a constant supply flowrate the value of percentage useful flow becomes less abstract and can be viewed as concisely as the useful flowrate, thus it can be considered a measure of the efficiency of the grinding setup used. It can be seen from Figure 46 that percentage useful flow approached a maximum of approximately 50% of the applied flow, a value more in agreement with previous works.

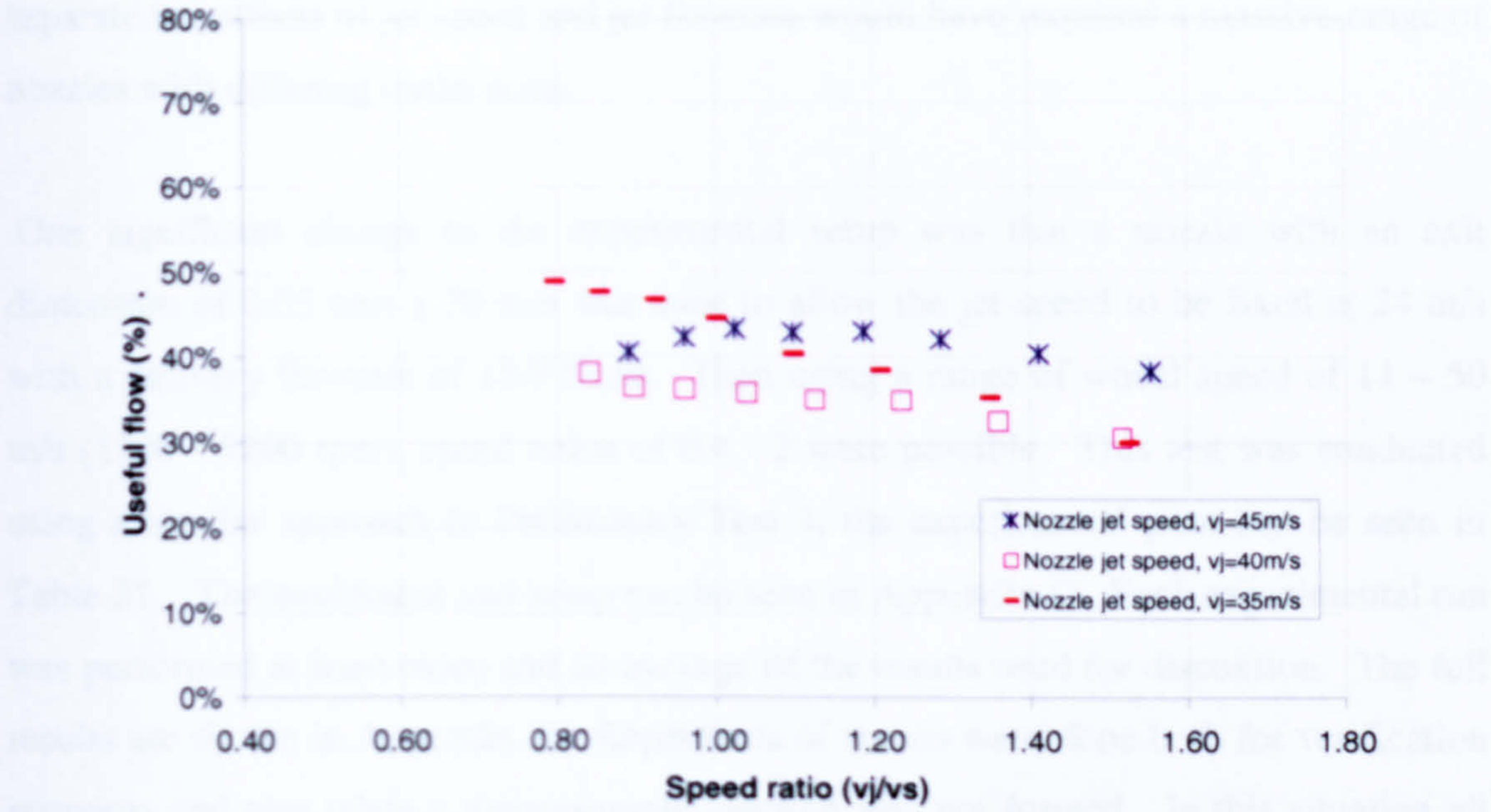

Figure 46, Results for Preliminary Test 3 showing percentage useful flow versus speed ratio for 3 fluid jet speeds, a=25 µm, v_w=2 mm/s, Q_d=18.9 l/min.

In regards to the speed ratio issue, Figure 46 shows the percentage useful flow against the speed ratio. For the jet speed of 45 m/s a trend appears to be visible showing a peak of percentage useful flow at a value close to a speed ratio of 1, when the wheel speed equals the jet speed. It would have been expected that the other two jet speeds might have shown a similar trend of having a peak at a speed ratio of 1. The test where the jet speed is 40 m/s appears to nearly show the same trend, however the test where jet speed is 35 m/s does not. The initial findings from the speed ratio graphs are difficult to interpret fully over the small range that was necessitated by the wide range of input values used. For the purposes of the overall project this test served to show that trends seem to exist and that at certain values of speed ratio key variations in a useful flow trend may occur.

After conducting this test it seemed that a follow-up test would be useful in order to establish if any trend exists over the larger range of jet speed/wheel speed ratios. This required a test where the speed range could be extended in both directions.

7.6.2 Abwood Speed Ratio Test

The purpose of this test was solely to assess the interaction of the speed ratio and useful flow over a larger range of wheel speeds. It was a practical necessity to vary the wheel speed rather than the jet speed. To keep a constant supply flowrate in order to

separate the effects of jet speed and jet flowrate would have required a massive range of nozzles with differing outlet sizes.

One significant change to the experimental setup was that a nozzle with an exit dimension of 0.65 mm x 20 mm was used to allow the jet speed to be fixed at 24 m/s with a delivery flowrate of 18.9 l/min. Then using a range of wheel speed of 11 – 50 m/s (1200 - 5200 rpm), speed ratios of 0.4 - 2 were possible. This test was conducted using a similar approach to Preliminary Test 3, the experimental plan can be seen in Table 21. The equipment and setup can be seen in Appendix C. Each experimental run was performed at least twice and an average of the results used for discussion. The full results are shown in Appendix A. Repetitions of results were done both for verification purposes and also when a thermocouple junction was not formed. In this situation all the remaining data; useful flow, power, could still be recorded and would not have been affected by the lack of a thermocouple junction.

Test No.	Jet speed, v_j (m/s)	Wheel speed, v_s (m/s)	Ratio (v_j/v_s)
1	24.3	11.6	*2.10*
2	24.3	12.0	*2.01*
3	24.3	12.8	*1.89*
4	24.3	13.5	*1.80*
5	24.3	14.3	*1.70*
6	24.3	15.1	*1.60*
7	24.3	16.2	*1.50*
8	24.3	17.4	*1.40*
9	24.3	18.8	*1.29*
10	24.3	20.2	*1.20*
11	24.3	22.2	*1.09*
12	24.3	24.1	*1.01*
13	24.3	26.5	*0.92*
14	24.3	30.4	*0.80*
15	24.3	34.7	*0.70*
16	24.3	40.5	*0.60*
17	24.3	50.1	*0.48*

Table 21, Experimental plan for Abwood speed ratio test.

7.6.2.1 Results

At this stage the useful flow collection system provided repeatable and reliable results. Therefore the results from this test were not used to assess the equipment but only to analyse the results of the assumption that jet speed needs to match wheel speed.

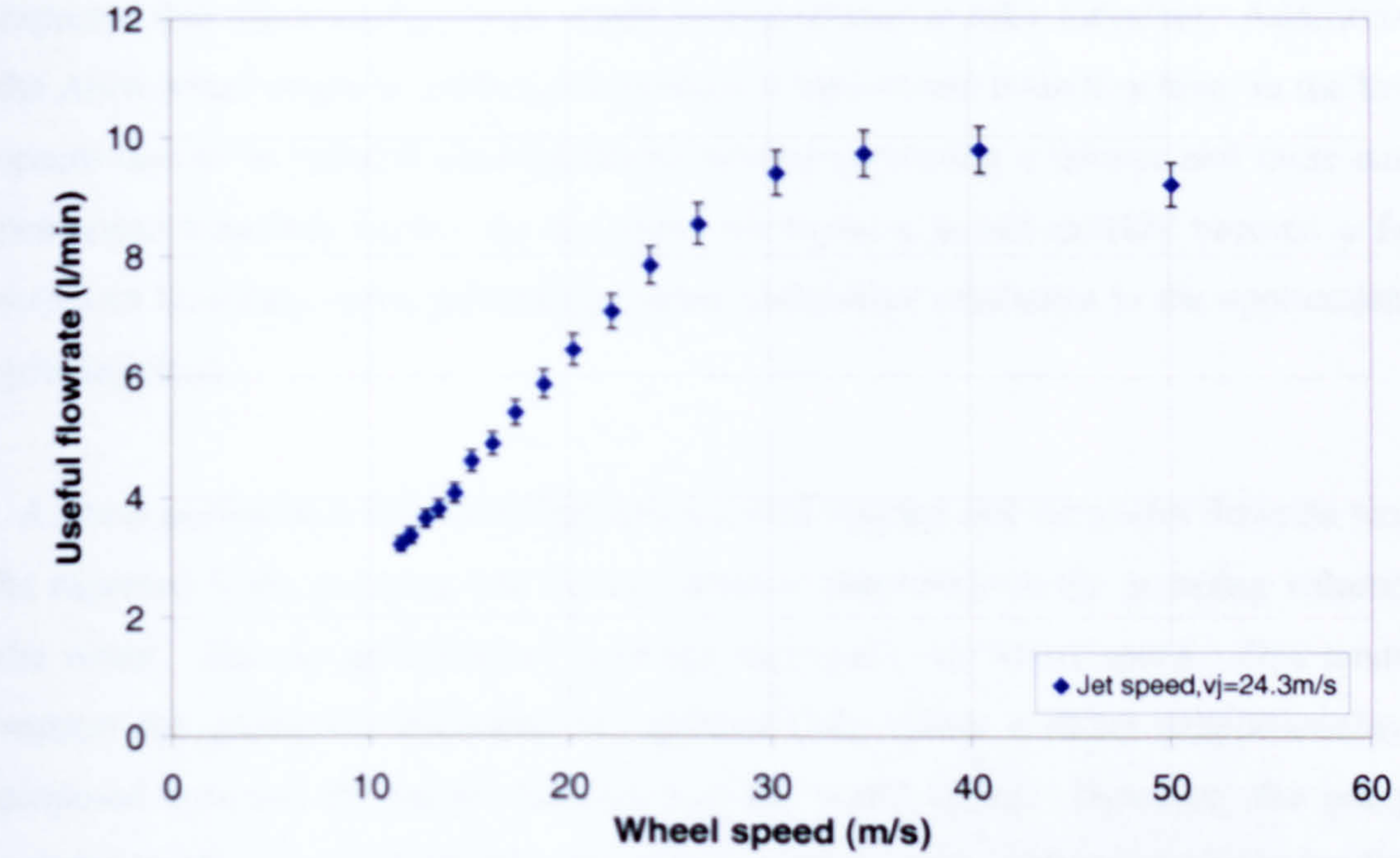

Figure 47, Results from Abwood speed ratio test showing useful flowrate versus wheel speed, a=25µm, v_w=6 mm/s, Q_d=18.9 l/min.

The useful flowrate results can be seen in Figure 47 plotted against wheel speed; and the percentage useful flow results can be seen in Figure 48 plotted against the speed ratio (v_j/v_s). Both results show a definite trend in regards to the amount of fluid that can pass through the grinding contact zone. Figure 47 shows how the wheel speed has a definite effect during this test. It can be seen that as the wheel speed increases the useful flow increase. In Figure 47 when the wheel speed is smaller than the jet speed the percentage useful flow is approximately linearly proportional to the wheel speed. This situation is due to a smaller air boundary existing around the wheel at low speeds. This air boundary layer can be penetrated quite easily with sufficient fluid speed in conjunction with a flowrate high enough so that the wheel is never short of fluid to pump through. However, at high wheel speeds, the air boundary layer is increased in thickness and also in its momentum. A higher jet speed is therefore required to penetrate the boundary layer. Also, a larger jet flowrate is required to ensure a sufficient quantity is supplied to satisfy the achievable useful flowrate after allowing for an increased rate of fluid rejection. When considering the air boundary layer as a key factor to fluid ingress it is necessary to consider the type of boundary layer that could be expected. A smooth wheel of this diameter would have a Reynolds number of between $3x10^5$ and $1x10^6$. A fully turbulent boundary layer would be expected when Re > $1x10^6$ and considering a rougher surface would be expected to lower this limit, it would be

expected that this boundary layer would be transitional to fully turbulent. Additionally the Altos wheel might be expected to produce a transitional boundary layer in the lower speeds due to its reduced circumference, thereby presenting a thinner and more easily penetrated boundary layer. As the speed increases it would quickly become a fully turbulent boundary layer, presenting a more substantial resistance to the application of grinding fluid.

A linear portion in relationship between the wheel speed and the useful flowrate would be expected if the pumping rate of the system is dependent on the pumping volume of the wheel. The pumped flowrate therefore increases with wheel speed. This tends to support the prediction according to equation (24), where a direct proportionality is proposed between the useful flowrate and the wheel speed. However, the pumped volume needs to be calibrated for the wheel condition and compared with the predicted value from the wheel porosity. These results suggest a good correlation between the Rowe theory of equation (24) and the values in the low speed ratio 'linear' region with this grinding wheel.

Figure 48 shows that the maximum percentage useful flow was approximately 50% of the applied flow for this experimental arrangement. It appears that this maximum percentage useful flow occurs as the nozzle jet speed approaches the wheel speed, where the speed ratio is less than 1. For this experiment the maximum percentage useful flow also represents the maximum useful flowrate. What is also clarified by Figure 48 is the relevance of the speed ratio factor. Although the results have been transformed due to the inverse ratio, thereby the linear portion referred to earlier now shows a curve, the points of interest become clearer. When the wheel speed reaches the jet speed the ratio is 1, all values below this represent the preferred region of operation for a manufacturer, high wheel speed and low jet speed. The region above a ratio of 1 represents higher jet speeds than wheel speeds and would realistically not be used by industry without explicit guidance pertaining to definitive benefits. It is this region that the manufacturers wish to avoid; indeed they would prefer not to approach it at all, preferring to work well below a ratio of 1. However, this region is of interest to this project as it represents a situation where the fluid supply flowrate can be considered plentiful to the pumping demands of the wheel. Below a ratio of 1 is most likely where

the effect of the air barrier will be substantial, because in this region the wheel speed is highest in comparison to the jet speed.

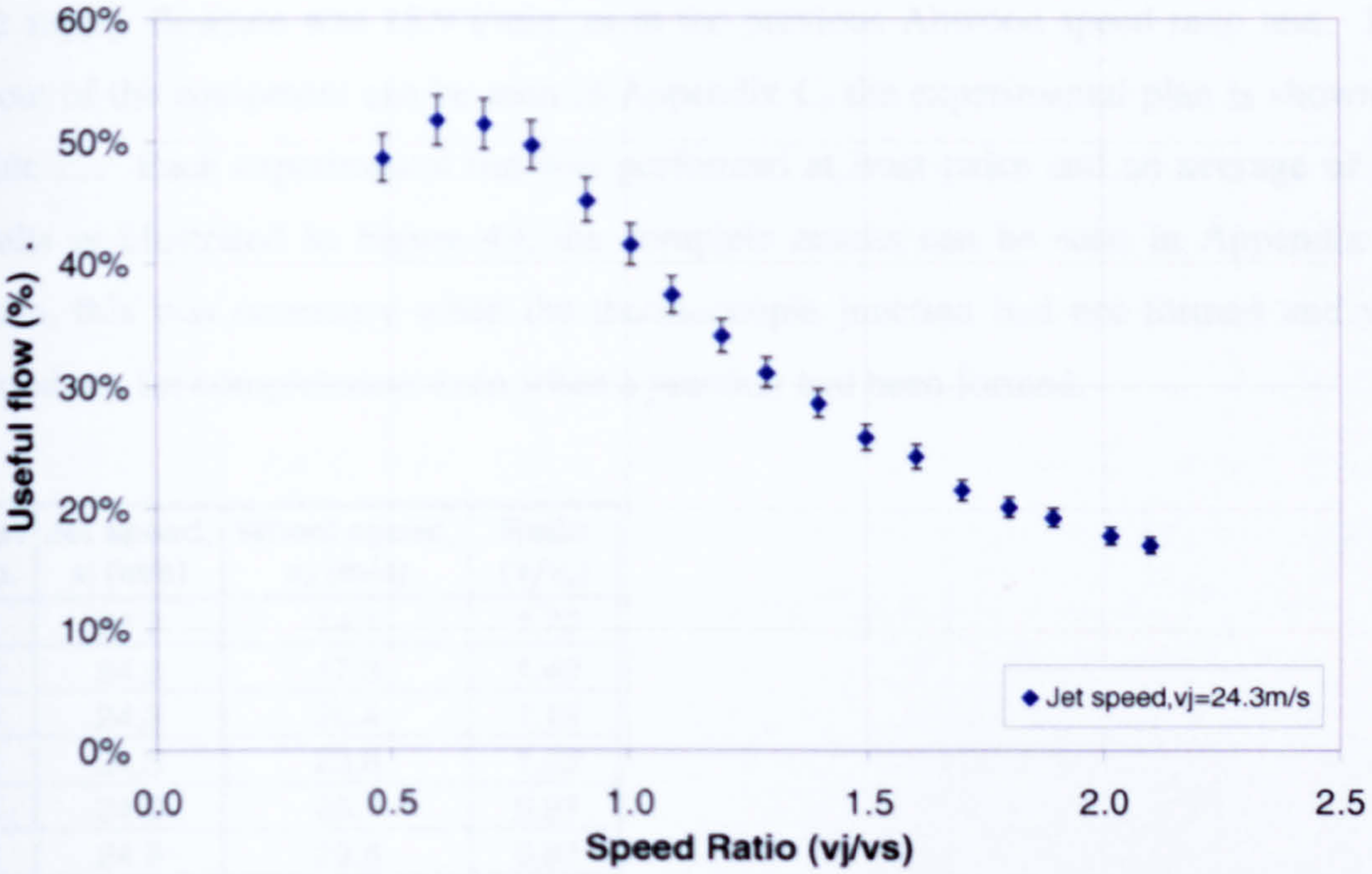

Figure 48, Percentage useful flow versus speed ratio for the Abwood speed ratio test, a=25 µm, v_w=6mm/s, Q_d=18.9 l/min using the Altos wheel.

The strong influence of wheel speed over the useful flow during this test and some of the other preliminary tests suggests that the pumping effect of the wheel may have a very large impact over the volume of flow that can pass through the contact zone. With this being the case the topography of the wheel will be an integral factor, as such the use of the convenient flow term with its basis in wheel topography becomes more appreciable.

7.6.3 Dominator Speed Ratio Test

In order to have a fuller picture of the effects of the wheel speed and the speed ratio on the useful flow a test was planned to measure the flow at higher-than-conventional wheel speeds and with a different wheel. This test used the Jones and Shipman Dominator Surface grinding machine. By using the stiffer machine with the faster spindle several factors could be addressed that were previously impossible to tackle, the most important of which were the higher wheel speeds and the different wheel porosity. The experiment was performed over a range of wheel speeds of 14 – 69 m/s, giving a speed ratio range of 0.35 – 1.7. The samples were made to give a 'grindable' length of 100 mm. The workpiece speed was again increased slightly up to 10 mm/s, this gave a collection period of 10 seconds. The slot nozzle was positioned roughly 5 mm from the

wheel periphery, with the jet stream parallel to the workpiece. The jet speed was kept constant and the wheel speed was varied to achieve the range of speed ratios required. The supply flowrate was 18.9 l/min, as in the previous Abwood speed ratio test. The layout of the equipment can be seen in Appendix C, the experimental plan is shown in Table 22. Each experimental run was performed at least twice and an average of the results is illustrated in Figure 49, the complete results can be seen in Appendix A. Again, this was necessary when the thermocouple junction had not formed and was carried out for completeness even when a junction had been formed.

Test No.	Jet speed, v_j (m/s)	Wheel speed, v_s (m/s)	Ratio (v_j/v_s)
1	24.3	14.1	*1.72*
2	24.3	17.3	*1.40*
3	24.3	20.4	*1.19*
4	24.3	23.6	*1.03*
5	24.3	26.7	*0.91*
6	24.3	29.8	*0.81*
7	24.3	33.0	*0.74*
8	24.3	36.1	*0.67*
9	24.3	39.3	*0.62*
10	24.3	42.4	*0.57*
11	24.3	45.6	*0.53*
12	24.3	48.7	*0.50*
13	24.3	51.8	*0.47*
14	24.3	55.0	*0.44*
15	24.3	58.1	*0.42*
16	24.3	61.3	*0.40*
17	24.3	64.4	*0.38*
18	24.3	68.8	*0.35*

Table 22, Experimental plan for Dominator speed ratio test.

7.6.3.1 Results

The testing in regards to the useful flow showed that the expected parabolic trend did repeat for the stiffer machine and the less porous wheel at higher wheel speeds, as shown in Figure 49. The gradient of the linear portion appears to be much steeper and not as pronounced when the speed ratio is high. However the linear portion does not pass through the origin as in the Abwood tests. This constant region at the lower wheel speeds suggests the relationship between wheel speed and useful flowrate may be more complicated for less porous wheels. It is postulated that this is related to a combination of the lower porosity of the wheel employed on the Dominator and its larger diameter. The low porosity would be expected to allow less useful flowrate at lower wheel speeds in the linear range and hence lead to a lower percentage useful flow. The larger wheel

diameter would be expected to lengthen the hydrodynamic wedge region at the grinding nip and the effect of this might increase useful flowrate at higher wheel speeds.

The linear portion of the graph, visible in Figure 49 between the wheel speeds of 30 m/s and 40 m/s, exists when the wheel speed equals the jet speed to where the wheel speed is nearly double the jet speed. Although not as linear in nature as the Abwood tests and of a much steeper gradient the point where it occurs and stops remains similar. The region of steep increase for the Dominator and the Flexovit wheel combination starts when the speed ratio is just below 1, and ends when the speed ratio is approximately 0.5. It can be stated that for the Flexovit wheel this region of linearity appears to be condensed, this is more easily seen in Figure 50.

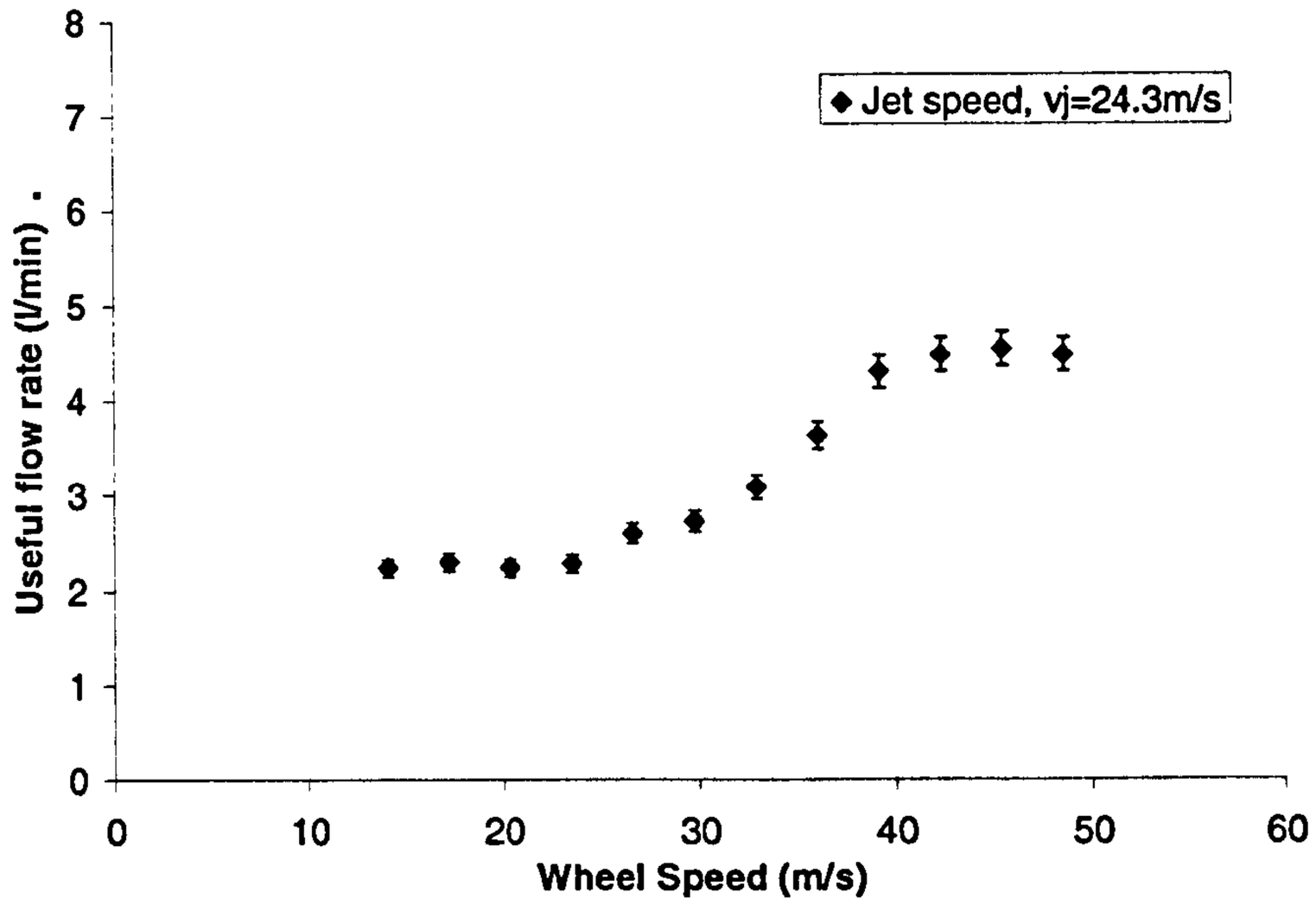

Figure 49, Useful flowrate versus wheel speed for the Dominator speed ratio test, when v_j = 24.3 m/s, q_d=18.9 l/min, using the Flexovit wheel on the Dominator grinding machine.

The reduced porosity of the Flexovit wheel suggests it should be capable of pumping less fluid for a particular wheel speed and supply flowrate. This is confirmed by Figure 49. However, Figure 49 appears to show that the useful flowrate only increases when the wheel speed exceeds jet speed. The wheel speed at which useful flowrate peaks is higher than for previous tests when the higher porosity wheel is used. The wheel speed for maximum useful flowrate is almost twice the jet speed.

According to previous results it would be expected that the linear portion should follow pass through the origin. Results at the lowest wheel speeds do not fit well with previous reasoning and results. Useful flowrate remains almost constant and much

higher in value than expected for very low wheel speeds suggesting that for this wheel the fluid jet easily penetrated the air barrier in this low speed range. It is conjectured that the nozzle was positioned so close to the wheel that it acted as a scraper. If this was the case it is possible that fluid attached to the boundary layer and was carried into the contact much more efficiently at low wheel speeds than would otherwise have been the case. Further investigation into the scraper effects would be advisable in this case.

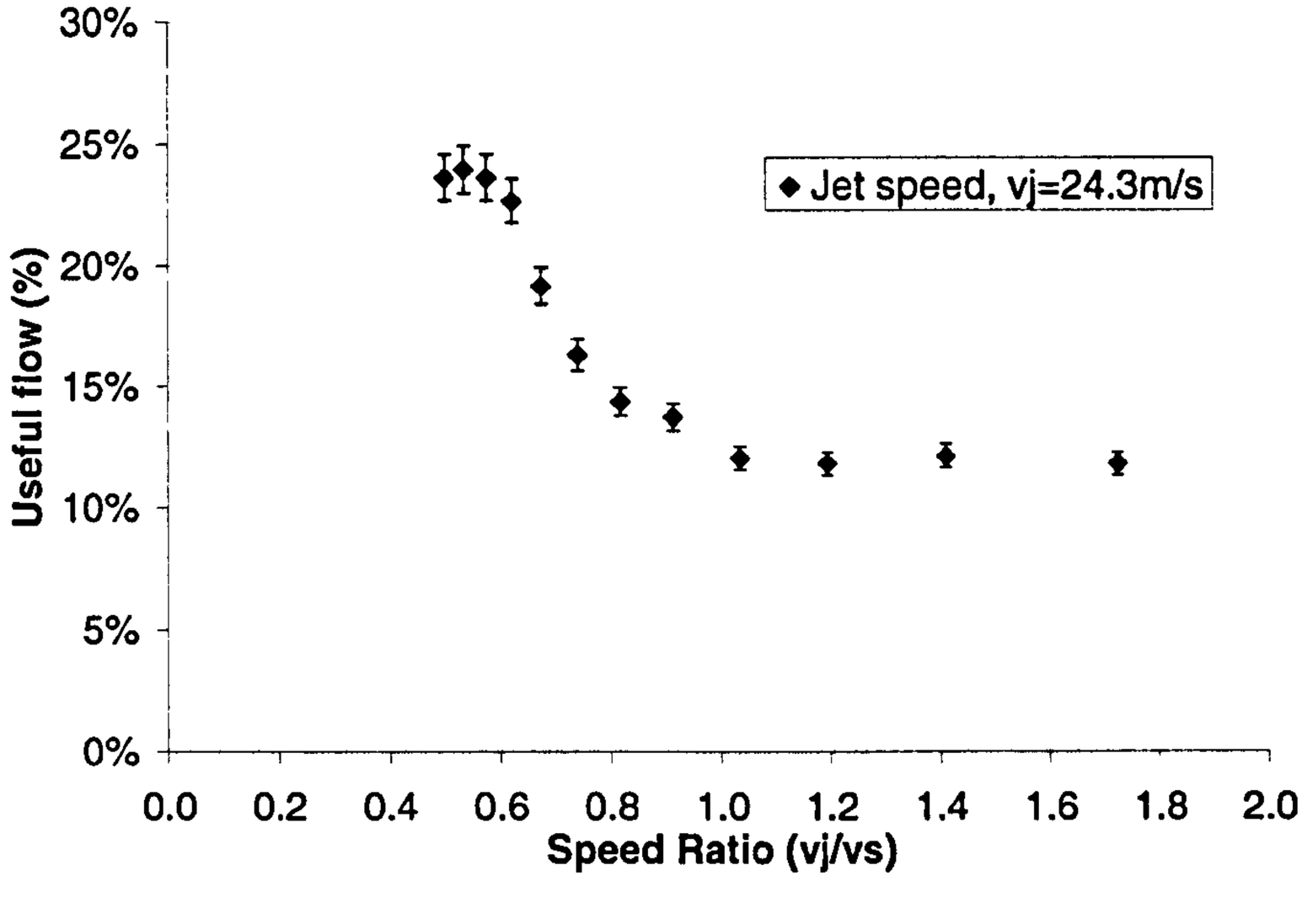

Figure 50, Percentage useful flow versus speed ratio for the Dominator speed ratio test, when v_j = 24.3 m/s, q_d=18.9 l/min, using the Flexovit wheel on the Dominator grinding machine.

As the speed ratio drops below a value of 1 the useful flow increases significantly with increasing wheel speed. The useful flowrate peaks at a speed ratio of approximately 0.5 for the Flexovit wheel compared with a ratio of roughly 0.7 for the Altos wheel. The overall shape of Figure 50 for the Flexovit wheel has similarities to the comparable Figure 48 for the Altos wheel. Above the speed ratio of 1, where the jet speed exceeds the wheel speed, the useful flowrate for the Flexovit wheel is relatively constant. This constancy in the results despite an increasing wheel speed appears contrary to previous prepositions. The region where the jet speed exceeds the wheel speed, i.e. when $v_j/v_s >$ 1.2, is not a region industry would be expected to operate, indeed it would be preferred by industry to operate well below $v_j/v_s = 1$. This region is of interest from an analytical viewpoint only, and as stated previously is not a target operating region for any manufacturer.

These results draw into question the need for matching exactly the wheel speed to the jet speed, shown in Figure 50 by the highest percentage useful flow being at a speed ratio of below one. Indeed there appears to be benefit in having the jet provide sufficient flowrate to the contact zone that the wheel can then utilise dependant solely on wheel speed. During these tests the supply conditions were favourable, in that at no point the wheel was starved of either power from the spindle or grinding fluid; and that the jet speed was of less consequence when the nozzle is positioned close enough to interrupt the air barrier.

During the testing at the higher wheel speeds with the Dominator above 50 m/s, the volume of flow collected tended to continue to increase rather than tail off as shown in previous tests. These top end results proved unreliable in repetition, likely due to the aggressive nature of the grinding being attempted. The sensitivity of these results to the nature of the wheel surface made repeatability questionable therefore they have been disregarded for analysis purposes; however they can still be seen in Figure 51.

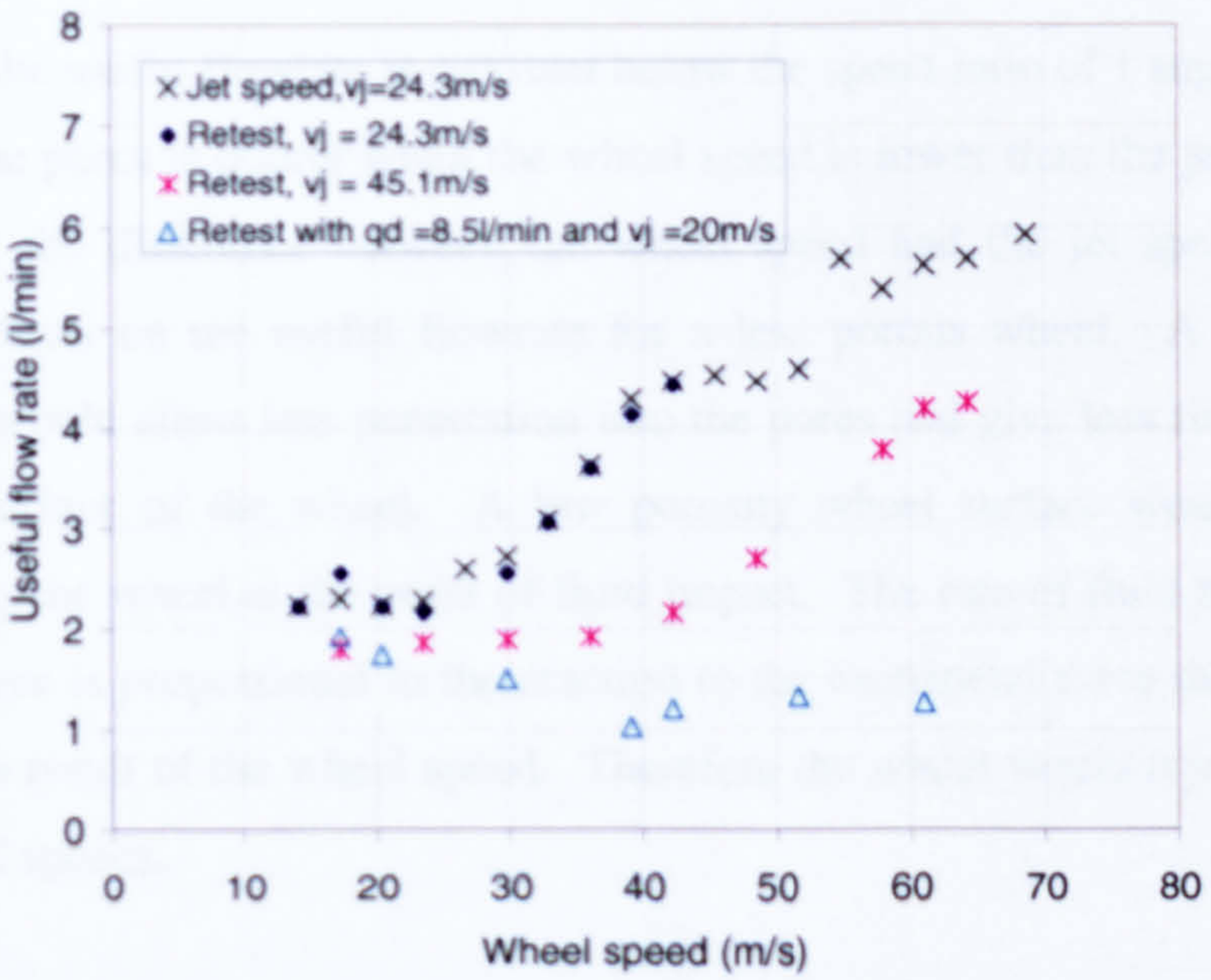

Figure 51, Complete set of results showing the speed ratio against useful flowrate for the Dominator speed ratio tests using the Flexovit wheel on the Dominator grinding machine, when q_d=18.9l/min unless otherwise stated.

Further to this as the trend was different at lower wheel speeds from the Abwood speed ratio test these results were repeated. The repetitions were carried out at different fluid input values, one set of tests were performed at a higher fluid jet speed of 45m/s,

the other test was performed at a lower supply flowrate of 8.5 l/min and jet speed of 20m/s. These tests were conducted in order to compare to a higher jet speed and to compare to a lower, possibly insufficient, flowrate. The complete set of results can be seen in Figure 51. In this figure the higher speed values have also been shown, as stated these values buck the trends shown in other results but are shown here for completeness.

What can be seen clearly in Figure 51 is the repeatability of the trends found in the first run of tests. Particular interest is found in tests conducted using a jet speed of 45m/s and the supply flowrate of 18.9 l/min. The importance of the speed ratio again is clearly visible, showing the steep increase in useful flowrate as the wheel speed approximately matches the jet speed. The constant portion at low wheel speeds again occurs up to the steep gradient, the reasoning for this is not clear, what is clear however is that for the Flexovit wheel the speed ratio is of paramount importance. Again support is found for advising a user to operate at a speed ratio of 0.5-0.9, this can be seen clearly in the speed ratio graph shown in Appendix A.

The fact that the useful flowrate is constant below the speed ratio of 1 suggests that the ability to fill the pores is poorer when the wheel speed is lower than the jet speed. It is postulated that the difference between the wheel speed and the jet speed may have exaggerated effects on the useful flowrate for a less porous wheel. A low porosity wheel surface would allow less penetration into the pores and give less fluid adherence space at the surface of the wheel. A low porosity wheel surface would allow less penetration into the wheel at the point of fluid impact. The rate of fluid rejection from the wheel surface is proportional to the reaction to the centripetal force the fluid would experience as a result of the wheel speed. Therefore the wheel would reject more fluid at higher wheel speeds.

The balance of fluid held at the wheel surface and fluid rejected due to reaction forces would need to be considered alongside the speed ratio. The nature of the difference between the wheel speeds can be described as follows. When the wheel speed matches the jet speed the fluid jet will impact on a surface moving at the same speed. The centripetal reaction of the wheel upon the fluid stream would be lower; the momentum would be preserved due to the similar directions of motion. If the jet speed is below the wheel speed the wheel will be required to accelerate the fluid upon impact. As the jet stream impinges on the wheel with sufficient flowrate an accommodating wheel will

entrain, within its large pores, a fluid jet that has sufficient speed to penetrate the air barrier. A less accommodating wheel, one with a more closed surface, will not be able to deal with the different momentums by entraining fluid as efficiently. As jet speed exceeds the wheel speed a low porosity wheel surface that cannot absorb excess fluid by forced penetration will tend to reject the oncoming fluid based purely upon the differing speeds. Momentum preservation will tend to cause the fluid to deflect from the wheel surface as the fluid cannot accelerate a wheel that has its speed kept constant by the grinding machine spindle. Consequently, one might expect the speed ratio to have a more pronounced effect on useful flowrate due to surface porosity.

The results for the low jet flowrate of 8.5 l/min show useful flowrate reducing as wheel speed increased. This tends to confirm that insufficient flowrate leads to starvation. A low jet flowrate means the jet momentum is reduced. As the wheel speed is increased, the air boundary layer is increased and the jet momentum is insufficient to penetrate the air barrier. At the lowest wheel speed, the percent useful flowrate approaches 25 % but as wheel speed increases this values falls.

7.7 Jet Flowrate/Speed Tests

In analysing the useful flow in reference to the delivery conditions it became obvious that separating the effects of the jet flowrate, m_j from the jet speed v_j would be important. For the majority of testing to this point one of these two values were kept constant. This meant that the analysis of the differentiable effects of these parameters has not been fully addressed. Therefore a test was devised that would attempt to qualify this issue; this meant varying the flowrate whilst keeping the jet speed constant and vice versa. Without a very large range of nozzle sizes or a nozzle with an adjustable height it was impossible to completely maintain the flowrate as a constant. Therefore the flowrate is maintained as tightly as possible for each range of jet speeds, v_j. The jet speed was varied by changing the nozzle exit height. The test was conducted on the Dominator grinding machine using the Flexovit grinding wheel. The experimental plan can be seen in Table 23

Test No.	Nozzle height (mm)	Jet speed, v_j (m/s)	Jet flowrate, m_j (l/min)	Wheel speed, v_s (m/s)	Ratio (v_j / v_s)
1	0.50	40	24.0	30	*1.33*
2	0.50	30	18.0	30	*1.00*
3	0.50	20	12.0	30	*0.67*
4	0.50	10	6.0	30	*0.33*
5	0.65	30	24.0	30	*1.00*
6	0.65	20	16.0	30	*0.67*
7	0.65	10	8.0	30	*0.33*
8	0.40	40	19.0	30	*1.33*
9	0.40	30	14.0	30	*1.00*
10	0.35	40	17.0	30	*1.33*
11	0.85	20	20.0	30	*0.67*
12	0.85	10	9.8	30	*0.33*

Table 23, Experimental plan for jet speed/flowrate test.

7.7.1 Results

The results from these tests show the difficulty of trying to differentiate the effects of these two intrinsically linked parameters. Figure 52 shows the useful flowrate against the jet flowrate. Figure 52 shows that there is little variation in useful flowrate between a supply flowrate of 6 l/min and 24 l/min. The lack of major variation in this constant wheel speed test further suggests that the wheel speed has the strongest effect on the useful flowrate in comparison to all other input parameters. From this test it can be seen that the maximum useful flowrate is ~2.2 l/min when v_s=30 m/s and when either v_j=10 m/s with m_j=8 l/min; or v_j =20 m/s with m_j =16 l/min. This shows approximate agreement with the Dominator speed ratio test, with the same wheel and same equipment and methods. During this test useful flowrate was ~2.7 l/min when v_s=30 m/s, v_j=24 m/s and m_j=18.9 l/min. The setup for this Dominator speed ratio test can however be more readily compared to Tests 2 and 11 for this trial, where v_s=30 m/s, v_j=20 m/s, m_j=20 l/min and v_s=30 m/s, v_j=30 m/s and m_j=18 l/min. For both of these tests the useful flowrate is approximately 1.6 l/min, much below the equivalent Dominator tests. This test was repeated and an average is presented, when useful flowrate varies little the effect that even minor variation in input parameters can have is significant. What can be definitely concluded is that for the Flexovit wheel running at 30 m/s up to 2.5 l/min useful flow is achievable, whether it is necessary to input the effort required to reach this value would be dependant upon the process requirements.

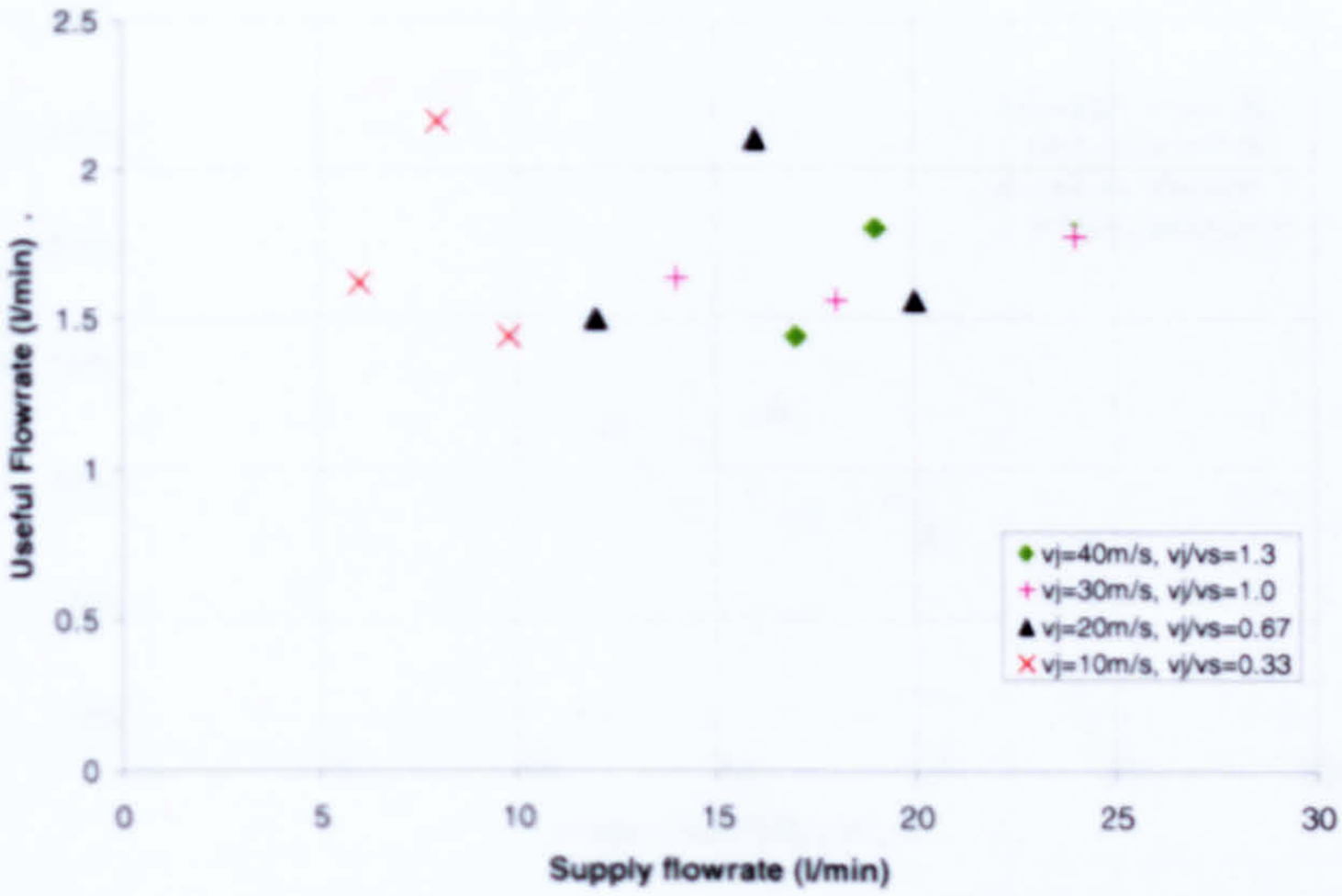

Figure 52, Useful flowrate versus supply flowrate for the jet speed/flowrate test, when v_s = 30 m/s, a=30 µm, v_w=10 mm/s, using the Flexovit wheel on the Dominator grinding machine.

What little variation there is between the values is difficult to explain. The consistency of the useful flowrate values is in general agreement with the results from the lower speed ratio tests on the Dominator. Examination of Figure 52 and more specifically with the jet speed of 10 m/s shows the variation that can exist from one test to the next, in this case nearly 30%. Where the results have proven slightly more consistent, for example between the results for the jet speeds of 30 and 40 m/s, a slight increase in useful flowrate can be seen when the jet speed is increased. When considering the fact that the useful flowrate has remained constant the percentage useful flow should be considered. Examination of this parameter shows how the amount of rejected flow increases as the supply flowrate is increased; shown by the decrease in percentage useful flow visible in Figure 53. The grinding situation attempted could be considered favourable, at no point was it expected that the grind would result in workpiece burn. Indeed throughout testing both the grinding zone temperature and the grinding power remained within tolerable limits.

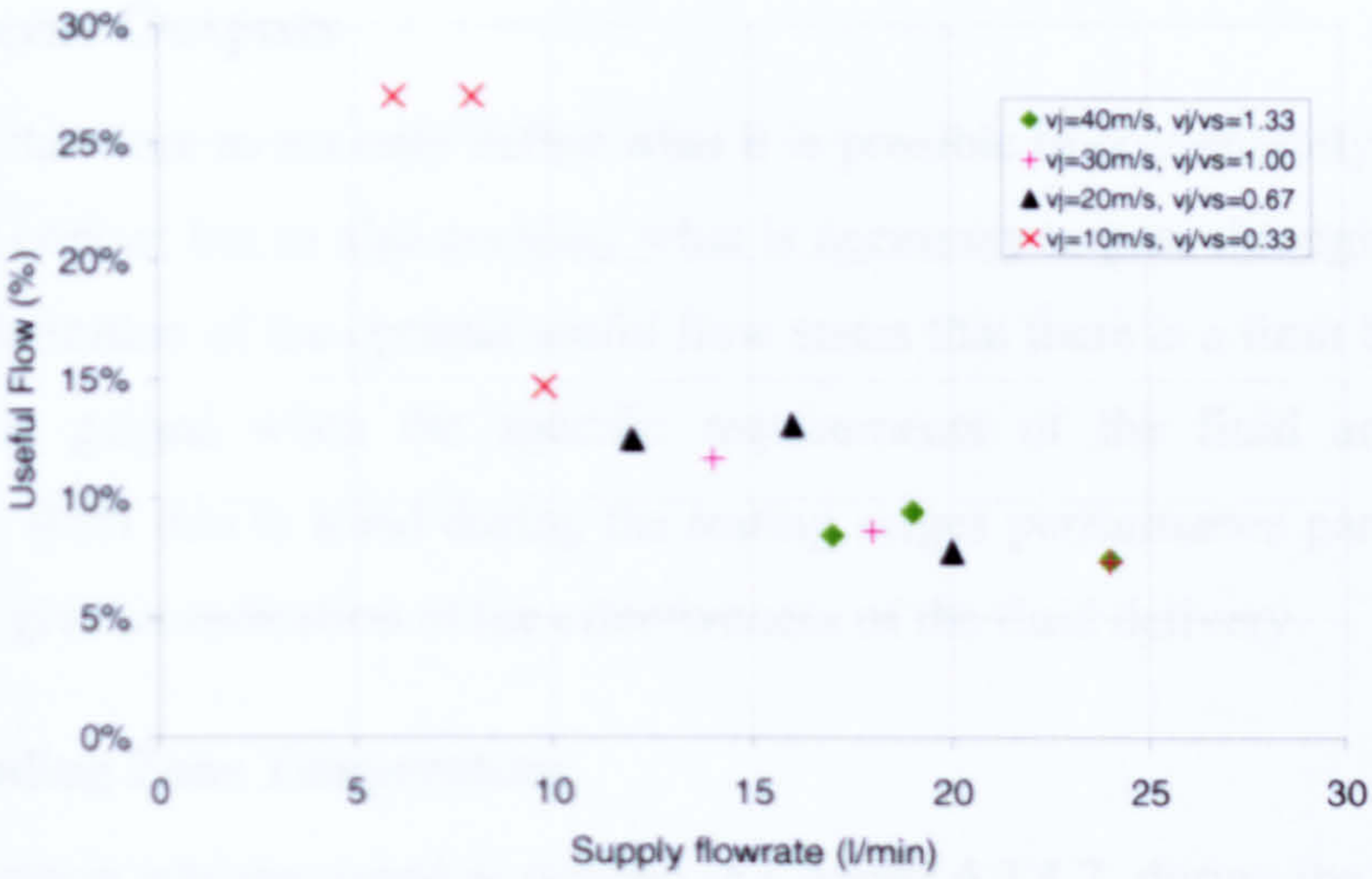

Figure 53, Percentage useful flow versus supply flowrate for the jet speed/flowrate test, when v_s = 30 m/s, a=30 μm, v_w=10 mm/s, using the Flexovit wheel on the Dominator grinding machine.

The results displayed in Figure 52 can be examined further by splitting the parameters down into groups of similar supply flowrates. This is done with several of the results by grouping the flowrates of around 12 l/min and 22 l/min, illustrated in Figure 54. What can be seen is how the minimal variation that does exist could be more affected by jet speed than jet flowrate. A definite upward trend in useful flowrate is visible as the jet speed is increased. The increase is slight though, and it could be argued that it can be attributed to the very slight variation in the flowrates. What is clear from this result however is that the increase of 10 l/min in applied flowrate has had little effect on the useful flowrate. This reinforces the idea that increasing the supply flowrate has negligible effects if the jet speed is not sufficient.

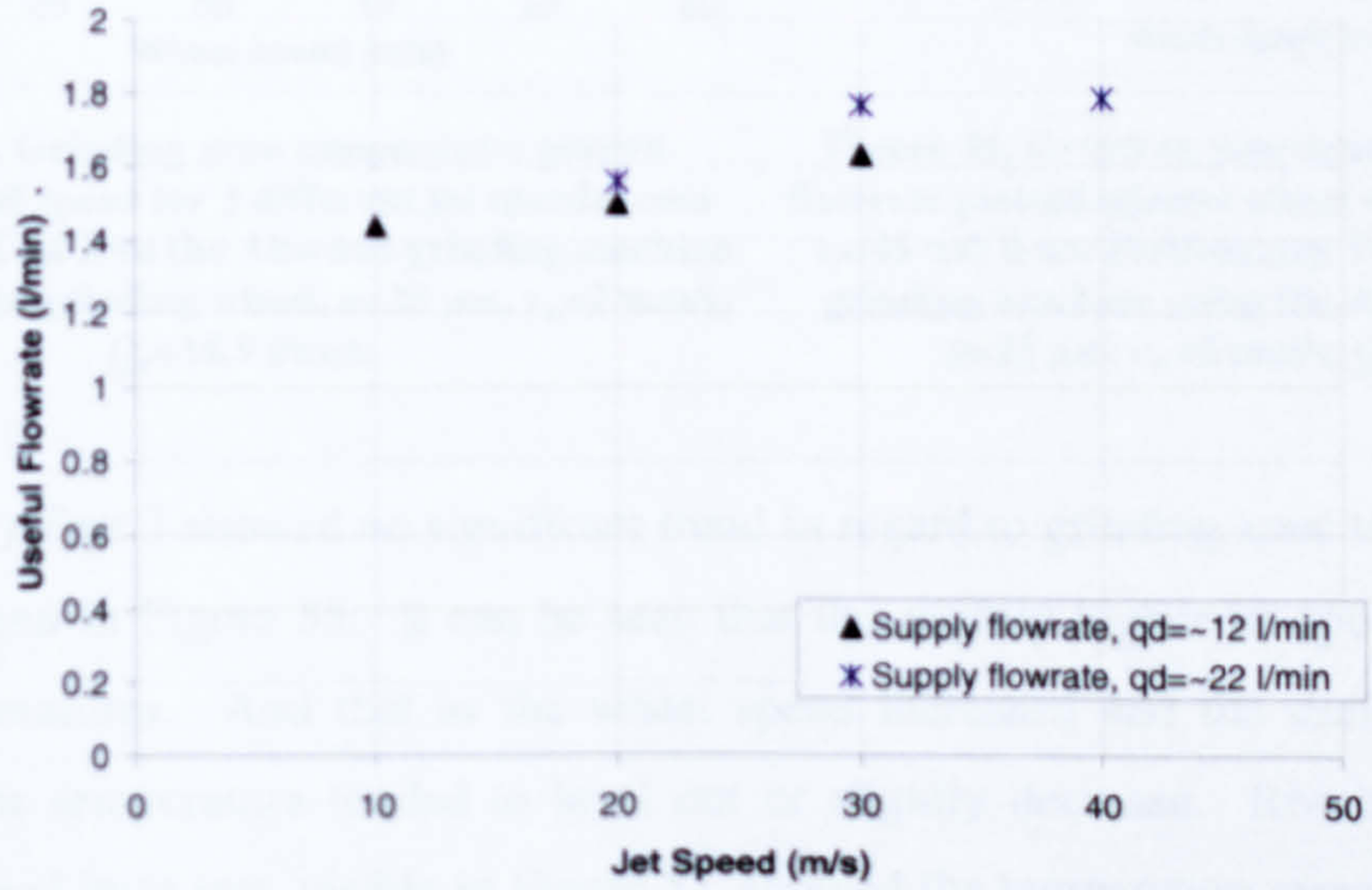

Figure 54, Useful flowrate versus jet speed for the jet speed/flowrate test for various supply flowrates, when v_s = 30 m/s, a=30 μm, v_w=10 mm/s, using the Flexovit wheel on the Dominator grinding machine.

7.8 Process Outputs

It is key to the work to not only define what it is possible to conveniently pass through the grinding contact but to also consider what is necessary to pass through the grinding zone. The definition of the optimal useful flow states that there is a limit beyond which no benefit is gained when the specific requirements of the fluid are considered separately. With this in mind during the testing stages performance parameters were evaluated to give an indication of the effectiveness of the fluid delivery.

7.8.1 Grinding Zone Temperature

The temperature was measured as defined in Chapter 4.2.4.2 during the Taguchi tests and several of the speed ratio tests. The purpose was to monitor the possible onset of thermal damage, for the more severe grinding trials visual effects such as temper colours were visible along with less tangible effects of noise, bounce and misting. Excessive temperatures also tend to be accompanied by power spikes, which are discussed in the following chapters.

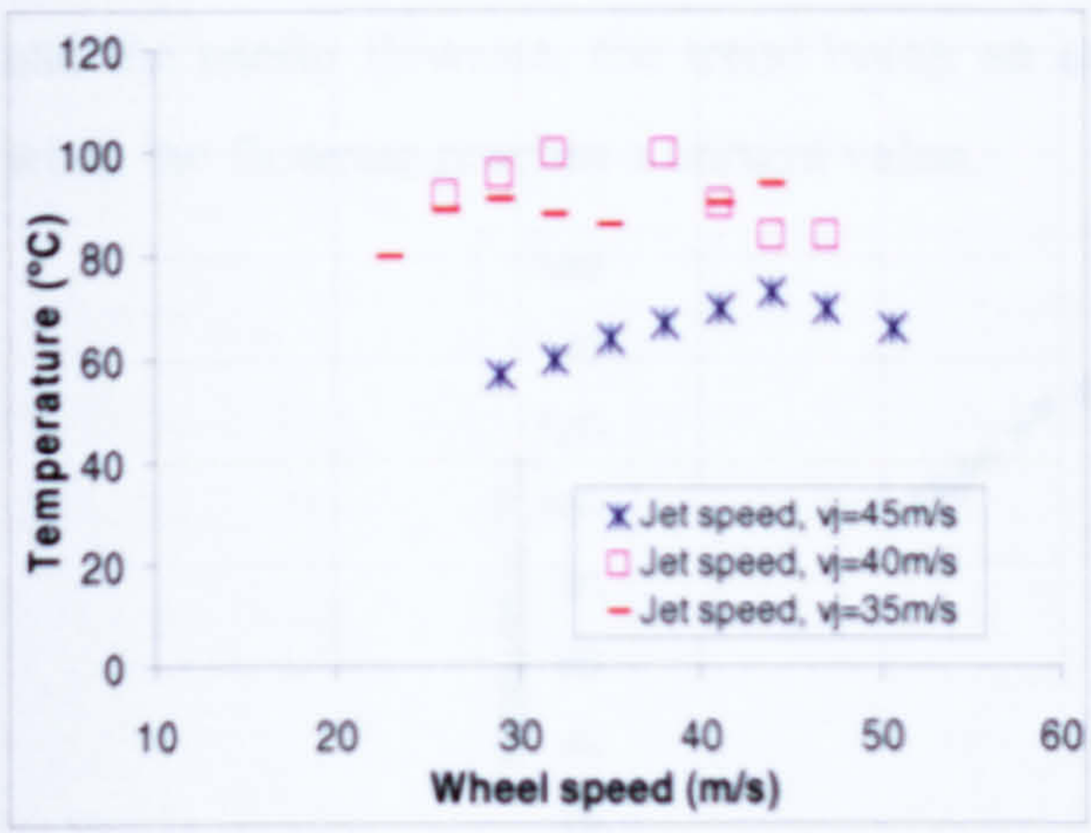

Figure 55, Grinding zone temperature plotted against wheel speed for 3 different jet speeds from Preliminary Test 3 on the Abwood grinding machine using the Altos grinding wheel, a=25 µm, v_w=2 mm/s, Q_d=18.9 l/min.

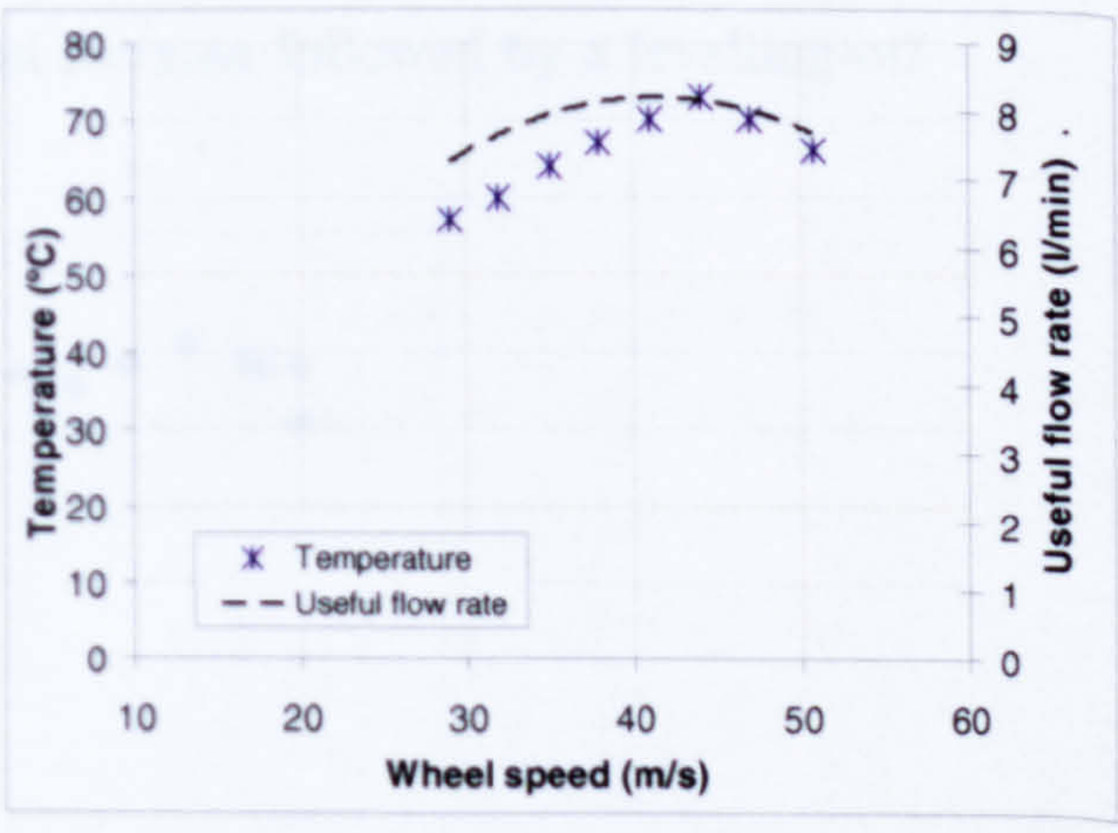

Figure 56, Grinding zone temperature and useful flowrate plotted against wheel speed with a jet speed, v_j=45 m/s from Preliminary Test 3 on the Abwood grinding machine using the Altos grinding wheel, a=25 µm, v_w=2 mm/s, Q_d=18.9 l/min.

Preliminary Test 3 showed no significant trend in regard to grinding zone temperature, as can be seen in Figure 55. It can be seen that the slightly higher jet speeds had the lower temperatures. And that as the wheel speed increased and the useful flowrate increased the temperature tended to level out or slightly decrease. Results from the Abwood speed ratio test, visible in Figure 57, showed the temperature remained within tolerable limits suggesting a favourable grind was being performed with adequate useful flow. The temperature again had a tendency to increase and then level off, with the

increase being mainly due to the increasing wheel speed. It is worth noting at this point that the energy partitioning within the contact zone will have had a key influence on the workpiece surface temperatures.

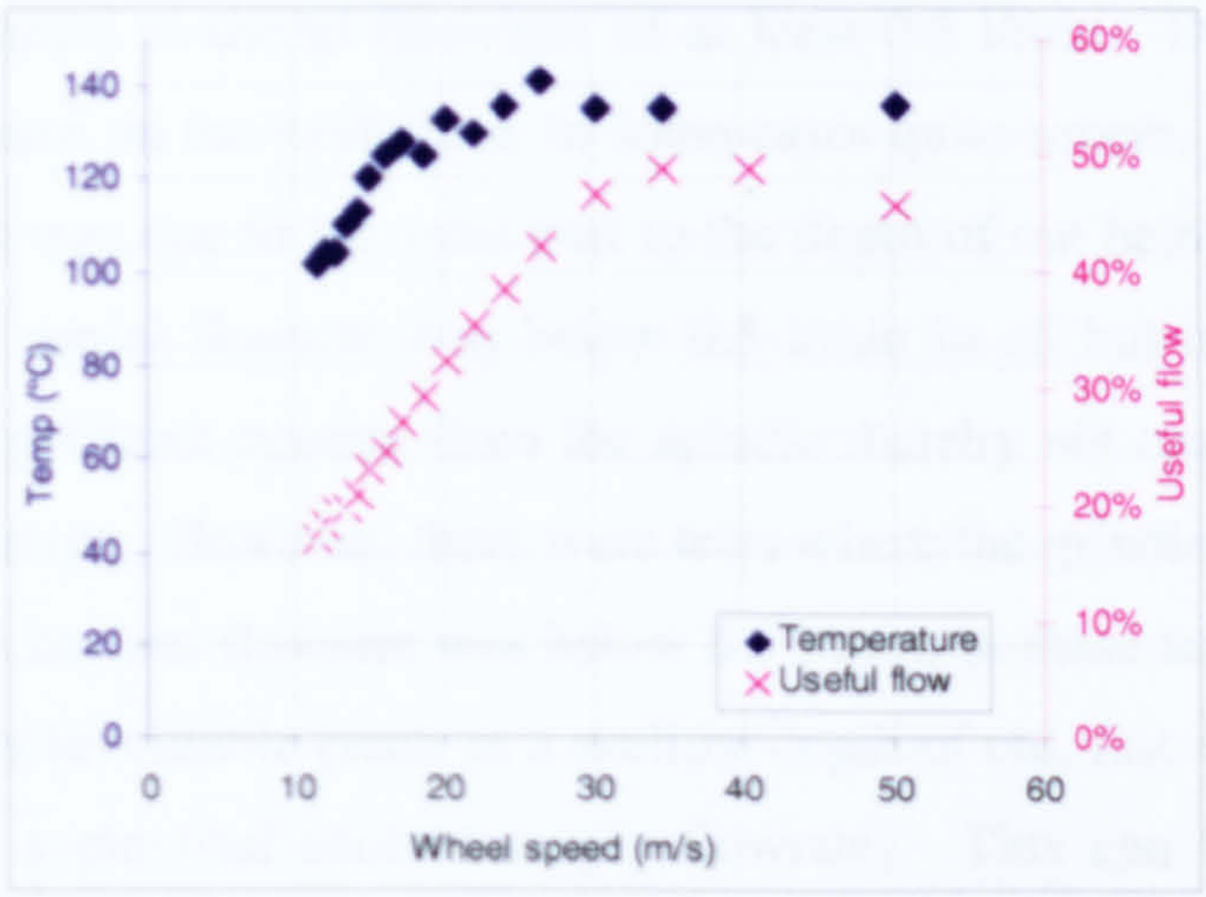

Figure 57, Temperature and percentage useful flow plotted against wheel speed from the Abwood speed ratio test on the Abwood grinding machine using the Altos grinding wheel when a=25 µm, v_w=6 mm/s, Q_d=18.9 l/min.

From Figure 58 it can be seen that a trend exists between the grinding zone temperature and the useful flowrate, the trend being an initial increase followed by a levelling-off when the flowrate reaches a certain value.

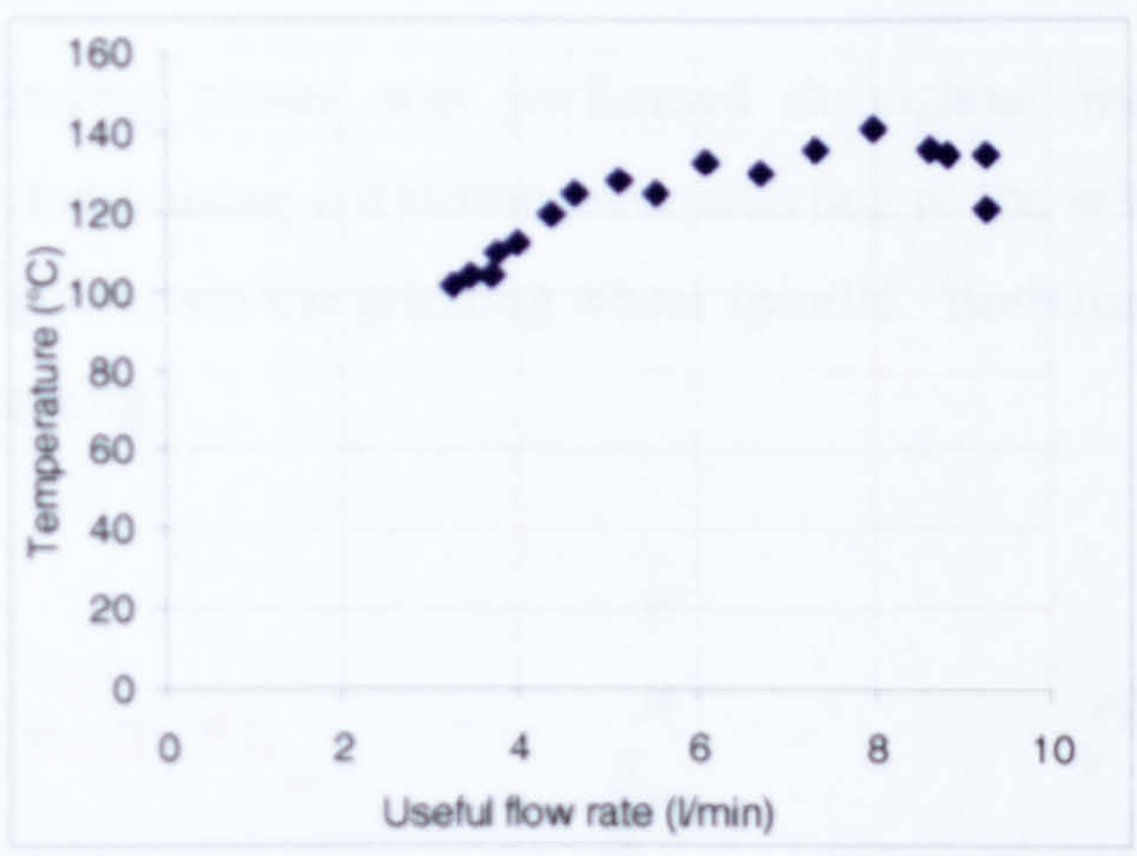

Figure 58, Temperature plotted against useful flowrate from the Abwood speed ratio test on the Abwood grinding machine using the Altos grinding wheel when a=25 µm, v_w=6 mm/s, Q_d=18.9 l/min.

Finally the Taguchi testing is considered in regards to temperature. Although the test was designed around the measurement of the useful flow, and as such the 'high' and 'low' were picked only to affect the useful flowrate, it is possible to examine the results in reference to grinding zone temperature. The extreme range of the parameters unfortunately did not lend itself well to temperature measurement, as such only half of

the tested values picked up temperature readings. It is however still possible to conclude qualitatively from these results based on the measured and visible thermal effects. For the three lowest temperatures from the tests a useful flow of 6-15% was measured, this equated to useful flowrates of at least 0.5 l/min. During several tests there was visible burn on the workpiece, in some cases quite severe, this can be seen in Appendix C. This was due in the most part to the depth of cut being the 'high' value. In these cases the useful flowrate was below 0.5 l/min in all but one test, where the author observed significant bounce from the spindle thereby not ensuring a constantly closed grinding contact. However, there were tests where the grinding temperature was acceptable and the coolant flowrate was below 0.5 l/min, in these tests the grind being attempted was very favourable (such as a shallow depth of cut, fast wheel speed with a fast workpiece or a plentiful coolant supply flowrate). This can be summarised by saying that in regards to temperature as a grinding process assessor that insufficient useful flowrate with large depth of cut and slow workpiece speeds can lead to thermal damage. Also it can be stated that a low useful flowrate is acceptable provided there is a small depth of cut and a high workpiece speed.

7.8.2 Grinding Power

Measuring the grinding power was performed throughout the testing phase by measurement of the force using a dynamometer attached to the workpiece or by direct measurement of the power via the grinding wheel spindle. Both methods proved robust and reliable during testing.

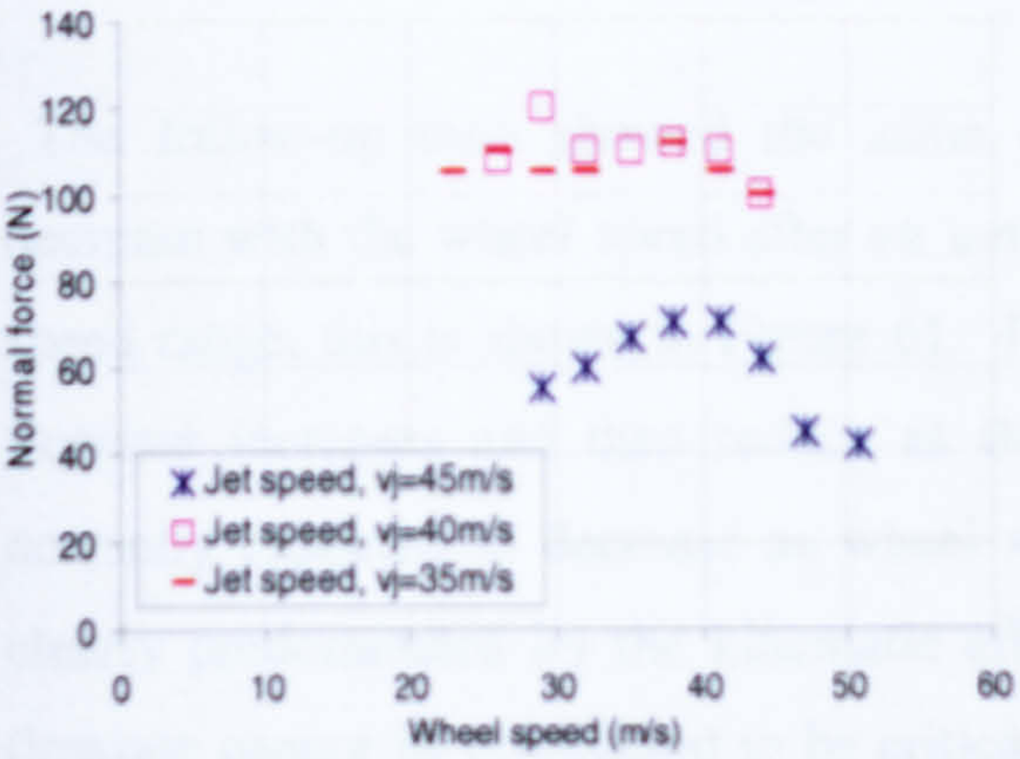

Figure 59, Tangential force against wheel speed for 3 different jet speeds from Preliminary Test 3 on the Abwood grinding machine using the Altos grinding wheel, a=25 µm, v_w=2 mm/s, Q_d=18.9 l/min.

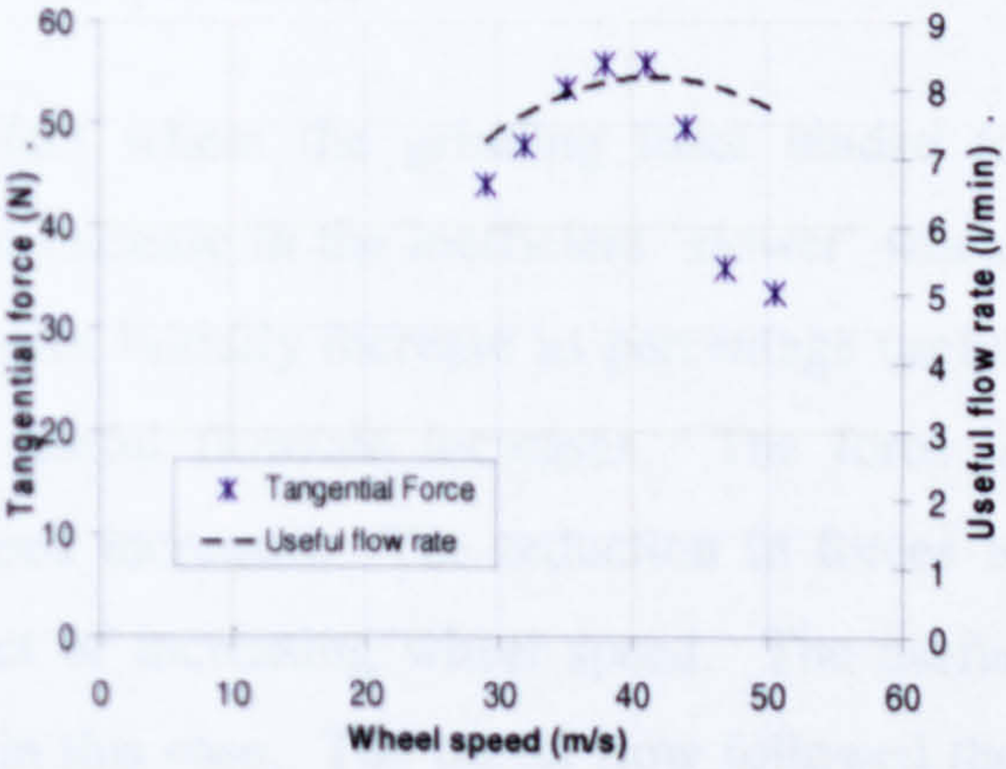

Figure 60, Tangential force and useful flowrate against wheel speed when jet speed = 45m/s from Preliminary Test 3 on the Abwood grinding machine using the Altos grinding wheel, a=25 µm, v_w=2 mm/s, Q_d=18.9 l/min.

For Preliminary Test 3, which was the first test equipped for force measurement the power remained low, again reinforcing the interpretation that this test had favourable grinding conditions, this can be seen in Figure 59 and in more detail in Figure 60 when plotted with useful flowrate. The force shows similar trend to the temperatures from Figure 55. Indeed Figure 60 shows how the force can increase as the wheel speed increases; however as the useful flowrate levels-off the force also tends to level-off or even drop. This is accompanied by the drop in useful flowrate expected when the wheel speed exceeds the jet speed, as proportionally less fluid is being carried by the wheel this could have an effect on force being measured. What can be seen is a general decreasing trend as the wheel speed increases, this is expected as a faster wheel speed means a smaller grain depth of cut.

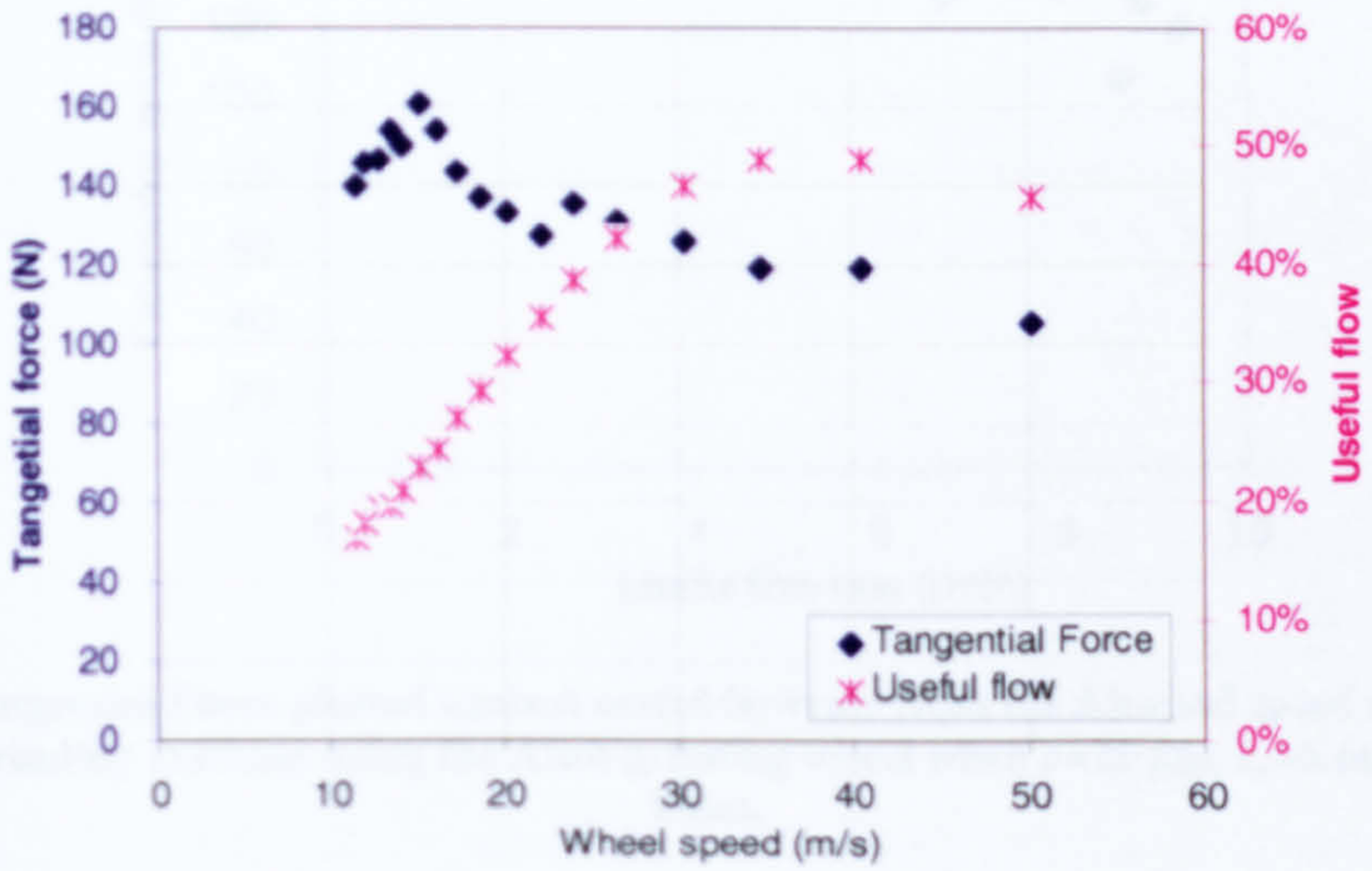

Figure 61, Tangential force and useful flow plotted against wheel speed from the Abwood speed ratio test on the Abwood grinding machine using the Altos grinding wheel when a=25 µm, v_w=6 mm/s, Q_d=18.9 l/min and v_j =24.3 m/s.

The follow-up tests showed the same effect where the grinding force tended to decrease with the wheel speed after an initial increase in the inefficient 'slower' wheel speed range, this is shown in Figure 61. Forces initially increase as percentage useful flowrate increases and then reduce as the useful flowrate increases. The force is normally expected to decrease as wheel speed increases. The reduction in forces is clearly predominated by the kinematic effect of increasing wheel speed. The useful flowrate cannot be considered to be critical in this case. The useful flow followed the same trend as the force, suggesting that there was always sufficient flowrate and that the wheel speed had the controlling influence over the tangential force.

This can be more interestingly displayed as shown in Figure 62, this illustrates the effect of useful flowrate appears to have on the tangential force, it can be seen that the force tends to decrease as the useful flowrate increases, barring one spurious point it could be considered to level-off at a useful flowrate of around 6 l/min. The initial increase is where the process is not receiving enough useful flow, beyond 4 l/min the flow appears to positively affecting the process and then beyond 6 l/min the benefits begin to tail off. To make definitive statements on these results is difficult as the purpose of the work was not to conduct large volumes of tests to directly prove the effect the useful flowrate has on the complex property of grinding force.

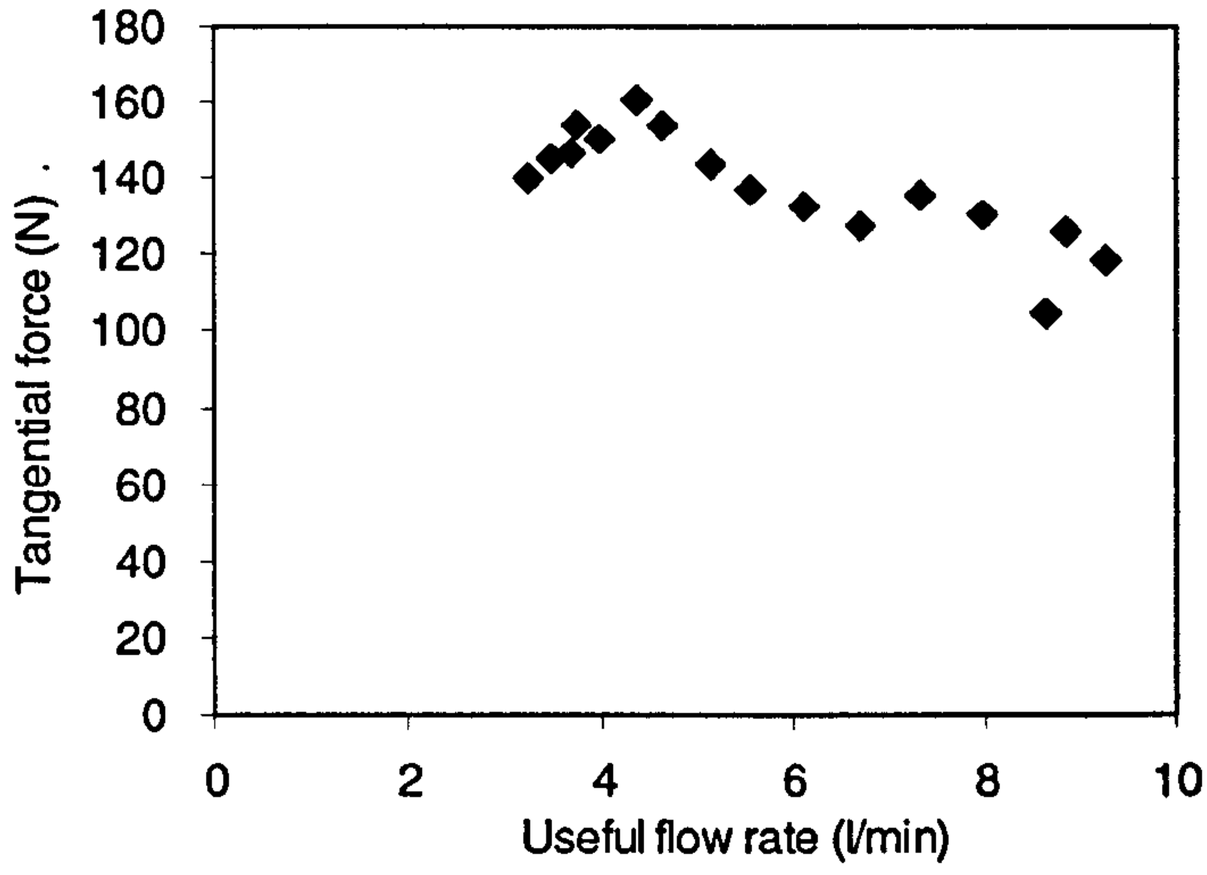

Figure 62, Tangential Force plotted against useful flowrate from the Abwood speed ratio test on the Abwood grinding machine using the Altos grinding wheel when a=25 µm, v_w=6 mm/s, Q_d=18.9 l/min.

During the Taguchi tests the power results were sufficient to draw some tentative conclusions. Again the values of high and low have affected the overall validity bringing the results to approximately an 80% confidence level. Statistically this is a low value and where the test designed to focus solely on power it would require re-designing. However, as with the temperature some qualitative conclusions can still be drawn. Analysis of the direct effects charts appears to show that the dressing condition, the wheel surface speed and the depth of cut have the biggest effect over the power readings.

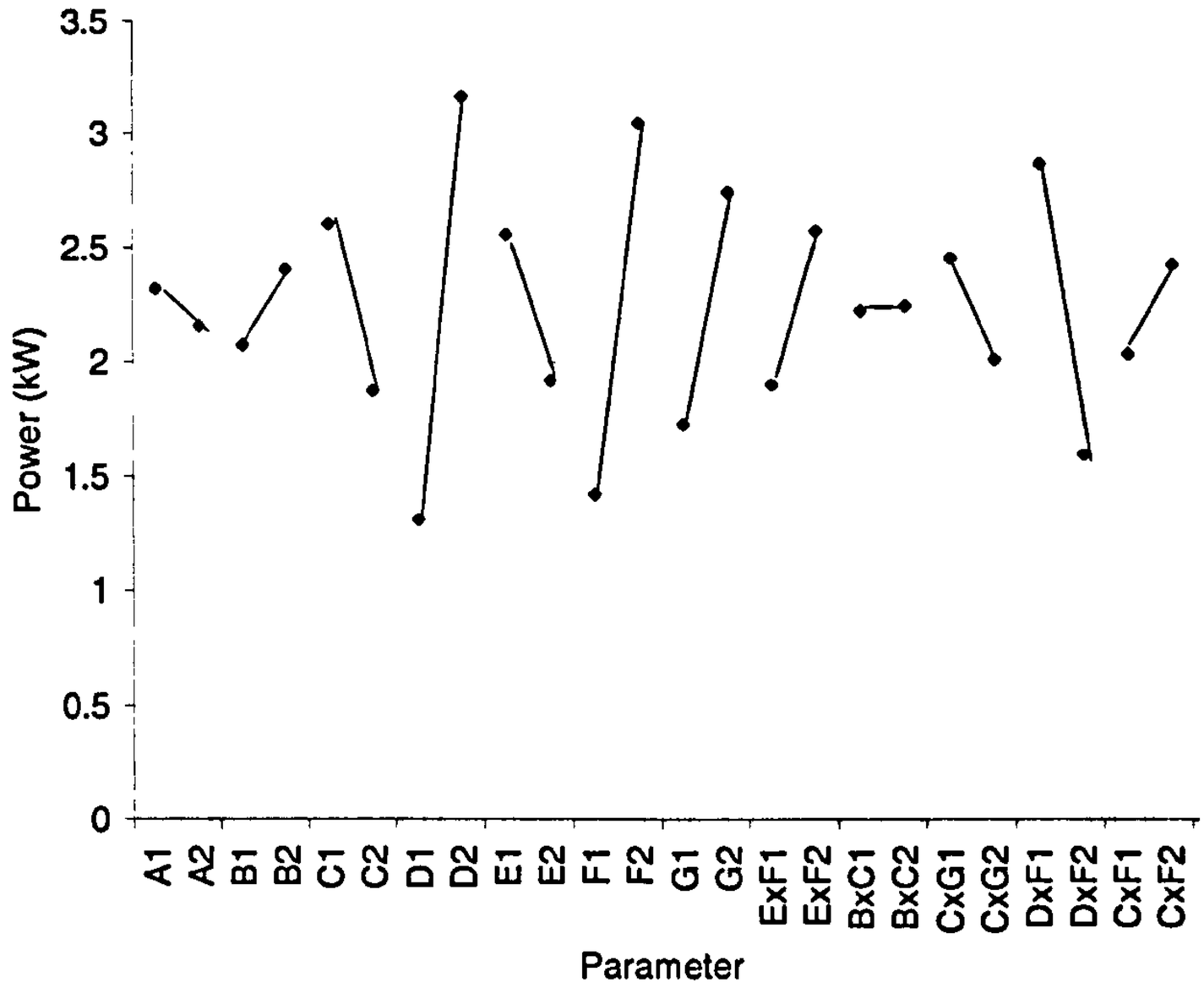

Figure 63, Direct effect chart for grinding power from the Taguchi test on the Dominator grinding machine using the Flexovit wheel. A = Material Type, B = Nozzle position, C = Jet Speed, D = Dressing condition, E = Work piece surface speed, F = Wheel surface speed and G = Engagement, Actual depth of cut.

These trends agree with what is generally understood to be true in the grinding industry. This validates some of the trends beyond the statistical methods. Several of the highest power readings from the Taguchi tests correlated to high useful flowrates, however these were the tests that experienced severe burn and significant juddering and bounce during the grind. Of the other tests where moderately high levels of power were measured there was an even spread of high to low useful flowrates, suggesting that the power is not significantly affected by the useful flowrate. Indeed the lowest useful flowrate measured did not have a high power reading.

Tentative conclusions can be made on the impact of sufficient flowrates and insufficient flowrates. The Taguchi tests provided limited insight into the power in regards to the useful flowrate. Earlier testing showed a possible correlation of useful flowrate to force, the exact trends are not clear as the far more influential factor of wheel speed masks the lesser effect of useful flowrate. The force when viewed in regards to speed ratio showed some effect, this ratio has been shown to affect the useful flowrate strongly and thus it could be stated that any correlation could be attributed to the useful flowrate achieved. This is not proof of a direct effect but certainly implies a relationship that should be investigated in depth during a subsequent project.

This series of testing shows a trend regarding the useful flow and the grinding force in reference to the speed ratio. The extent and influence of this trend still needs further verification, it is postulated that this effect may change when the wheel speed is above a certain value.

7.8.3 Surface Roughness

The direct effects charts extracted from the Taguchi test showed the main effects can be attributed to parameters D, F and to a lesser extent G. The confidence ratios for these parameters were just below 90%, a value that can be considered statistically low, suggesting the smaller effects should be scrutinised carefully in terms of their true influence. This is due to the appropriateness of the parameters chosen, for a test focussed solely on surface roughness the limits would have been different. It should be noted however that the dressing condition and wheel speed would be expected to strongly influence the surface roughness, thus agreeing with accepted industrial knowledge.

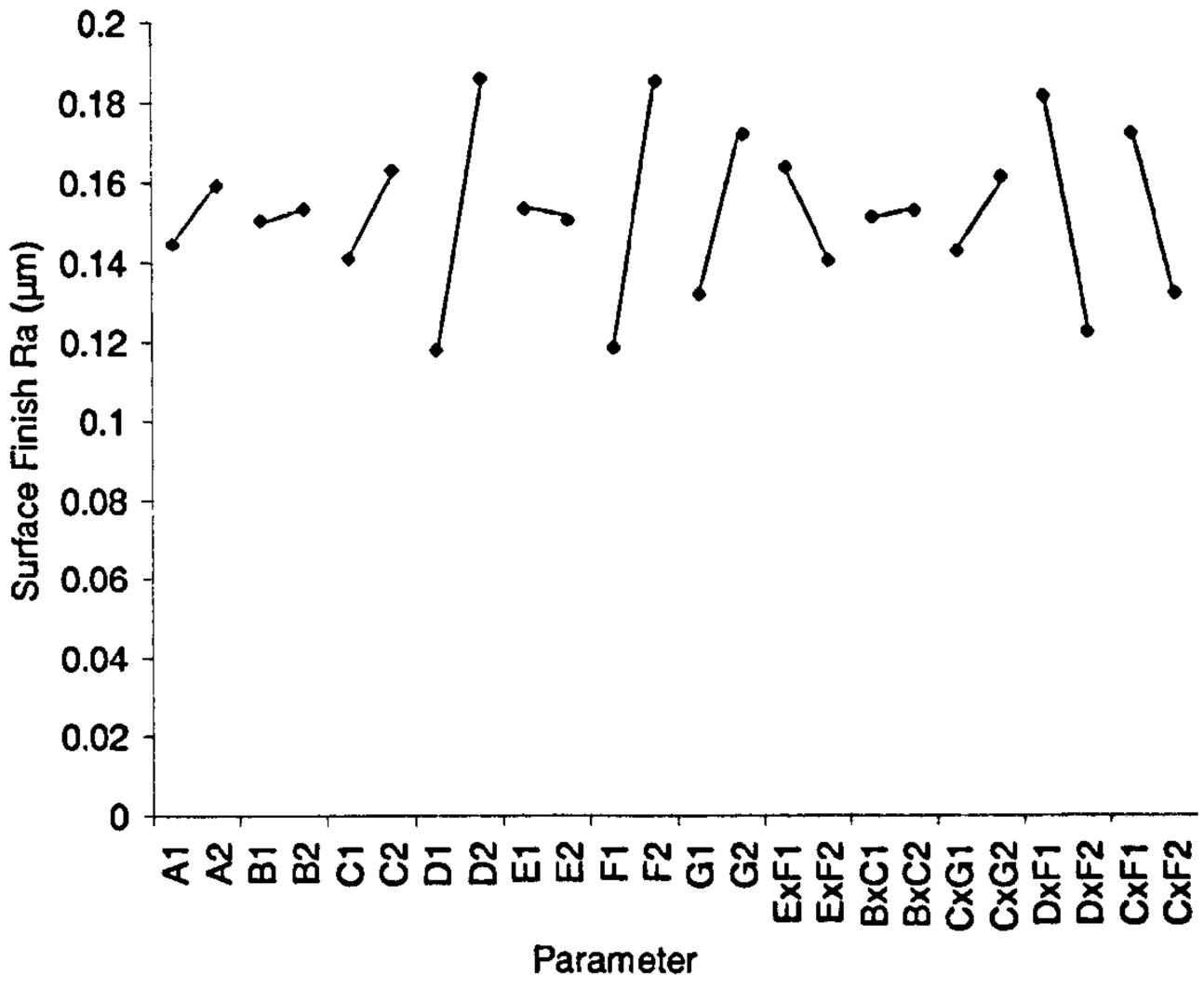

Figure 64, Direct effect chart for surface roughness, *Ra* from the Taguchi test on the Dominator grinding machine using the Flexovit wheel. A = Material Type, B = Nozzle position, C = Jet Speed, D = Dressing condition, E = Work piece surface speed, F = Wheel surface speed and G = Engagement, Actual depth of cut.

Examination of the data from these tests shows that for the best five surface roughness's not less than 0.6 l/min of useful flowrate was achieved, showing no influence from the nozzle flowrate/speed. Two out of the three worst surface

roughness's corresponded to measurements of useful flowrate lower than 0.6 l/min, also correlating to the fine dressing condition and the fast wheel speed.

To summarise, there is a correlation between grinding and dressing conditions and surface roughness. These effects tend to mask direct effects that might be attributed to useful flowrate. Any direct effect would need to be investigated with a more conventional analysis of effects of useful flowrate under carefully controlled experiments where effects of dressing and grinding conditions are eliminated.

Chapter 8. Topography Trials

8.1 Aim

The hypothesis of the project is that there is a correlation between the surface topography of the grinding wheel and the amount of flow that can be passed through the grinding zone. It was anticipated that a correlation could lead to a predictive model that would require minimal or no extra testing and understanding of the wheel to predict an achievable useful flowrate.

8.2 Approach

In approaching this issue from the standpoint of convenient flow it becomes necessary to define some wheel characteristics that are not standard and can maybe be varied and controlled, namely the surface topography of the grinding wheel. The topography is mainly dependant on two factors, these being the manufacturer's design specification and the dressing applied to a wheel by the user. The relevant parts of the specification will be the grain size, bonding type and the level of porosity. Certain types of wheels lend themselves to the need for further verification beyond the range of this work, such as the Spherowin™ technology used by Winterthur, Germany. The Spherowin™ technology creates porosity by the introduction of micro-bubbles in addition to bonding material and abrasive grains.

It is known that dressing will affect the performance of a wheel; this is generally understood to be the effect of removing wheel loading and creating new cutting faces. However, the practice of dressing may affect the fluid carrying capability of the wheel, this is most certainly true in regards to re-opening pores by removing swarf from within them. Dressing may also provide benefit from the effect of bond fracture and therefore the creation of new pores roughly the size of the abrasive grains that have been removed.

The basic model for useful flow has been described previously as the Rowe model, found in Marinescu *et al* (2004) as

$$Q_u = v \times b_s \times h_{uf} \tag{39}$$

This can be re-written for 2 dimensional convenient flow as follows.

$$Q_c' = v_s . \phi_b . h_{pores} \tag{40}$$

Where v = characteristic speed, b_s = grinding wheel width, h_{uf} = Equivalent fluid film thickness, h_{pores} = Average pore depth and ϕ_b = Bulk wheel porosity.

The model shown in equation (39) is the basis of all models developed to date. From this equation the heavy dependence on a value of speed is clear, this is generally the grinding wheel speed, v_s. The definition of the equivalent fluid layer thickness, h_{uf} is where most variations in modelling exist. The proposition of this work is that the fluid layer and hence useful flow can be intrinsically linked to what is referred to within this work as the convenient flow. This being the amount of fluid a wheel can transport based on its surface topography.

By analysing the structure of the topography of the wheel surface and approximating the amount of fluid the wheel can carry, without excessive fluid penetration, it may be possible to approximate a target for supply flowrate based on approaching or surpassing the value of convenient flow.

8.3 Experimentation

In order to support the theory that the fluid carrying capability of the wheel is an integral factor in useful flow, several experiments were undertaken to measure the surface topography and the useful flow. Some initial tests were carried out, with the purpose being to test the equipment and develop the systems that would be required in analysis. The first test was designed to measure and quantify the surface topography of a grinding wheel dressed using various values of dressing depth and dressing lead. Quantifying the values of surface topography allows the fluid carrying capability of the wheel, or the convenient flow to be approximated. By varying the dressing during these tests the influence of this factor on the convenient flow can be approximated. The second was to test the effect the bedding-in process has on the surface topography. The third was to analyse two wheels of varying porosity and grain size. These values can then be compared to the measured amounts of fluid collected during the grinding trials.

8.3.1 Initial Topography Tests

In order to begin the analysis some initial testing was planned to verify the process of capturing and analysing the surface topography of the wheel, as described and used by Cai (2002). This initial test used the Microset 101RF replica type substance described in Chapter 4.3.1, to take an impression of the wheel surface. This impression was then

measured using the OSP100A optical scanner so a topography could be recreated with software techniques.

Initial testing was conducted on the Altos grinding wheel. One such result can be seen in Figure 65, this initial image shows the negative impression that the replica gives, thus the high spots in the image correlate to pores within the wheel structure. This shows the image prior to the inversion and filtering technique described earlier. A large sample area (20 mm x 15 mm) was used for the first test so an overall view of the wheel could be produced. The left and right edges of the sample clearly show the curvature of the wheel. Later techniques removed this distortion so a clearer view can be taken and the curvature of the wheel can be disregarded. This initial test proved the validity of the processes, in good agreement with Cai (2002).

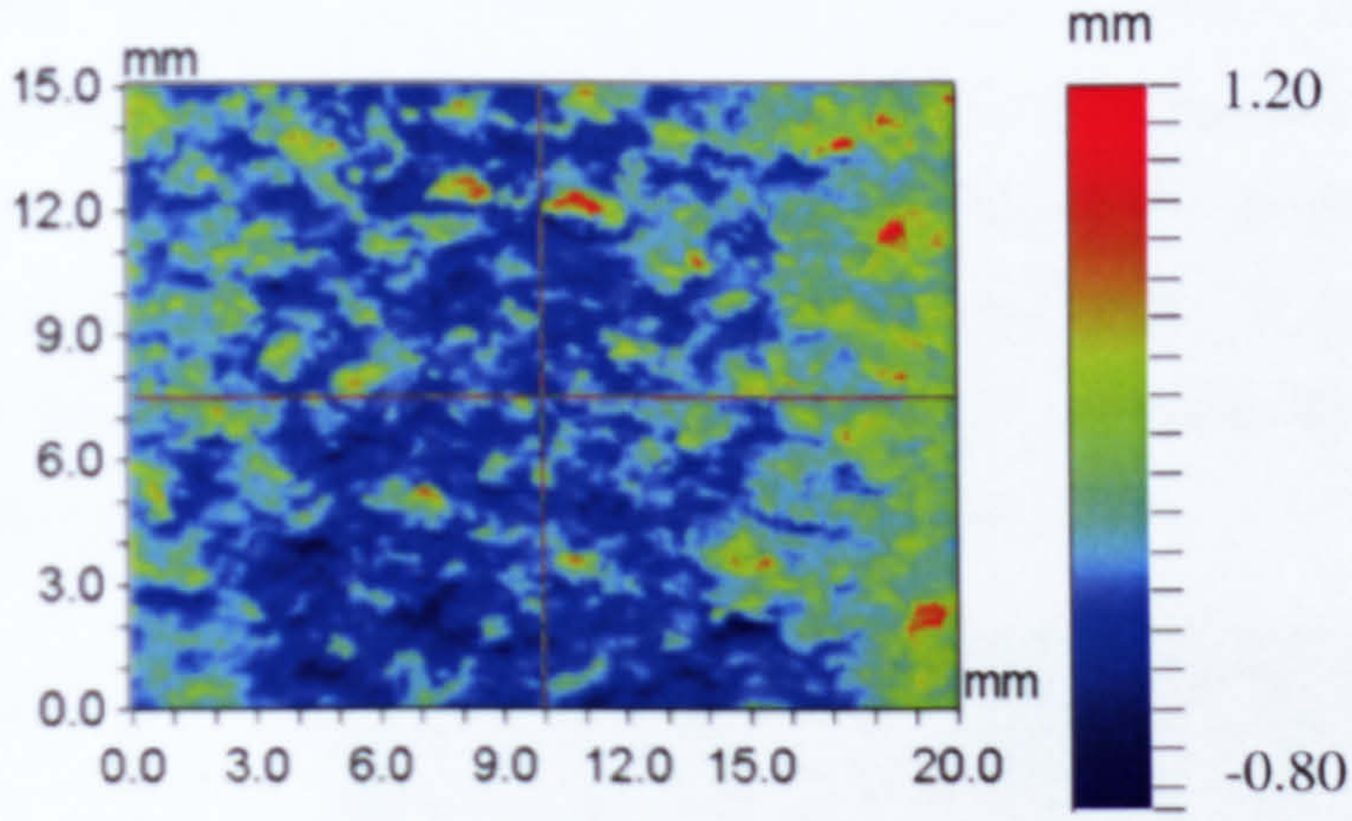

Figure 65, Preliminary contour plot of the wheel replica.

8.3.2 Dressing tests

In order to investigate the effect dressing has on wheel surface topography a test was conducted where dressing was varied over a range of overlap ratios.

Krishnan (1995) stated that dressing depth has an effect on useful flow but that dressing lead was largely ineffectual. If this is true then varying the dressing depth will have an obvious effect on the topography; thus any measurement parameter used during this test that shows a significant change can be used as an estimator of the fluid carrying capacity of the wheel. This can be further clarified by using the test where dressing lead is varied and checking that any variation is minimal. The test was conducted using the plan shown in Table 24.

Test Order	Dressing Parameters						Overlap ratio, Ud
	Dressing feed rate, f_d		Dressing depth, a_d		No. of passes		
1	50	mm/min	20	µm	2		10
2	50	mm/min	5	µm	2		10
3	250	mm/min	20	µm	2		2
4	500	mm/min	20	µm	2		1
5	750	mm/min	20	µm	2		0.67

Table 24, Topography test experimental plan.

8.3.2.1 Results

The intention of the topography test was to show how the dressing parameters can affect the surface topography of the wheel. However, Figure 67 shows how the principal surface roughness parameters exhibit minimal variation due to the changes to the dressing variables. It is the R_t value (peak to trough distance) that shows any reasonable variation. However it is known that the R_t value is strongly affected by the extreme values that may exist within a sample. The large variations in the value of R_t cannot have resulted from dressing variations alone. In Figure 66 the R_t is 2mm, this cannot have been directly attributed to 2 dressing passes each at 20 µm depth of cut. A visual check was performed on the surface of the sample to verify the scale of the variation was in the order of millimetres rather than microns.

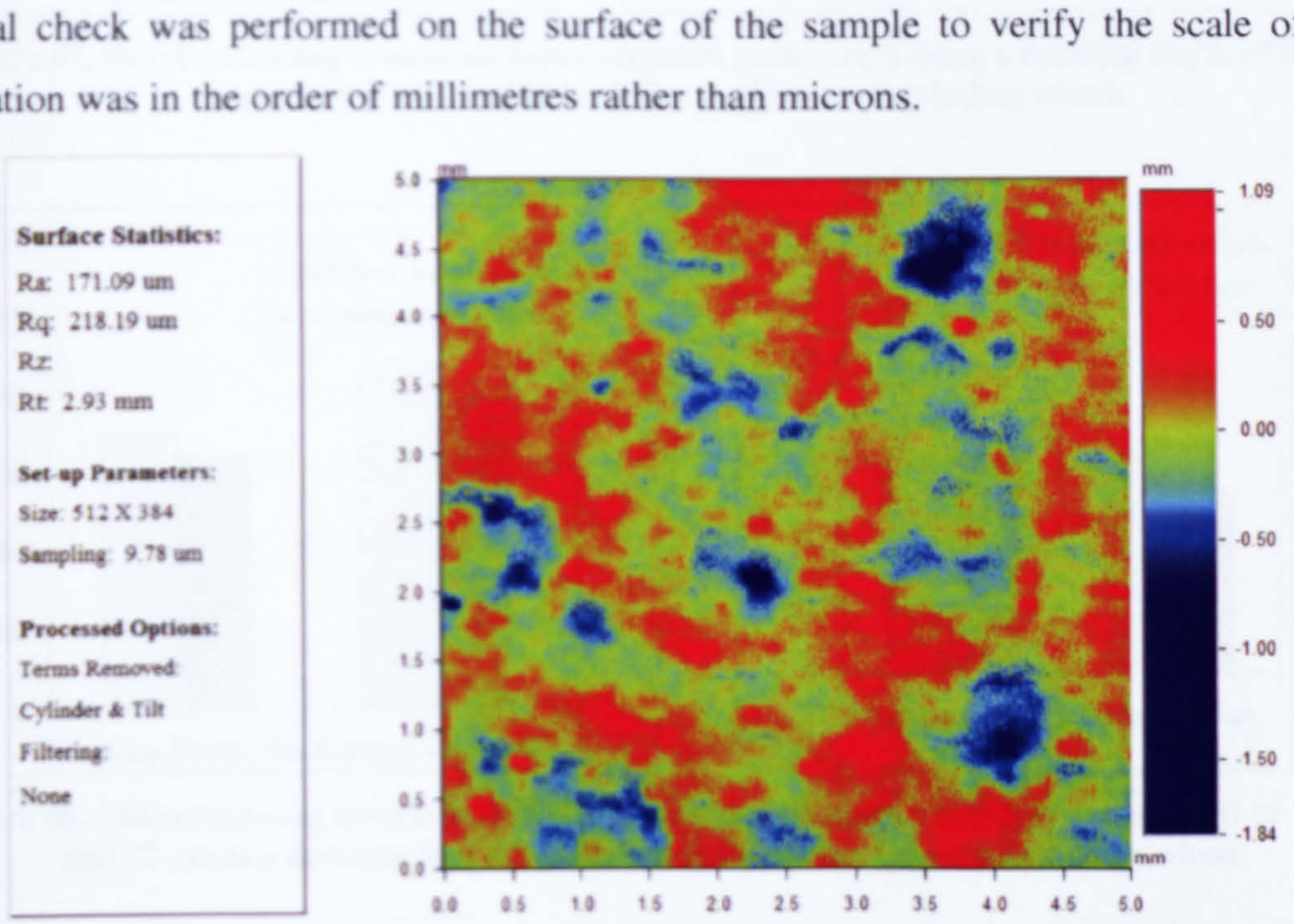

Figure 66, Wyko analysis of topography data in initial testing of the Universal wheel.

Although dressing is known to improve grinding performance by exposing new cutting faces and cleaning the wheel of swarf it does so without making large scale changes to the surface topography of the wheel. The more significant voids exist as a function of

the wheel type. The measurement of R_t (approximately 2 mm) shown in Figure 65 for the Altos wheel and then Figure 66 for the universal wheel with a reasonably porous matrix are several times larger than the values Cai (2002) reports for a vitrified bond cBN wheel (R_t = 0.5mm, for similar measurement method); thus defining the wheel structure is the over-riding factor in fluid pore space availability. However, it should be mentioned that a significantly robust dressing pass (very fast feed rate, f_d or very deep dress depth, a_d) could cause extra pore spaces to occur via bond fracture, so it should be noted that in some cases the dressing can have an effect.

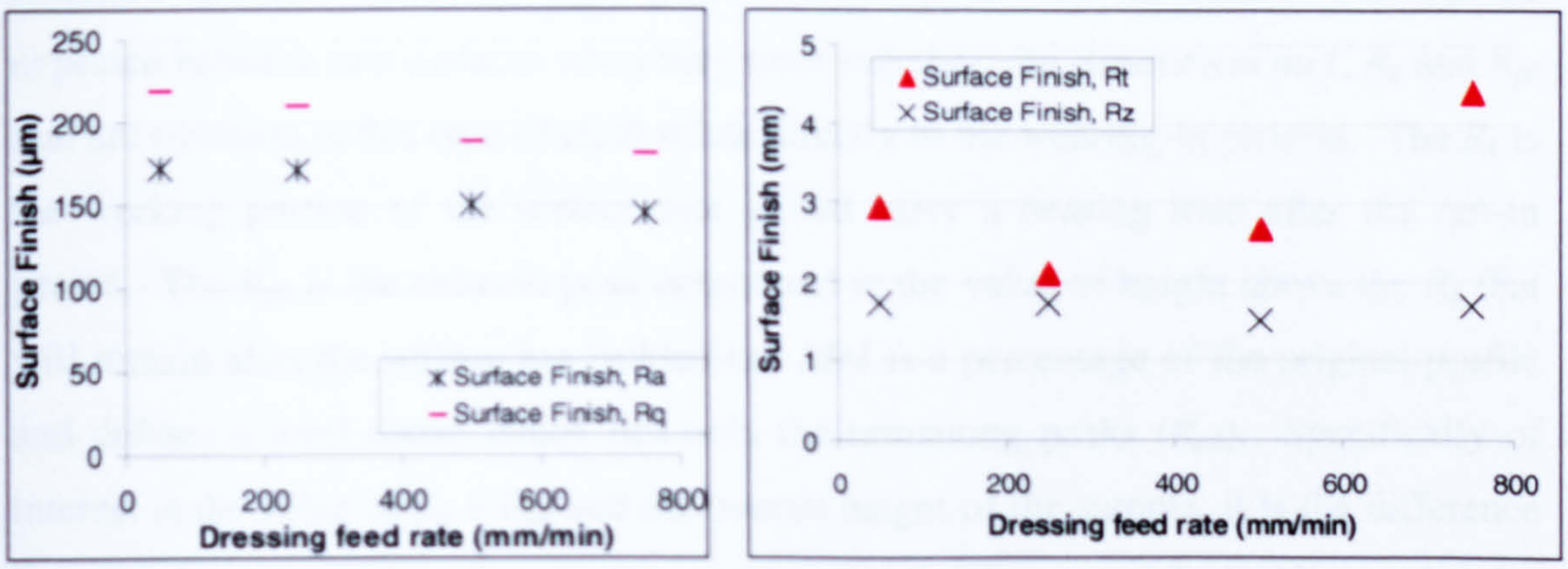

Figure 67, Graphs showing several surface roughness parameters using a dressing depth of 20 µm and a range of dressing leads for the Universal grinding wheel.

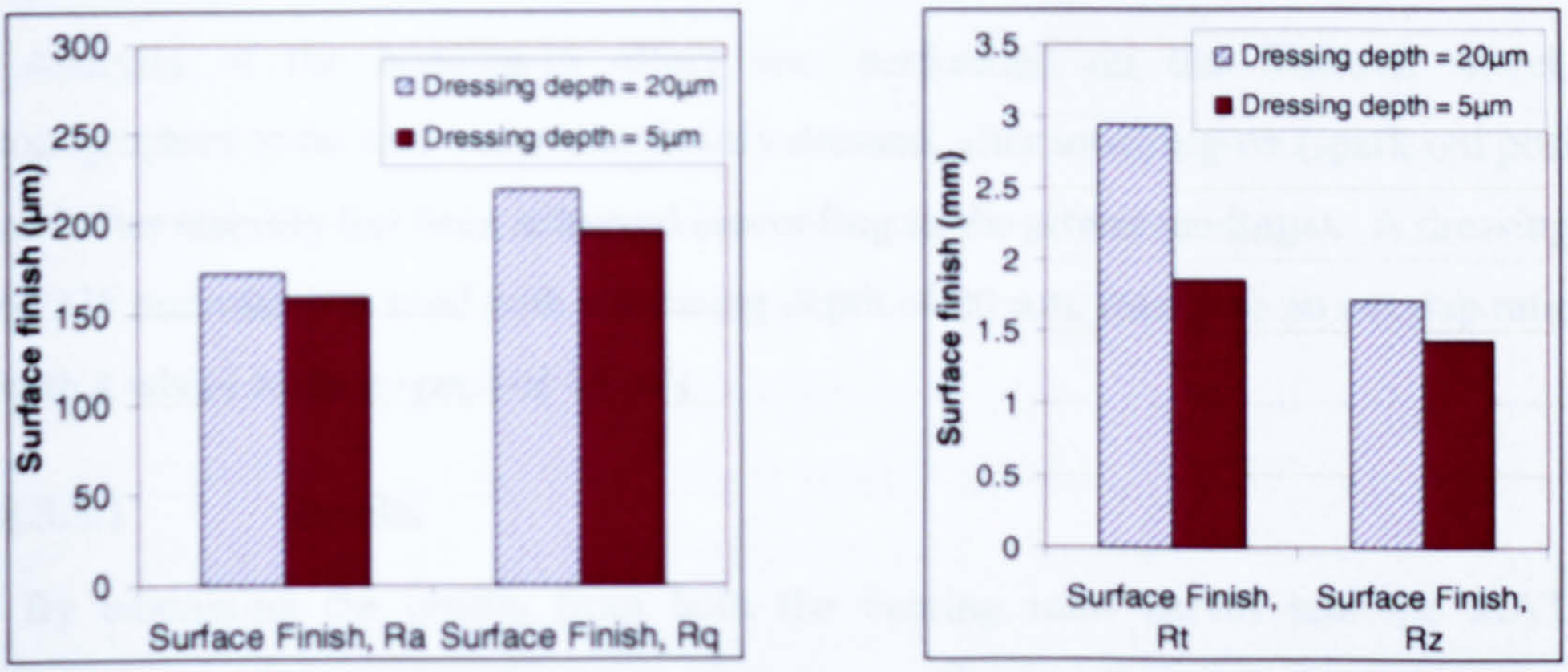

Figure 68, Charts showing several surface finish parameters using a depth of dressing cut of 5 µm and 20 µm at a dressing feed rate of 50 mm/min for the Universal grinding wheel.

8.3.3 Bedding-in tests

Most analysis of wheel surfaces is performed on either freshly dressed wheels or heavily used wheels. It is known that just after dressing a grinding wheel in use will show unstable power characteristics due to the larger/weaker peaks being removed. The remaining stronger peaks of the wheel carry the load and perform the actual material

removal. This is known commonly as the bedding-in process, run-in process or wear-in process and is when the 'weaker' peaks of the surface topography are removed by direct contact with a workpiece. It is therefore necessary to investigate the effect that the bedding-in process has on the surface topography.

This bedding-in is common to other mating-surface processes such as bearings and as such has led to various surface roughness parameters being defined. Most notable are the ones which relate to a graph called a Bearing Ratio Curve, as defined in the British Standard EN ISO 13565-2. This graph shows the amount of contact that can be expected between two surfaces when they mate together, the parameters *mr1*, R_k and R_{pk} that are common to this type of chart relate directly to the wearing-in process. The R_k is the working portion of the surface that would carry a bearing load after the run-in period. The R_{pk} is the reduced peak height and is the value of height above the R_k that will remain after the surface has bedded-in. *Mr1* is a percentage of the original profile and defines a level above which lies only the remaining peaks (R_{pk}). Specifically of interest is the value of $R_k + R_{pk}$ and the overall height of the sample, it is the difference between these two values that can be considered in bearing terms the bedding-in height. A diagram explaining these parameters can be found in Appendix C.

Analysis of the bedding-in effect was performed on the Flexovit wheel, the topographies to be analysed were; freshly dressed, after touching-on (spark out position) and after stability has been achieved (according to the power readings). A dressing lead of 375 mm/min was used with a dressing depth of 20 µm; this gave an overlap ratio of 2 with a wheel surface speed of 45 m/s.

8.3.3.1 Results

By examining the results from both the bearing ratio curves and the MATLAB analysis some interesting features can be seen. The small sample bearing ratio curve predicts that the load will be carried at a height of ~252 µm, this is given by the sum of the positive R_k value, labelled on the left side of the bearing ratio curve as Z, and the R_{pk} value, seen in Figure 69. When compared to the measured peak value of 628 µm it can be expected that 380 µm will be removed during the bedding-in process. This position of load carrying height is analogous to a worn-in or bedded-in height, as described in previous chapters. This can be compared to the test results where the worn-in peak height is 404 µm, visible in Figure 70.

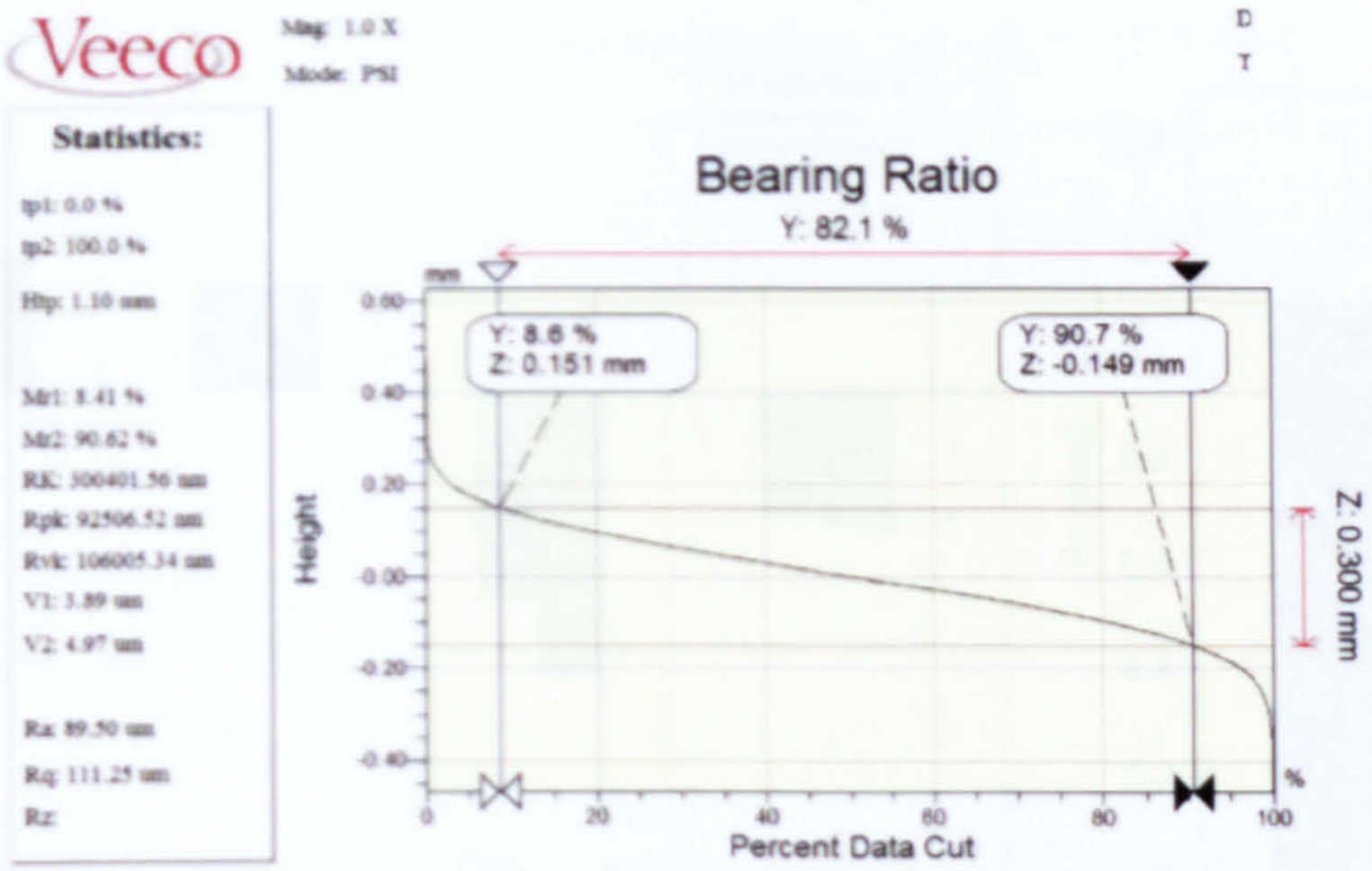

Figure 69, Bearing ratio curve for the freshly dressed small sample of the Flexovit grinding wheel, note the markers on the curve showing the positive and negative values that sum to give the R_k value.

The situation the Bearing Ratio curve describes is analogous but not directly comparable, a bearing ratio curve applies to materials of similar hardness. In grinding this is obviously not the case as the grinding wheel (more specifically the abrasive grain) is magnitudes harder than the workpiece. Although the wheel will wear slightly due to the bedding-in processes it will not be expected to wear as much as it's opposing surface and the amount of wear will depend heavily on the surface it is in contact with. It can also be seen in Figure 70 that there is a slight increase in peak height from the 1 pass to the 100 passes result. This is due to the exact positioning of the sample on the surface of the wheel. The value of peak height is dependant on the level that the system defines as zero. This zero is decided based on the arithmetic mean of all the points. Examination of both the filtered and unfiltered results show that the peak removal is roughly 50% of the overall peak height of the pores (see Figure 70), this relates to 15% of the overall peak-to-trough height in the sample, as shown in Figure 71. All results are shown in Appendix C. The more easily comparable value is the R_t given in Figure 71, this values shows a decrease of ~170 μm between the freshly dressed and worn-in wheel states. It can also be seen from Figure 71 that the majority of removal of these extraneous peaks happens very quickly after dressing, possibly within a few passes of a grinding wheel.

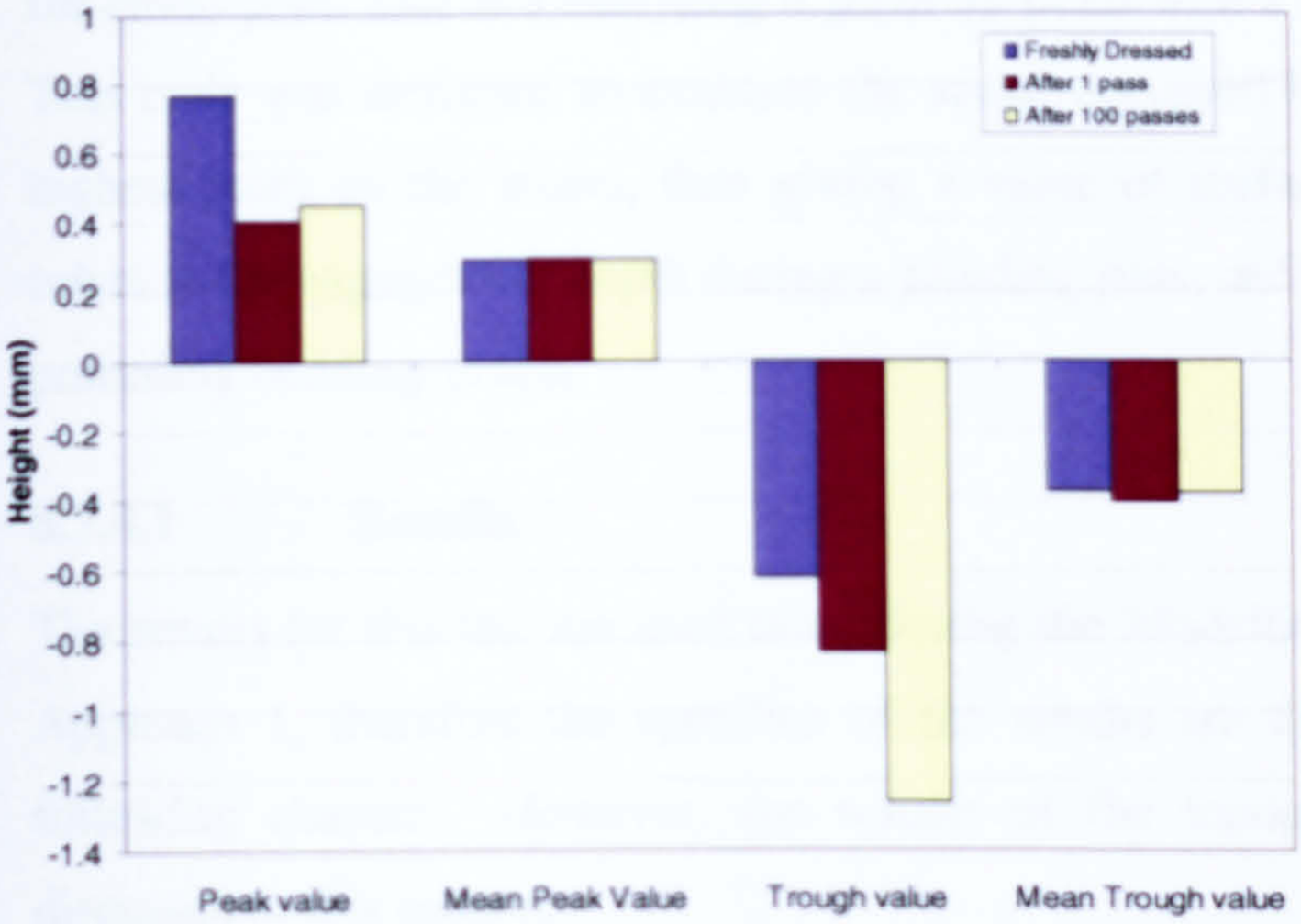

Figure 70, Peak height using a small sample of the Flexovit wheel.

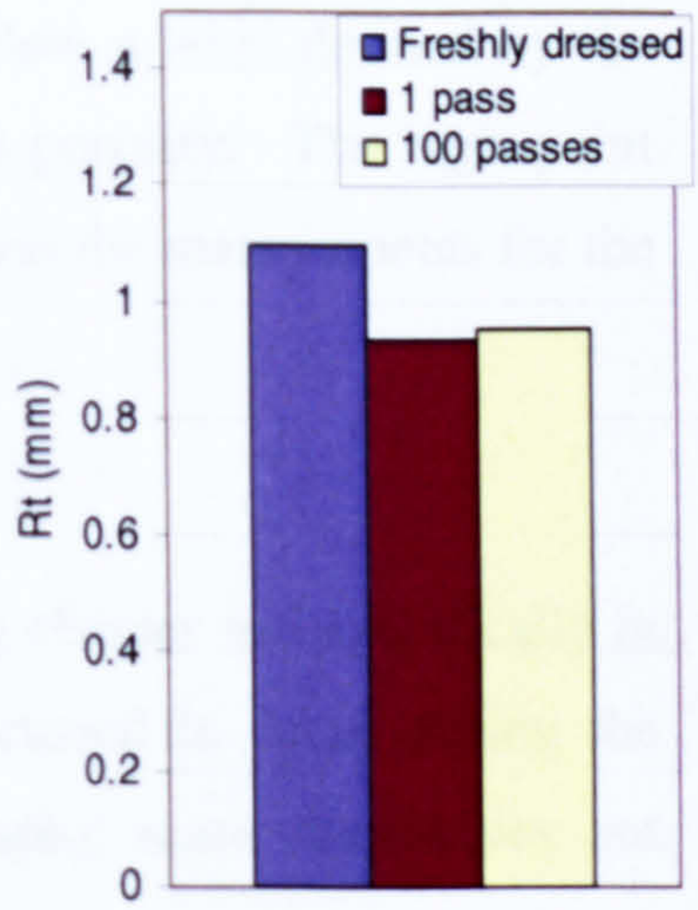

Figure 71, Values of R_t using a small sample of the Flexovit wheel.

Analysis of the surfaces also allowed a mean to be taken of the heights of the peaks, it was found that the difference between the mean of the maximum heights and troughs varied little through all the samples. It also becomes apparent that the mean peak height value for the wheel in any state is similar to the worn-in value predicted by the bearing ratio curve. This is shown in the bearing ratio curve in Figure 69, and was described previously as 252 μm roughly agrees with the mean peak value of 260 μm shown in Figure 70. This process of averaging the highest points is found to remove less than 1% of the points within the sample.

8.3.4 Grinding trials

In order to correlate the topography to the useful flow testing, it was necessary to take samples from the grinding wheels which had been used for useful flow collections trials. These were the Altos and Flexovit wheels. All samples were taken during the ground-in steady state for the wheel surface. Sampling was performed in two ways; one was as larger sample of 19 mm x 25 mm and another 'close-up' of 5 mm x 5 mm. This allowed evaluation of both the averaged values and the individual feature values. It can be seen from Figure 72 that the smaller sample size is a close-up of a section of the large sample (noting the slightly different scales employed in each image).

The purpose of these tests were to approximate the space available within the surface of the wheel that can be conveniently occupied by fluid. This was achieved by taking

the cloud point data and analysing it point by point with a user-created MATLAB code. This code was designed to evaluate the space occupied below a level defined by the highest point on the wheel, thus giving a value of surface porosity. The high point refers to the engagement depth during a grinding pass, and was the main impetus for the preceding bedding-in test.

8.3.4.1 Results

The results for this test are used more during the Modelling chapter and specifically in Approach 1, therefore the specifics of the results are discussed in detail during the following chapter. However, the results of the topography scans themselves are discussed in this section.

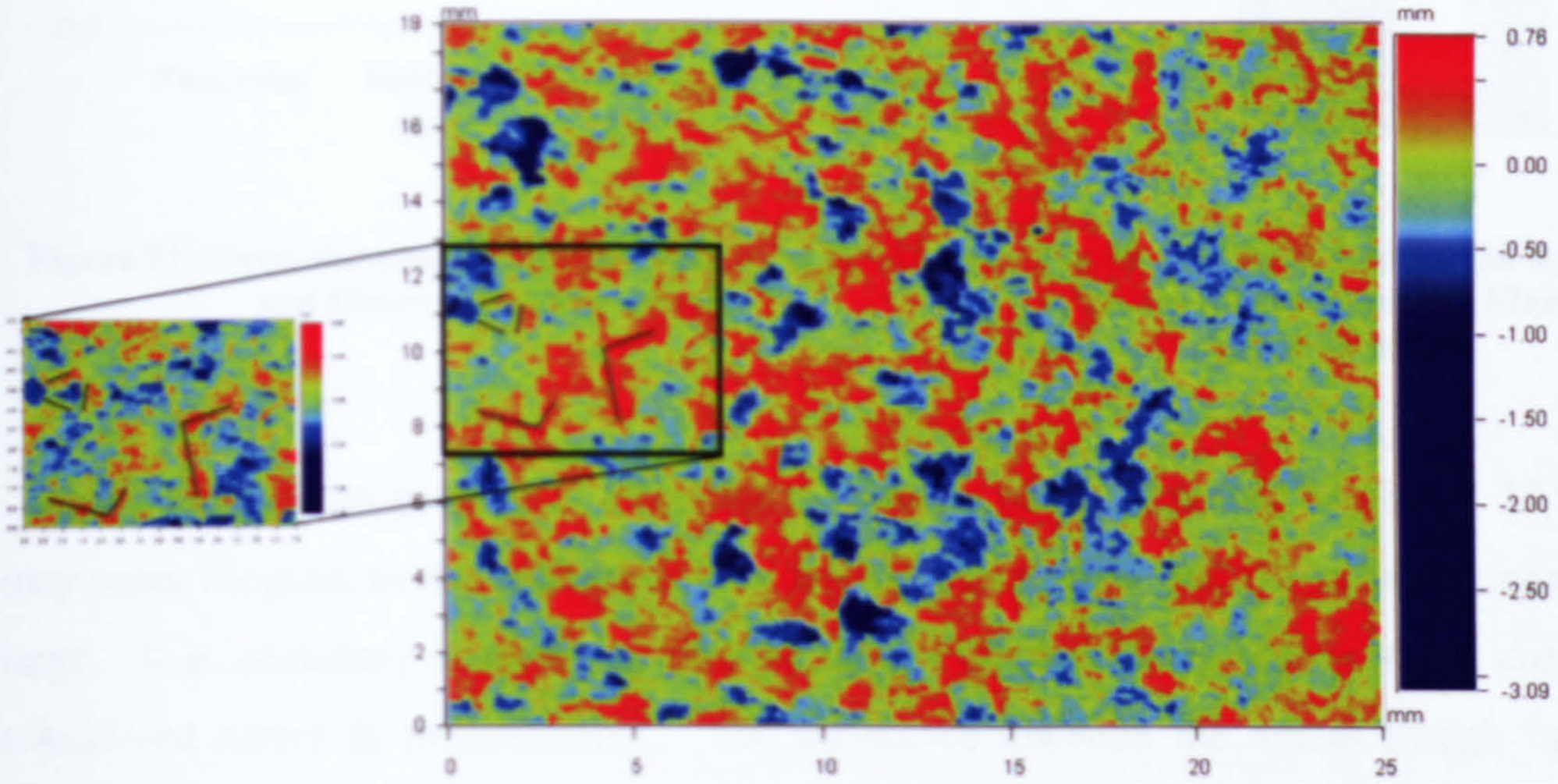

Figure 72, Diagram showing the smaller sample in reference to the larger sample, with key features identified.

Analysis of these samples required some features to be clearly defined, the most important being the highest point of the analysis as a reference. This high point was found to be somewhat ambiguous depending on the interpretation of the wheel curvature by the Wyko Software. An example of a contour map is visible in Figure 72. The peak values from the same wheels do not seem to correlate, however by taking an average of the peaks through the sample a reliable value is reached showing consistency between wheel types. This is logical as the samples are not taken in the exact same position on the wheel so variation in exact peak height is to be expected. The small sample was found to have less than 30 peaks per sample, this made it susceptible to population fluctuations. What can also be seen in Figure 73 is the variation in the

trough value for the larger sample, this shows the open nature of the structure of the Altos wheel. As mentioned previously, the Altos wheel was a one-off designed to have an extremely open bond type and with the large/long grains used the surface tends to have large voids.

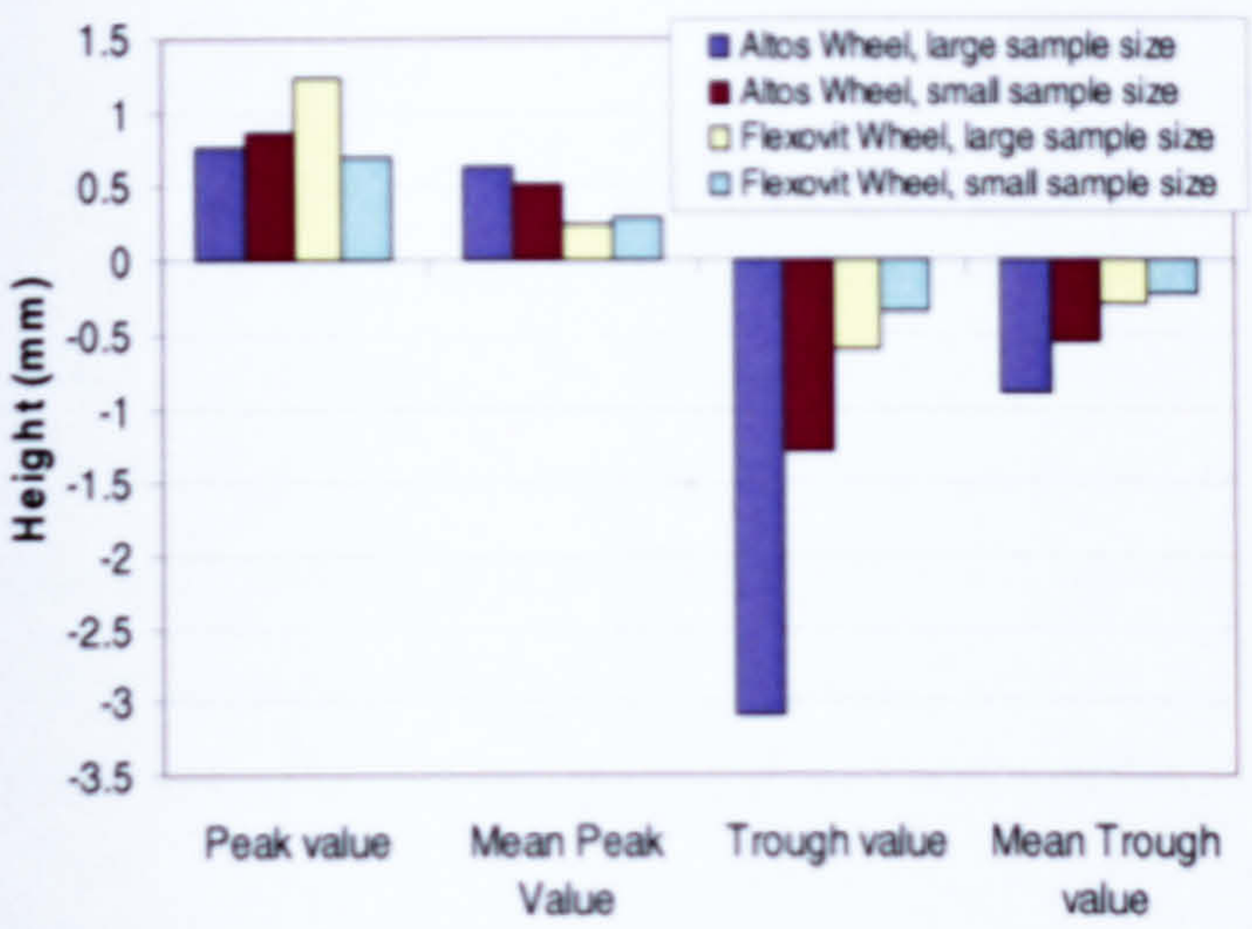

Figure 73, Chart showing topography data from the Altos and Flexovit grinding wheels.

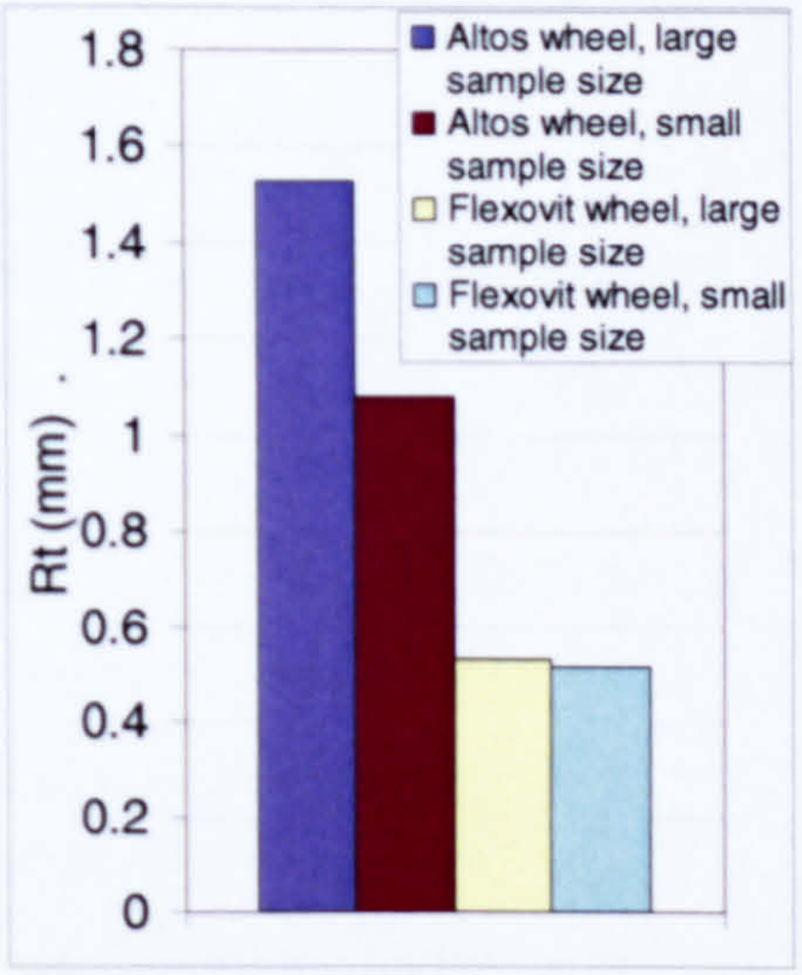

Figure 74, Chart showing the R_t of the means for the Altos and Flexovit grinding wheels.

During analysis an average is taken for the lowest point. Looking at Figure 73 this may seem illogical as the difference between the mean value and the extreme value is large. It is necessary however to remove these extreme trough values, these can be considered errors in measurement. The difference between the actual trough value (lowest point in the sample) and the mean trough value is representative of less than 0.5% by volume of the overall sample. This small volume represents pores of considerable size, however these pores are infrequent and sporadic in the Altos wheel; for example in the 19 mm x 25 mm sample only 3 such pores existed and in the smaller sample size there is none of the same magnitude. In the smaller samples there is no need to account for this possibility as the samples taken never had the extreme pores/errors. Indeed for similar testing on the other grinding wheels this situation was even sparser.

The evaluation of wheel surface porosity and the use of these results for comparative purposes is given in the next chapter.

Chapter 9. Modelling

9.1 Introduction

The final part of the work is to use the knowledge from the testing procedures to predict the amount of useful flow that can be achieved; or to predict the amount of flow that needs to be applied to achieve a good grind. These two approaches are different and each is defined.

One method is based on the topography work and defines what can be achieved if the pores of the wheel are filled or nearly filled. This is then compared with the experimental work to define a value of the percentage of the pores that are filled. The second approach uses the grinding trials to approximate a value of convenient flow that can be achieved during a grinding trial based on the equivalent fluid film thickness, h_{uf}. This value of h_{uf} is then compared to known physical data from the grinding wheel.

9.2 Approach 1

The first approach uses the idea that the pores can be filled completely with fluid, and that the full pores would approximately define a value of *maximum* useful flow or convenient flowrate. This value is then adjusted to account for the assumption that the pores can never be completely filled. This gives a value of achievable useful flow, based on the wheel surface topography; this value is always dependant upon a sufficient supply flowrate and jet speed and should never be considered independently of these factors.

Using a code developed in MATLAB, profiles of the wheel surface were re-created from the surface samples and used to calculate the space available on average throughout the sample. By coupling the profiles with the results of the bedding-in analysis and an assumed wheel speed, a value of useful flow could be approximated for what could be described as a rotationally symmetrical grinding wheel. This idealised wheel surface is obviously not representative of the true surface of a grinding wheel, instead it would resemble a multi grooved vee-belt pulley wheel. A factor must be used in order to account for this distorted situation, it has been postulated that the bulk wheel porosity would be suitable for such an adaptation. This analysis system allows an approximation of the wheel carrying capabilities to be performed for each sample. This can be seen in Figure 76 and Figure 77.

9.2.1 Methodology

The most important part of this approach is the MATLAB code producing the value of convenient flow. The program performing this calculation can be seen in Appendix D. The MATLAB code starts by extracting important values from the sample. These include several key features, such as the highest and lowest points throughout the entire data set. The value of lowest position is taken from finding the minimum of the entire dataset. This value represents the lowest point of measurement into the wheel, the depth of the deepest pore. The code then breaks the sample down into 2D strips of data, each individual line-scan of a given sample. The value of the highest point is taken by putting the maximum value from each line scan into a vector and then taking an arithmetic mean of this vector. This highest value is needed to represent the point where the grains of the wheel have penetrated into the impermeable workpiece, thus creating a physical boundary to fluid flow. This average of the highest point gave a reliable value of the expected point of contact with the wheel and the workpiece, as discussed during the bedding-in tests in Chapter 8.3.3. This allows the program to create a representation of an area that is bounded by the impermeable workpiece and the deepest point of the wheel surface. This calculated value is used by the program as a way of working out the amount of space that would be available for fluid if the grains were removed from the surface. This value of total area is used for reference during the analysis to predict a volume of useful flow.

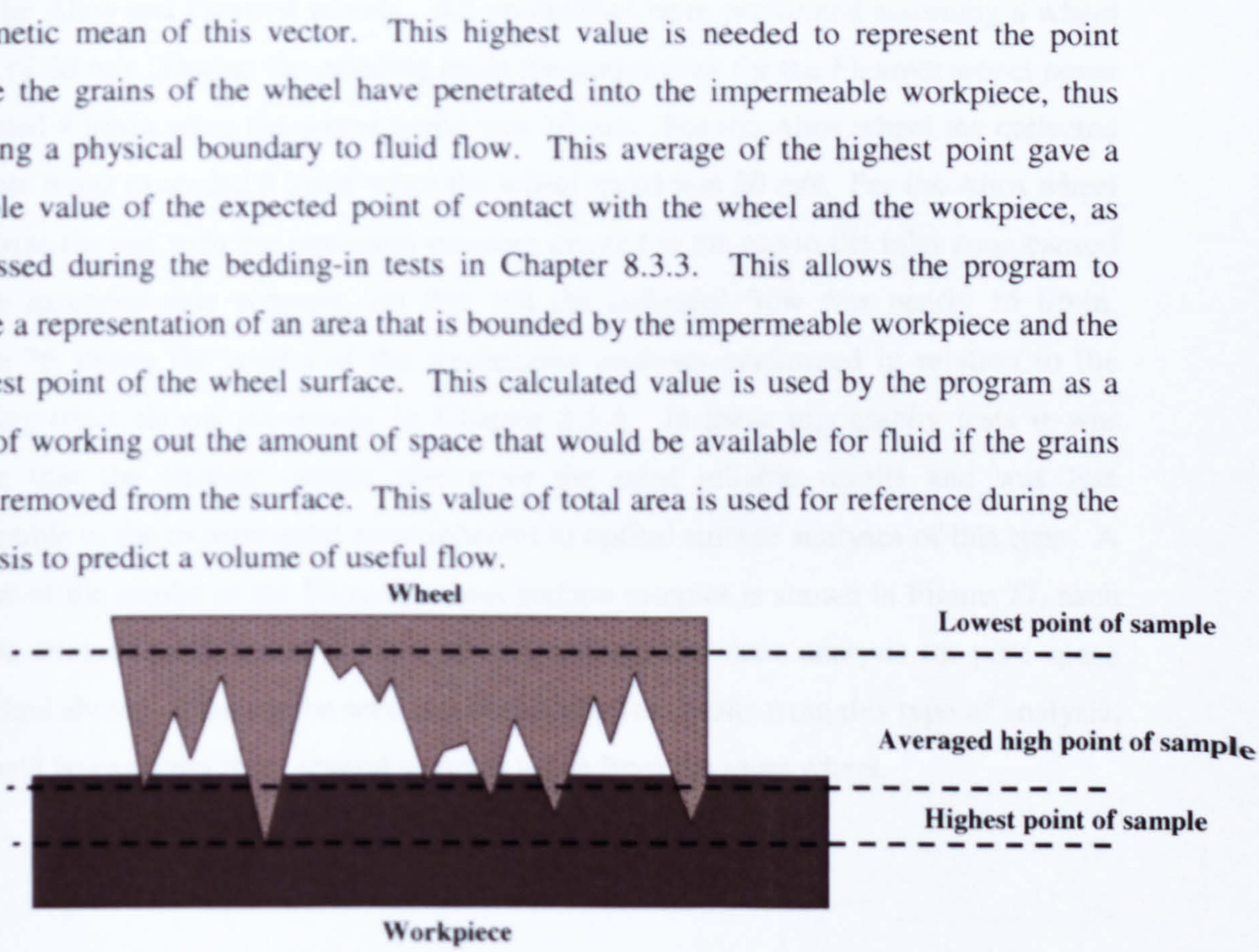

Figure 75, Illustration of wheel/workpiece interface used for MATLAB analysis

The code then scans each point on the line and integrates it to calculate the value of the total area that is occupied by the grinding wheel, thus the remaining area is the value of pore space in the grinding wheel surface that can be occupied by grinding fluid. This value is then combined with the wheel speed and the bulk wheel porosity (to remove the aforementioned 'vee-belt' effect) giving a value of convenient flow.

This method relies purely on the wheel surface topography and the wheel speed and can be used universally wherever the exact wheel surface topography is known. The value of convenient flow achieved here assumes that the pore space available (represented in Figure 75 by the internal white area) within the wheel is completely filled with fluid. Further to this the calculated value of convenient flow assumes a plentiful supply of fluid, thus is only valid in conjunction with a well designed fluid application system.

9.2.2 Findings

The values shown in Figure 76 can be compared to the useful flow trials performed on both the Altos and Flexovit wheels. All predictions were performed assuming a wheel speed of 30 m/s. During the grinding trials the useful flow for the Flexovit wheel never exceeded 4 l/min when the wheel speed was 30 m/s. For the Altos wheel the collected flowrate never exceeded 8 l/min when the wheel speed was 30 m/s. For the Altos wheel there was the test with the unnatural pressure created at the nip to the inlet zone caused by the extended side scrapers, for this test the collected flow was nearly 15 l/min. Figure 76 shows the results of the topography analyses performed in relation to the grinding trials shown previously in Chapter 8.3.4. In these topography tests it was shown that the smaller sample size gave the most reliable results and was less susceptible to the experimental error inherent to optical surface analyses of this type. A full set of the results of the Flexovit wheel surface samples is shown in Figure 77, each sample relates to a different test but all can undergo the same analysis for pore space described above. What can be seen is a consistency of results from this type of analysis, as would be expected from several samples taken from the same wheel.

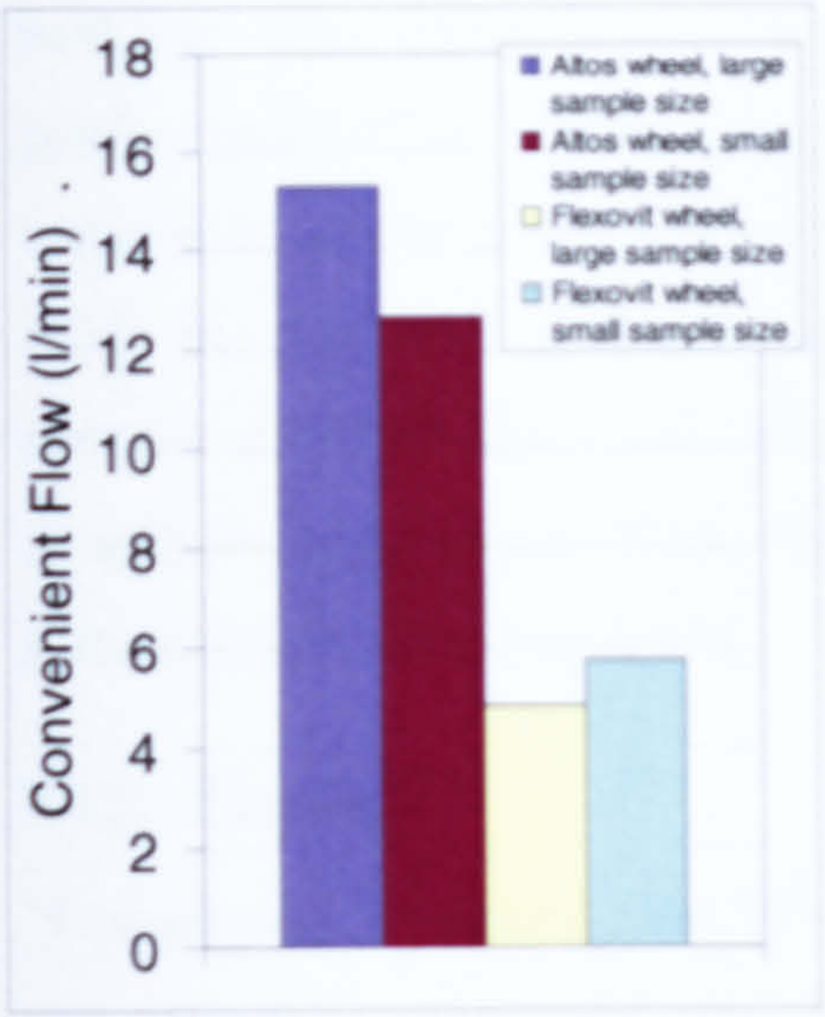

Figure 76, Calculated convenient flowrate for the Altos and Flexovit wheels when v_s=30 m/s.

Figure 77, Convenient flowrate approximations from all topography tests with the Flexovit wheel when v_s=30 m/s.

Comparing experimentally measured maximum useful flowrate with calculated convenient flowrate it can be concluded that for the Flexovit wheel it is possible to fill between 50% and 60% of the available space within the wheel surface. For the Altos wheel it is possible to fill 60% to 70% of the available space within the wheel surface. This method has shown the definition of the surface topography as a key factor to the identification of the fluid carrying capabilities of a grinding wheel.

9.3 Approach 2

A second approach is to predict a value of useful flowrate based on the equivalent fluid thickness layer found during the grinding trials. This value can be used to model the requirements of the fluid delivery system needed for a given grinding process. The process assumes the fluid carrying capabilities of the wheel are a consequence of the topography of the wheel and are controlled primarily by the wheel speed. Exactly how the fluid is transported is inconsequential as the prediction is based on an equivalent fluid thickness derived from experiment or estimated from known variables. This methodology leads to the prediction of an achievable useful flowrate, again this value is dependant upon the fluid supply being sufficient.

9.3.1 Methodology

Throughout the grinding trials the equivalent fluid layer thickness, h_{uf} was evaluated from the measured useful flow results so that an impression of the tendencies could be

built up. This approach is based around equation (24), where h_{uf} is used directly to predict useful flow. Developing this further required a deeper understanding of what value of h_{uf} can be achieved during experimentation. Indeed it would be ideal if the h_{uf} could be compared to the values indicative of wheel surface topography such as abrasive grain diameter and bulk wheel porosity. Therefore this approach revolved around the comparison of experimentally derived values of h_{uf} to the known physical parameters of a grinding wheel.

9.3.2 Findings

Comparison is made to the Abwood speed ratio test and the Dominator speed ratio tests described previously. For the Altos wheel on the Abwood grinding machine the equivalent fluid layer thickness, h_{uf} was found by experiment to be in the region of 120-200 μm. When utilising an h_{uf} of 200 μm in equation (24) and comparing to the Abwood speed ratio tests the results are promising, as can be seen in Figure 78. A strong correlation can be seen for wheel speed up to 30 m/s. This suggests that when there is adequate fluid supplied the useful flowrate is strongly dependant on the wheel speed, this in turns leads to the conclusion that the wheel topography responsible for pumping the fluid is key to the value of useful flow. It can also been seen that this relationship is only true for a certain range of speed ratios.

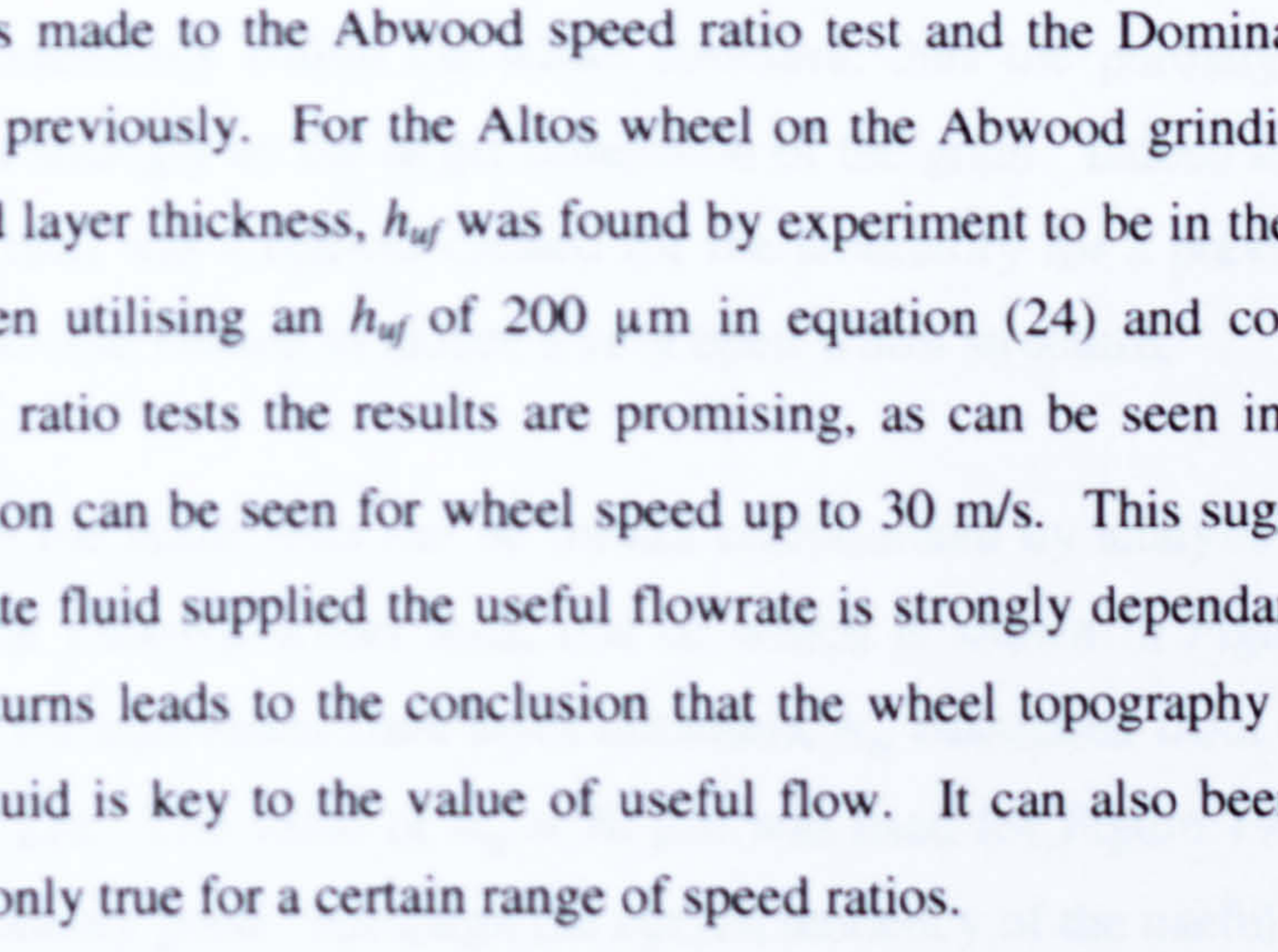

Figure 78, Graph showing the prediction of useful flow based on an approximated h_{uf} and the results from the Abwood speed ratio test using the Abwood grinding machine and the Altos grinding wheel, when v_j=24.3 m/s, Q_d=18.9 l/min.

When compared to the surface topography results the value of h_{uf} approximates well to a fifth of the difference between the mean height and depth of the surface topography (where this value is approximately 1.1 mm, see Figure 74) and correlates well to the

value of R_{pk} which averages around 190 μm for all Altos samples (see Appendix A). The use of equation (24) taken from Marinescu et al (2005) proves difficult to use when considering the grain aspect ratio. Use of grain diameter proves conceptually difficult when considering the Altos wheel where the aspect ratio of an average abrasive grain is 10:1, at this high ratio the diameter has no simple physical relevance. Using a value of d_g of 1000 μm for the Altos wheel does not correlate with the results shown within this work. Considering the 10:1 aspect ratio, a characteristic grain length is maybe more appropriate. The approximation that can be made is that h_{uf} is a fifth of the grain length (rather than diameter in the case of the Altos wheel). This assumption is made as the grains will lie randomly within the wheel structure, thus the porosity is likely to be controlled more strongly by the larger dimension of the grain. Indeed in the case of the Altos wheel, which was a one-off created for the laboratory for a previous project, the large aspect ratio was chosen to induce a very open wheel structure.

The results for the Altos tests can be further corroborated by analysis using the same approach for the Flexovit wheel tests, one of which is shown in Figure 79. For the Flexovit wheel the equivalent fluid layer thickness, h_{uf} calculated from experiment was between 40-80 μm. The value of h_{uf} = 70 μm was used for Figure 79; the fit for this value was reasonably good. Although the curved tendency of the useful flow results for this combination of grinding wheel and grinding machine tended to increase the error.

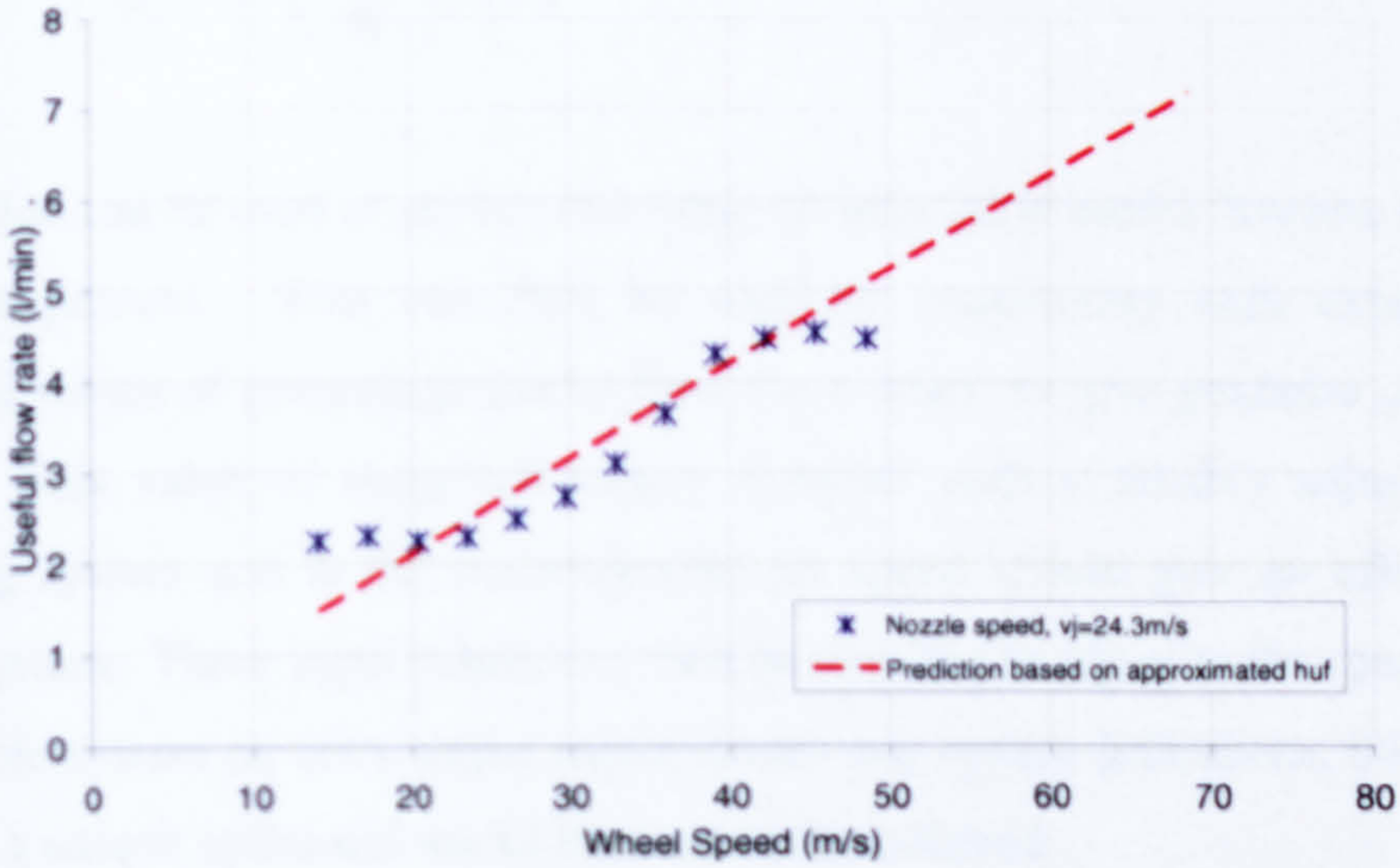

Figure 79, Graph showing the prediction of useful flow based on an approximated h_{uf} and the results from the Dominator speed ratio test using the Flexovit grinding wheel, when v_j=24.3 m/s, Q_d=18.9 l/min.

This value of h_{uf} can again be compared to values obtained from topography analysis, where it is approximately a fifth of the difference between the mean height and depth of the surface topography (where this value is approximately 0.5 mm). Observation of the bearing ratio curve for the Flexovit wheel sample shows R_{pk} to be on average 80 µm, see Figure 69. The good agreement for these values suggests they can be utilised in the decision making for the fluid application process. When considering h_{uf} in regards to the grain diameter for the Flexovit wheel the results prove slightly more promising. With an average grain diameter, d_g of approximately 350 µm the h_{uf} is approximated well by using the same value of a fifth stated previously. This provides good agreement to the calculations made for the Altos wheel for the achievable value of convenient flow, again it should be stated that this comes with the proviso of a favourable fluid application system. This approach can be combined with the wheel specification data to give the following equation for predicting the achievable useful flowrate.

$$\dot{Q}_u = v_s \cdot b_s \cdot \frac{1}{5}\left(\frac{15.2}{M}\right)[mm] \tag{41}$$

Where M is the grit size from the wheel specification.

Equation (41) could be modified to include the bulk wheel porosity value, ϕ and the value of expected pore filling as shown in equation (42)

$$\dot{Q}_u = v_s \cdot b_s \cdot \phi \cdot f \cdot \left(\frac{15.2}{M}\right)[mm] \tag{42}$$

This equation can be used to predict the value of achievable useful flowrate for a given wheel and process. This can then be used in conjunction with experimentally determined values of percentage useful flow for a wheel to give guidance on a supply flowrate. This value of suggested supply flowrate with a suitably adjusted nozzle positioning system and at the recommended jet speed should give an efficient fluid delivery system. These input values can then be tweaked to adjust to the specific nature of the whole system on both output requirements and system limitations, this tweaking will allow a unique optimised useful flowrate to be achieved.

At this point it seems reasonable to compare this approach to the experimental data available from researchers who have measured useful flow in the past. Engineer *et al* (1992) produced results by measuring useful flow. He also supplied sufficient data to

be able to compare results to the predictions within this work. The graph shown in Figure 5 illustrates the amount of flow collected at various supply flowrates using varying wheels. The wheel specification is provided in full so the approach using an approximation of the h_{uf} from grain size can be employed. By using equation (42) the following can be deduced.

$$\dot{Q}_u = 30[m/s] \cdot 19[mm] \cdot 0.5 \cdot \frac{1}{2} \cdot \left(\frac{15.2}{M}\right)[mm]$$

Where v_s=30 m/s, b_s=19 mm and M=60.

$$\dot{Q}_u = 3.61 \times 10^{-5} m^3/s = 2.2 l/\min$$

This gives a value of useful flowrate that could be achieved if the jet speed, v_j where much higher for the grinding performed during Engineer's tests. As the grain size is the same for all the grinding wheels used during the tests the value of achievable useful flowrate varies only due to the changing wheel porosities. It can be seen from the range of jet speeds used in Figure 80 that at no point is the speed ratio approaching 1. The values of collected flow found by Engineer are at the most 50% of the achievable useful flow. This can be explained by comparing to the results of the Dominator speed ratio test where the Flexovit wheel is used, this wheel is similar in nature to the 38A60I8VBE used by Engineer. In the Dominator speed ratio tests roughly 2.2 l/min useful flowrate is achieved with a nozzle jet speed of 24.3 m/s and the jet flowrate of 18.9 l/min, comparing this to the 0.3 l/min achieved by Engineer using a nozzle jet speed of 0.6 m/s and a flowrate of 4.1 l/min. When the Engineer value of useful flowrate is scaled up so the supplied flowrates match, the values of useful flowrate are similar. In fact any remaining difference can be assumed to be due to the effect of the jet speed not being similar to the wheel speed.

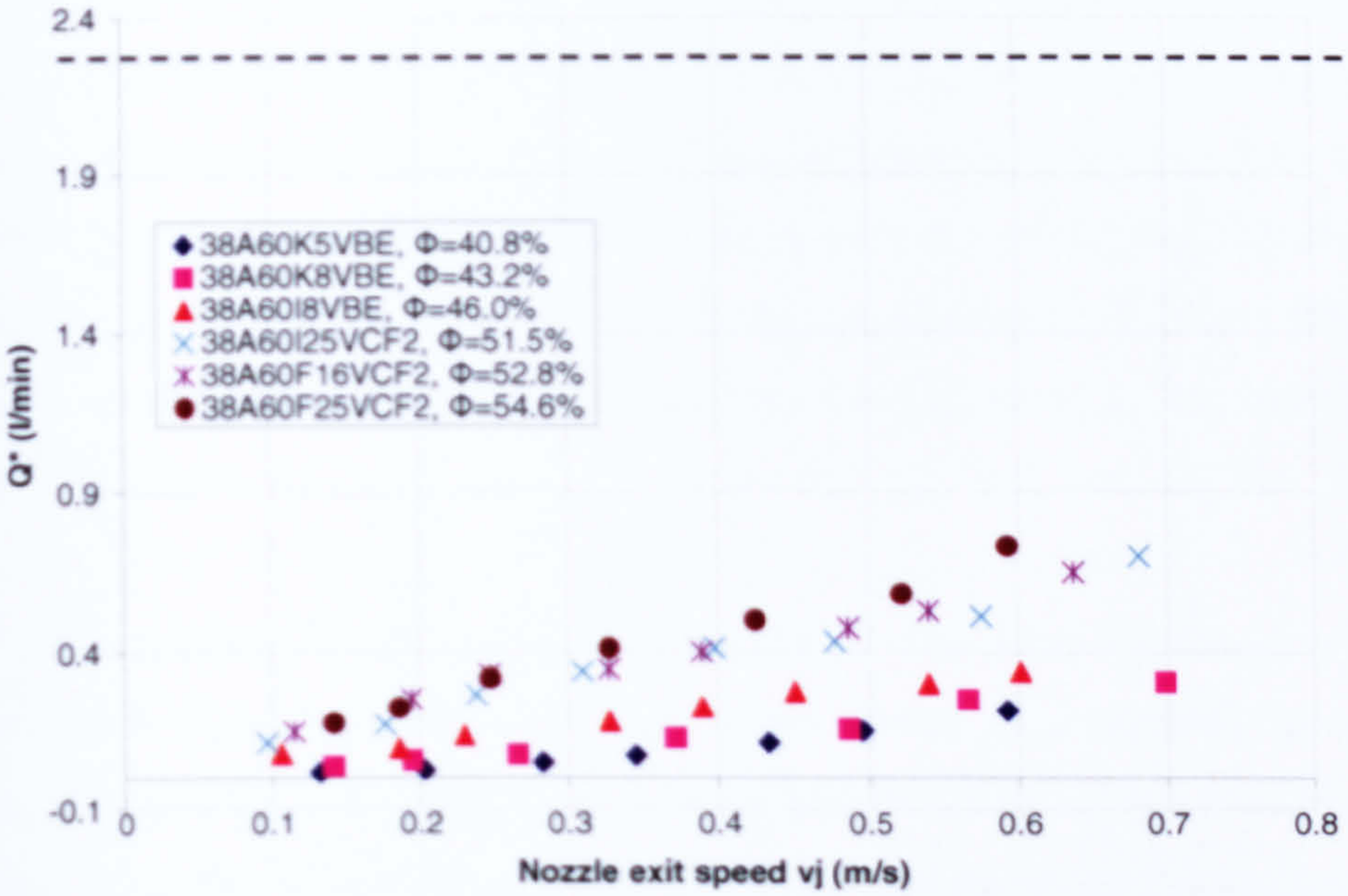

Figure 80, Useful flowrate versus nozzle exit speed for grinding wheels of various bulk porosities Φ, showing the calculated achievable useful flowrate when v_s=30 m/s, a=12 μm, s_d=160 μm, v_w=0.09m/s, b_s=19 mm and d_s=250 mm. (Engineer *et al*, 1992).

A further comparison has also been performed for direct correlation to results from this project this is shown in Appendix A. This additional work compares the results from Preliminary Test 3 with the prediction from equation (42). For this test equation (24) proved difficult to interpret. This is due to the effect of an average grain aspect ratio of 10:1. However, equation (42) can also be added to these results to see the applicability of this model, again it proves to show close alignment to the measured results. In this test the prediction of the useful flow can be seen to follow the upward linear trend found during previous tests, this again shows that the linearity tails off at around where the wheel speed approaches the jet speed.

Chapter 10. Discussion

The aim of this work was to provide further understanding of the term useful flow in grinding applications. Providing a deeper understanding would allow savings to be made in industry regarding the amount of coolant required for a process. This would in turn have implications for the environmental impact the manufacturing industry makes as a whole. As discussed earlier even small savings in coolant delivery volume and application speed can result in significant savings when scaled up to multiple machines in many companies.

One of the key developments required for this project was the design and manufacture of a useful flow collection system. Without such a device the analytical testing would not have been possible and any advance in modelling would have been unverifiable and redundant. As shown in Chapter 6, a fully developed and thoroughly tested system was designed and implemented on two very different surface grinding machines. The nature of the arrangement allowed any material, any wheel type, any wheel speed, any depth of cut and any coolant application speed or flowrate to be tested. There were restrictions in terms of the workpiece geometry and the worktable speed, but beyond that there was tremendous scope afforded by the useful flow collection system that was developed for this project.

With a reliable and repeatable useful flow collection system developed the onus then moved onto testing the parameters that may affect the useful flowrate on any given system. This was approached firstly with a fractional factorial methodology so that as many aspects could be addressed as possible. Wheel speed, jet speed and flowrate were found to have the strongest effects on useful flowrate. Interestingly, and for the first time, the combined effect of jet speed/flowrate and wheel speed was found to have a significant effect on the amount of useful flowrate achievable for a given process. This provided new understanding well beyond previous views that jet speed must match wheel speed.

The project then moved onto full factorial testing of fewer parameters. Using full factorial testing it was possible to examine in greater detail the relationships that had been discovered qualitatively during the Taguchi testing. The key requirement at this stage were to further investigate the effect of wheel speed, jet speed and jet flowrate on useful flowrate

The wheel speed testing proved that the effect was a nearly linear proportionality up to a point defined by a value of speed ratio (v_j/v_s). The linear proportionality found lent credence to the initial proposition that the topography of the wheel is the predominant effect over the amount of flow that can pass through the contact zone. Indeed this linear relationship would be expected if the volume of flow is dependant on the fluid pumping capability of the wheel. The fluid pumping capability can only be dependant on topography and speed of the wheel. The type of wheel and the speed at which the grinding fluid is applied can affect this linearity. It was found that a low porosity wheel (approximately 45 %) with a visibly closed structure is more affected by the ratio of wheel speed and the jet speed.

The speed of the jet flow can also be considered key to the work as a slow jet of sufficient flowrate will approach the situation of flood cooling which for high wheel speeds has been shown to be ineffectual (see Figure 7 and Figure 8). Jet speed and its effect on useful flowrate has been considered on two fronts, one is in regards to the speed ratio value mentioned previously and the other is in regards to combined and separate effects it has with jet flowrate. When considering the speed ratio the desire is to avoid matching the jet speed to the wheel speed; something which is becoming a costly process in the modern environment of increasing wheel speeds. Testing has shown that there is little point in having jet speed exceed wheel speed, it has been found that this serves only to decrease percentage useful flow thus increasing rejection and lowering efficiency. The Altos tests show clearly a trend between the jet speed and the wheel speed when the flowrate can be considered sufficient. What can be seen from Figure 48 is that the maximum achievable percentage useful flow was 50 % when the jet speed was approximately 70 % of wheel speed. It could be concluded from this that the best ratio is $v_j = 0.7v_s$, this situation should provide the highest utilisation of the fluid being applied. It should however be noted that the useful flow is 45-50 % for the ratio range of $0.5 < v_j / v_s < 0.9$, it could therefore be said that for a suitably 'easy' grind there is benefit in dropping the ratio to 0.5 or below without losing too much in terms of process outputs. It has been shown from both the Abwood and the Dominator speed ratio tests that the largest volume of useful flowrate will be achieved in the region where the speed ratio is between 0.5-1, indeed for both tests conducted the ideal ratio was approximately 0.6. It has also been shown from the Taguchi results that in a situation

where grinding could be considered 'easy' (for example when needing only a shallow cut, or a conventional cut with a well suited wheel) this ratio can be lowered significantly. In general terms the jet speed is required to penetrate the air barrier that is generated around the spinning grinding wheel. A high wheel speed and powerful air barrier will tend to increase the rejection of fluid, thus lowering the percentage useful flow. A lower percentage useful flow could be considered an inefficient state of operation as effort employed to apply the rejected fluid would be wasted. Work within the AMT Research Laboratory has shown that the percentage useful flow could be increased using a pre-nozzle scraper. This may allow more fluid to adhere to the wheel surface. However, the topography limits discussed earlier will still tend to limit what can be carried through the grinding zone and be considered useful flowrate.

Analysis of the supply flowrate has been clouded in the past by being allied to changes in jet speed, thus masking the individual effects. This had been necessary to limit the requirements of the fluid application system being used. Work within this thesis shows the effect jet flowrate can have on the useful flowrate. It has been shown that the topography limits the amount of flowrate that can be achieved and be considered useful. When accompanied with the expected value of percentage useful flow which is difficult to exceed for a given wheel (approximately 50 % for the Altos wheel and 30 % for the Flexovit wheel), applying more flowrate to the grinding zone merely decreases the percentage useful flow. Testing where the jet flowrate and jet speed are varied independently has shown that increasing the flowrate beyond the achievable value provides no gain in terms of useful flow.

During the testing temperature, power and force were recorded. The main purpose was to verify the quality of the grind that had been performed based on the useful flowrate that had been achieved. Results in this regard were representative rather than conclusive. During the Taguchi test temperature, power and surface roughness were all recorded, but as the analysis was designed for maximum variation of useful flow the results of these other parameters suffered. Consequently the confidence intervals found were low making conclusions tentative, however results could still be interpreted. Figure 57 showed the results from the Abwood speed ratio test and was indicative of the results from the other tests. What is visible is an increasing temperature as useful flowrate increased; though this is mostly due to the kinematic effect of increasing wheel

speed. A noticeable and important effect was the tendency for the grinding zone temperature to stabilise as the useful flowrate reached a peak, even when the wheel speed kept increasing. For the Abwood testing the force was measured. What can be seen from the Abwood test shown in Figure 61, is that as the wheel speed is increased the force tends to drop. This would be expected for constant specific energy and indicates that the reduced chip thickness with increasing wheel speed was insufficient to increase specific energy sufficiently to increase force. There has to be a substantial increase in specific energy before forces increase with wheel speed. This drop was consistent throughout the scale of the wheel speeds tested even when the wheel speed exceeded the jet speed.

The initial proposition of the surface topography being of utmost importance to the useful flowrate required that a means of measuring the topography be found. The analysis of the topography was conducted using methods proven within the Laboratory; however the author still conducted preliminary trials to verify that results could be relied on.

The author started by testing the effect of dressing on the wheel surface. It was found that the dressing did not have significant effect on the large scale variations within the topography. Variation induced by the dress was not found to affect the nature of the pores within the wheel surface. It is these pores that carry the fluid through the contact zone. It was suspected dressing may affect the wheel surface by bond fracture, thus opening 'grain-sized' pores. This was not found to be frequent within the dressing parameters used for this test. It could be concluded that only an 'aggressive' dress could affect the wheel surface enough to vary the achievable useful flowrate. It should be noted that the cleaning effect of a dress would re-open the wheel surface for fluid. However, the specific type of dress performed, beyond the previously mentioned aggressive approach, would not affect the wheel surface topography, in regards to useful flowrate, in any way.

The estimation of useful flowrate from the wheel surface topography relied upon the measurement of porosity across a plane through the wheel. This planar measurement required sensible measures of the upper (peak grain height) and lower limits (pore depth) of the wheel surface. It is known that dressing a wheel often leads to instability

in the power readings during the first few grinding passes, this is due to the wheel bedding-in and the 'weaker' grain peaks being removed. Each measurement of the surface topography tended to be taken directly after a dress, therefore it was necessary to know how much was removed from the peak height during the bedding-in process. Thus a test was planned to measure the topography immediately after a dress, then after 1 grinding pass (when the wheel would still be unstable) and then after 100 grinding passes (when the wheel can be considered stable). This test showed that some of the peak height measured is removed during the bedding-in process as expected. It was found that this process removed approximately 15 % of the peak-to-trough height. Due to the nature of the predictive model, this difference has the potential to induce a 40 % error into the prediction of the achievable useful flowrate.

The final use for the topography measurements was to take samples from the grinding wheels that have been used during useful flow collection trials. These samples could then be analysed and used to predict the achievable useful flowrate, this could then be compared to the values found during testing. The samples showed the variation that can be expected between different wheel types, this is shown in Figure 76. The topography based predictions stated the Altos wheel could have a convenient useful flowrate of around 13 l/min when v_s is 30 m/s; and the Flexovit wheel approximately 5 l/min at the same wheel speed. These values are both based on the pores being completely filled with coolant. By comparison to the experimental values of useful flowrate it was found that it may only be convenient to fill ~60 % of the available pore space. This leads to the conclusion that in the case of these wheels the achievable useful flowrate is roughly 60% of the convenient flowrate. The result of Preliminary Test 2 shows that the value of convenient useful flowrate can be exceeded with suitable, if unorthodox, grinding zone inlet conditions, in this test the measured useful flowrate reached 17 l/min.

One of the goals of this project was to find a way to predict the achievable useful flowrate based on readily available parameters. The supposition that the topography of the wheel was a key parameter suggested a value from the wheel specification would be preferable. During testing the author used measured values of useful flowrate to correlate to the parameter h_{uf}. It was found that for the wheels under analysis the Rowe equation defined in equation (24) should be adapted by having the h_{uf} equivalent to a fifth of the grinding wheel grain size, d_g. This value of a fifth was related to a

multiplication of the bulk wheel porosity and an assumed value of filling half of the pores space. This allows the user to predict the achievable useful flowrate as v_s approaches v_j. It can then be proposed that as the wheel speed exceeds the jet speed the useful flowrate will not exceed the value reached when $v_j = v_s$. It should be noted that the achievable useful flowrate may not be the optimal useful flowrate, as has been shown during the Taguchi trials a significantly lower useful flowrate can be sufficient for a shallow cut grinding situation.

As stated previously optimisation is extremely process dependant, so for the tests conducted during this project the optimised values can be considered as follows. The values of useful flow taken from the speed ratio tests can be considered un-optimised, as they are based only on what was collected during trials where good surface finishes and reasonable grinding power levels were maintained. However, the Taguchi trials provided analysis involving 'poor' grinding scenarios. Indeed as was highlighted in Chapter 7.8 it was below a level Q_u = 0.5 l/min when the process parameters deteriorated significantly. With this in mind it could be considered that for the Flexovit wheel on the Jones and Shipman Dominator could have an optimised useful flowrate of 0.5 l/min. This value relates to an h_{uf} of 45 µm, so where the value of 45 µm relates to the achievable useful flowrate, a value of h_{uf}=45 µm is optimal in terms of reducing the fluid/power requirements of the process. This can be then be used to approximate the flow that needs to be applied via the nozzle. Chapter 7.6.3 describes how for the Flexovit wheel the maximum achieved useful flow was 30 %. If it is assumed that 30 % is a reasonable amount of flow utilisation for a well specified nozzle type and position, then the user needs to apply 0.67 l/min per mm of wheel width at a suitable nozzle jet speed.

The speed of the jet flow can also be considered key to the work as a slow jet of sufficient flowrate will approach the situation of flood cooling which for high wheel speeds has been shown to be ineffectual (see Figure 7 and Figure 8). The Altos tests show clearly a trend between the jet speed and the wheel speed when the flowrate can be considered sufficient. What can be seen from Figure 48 is that the maximum achievable percentage useful flow was 50 % when the jet speed was approximately 70 % of wheel speed. It could be concluded from this that the best ratio is $v_j = 0.7v_s$, this situation should provide the highest utilisation of the fluid being applied. It should

however be noted that the useful flow is 45-50% for the ratio range of $0.5 < v_j / v_s < 0.9$, it could therefore be said that for a suitably 'easy' grind there is benefit in dropping the ratio to 0.5 or below without losing too much in terms of process outputs.

Chapter 11. Conclusions

A reliable and repeatable novel useful flow collection system has been developed, incorporating automatic operation of a timed flow collection arrangement. This system has proven transferable between surface grinding machines and is adaptable to external cylindrical grinding with minimal further development.

Taguchi testing has shown the most significant factors affecting the useful flow are wheel speed, jet speed, jet flowrate and the combined effect of these three parameters. The relationship between useful flowrate and wheel speed has been shown and expanded upon using the Speed ratio term. Approximate relations between maximum useful flow and speed ratio are shown.

It has been found that useful flowrate is affected significantly by grinding wheel surface topography and that achievable useful flowrate can be estimated from grain size using the adapted Rowe equation. A simple and easily applied model has been developed and can be used requiring knowledge of grinding wheel speed, average grain size and bulk wheel porosity. It has also been shown that the approximate pore space available in the grinding wheel surface can be calculated via analysis of impressions of the wheel surface.

Further to this it has been shown that jet speed has an effect on useful flowrate when viewed in relation to the wheel speed. A decision on jet speed should be made based on the wheel speed required and the severity of the grind being attempted. Jet flowrate is also found to be effectual on the useful flowrate but only up to a point. When increasing the jet flowrate beyond this value it becomes very difficult to increase the useful flowrate, thus further increases in jet flowrate only serve to lower percentage useful flow. In this region where there is no benefit in increasing jet flowrate the only way to increase useful flow is to increase jet speed. The benefit of having enough useful flowrate has been shown and guidance has been provided both on predicting the amount of jet flowrate and also on the jet speed that should be used.

11.1 Contribution to knowledge

The following can be considered novel and show the unique contributions to knowledge this project has achieved.

- A design framework for the collection of useful flow.
- A fractional factorial test covering many grinding variables proving conclusively the key variables as wheel speed and jet speed.
- Experimental proof of the effect of the combination of wheel speed and jet speed over useful flow rate.
- Understanding of the effect on useful flowrate of varying key input variables.
- A guideline of jet speed for a given wheel speed.
- $v_j = 0.6\ v_s$.
- Values of expected percentage useful flow for a given wheel type.
- A program to analyse a grinding wheel surface impression and output a value of convenient flowrate.
- A model for a predicting useful flowrate through a surface grind based on standardised wheel values and experimental knowledge.

Chapter 12. Suggestions for Further Work

The following areas are suggested for further work into the subject surrounding this project:

- More grinding wheels should be analysed to verify the relationship between the grain size and the useful flowrate. A test involving wheels of similar and differing grain size and bulk porosity would allow the model to be verified and advanced.

- Adaptation of the useful flow collection system to the cylindrical grinding process. This would allow faster wheel speeds to be tested and analysis of whether the differing kinematics affect the relationship the grinding wheel has with the useful flow.

- Further benefit could be gained from insight into the fluid penetration into the wheel and at what position the penetrating fluid actually re-emerges from the wheel. This would provide insight into the need to force fluid beyond the surface pores and clarity surrounding what depth of penetration the fluid remains useful.

- There would be benefit in adapting the system to be used on a HEDG grinding machine. The application of fluid is considered critical in this process. However, some suspect that at extremely high removal rates HEDG becomes a practically dry grinding process, this is due to the large arc of contact and aggressive feeds and speeds. The application of the useful flow collection system might provide insight into the amount of fluid that usefully passes through the HEDG contact zone. It would show whether all the useful flow is 'burnt out' or whether it re-emerges as fluid. This raises the further question as to the ability of collected flow to accurately represent useful flow where a proportion of the flow is vaporised.

References

Akiyama, T., Shibata, J. & Yonetsu, S., 1984, Behaviour of grinding fluid in the gap of the contact area between the grinding wheel and a workpiece – A study on delivery of grinding fluid, *Proceedings of the Fifth International Conference on Production Engineering*, Tokyo, pp 52-57.

Alden, G. I., 1914, Operation of grinding wheels in machine grinding, *Transactions of ASME*, 36, pp 451-460.

Axinte, D., Axinte, M and Tannock, J.D.T., 2003, A multicriteria model for cutting fluid evaluation, *Proceedings of the Institution of Mechanical Engineers, Part B: Journal of Engineering Manufacture*, Vol 217, n10, pp 1341-1353.

Baines-Jones, V.B., Morgan, M.N., Allanson, D.R. & Batako, A.D.L., 2005, Grinding fluid delivery system design - nozzle optimisation, *GERI Annual Research Symposium*, Available from http://www.ljmu.ac.uk/geri/geri_docs/GARS2005papers_vadim.pdf

Baines-Jones. V., Batako, A.D.L and Morgan, M.N., 2007, Computational fluid dynamics analysis of grinding fluid nozzles, *3rd GERI Annual Research Symposium GARS-2007*, Liverpool, UK, 27 June 2007.

Batako, A.D.L, Rowe, W.B. and Morgan, M.N., 2005, Temperature measurement in high efficiency deep grinding, *International Journal of Machine Tools & Manufacture*, Vol. 45, pp.1231-1245.

Brinksmeier, E. & Minke, E., 1993, High Performance Surface Grinding- The Influence of Coolant on the Abrasive Process, *Annals of the CIRP*, Vol. 42, n 1, 1993, pp 367-370.

Brinksmeier, E., Heinzel, C. and Wittman, M., 1999, Friction, Cooling and Lubrication in Grinding, *CIRP Annals - Manufacturing Technology*, Vol. 48, n 2, 1999, pp 581-598.

Brucher, T., 1996, *Kühlschmierung beim Schleifen keramischer Werkstoffe*, Dr.-Ing. Diss., Universität Bremen, VDI-Verlag, Düsseldorf.

Cai, R., 2002, *Assessment of Vitrified cBN Wheels for Precision Grinding*, Ph.D. Thesis, Liverpool John Moores University, Liverpool, UK.

Carslaw, H. and Jaeger, J.C., 1959, *Conduction of Heat in Solids*, Oxford Science Publications, Oxford University Press.

Chang, C.C., 1994, *An Analysis of Coolant Flow and Heat Transfer in Grinding*, Ph.D. Thesis, University of Pittsburgh.

Chang, C.C., Wang, S.H. and Szeri, A.Z., 1996, On the Mechanism of Fluid Transport across the Grinding Zone, *Journal Of Manufacturing Science And Engineering-Transactions Of The ASME*, Vol. 118 (3), pp 332-338.

Council Directive on the disposal of waste oils 75/439/EEC, Article 1.

Cui, C., 1995, *Experimental Investigation of Thermofluids in the Grinding Zone*, Ph.D. Thesis, University of Connecticut.

Dagnall, H., 1997, *Exploring Surface Texture*, Taylor and Hobson Publication, List No. 600-14/98.

Directive 2000/76/EC of the European Parliament and of the Council of 4 December 2000,
Available from *http://europa.eu.int/eur-lex/lex/LexUriServ/LexUriServ.do?uri=CELEX:32000L0076R(01):EN:HTML*, accessed 1st Oct 2006.

Ebbrell, S., Woolley, N.H., Tridimas, Y.D., Allanson, D.R. & Rowe, W.B., 2000, The Effects Of Cutting Fluid Application Methods On The Grinding Process, *International Journal of Machine Tools and Manufacture*, v 40, n 2, Oct, pp 209-223

Engineer, F., Guo, C. and Malkin, S., 1992, Experimental Measurement of Fluid Flow through the Grinding Zone, *Journal Of Engineering For Industry-Transactions Of The ASME,* Vol 114, February, pp 61-66.

EU Council Directive 75/439/EEC, June 1975, Available from *http://europa.eu.int/eur-lex/lex/LexUriServ/LexUriServ.do?uri=CELEX:31975L0439:EN:HTML*. Accessed 1st Oct 2006.

Ganesan, M., Guo, C., and Malkin, S., 2001, Analysis of hydrodynamic forces in grinding, *Abrasives Magazine*, Oct-Nov, pp 6-12.

Greenwood, J.A. and Tripp, J.H., 1967, The Elastic Contact of Rough Surfaces, *Journal of Applied Mechanics*, March, pp153-159.

Guest, T. J. J., 1915, *Grinding Machinery* (London: Edward Arnold).

Guo, C and Malkin, S., 1992, Analysis of Fluid Flow through the Grinding Zone, *Journal of Engineering for Industry-Transactions Of The ASME*, Vol. 114 (4), Nov, pp 427-434.

Gviniashvili, V.K., 2003, *Fluid application system optimisation for high speed grinding*, Ph.D. Thesis, Liverpool John Moores University.

Gviniashvili, V.K., Morgan, M.N., Woolley, N.H. and Rowe, W.B., 2004, Useful Flowrate in Grinding, *International Journal of Machine Tools & Manufacture*, Vol. 44, May 2004, pp 629-636.

Hahn, R.S., 1966, On the Mechanics of the Grinding Process Under Plunge Cut Conditions, *Journal of Engineering for Industry-Transactions of the ASME,* pp 72-80.

Hazardous Waste Reduction EU Life-Environment project, 2005, available from *http://www.hazred.org.uk/* . Accessed 1st Oct 2006.

Howes, T.D., 1990, Assessment of the Coolant and Lubricative Properties of Grinding Fluids, *Annals of the CIRP*, Vol 39, n 1, 1990, pp 313-316.

Howes, T.D., Neailey, N. & Harrison, A.J., 1987, Fluid Film Boiling in Shallow Cut Grinding, *Annals of the CIRP*, Vol 36, pp 223-226.

Irani, R.A., Bauer, R.J. and Warkentin, A., 2005, A Review of Cutting Fluid Application in the Grinding Process, *International Journal Of Machine Tools & Manufacture*, Vol. 45, pp 1696-1705.

Kim, N.K., Guo, C. & Malkin, S., 1997, Heat Flux Distribution and Energy Partition in Creep-Feed Grinding, *Annals of the CIRP - Manufacturing Technology*, Vol. 46, n 1, 1997, pp 227-232.

Klocke, F., Baus, A. & Beck, T., 2000, Coolant Induced Forces in CBN High Speed Grinding with Shoe Nozzles, *Annals of the CIRP - Manufacturing Technology*, Vol. 49, n 1, 2000, pp 241-244.

Kovacevic, R and Mohan, R., 1995, Effect of High Speed Grinding Fluid on Surface Grinding Performance, *1st International Machining and Grinding Conference*, 12-14 Sept, Dearborn, Michigan, pp 919-931.

Krishnan, N., Malkin, S. & Guo, C., 1995, Fluid Flow Through the Grinding Zone in Creep Feed Grinding, *1st International Machining and Grinding Conference*, 12-14 Sept, Dearborn, Michigan, pp 919-931.

Malkin, S and Anderson, R.B., 1972, Active Grains and Dressing Particles in Grinding, *Proceedings of the International Grinding Conference*, Pittsburgh, p161.

Malkin, S., 1989, *Grinding Technology-theory and applications of machining abrasives*, Ellis Howard Publishing Limited, ISBN 0-85312-756-5.

Manufacturing Technologies website, *Basic Facts Brochure*, Spring 2006. Available from http://www.mta.org.uk/02_01_facts.php, Accessed 1st Oct 2006.

Manufacturing Technologies website, *Q3 data confirms machine tool market still buoyant*, Press release 18th Dec 2006. Available from http://www.mta.org.uk/viewPressRelease.php?id=46, Accessed 1st Oct 2006.

Marinescu, I.D., Rowe, W.B., Dimitrov, B & Inasaki, I, 2004, *Tribology of Abrasive Machining Processes*, William Andrew Publishing, New York, ISBN 0-8155-1490-5.

Metzger, J.L., 1986, *Superabrasive Grinding*, Butterworth and Co. Publishing

Morgan, M.N., Rowe, W.B., Black, S.C.E. & Allanson, D.R., 1998, Effective thermal properties of grinding wheels and grains, *Proceedings of the Institution of Mechanical Engineers, Part B: Journal of Engineering Manufacture*, Vol 212, n B8, pp 661-669.

Ott, H.W., 1991, *Zuführsysteme für Kühlschmierunstoff beim Schleifen*, Seminar "Kühlschmierstoffe in der spanenden Fertigung", Deutsches Industrieforum für Technologie (DIF), Frankfurt, 21-22 October.

Peters, J., Snoeys, R. & Decnaut, A., 1968, A Sonic Testing of Grinding Wheels, *Proceedings of the Ninth International Machine Tool Design and Research Conference*, p1113.

Practical Environmental Advice for Business, *GG199 Optimising the Use of Metalworking Fluids*, Sept 1999, Available from *http://www.envirowise.gov.uk/home.aspx* . Accessed 1st Oct 2006.

Professional Engineering, September 2006, Institute of Mechanical Engineers Trade Magazine vol. 19, no.17.

Qi, H.S., 1995, *A Contact Length Model For Grinding Wheel-Workpiece Length Contact*, Ph.D. Thesis, Liverpool John Moores University.

Qi, H.S., Rowe, W.B. & Mills, B., 1997, Experimental Investigation Of Contact Behaviour In Grinding, *Tribology International, v* 30 (4) pp 283-294. ISSN 0301-679X

Ramesh, K., Huang, H. and Yin, L., 2004, Analytical and experimental investigation of coolant velocity in high speed grinding, *International Journal of Machine Tools & Manufacture*, Vol. 44, Aug 2004, pp 1069-1076.

Rogers, G. F. C. & Mayhew, Y. R., 2001, *Thermodynamic and Transport Properties of Fluids*, Blackwell Publishers, Oxford, ISBN 0-631-19703-6.

Rowe, W.B., Black, S.C.E., Mills, B., Morgan, M.N. & Qi, H.S., 1997, Grinding Temperatures And Energy Partitioning, *Proceedings of the Royal Society of London, Series A: Mathematical, Physical and Engineering Sciences*, v 453, n 1960, May 8, 1997, pp 1083-1104

Rowe, W.B. and Jin, T, 2001, Temperatures in High Efficiency Deep Grinding (HEDG), *Annals of the CIRP -Manufacturing Technology*, 50 (1): pp205-208.

Rowe, W.B., Morgan, M.N., Batako, A.D. and Jin, T., 2003, Energy and Temperature Analysis in Grinding, Keynote Paper, *6th International Conference LAMDAMAP*, 1-4th July, pp 3-23, ISBN 1-85312-990-9.

Rowe, W.B., Morgan, M.N. and Batako, A.D.L., 2005, *HEDG Technical report to EPSRC*. EPSRC Grant ref no. GR/R68795/01.

Schlichting, H., 1968, *Boundary-Layer Theory*, 6th Edition, New-York McGraw Hill Book Company.

Schumack, M.R., Chung, J.B., Schultz, W.W. and Kannatey-Asibu Jnr, E., 1991, Analysis of Fluid Flow under a Grinding Wheel, *Journal of Engineering For Industry-Transactions Of The ASME*, Vol. 113 (2), May, pp 190-197.

Shaw, M.C., 1996, *Principles of Abrasive Processing*, Oxford University Press.

Stephenson, D.J., Jin, T. & Corbett, J., 2002, High Efficiency Deep Grinding of a Low Alloy Steel with Plated CBN Wheels, *Annals of the CIRP -Manufacturing Technology*, 51 (1): pp241-244.

Tawakoli, T., 1990, Hochleistungs-Flachschliefen: Technologie, Verfahrensplanung und wirtschaftlicher Einsatz, Dr.-Ing. Diss., TU Berlin.

Venables, M, 2006, *VIPER grinding gets more bite*, Machinery, Vol. 164, n 4127, August, pp 31-32

Vits, R., 1985, Technologische *Aspekte der Kühlschmierung beim Schleifen*, Dr-Ing. Diss, RWTH Aachen.

Vits, R., 1989, Fertigungsverfahren Band 2, VDI-Verlag, Dusseldorf.

Waste Exchange UK Initiative, Jan 2000, Available from *http://www.wasteexchangeuk.com/*. Accessed 1st Oct 2006.

Webster, J.A., Cui, C & Mindek Jr, R.B., 1995, Grinding Fluid Application System Design, *Annals of the CIRP - Manufacturing Technology*, v 44, n 1, 1995, pp 333-338.

Wu, H & Morgan, M.N., 2005, Measuring The Velocity of Fluid in a Grinding Model Using Laser Doppler Anemometry Technique, *GERI Annual Research Symposium*, available from http://www.ljmu.ac.uk/geri/geri_docs/GARS2005papers_wu.pdf

Yasui, H. and Tsukuda, S., 1983, Influence of Fluid Type on Wet Grinding, *Bulletin of the Japan Society of Precision Engineering*, Vol. 17, No.2, pp133-134.

Appendix A. Supplementary Test Results

Test No,	Jet speed		Wheel speed		Ratio (v/v_s)	Useful Flowrate		Max Forces, F		Max temp
						Volumetric	%	y, Ft	z, Fn	
1	4 45 m/s		7 29 m/s		1.55	7.25 l/min	***38.3%***	44N	55N	57 C
2	4 45 m/s		8 32 m/s		1.41	7.64 l/min	***40.4%***	48N	60N	60 C
3	4 45 m/s		9 35 m/s		1.29	7.96 l/min	***42.1%***	53.6N	67N	64 C
4	4 45 m/s		10 38 m/s		1.19	8.14 l/min	***43.0%***	56N	70N	67 C
5	4 45 m/s		11 41 m/s		1.10	8.12 l/min	***42.9%***	56N	70N	70 C
6	4 45 m/s		12 44 m/s		1.02	8.2 l/min	***43.3%***	49.6N	62N	73 C
7	4 45 m/s		13 47 m/s		0.96	8.02 l/min	***42.4%***	36N	45N	70 C
8	4 45 m/s		14 51 m/s		0.89	7.68 l/min	***40.6%***	33.6N	42N	66 C
9	5 39 m/s		6 26 m/s		1.52	5.78 l/min	***30.5%***	94N	108N	92 C
10	5 39 m/s		7 29 m/s		1.36	6.14 l/min	***32.5%***	82N	120N	96 C
11	5 39 m/s		8 32 m/s		1.23	6.6 l/min	***34.9%***	80N	110N	100 C
12	5 39 m/s		9 35 m/s		1.12	6.62 l/min	***35.0%***	70N	110N	80 C
13	5 39 m/s		10 38 m/s		1.04	6.78 l/min	***35.8%***	78N	112N	100 C
14	5 39 m/s		11 41 m/s		0.96	6.87 l/min	***36.3%***	77N	110N	90 C
15	5 39 m/s		12 44 m/s		0.90	6.9 l/min	***36.5%***	76N	100N	84 C
16	5 39 m/s		13 47 m/s		0.84	7.22 l/min	***38.1%***	64N	80N	84 C
17	6 35 m/s		5 23 m/s		1.52	5.68 l/min	***30.0%***	84N	105N	80 C
18	6 35 m/s		6 26 m/s		1.35	6.68 l/min	***35.3%***	88N	110N	89 C
19	6 35 m/s		7 29 m/s		1.21	7.28 l/min	***38.5%***	84N	105N	91 C
20	6 35 m/s		8 32 m/s		1.10	7.64 l/min	***40.4%***	84N	105N	88 C
21	6 35 m/s		9 35 m/s		1.00	8.44 l/min	***44.6%***	104N	130N	86 C
22	6 35 m/s		10 38 m/s		0.92	8.84 l/min	***46.7%***	78N	112N	108 C
23	6 35 m/s		11 41 m/s		0.85	9.02 l/min	***47.7%***	84N	105N	90 C
24	6 35 m/s		12 44 m/s		0.80	9.26 l/min	***48.9%***	80N	100N	94 C

Table of results from Preliminary test 3.

Datasheet and raw data for Jet speed/flowrate test.

Nozzle Data		Supply Data	Wheel data			Flow Values				Collected Flowrate	Power		
Nozzle Height	Speed, vj	Flow rate	Wheel speed, Vs		Ratio (vj / vs)	Useful fluid without conatainer	retest	with container	sec		Average	Test	Re-test
0.50 m/s	40.0 m/s	24.0 l/min	1 30.0 m/s	1900.0 rpm	1.33	295	515	515 g	10	0.02974 l/s	73.2 W	102.0 W	117.5 W
0.50 m/s	30.0 m/s	18.0 l/min	1 30.0 m/s	1900.0 rpm	1.00	260	480	480 g	10	0.02600 l/s	140.8 W	138.7 W	142.9 W
0.50 m/s	20.0 m/s	12.0 l/min	1 30.0 m/s	1900.0 rpm	0.67	250	470	470 g	10	0.02500 l/s	189.4 W	189.4 W	W
0.50 m/s	10.0 m/s	6.0 l/min	1 30.0 m/s	1900.0 rpm	0.33	270	490	490 g	10	0.02700 l/s	57.9 W	57.9 W	W
0.65 m/s	30.0 m/s	24.0 l/min	1 30.0 m/s	1900.0 rpm	1.00	295	520	515 g	10	0.02950 l/s	105.0 W	105.0 W	W
0.65 m/s	20.0 m/s	16.0 l/min	1 30.0 m/s	1900.0 rpm	0.67	350	560	570 g	10	0.03500 l/s	126.3 W	126.3 W	W
0.65 m/s	10.0 m/s	8.0 l/min	1 30.0 m/s	1900.0 rpm	0.33	360	580	580 g	10	0.03600 l/s	155.4 W	155.4 W	W
0.40 m/s	40.0 m/s	19.0 l/min	1 30.0 m/s	1900.0 rpm	1.33	300	520	520 g	10	0.03000 l/s	111.0 W	103.1 W	118.9 W
0.40 m/s	30.0 m/s	14.0 l/min	1 30.0 m/s	1900.0 rpm	1.00	272.5	500	492.5 g	10	0.02725 l/s	120.7 W	128.6 W	112.8 W
0.35 m/s	40.0 m/s	17.0 l/min	1 30.0 m/s	1900.0 rpm	1.33	240	460	460 g	10	0.02400 l/s	89.7 W	128.9 W	140.1 W
0.85 m/s	20.0 m/s	20.0 l/min	1 30.0 m/s	1900.0 rpm	0.67	260	480	480 g	10	0.02600 l/s	128.3 W	115.2 W	141.4 W
0.85 m/s	10.0 m/s	9.8 l/min	1 30.0 m/s	1900.0 rpm	0.33	240	460	460 g	10	0.02400 l/s	136.7 W	133.4 W	140.0 W

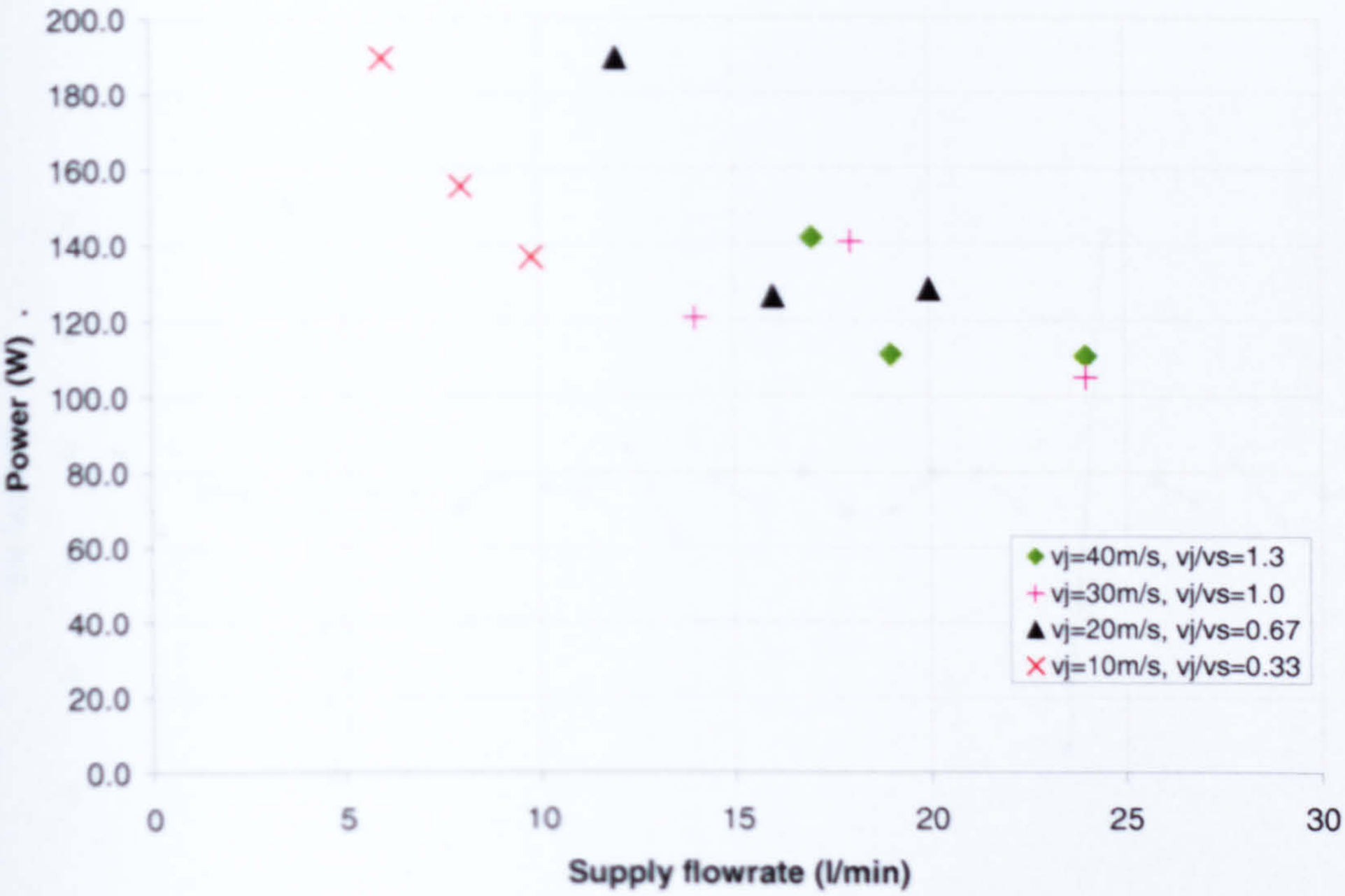

Power against flowrate for varying jet speeds for the Jet speed/flow rate test

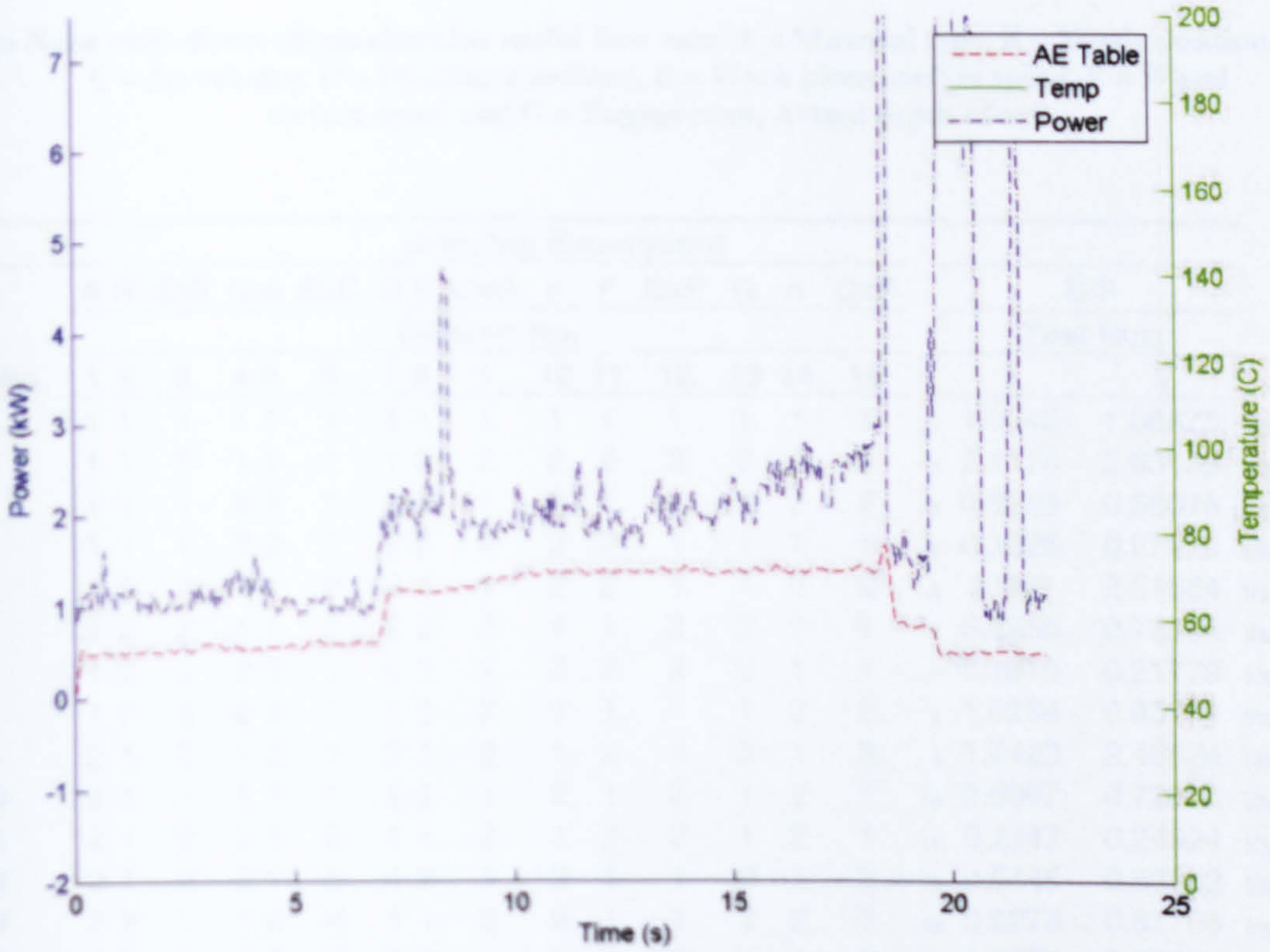

Typical Matlab display of the DAQ outputs for Jet speed/flow rate test, results shown from test

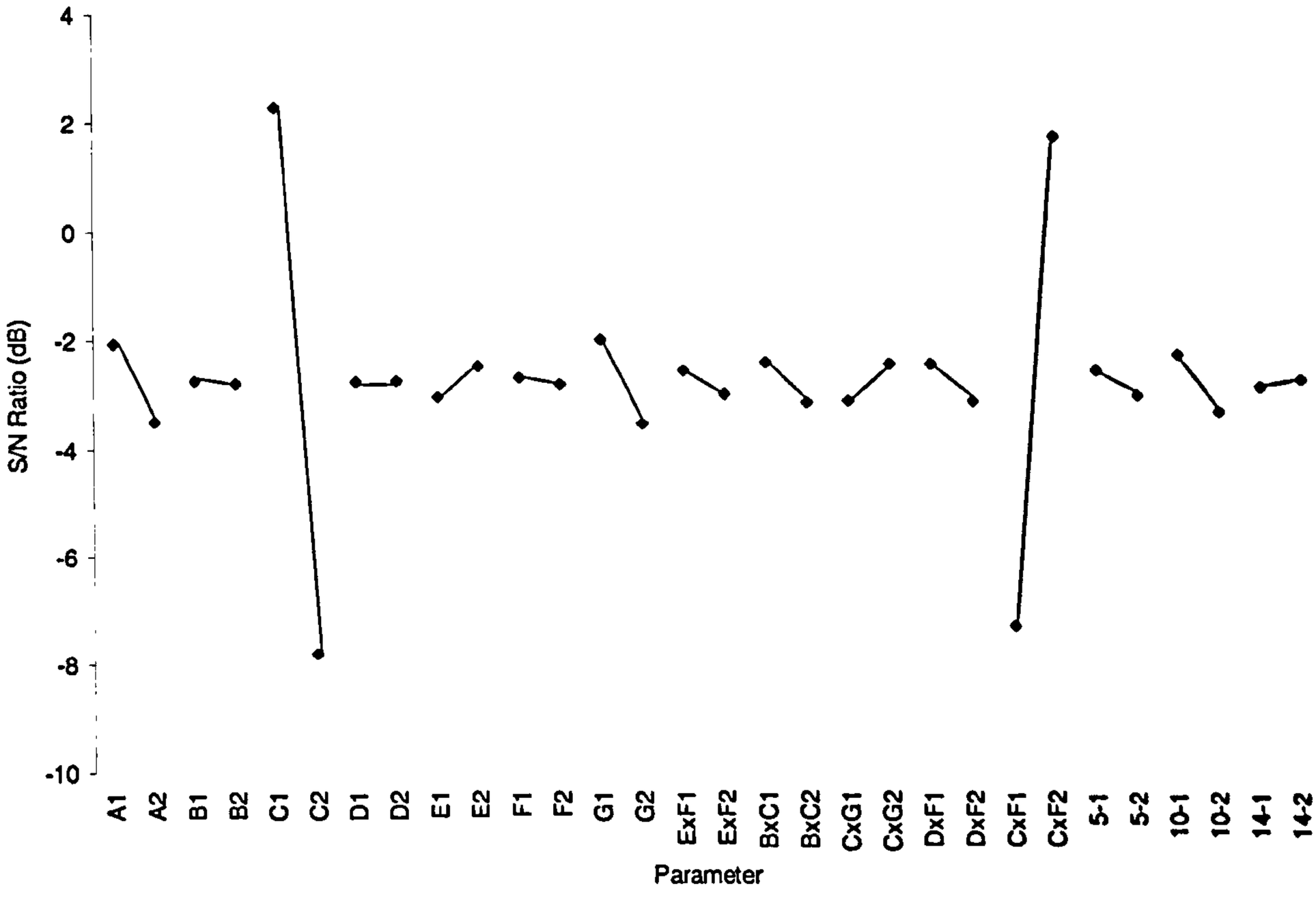

Signal to Noise ratio direct effects chart for useful flow rate. A = Material type, B = Nozzle position, C = Jet velocity, D = Dressing condition, E = Work piece surface speed, F = Wheel surface speed and G = Engagement, Actual depth of cut.

	Grinding Experiment															U/F		
	A	B	ExF	C	n	BxC	D	E	CxG	n	F	DxF	G	n	CxF			
	Column No.															Test Run		
Trial No.	1	2	3	4	5	6	7	8	9	10	11	12	13	14	15	i	ii	
1	1	1	1	1	1	1	1	1	1	1	1	1	1	1	1	1.0042	1.06473	Vs
2	1	1	1	1	1	1	1	2	2	2	2	2	2	2	2	2.1174	2.60133	Vs
3	1	1	1	2	2	2	2	1	1	1	1	2	2	2	2	0.6969	0.58076	Vs
4	1	1	1	2	2	2	2	2	2	2	2	1	1	1	1	0.3025	0.27223	Vs
5	1	2	2	1	1	2	2	1	1	2	2	1	1	2	2	2.069	2.51664	Vs
6	1	2	2	1	1	2	2	2	2	1	1	2	2	1	1	0.9256	0.72595	Vs
7	1	2	2	2	2	1	1	1	1	2	2	2	2	1	1	0.1815	0.21779	Vs
8	1	2	2	2	2	1	1	2	2	1	1	1	1	2	2	1.0284	0.90744	Vs
9	2	1	2	1	2	1	2	1	2	1	2	1	2	1	2	1.7423	2.46824	Vs
10	2	1	2	1	2	1	2	2	1	2	1	2	1	2	1	0.6897	0.72595	Vs
11	2	1	2	2	1	2	1	1	2	1	2	2	1	2	1	0.2347	0.24924	Vs
12	2	1	2	2	1	2	1	2	1	2	1	1	2	1	2	0.5445	0.53842	Vs
13	2	2	1	1	2	2	1	1	2	2	1	1	2	2	1	0.6279	0.61706	Vs
14	2	2	1	1	2	2	1	2	1	1	2	2	1	1	2	1.7725	2.72232	Vs
15	2	2	1	2	1	1	2	1	2	2	1	2	1	1	2	0.6824	0.68966	Vs
16	2	2	1	2	1	1	2	2	1	1	2	1	2	2	1	0.242	0.24803	Vs

Table of results from Taguchi experiment for Useful flow rate.

	Grinding Experiment															U/F	
	A	B	ExF	C	n	BxC	D	E	CxG	n	F	DxF	G	n	CxF		
	Column No.															Test Run	
Trial No.	1	2	3	4	5	6	7	8	9	10	11	12	13	14	15	i	ii
1	1	1	1	1	1	1	1	1	1	1	1	1	1	1	1	4.78%	5.07%
2	1	1	1	1	1	1	1	2	2	2	2	2	2	2	2	10.08%	12.39%
3	1	1	1	2	2	2	2	1	1	1	1	2	2	2	2	16.59%	13.83%
4	1	1	1	2	2	2	2	2	2	2	2	1	1	1	1	7.20%	6.48%
5	1	2	2	1	1	2	2	1	1	2	2	1	1	2	2	9.85%	11.98%
6	1	2	2	1	1	2	2	2	2	1	1	2	2	1	1	4.41%	3.46%
7	1	2	2	2	2	1	1	1	1	2	2	2	2	1	1	4.32%	5.19%
8	1	2	2	2	2	1	1	2	2	1	1	1	1	2	2	24.49%	21.61%
9	2	1	2	1	2	1	2	1	2	1	2	1	2	1	2	8.30%	11.75%
10	2	1	2	1	2	1	2	2	1	2	1	2	1	2	1	3.28%	3.46%
11	2	1	2	2	1	2	1	1	2	1	2	2	1	2	1	5.59%	5.93%
12	2	1	2	2	1	2	1	2	1	2	1	1	2	1	2	12.96%	12.82%
13	2	2	1	1	2	2	1	1	2	2	1	1	2	2	1	2.99%	2.94%
14	2	2	1	1	2	2	1	2	1	1	2	2	1	1	2	8.44%	12.96%
15	2	2	1	2	1	1	2	1	2	2	1	2	1	1	2	16.25%	16.42%
16	2	2	1	2	1	1	2	2	1	1	2	1	2	2	1	5.76%	5.91%

Table of results from Taguchi experiment for Percentage useful flow.

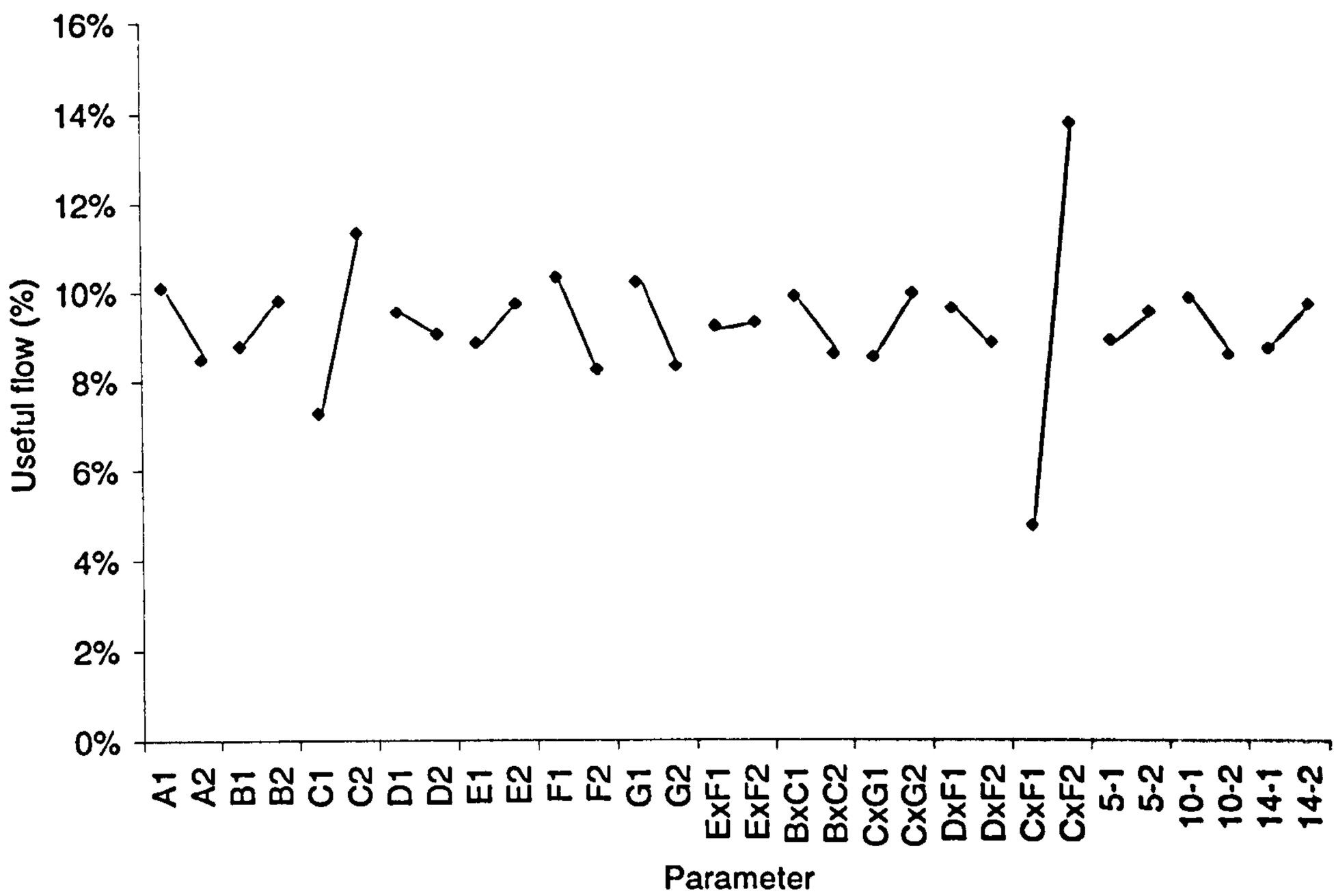

Direct effect chart for Percentage useful flow. A = Material Type, B = Nozzle position, C = Jet Speed/flowrate, D = Dressing condition, E = Work piece surface speed, F = Wheel surface speed and G = Engagement, Actual depth of cut.

ANOVA Results Table

Source	SS	*v*	V	F
A	0.00211	1	0.002106	2.64
B	0.00084	1	0.000845	1.06
C	0.01328	1	0.013283	16.66
D	0.00018	1	0.000182	0.23
E	0.00061	1	0.000606	0.76
F	0.00345	1	0.003446	4.32
G	0.00283	1	0.002833	3.55
EF	0.00001	1	5.3E-06	0.01
BC	0.00133	1	0.001327	1.66
CG	0.00166	1	0.001663	2.09
DF	0.00047	1	0.000472	0.59
CF	0.06476	1	0.064762	81.22
e	0.00239	3	0.000797	
T	0.09392	15		

ANOVA table for the percentage useful flow results, where SS is the Sum of the Squares for each variable, *v* is the degrees of freedom, V is the variance and F is the value from the F-test.

	Grinding Experiment															Surface finish		
	A	B	ExF	C	n	BxC	D	E	CxG	n	F	DxF	G	n	CxF			
	Column No.															Test Run		
Trial No.	1	2	3	4	5	6	7	8	9	10	11	12	13	14	15	i	ii	
1	1	1	1	1	1	1	1	1	1	1	1	1	1	1	1	0.10	0.07	µm
2	1	1	1	1	1	1	1	2	2	2	2	2	2	2	2	0.08	0.125	µm
3	1	1	1	2	2	2	2	1	1	1	1	2	2	2	2	0.2	0.15	µm
4	1	1	1	2	2	2	2	2	2	2	2	1	1	1	1	0.3	0.22	µm
5	1	2	2	1	1	2	2	1	1	2	2	1	1	2	2	0.17	0.14	µm
6	1	2	2	1	1	2	2	2	2	1	1	2	2	1	1	0.15	0.105	µm
7	1	2	2	2	2	1	1	1	1	2	2	2	2	1	1	0.12	0.15	µm
8	1	2	2	2	2	1	1	2	2	1	1	1	1	2	2	0.11	0.13	µm
9	2	1	2	1	2	1	2	1	2	1	2	1	2	1	2	0.3	0.22	µm
10	2	1	2	1	2	1	2	2	1	2	1	2	1	2	1	0.09	0.13	µm
11	2	1	2	2	1	2	1	1	2	1	2	2	1	2	1	0.145	0.155	µm
12	2	1	2	2	1	2	1	2	1	2	1	1	2	1	2	0.06	0.07	µm
13	2	2	1	1	2	2	1	1	2	2	1	1	2	2	1	0.18	0.2	µm
14	2	2	1	1	2	2	1	2	1	1	2	2	1	1	2	0.1	0.1	µm
15	2	2	1	2	1	1	2	1	2	2	1	2	1	1	2	0.065	0.095	µm
16	2	2	1	2	1	1	2	2	1	1	2	1	2	2	1	0.35	0.29	µm

Table of results from Taguchi experiment for surface finish, Ra.

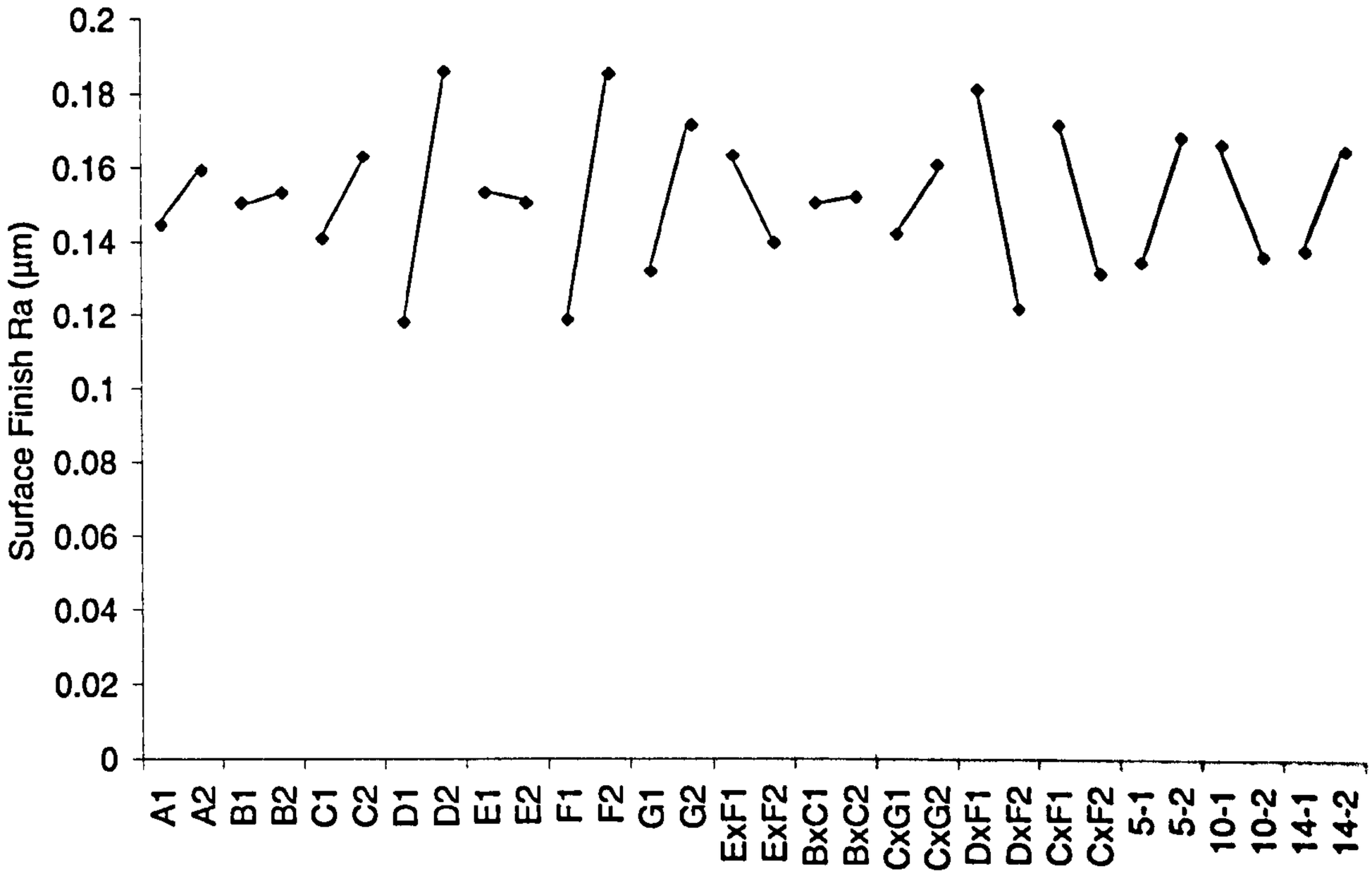

Direct effect chart for Surface finish. A = Material Type, B = Nozzle position, C = Jet Speed/flowrate, D = Dressing condition, E = Work piece surface speed, F = Wheel surface speed and G = Engagement, Actual depth of cut.

	Grinding Experiment															Power		
	A	B	ExF	C	n	BxC	D	E	CxG	n	F	DxF	G	n	CxF			
	Column No.															Test Run		
Trial No.	1	2	3	4	5	6	7	8	9	10	11	12	13	14	15	i	ii	
1	1	1	1	1	1	1	1	1	1	1	1	1	1	1	1	1.77	2.1	kW
2	1	1	1	1	1	1	1	2	2	2	2	2	2	2	2	1.708	1.644	kW
3	1	1	1	2	2	2	2	1	1	1	1	2	2	2	2	2.219	2.24	kW
4	1	1	1	2	2	2	2	2	2	2	2	1	1	1	1	1.57	1.3	kW
5	1	2	2	1	1	2	2	1	1	2	2	1	1	2	2	5.947	5.85	kW
6	1	2	2	1	1	2	2	2	2	1	1	2	2	1	1	3.351	3.61	kW
7	1	2	2	2	2	1	1	1	1	2	2	2	2	1	1	1.56	1.199	kW
8	1	2	2	2	2	1	1	2	2	1	1	1	1	2	2	0.612	0.456	kW
9	2	1	2	1	2	1	2	1	2	1	2	1	2	1	2	5.8	5.749	kW
10	2	1	2	1	2	1	2	2	1	2	1	2	1	2	1	0.19	0.47	kW
11	2	1	2	2	1	2	1	1	2	1	2	2	1	2	1	1.86	1.7	kW
12	2	1	2	2	1	2	1	2	1	2	1	1	2	1	2	1.45	1.423	kW
13	2	2	1	1	2	2	1	1	2	2	1	1	2	2	1	0.49	0.79	kW
14	2	2	1	1	2	2	1	2	1	1	2	2	1	1	2	1.09	1.129	kW
15	2	2	1	2	1	1	2	1	2	2	1	2	1	1	2	0.812	0.834	kW
16	2	2	1	2	1	1	2	2	1	1	2	1	2	2	1	5.391	5.355	kW

Table of results from Taguchi experiment for grinding power.

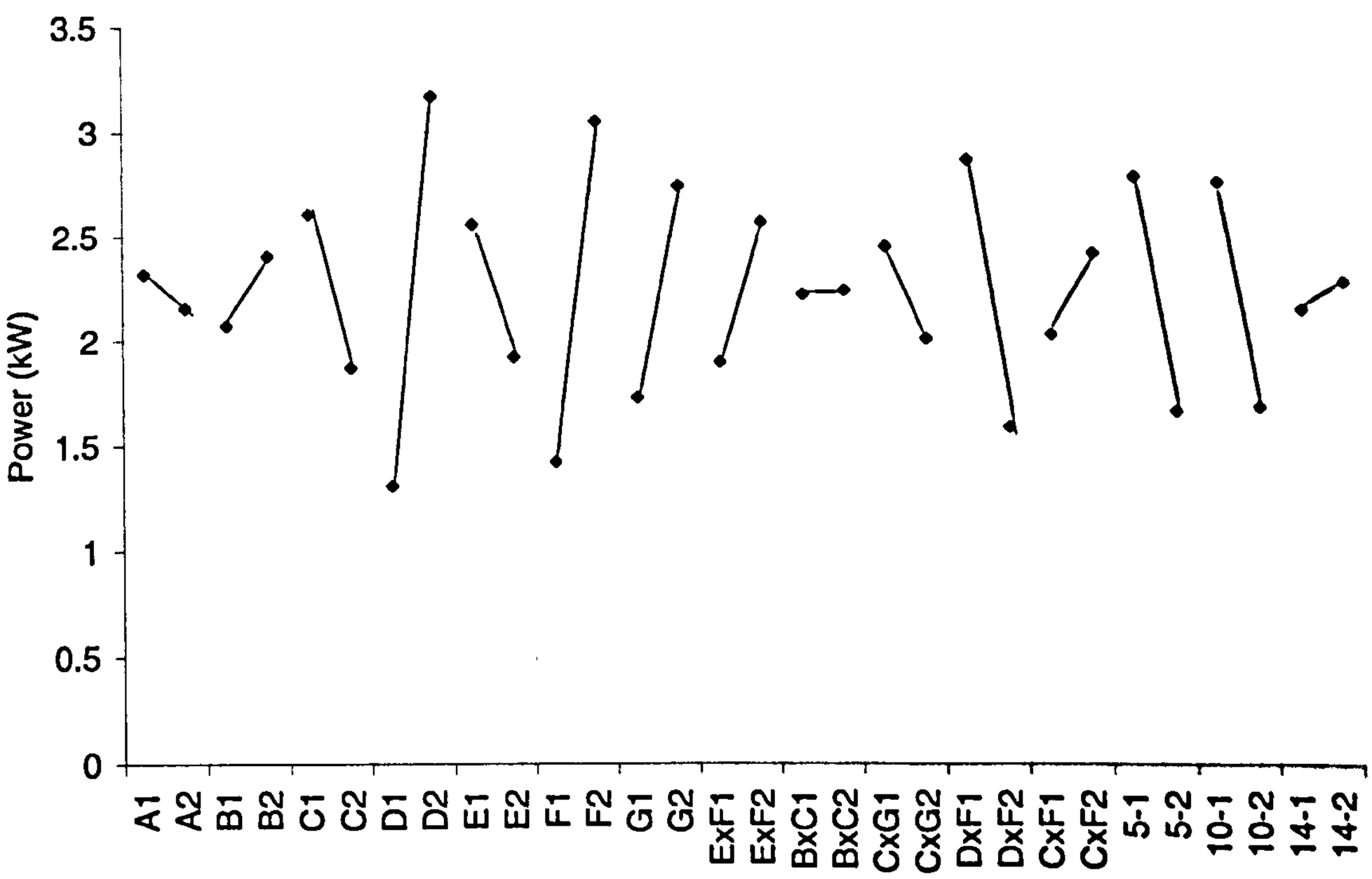

Direct effect chart for Power. A = Material Type, B = Nozzle position, C = Jet Speed/flowrate, D = Dressing condition, E = Work piece surface speed, F = Wheel surface speed and G = Engagement, Actual depth of cut.

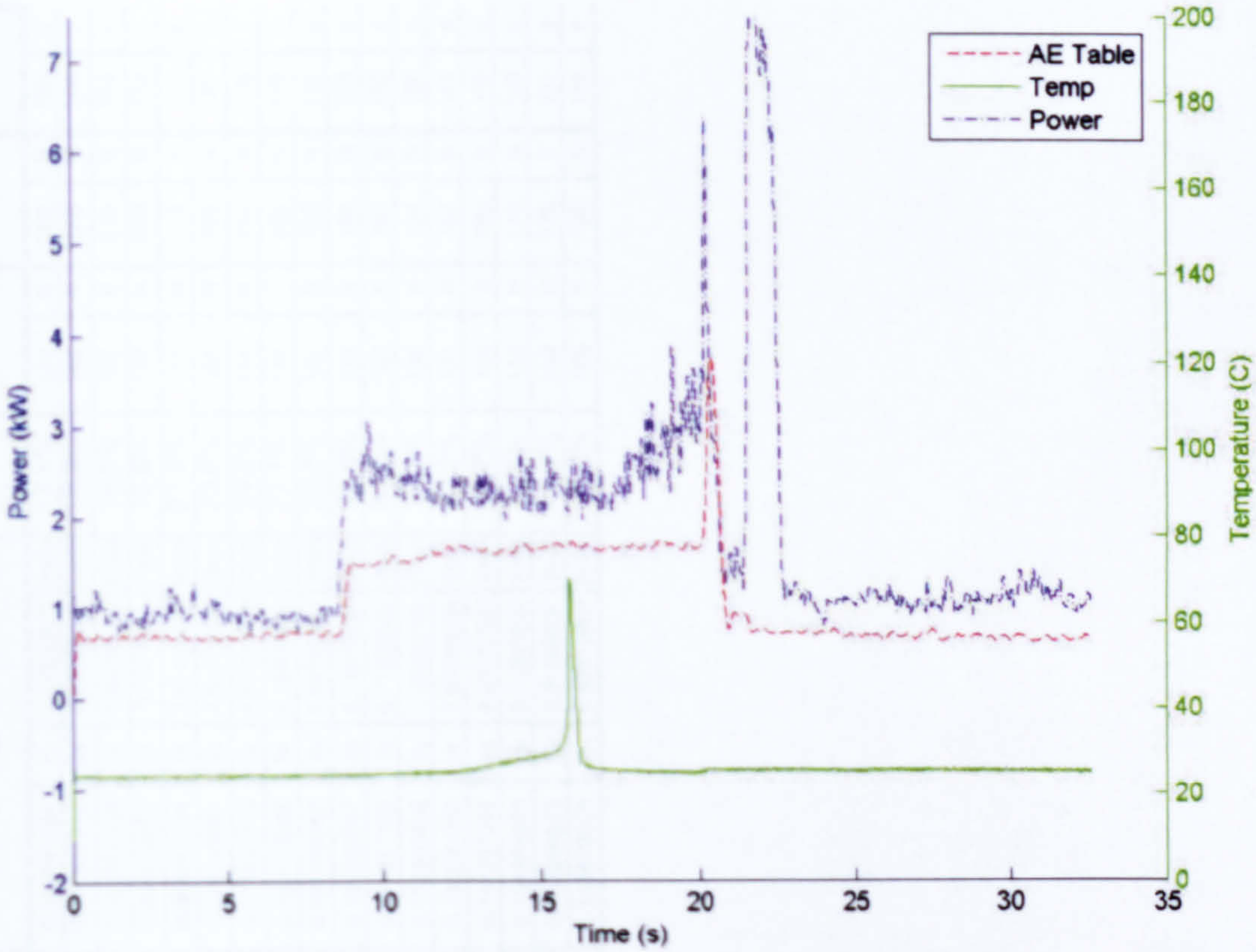

Example of Matlab display of the DAQ outputs for Taguchi tests on the Dominator grinding machine, results shown from test 12.

Table of results for Abwood speed ratio tests.

Nozzle Data		Wheel velocities				Useful Flow Values										Force (N)				Temp	
Nozzle speed, vj (m/s)	Nozzle Position		Wheel speed, vs (m/s)	(rpm)	Ratio (vj / vs)	retest			sec	rate				%	y, Ft		Z, Fn		Max	
24.3	5 mm	1	11.6	1200.0	2.10	1670	1676	g	10	0.054043154	l/s	3.24258923	l/min	17.1%	140	N	200	N	102	c
24.3	5 mm	2	12.0	1250.0	2.01	1682	1712	g	10	0.057672918	l/s	3.46037508	l/min	18.3%	146	N	208	N	104	c
24.3	5 mm	3	12.8	1330.0	1.89	1736	1750	g	10	0.061504336	l/s	3.69026013	l/min	19.5%	147	N	210	N	104	c
24.3	5 mm	4	13.5	1400.0	1.80	1780	1760	g	10	0.062512603	l/s	3.7507562	l/min	19.8%	154	N	220	N	110	c
24.3	5 mm	5	14.3	1480.0	1.70	1830	1797	g	10	0.066243194	l/s	3.97459165	l/min	21.0%	151	N	215	N	113	c
24.3	5 mm	6	15.1	1570.0	1.60	1940	1860	g	10	0.072595281	l/s	4.35571688	l/min	23.0%	161	N	230	N	120	c
24.3	5 mm	7	16.2	1680.0	1.50	1990	1906	g	10	0.077233313	l/s	4.63399879	l/min	24.5%	154	N	220	N	125	c
24.3	5 mm	8	17.4	1800.0	1.40	2080	1987	g	10	0.085400282	l/s	5.12401694	l/min	27.1%	144	N	205	N	128	c
24.3	5 mm	9	18.8	1950.0	1.29	2166	2057	g	10	0.092458157	l/s	5.54748941	l/min	29.3%	137	N	196	N	125	c
24.3	5 mm	10	20.2	2100.0	1.20	2260	2150	g	10	0.101835047	l/s	6.11010284	l/min	32.3%	133	N	190	N	133	c
24.3	5 mm	11	22.2	2300.0	1.09	2370	2250	g	10	0.111917725	l/s	6.71506352	l/min	35.5%	127	N	182	N	130	c
24.3	5 mm	12	24.1	2500.0	1.01	2524	2350	g	10	0.122000403	l/s	7.3200242	l/min	38.7%	136	N	194	N	136	c
24.3	5 mm	13	26.5	2750.0	0.92	2640	2460	g	10	0.133091349	l/s	7.98548094	l/min	42.2%	131	N	187	N	141	c
24.3	5 mm	14	30.4	3150.0	0.80	2780	2600	g	10	0.147207098	l/s	8.83242589	l/min	46.7%	126	N	180	N	135	c
24.3	5 mm	15	34.7	3600.0	0.70	2820	2670	g	10	0.154264973	l/s	9.25589837	l/min	48.9%	119	N	170	N	135	c
24.3	5 mm	16	40.5	4200.0	0.60	2840	2670	g	10	0.154264973	l/s	9.25589837	l/min	48.9%	119	N	170	N	121	c
24.3	5 mm	17	50.1	5200.0	0.48	2750	2567	g	10	0.143879814	l/s	8.63278887	l/min	45.6%	105	N	150	N	136	c

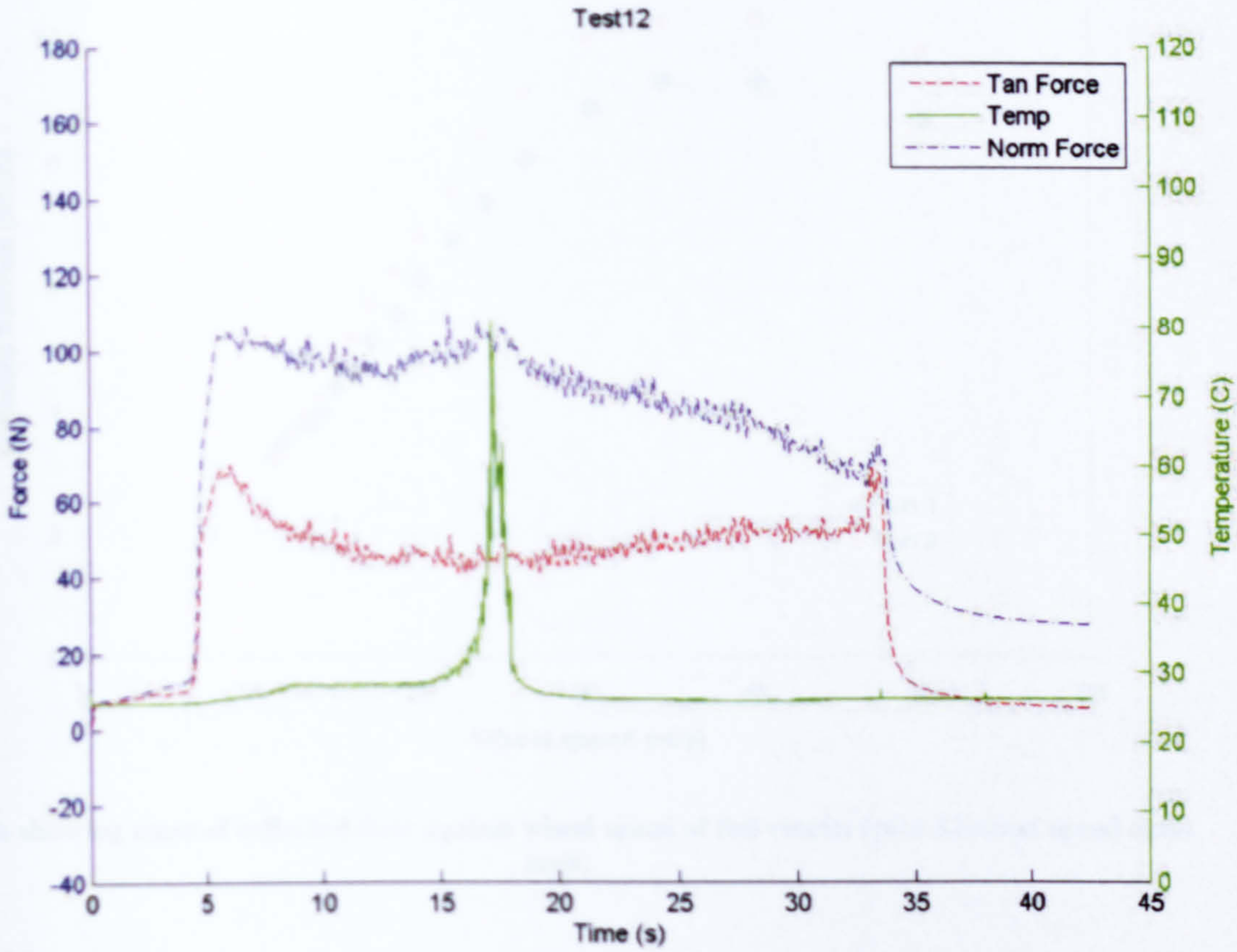

Typical Matlab display of the DAQ outputs for Abwood speed ratio test, results shown from test 12.

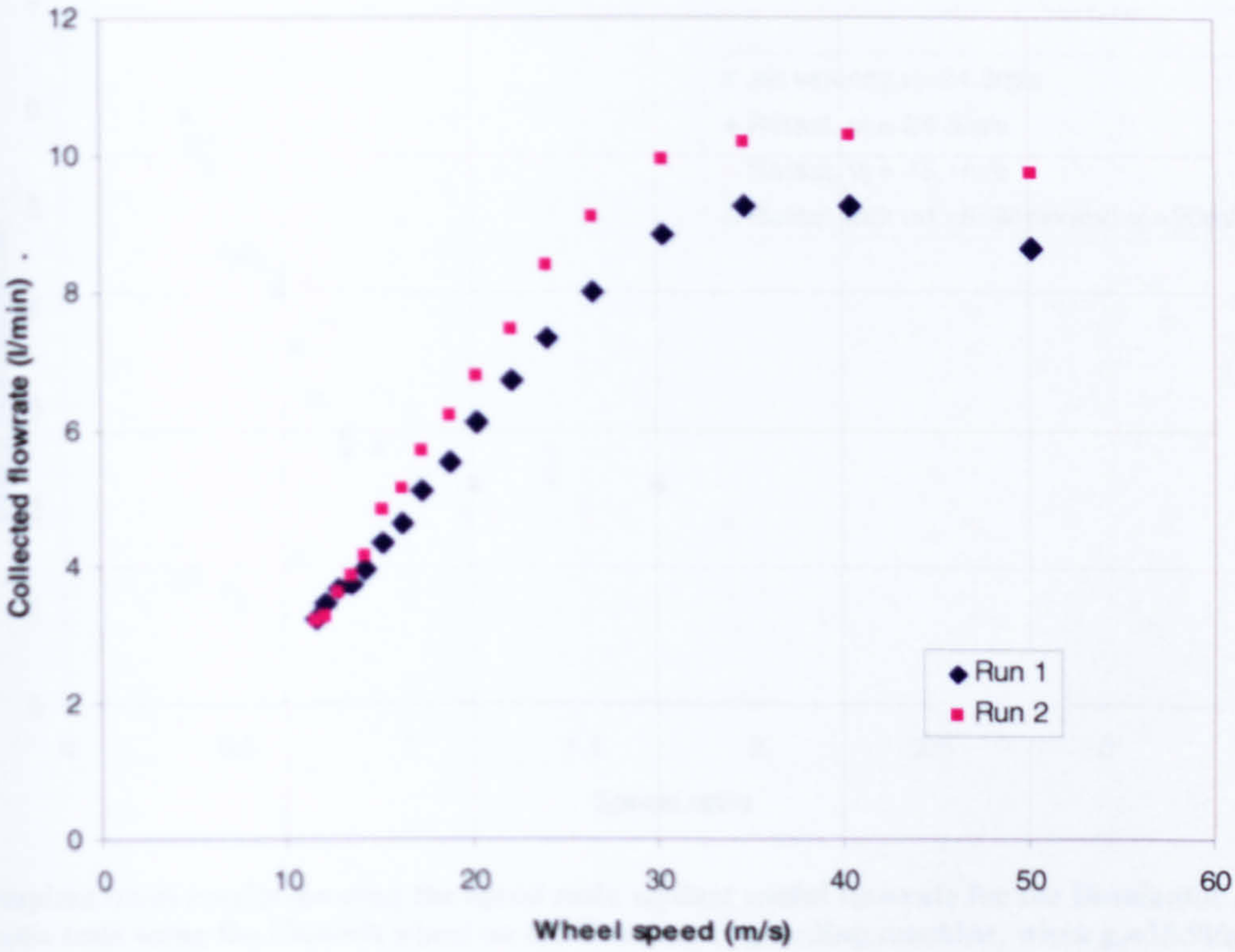

Graph showing mass of collected flow against wheel speed of full results from Abwood speed ratio tests.

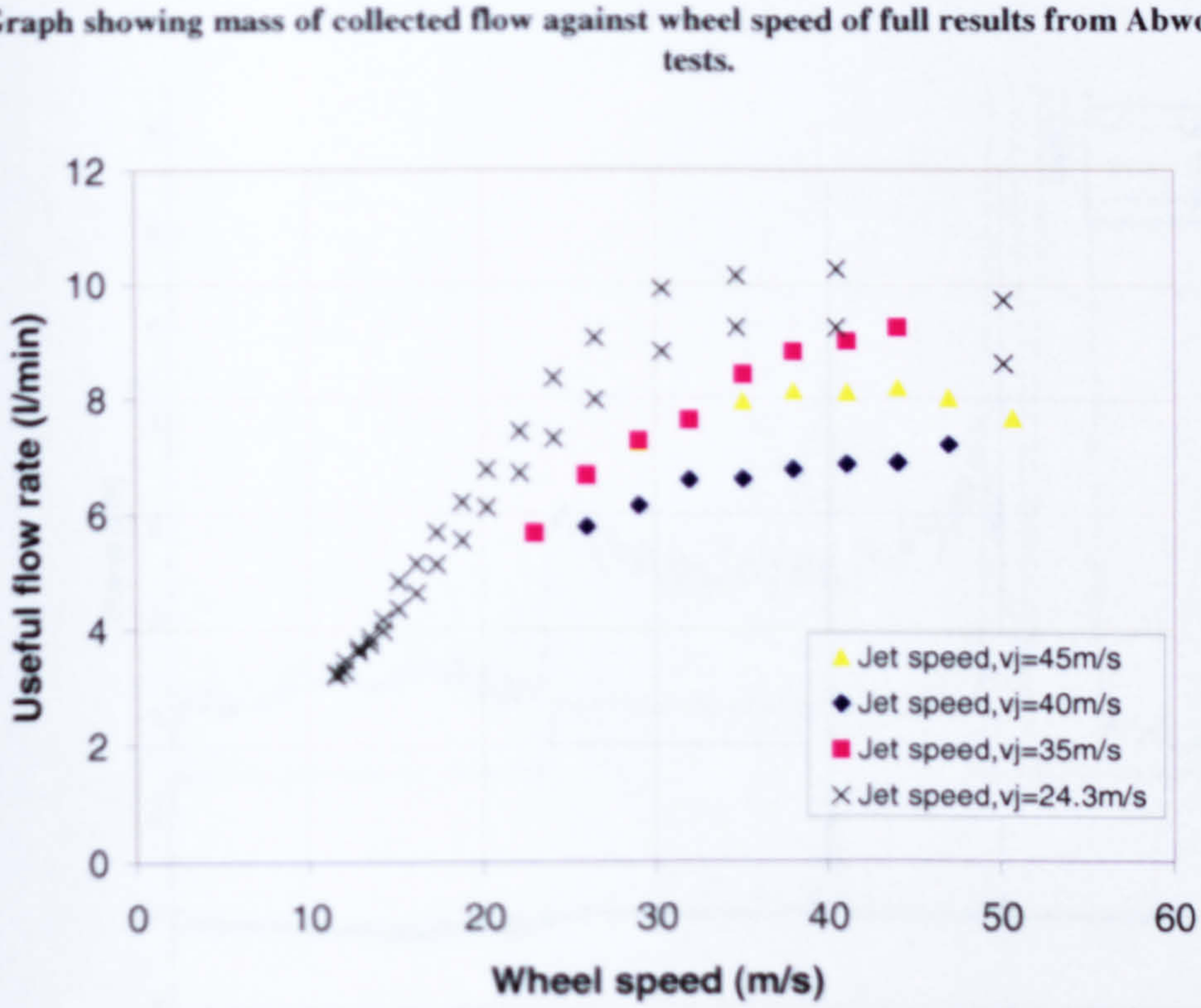

Complete set of results showing the Abwood speed ratio tests combined with the results from preliminary test 3 showing the useful flowrate against the wheel speed using the Altos wheel on the Abwood grinding machine, when q_d=18.9l/min.

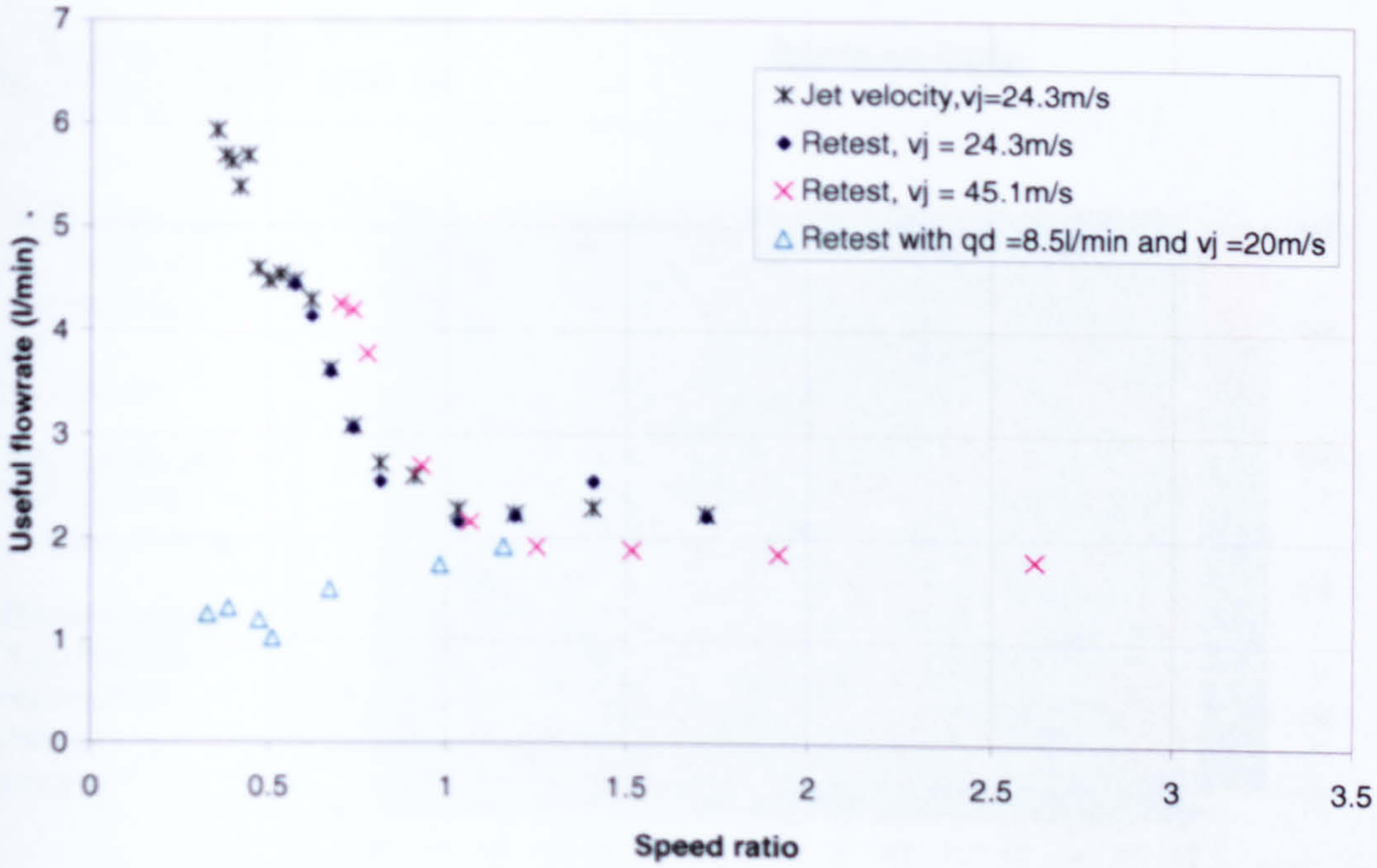

Complete set of results showing the speed ratio against useful flowrate for the Dominator speed ratio tests using the Flexovit wheel on the Dominator grinding machine, when q_d=18.9l/min.

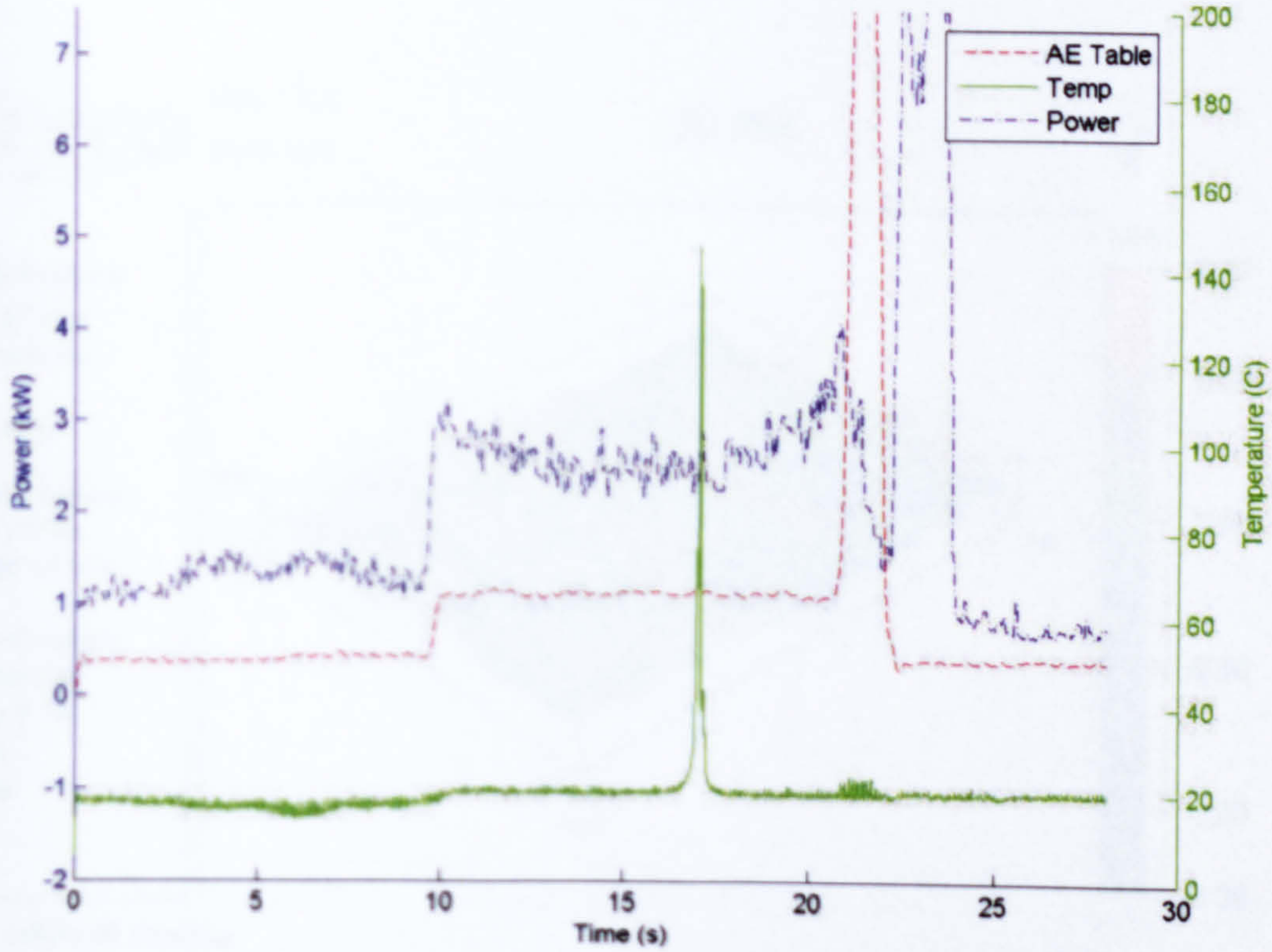

Typical Matlab display of the DAQ outputs for Dominator speed ratio test, results shown from test 4.

Veeco

Mag: 1.0 X

Mode: PSI

Surface Data

Surface Statistics:

Ra: 194.73 um

Rq: 240.95 um

Rz:

Rt: 2.16 mm

Set-up Parameters:

Size: 512 X 384

Sampling: 13.70 um

Processed Options:

Terms Removed:

Cylinder & Tilt

Filtering:

Low Pass

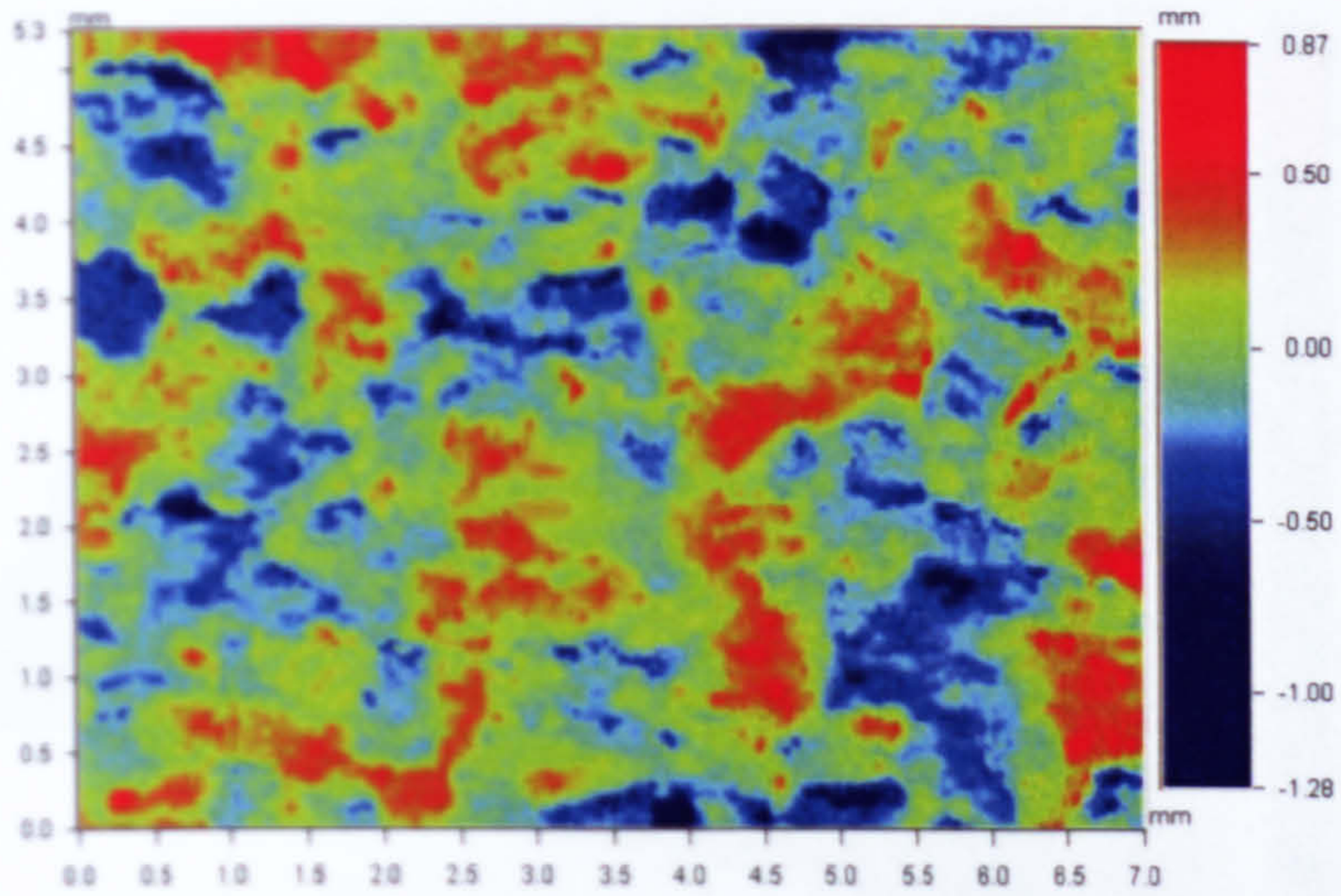

Title: OSP100 Profiler

Example of contour plot and key surface finish parameters generated by WykoVision software created with data taken from Uniscan system. The data comes from the Altos wheel.

Veeco

Mag: 1.0 X

Mode: PSI

3D Plot

Surface Statistics:

Ra: 194.73 um

Rq: 240.95 um

Rz:

Rt: 2.16 mm

Set-up Parameters:

Size: 512 X 384

Sampling: 13.70 um

Processed Options:

Terms Removed:

Cylinder & Tilt

Filtering:

Low Pass

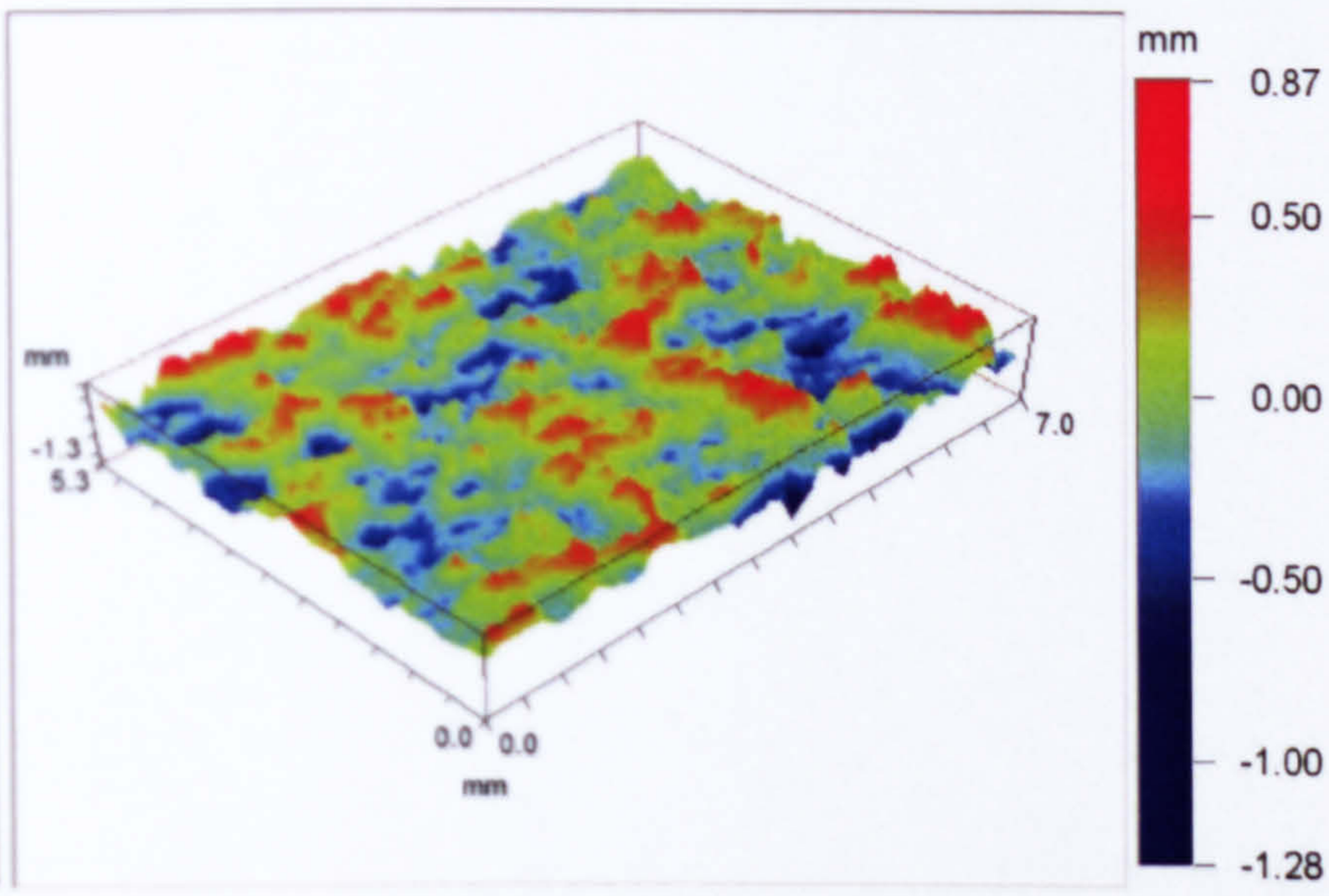

Title: OSP100 Profiler

Example of 3-D plot generated by WykoVision software created with data taken from Uniscan system. The data comes from the Altos wheel.

Veeco

3-Dimensional Interactive Display

Surface Stats:

Ra: 194.73 um

Rq: 240.95 um

Rt: 2.16 mm

Measurement Info:

Magnification: 1.00

Measurement Mode: PSI

Sampling: 13.70 um

Array Size: 512 X 384

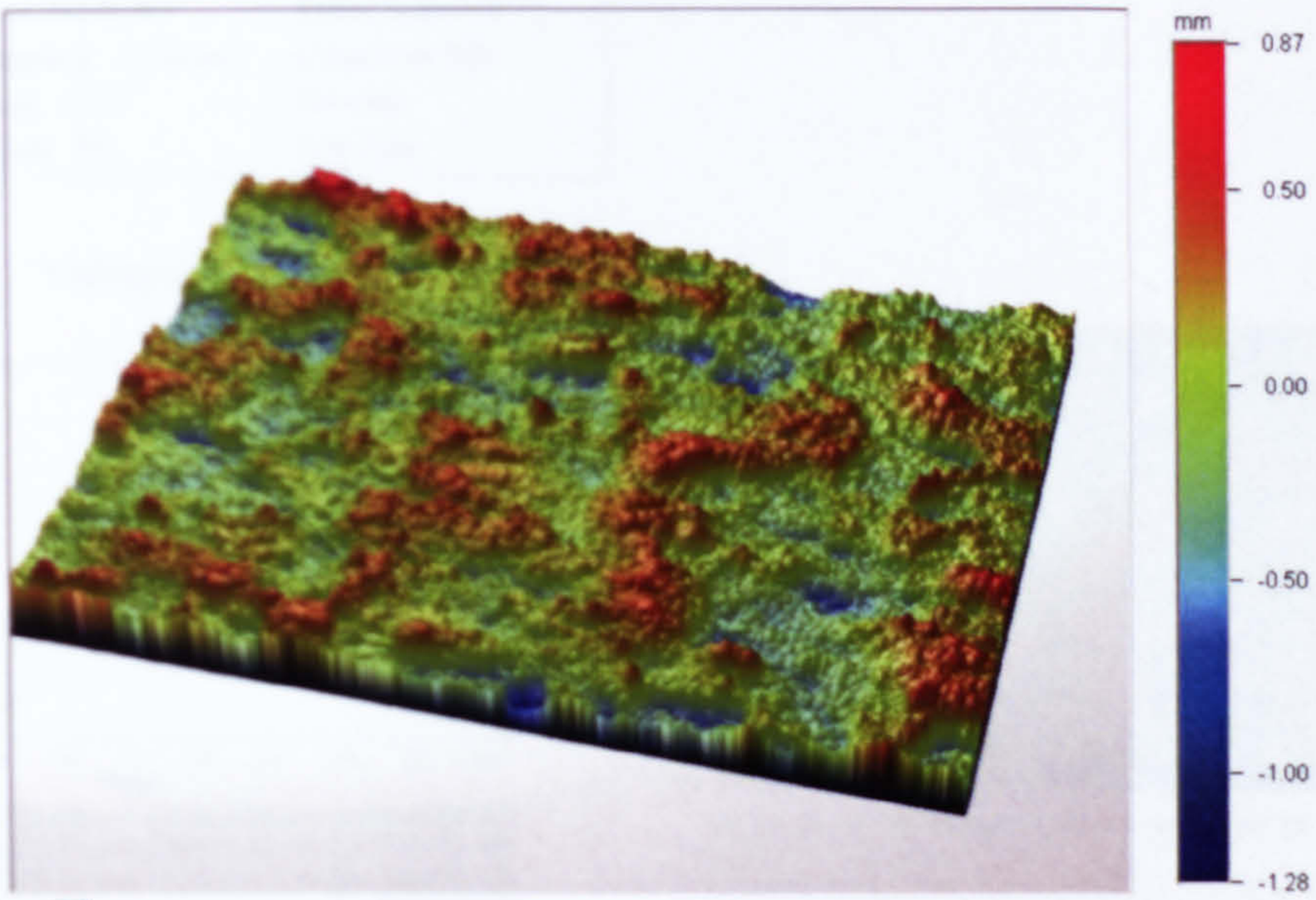

Title: OSP100 Profiler

Example of 3-D rendered image generated by WykoVision software created with data taken from Uniscan system. The data comes from the Altos wheel.

Title: OSP100 Profiler

Note:

Surface Statistics:	Set-up Parameters:	Processed Options:
Ra: 194.73 um	Size: 512 X 384	Terms Removed:
Rq: 240.95 um	Sampling: 13.70 um	Cylinder & Tilt
Rz:	Mag: 1.0 X	Filtering:
Rt: 2.16 mm	Mode: PSI	Low Pass

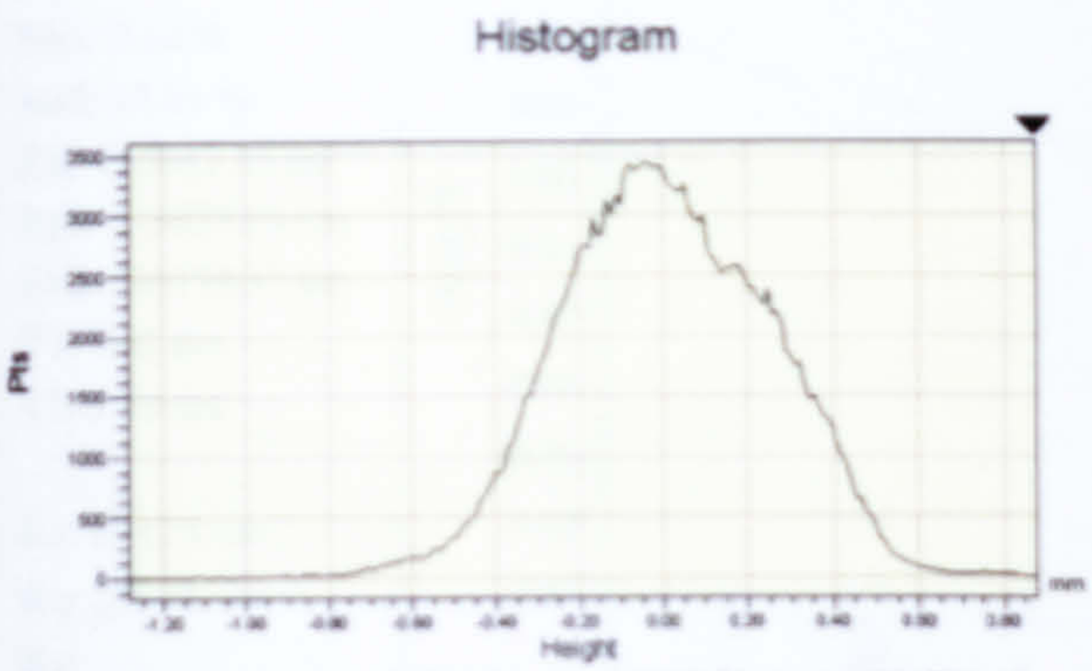

95% of data is between -451722.99 and 442866.03 nm (pv:894589.02)
90% of data is between -376275.73 and 388975.13 nm (pv:765250.85)
85% of data is between -376275.73 and 313527.86 nm (pv:689803.59)
80% of data is between -311606.63 and 302749.69 nm (pv:614356.32)

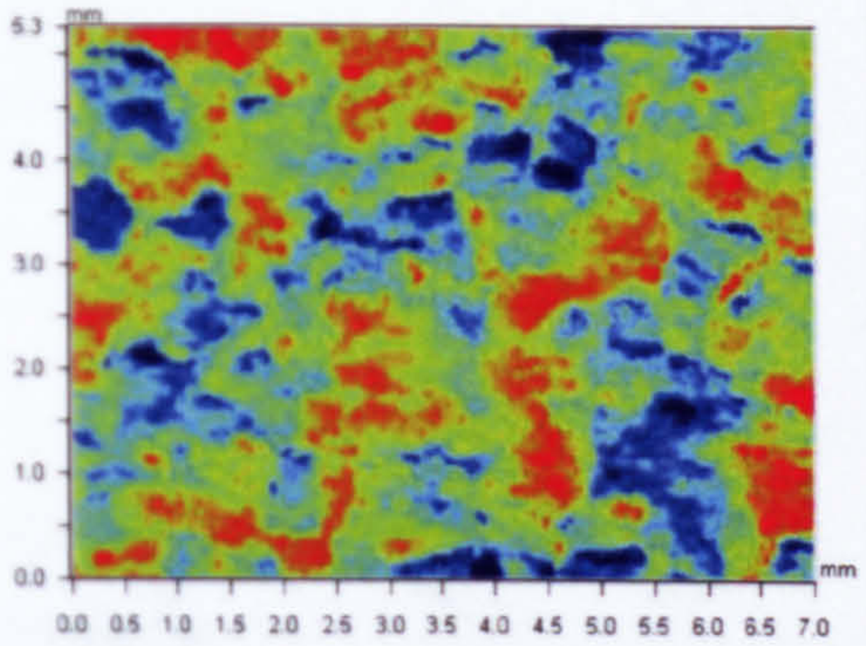

Example of point by point analysis displayed as a Histogram generated by WykoVision software created with data taken from Uniscan system. Also shown is a contour plot from the same dataset. The data comes from the Altos wheel.

Veeco

Mag: 1.0 X

Mode: PSI

Date: 07

Time: 14

Statistics:

tp1: 0.0 %

tp2: 100.0 %

Htp: 2.16 mm

Mr1: 9.60 %

Mr2: 92.03 %

RK: 655812.25 nm

Rpk: 179628.64 nm

Rvk: 230774.17 nm

V1: 8.62 um

V2: 9.20 um

Ra: 194.73 um

Rq: 240.95 um

Rz:

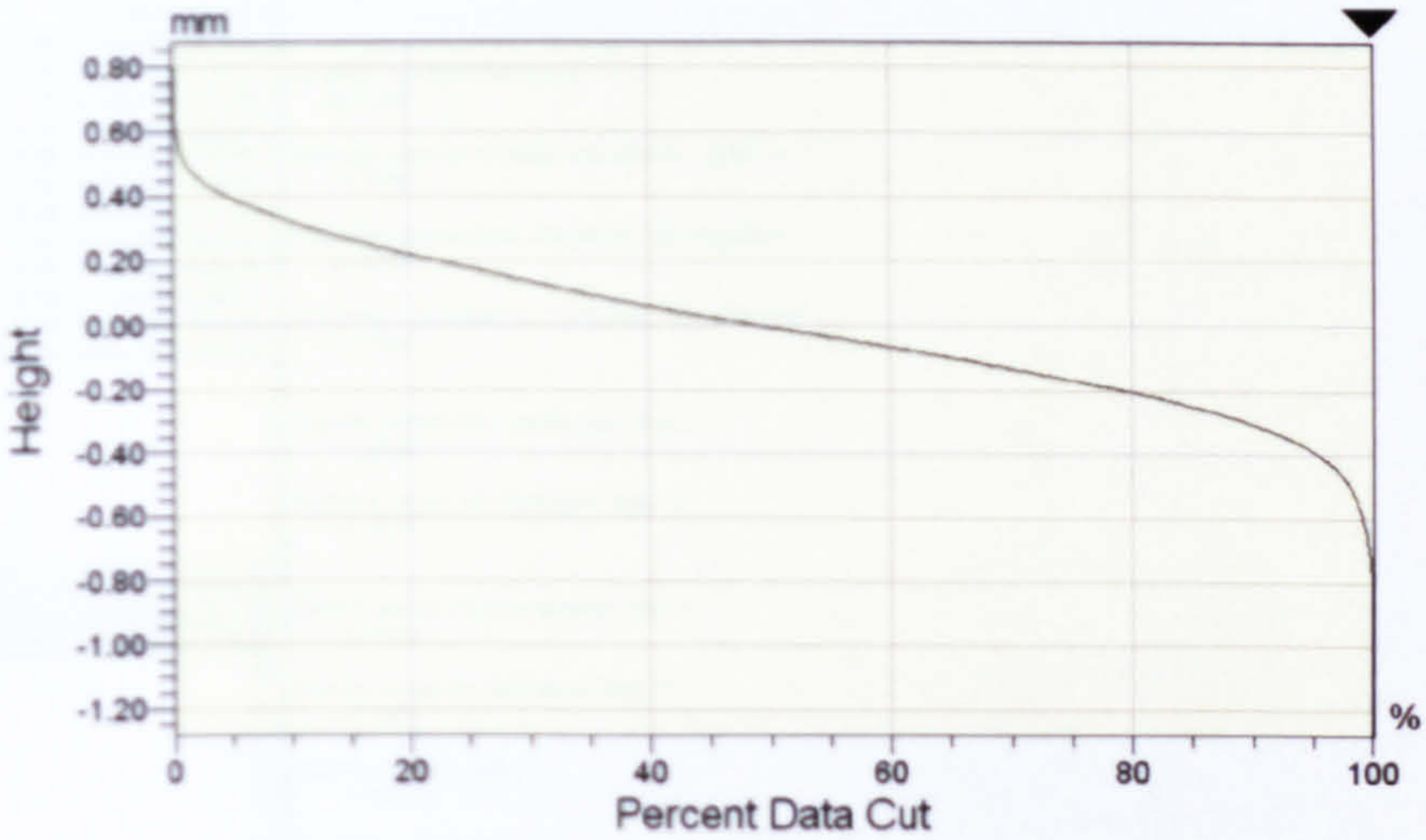

Title: OSP100 Profiler

Example of Bearing Ratio curve generated by WykoVision software created with data taken from Uniscan system. The data comes from the Altos wheel.

Veeco

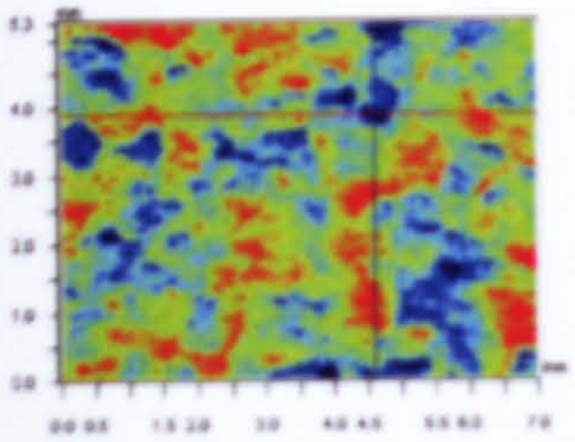

X	4.60	-	-	mm
Y	3.91	-	-	mm
Hi	-0.79	-	-	mm
Dist			-	mm
Angle			-	°

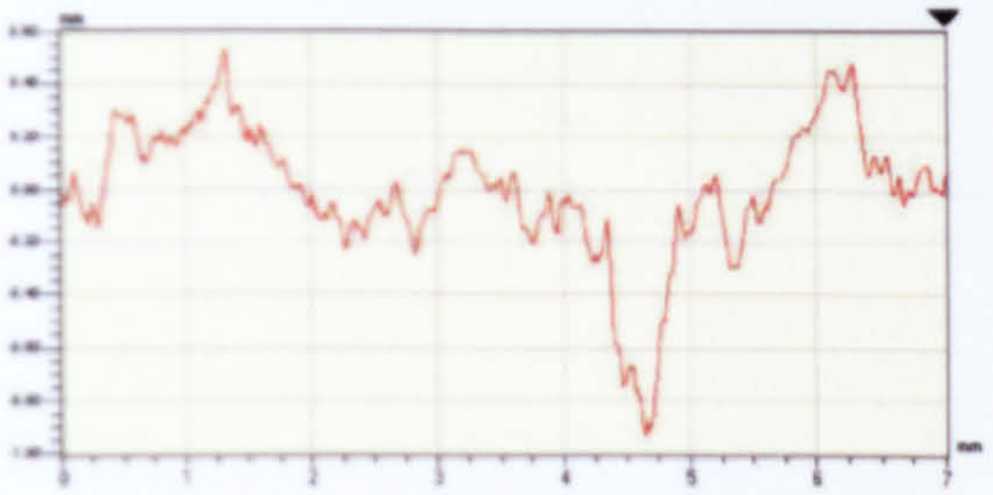

Rq	0.25 mm
Ra	0.18 mm
Rt	1.47 mm
Rp	0.53 mm
Rv	-0.94 mm

Angle	0.00 mrad
Curve	17.15 mm
Terms	None
Avg Ht	-0.01 mm
Area	-0.05 mm2

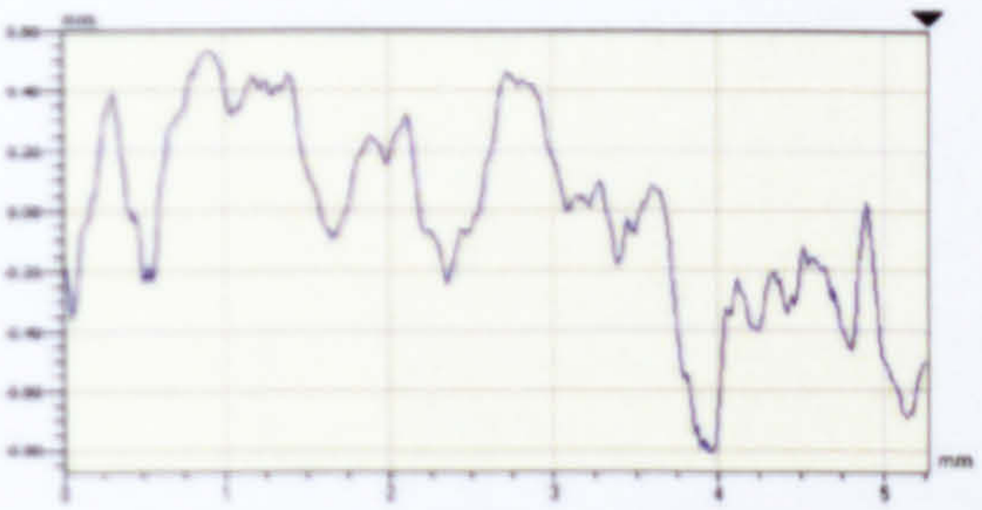

Rq	0.33 mm
Ra	0.27 mm
Rt	1.34 mm
Rp	0.53 mm
Rv	-0.81 mm

Angle	0.00 mrad
Curve	-9.53 mm
Terms	None
Avg Ht	-0.01 mm
Area	-0.06 mm2

Title: OSP100 Profiler

Example of 2-D analysis generated by WykoVision software created with data taken from Uniscan system. The data comes from the Altos wheel.

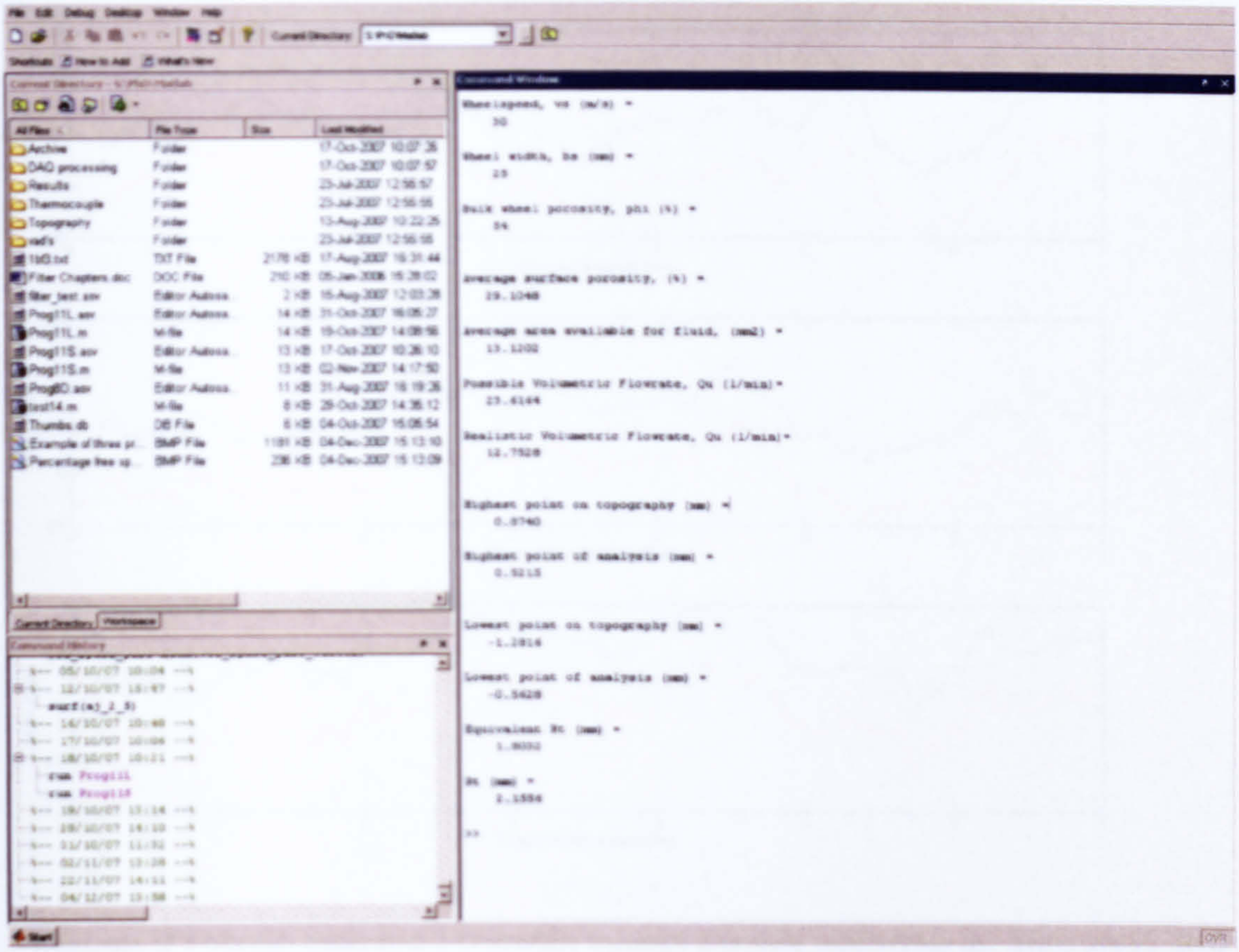

Example of outputs generated by Matlab code developed for this project with data from a topographical scan using the Uniscan optical scanning system. The data comes from the Altos wheel.

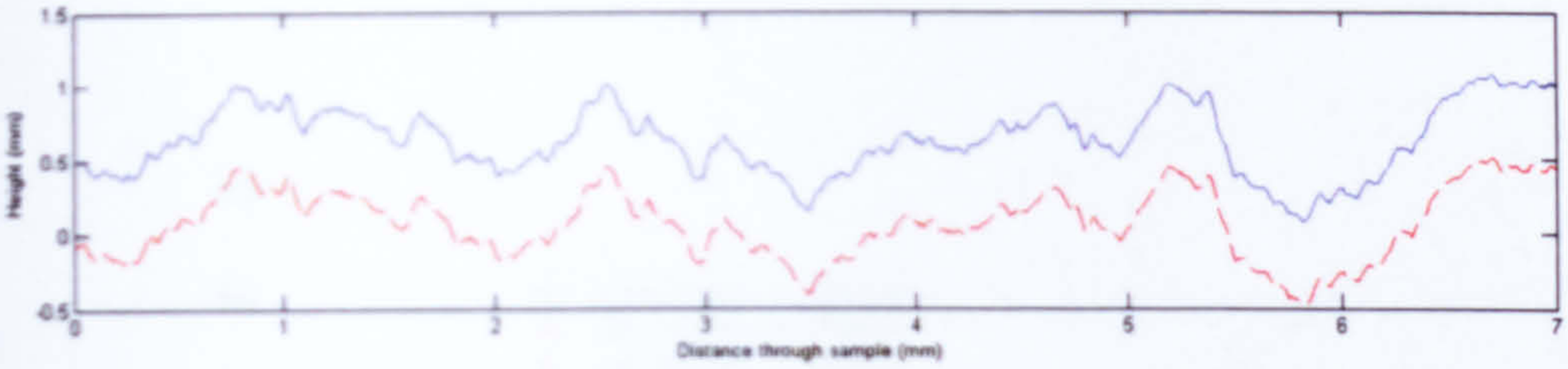

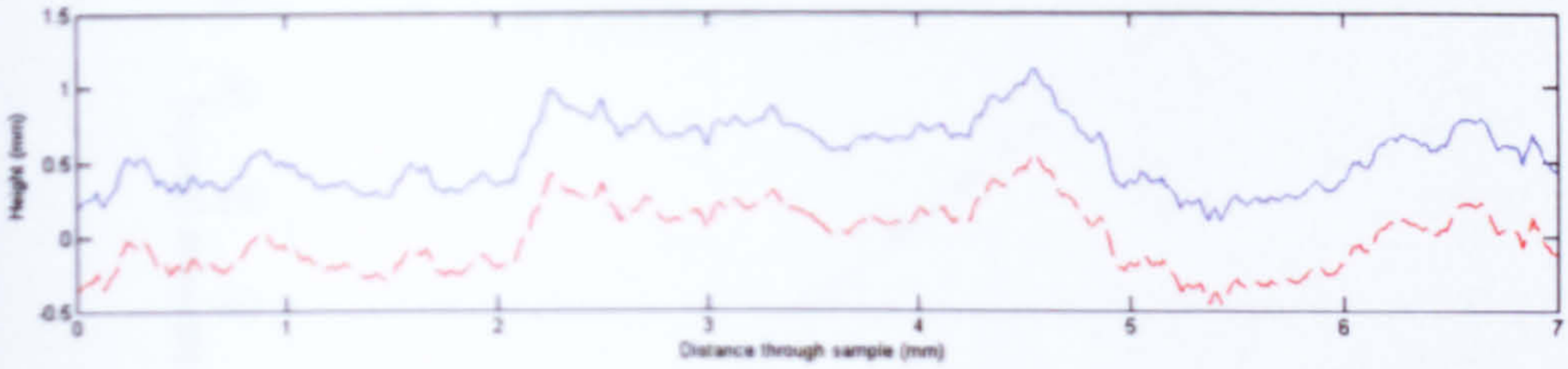

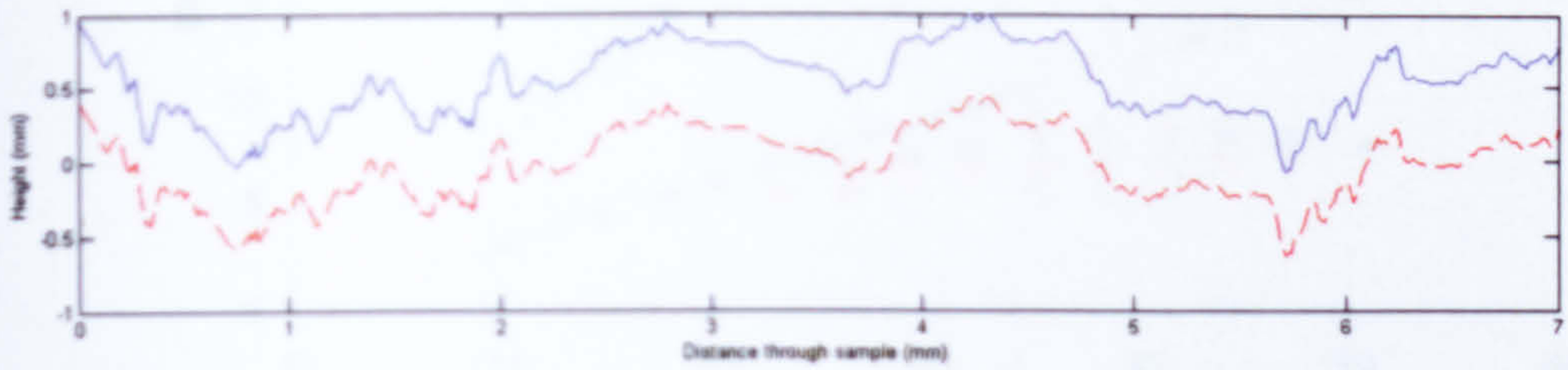

Example of 3 Matlab generated 2-D profiles through a sample taken from the Altos wheel. Red dashed line represents the raw data taken from the Uniscan output file. Blue line represents the adjusted data created for analysis purposes.

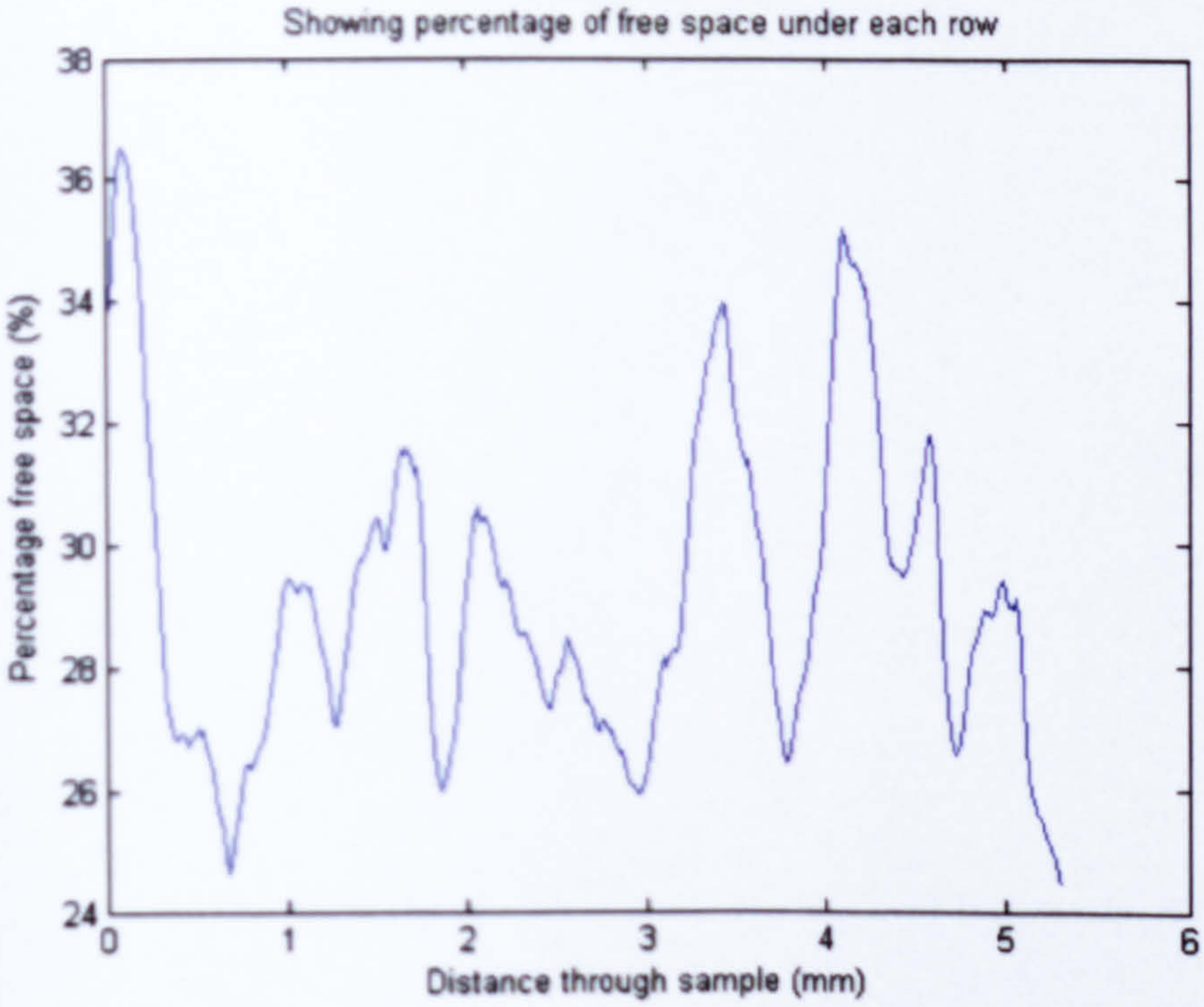

Example of analysis output from Matlab file showing the abstract term percentage free space at every 2-D slice through the sample.

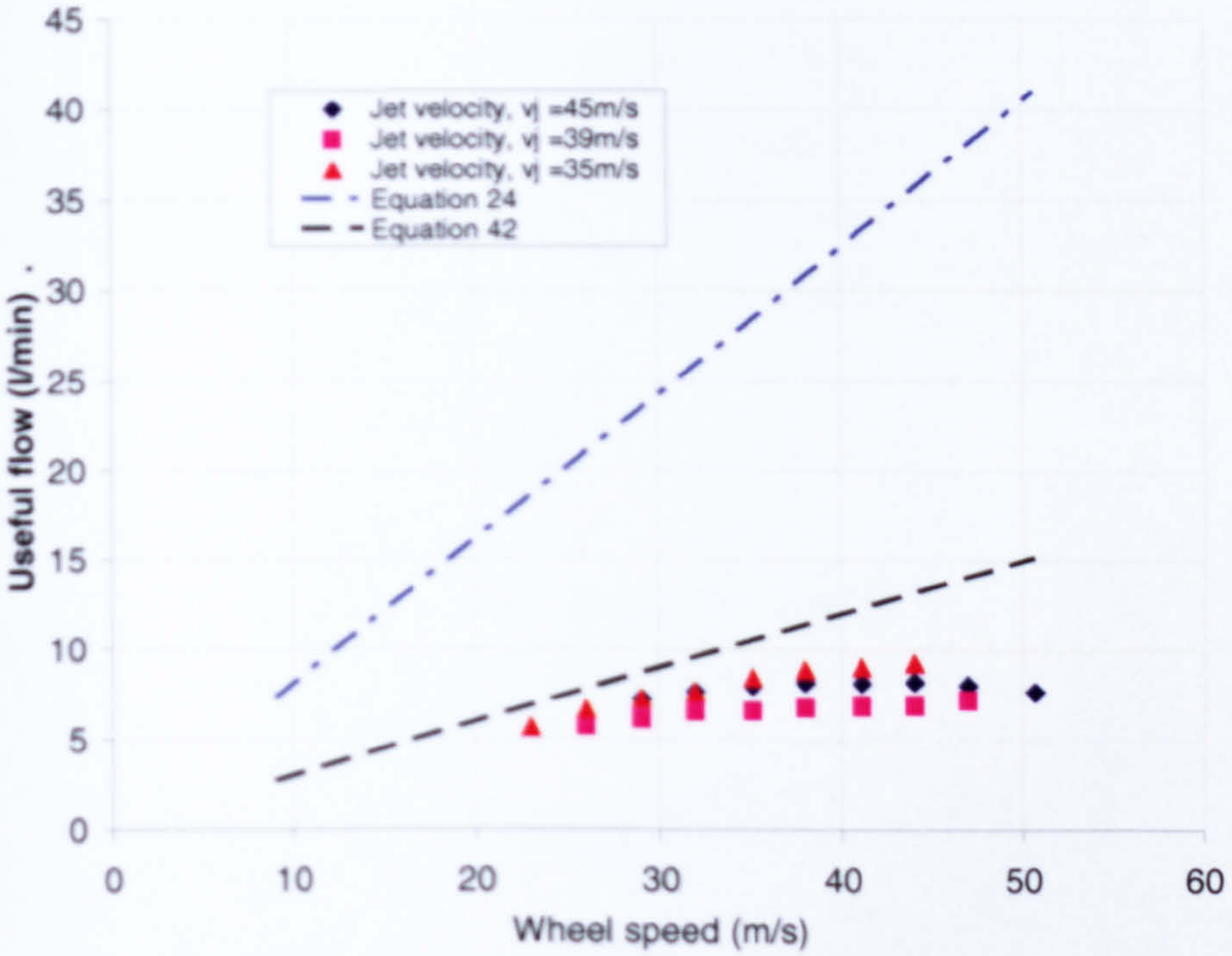

Results for Preliminary Test 3 showing percentage useful flow versus wheel speed for 3 fluid jet speeds; also showing equation (24) and equation Error! Reference source not found.**,** a**=25µm,** v_w**=2mm/s,** Q_d**=18.9l/min.**

Appendix B. Engineering Drawings

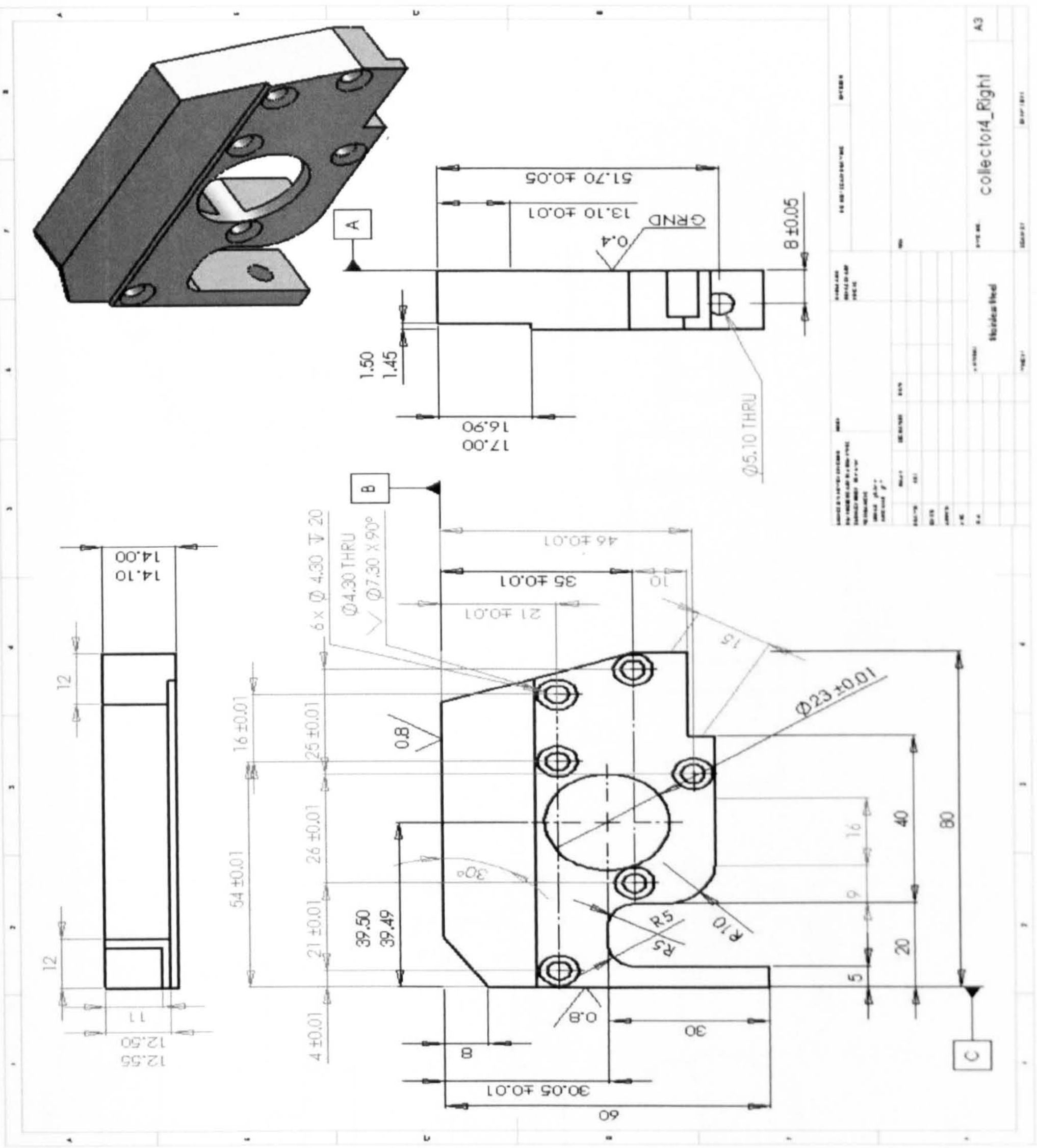

Engineering drawing of right half of Flow Director.

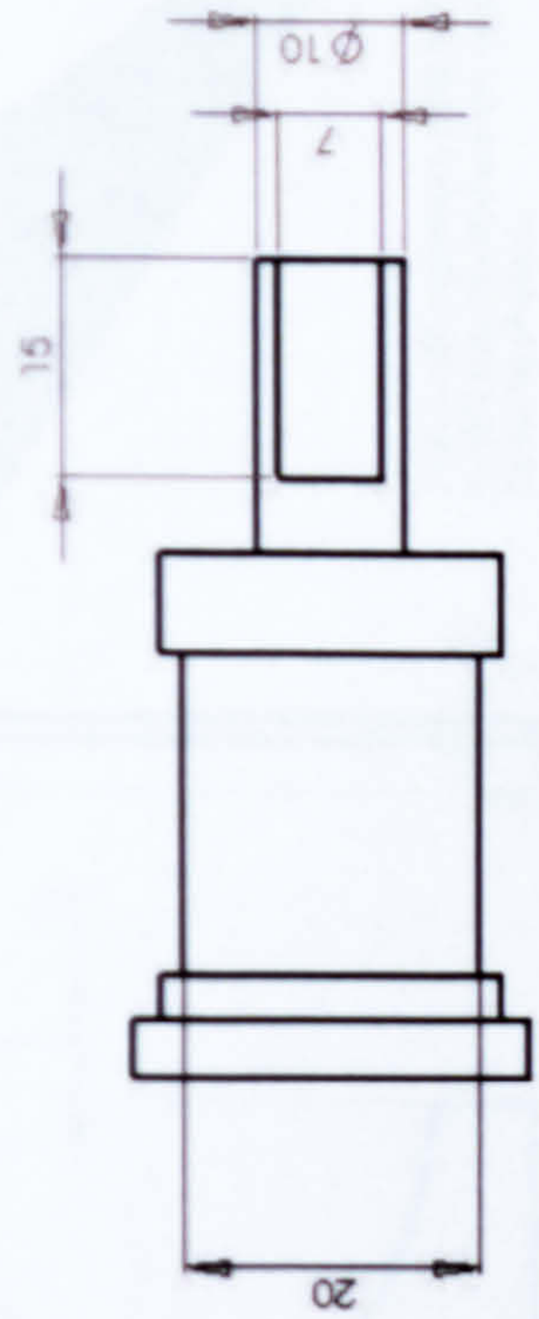

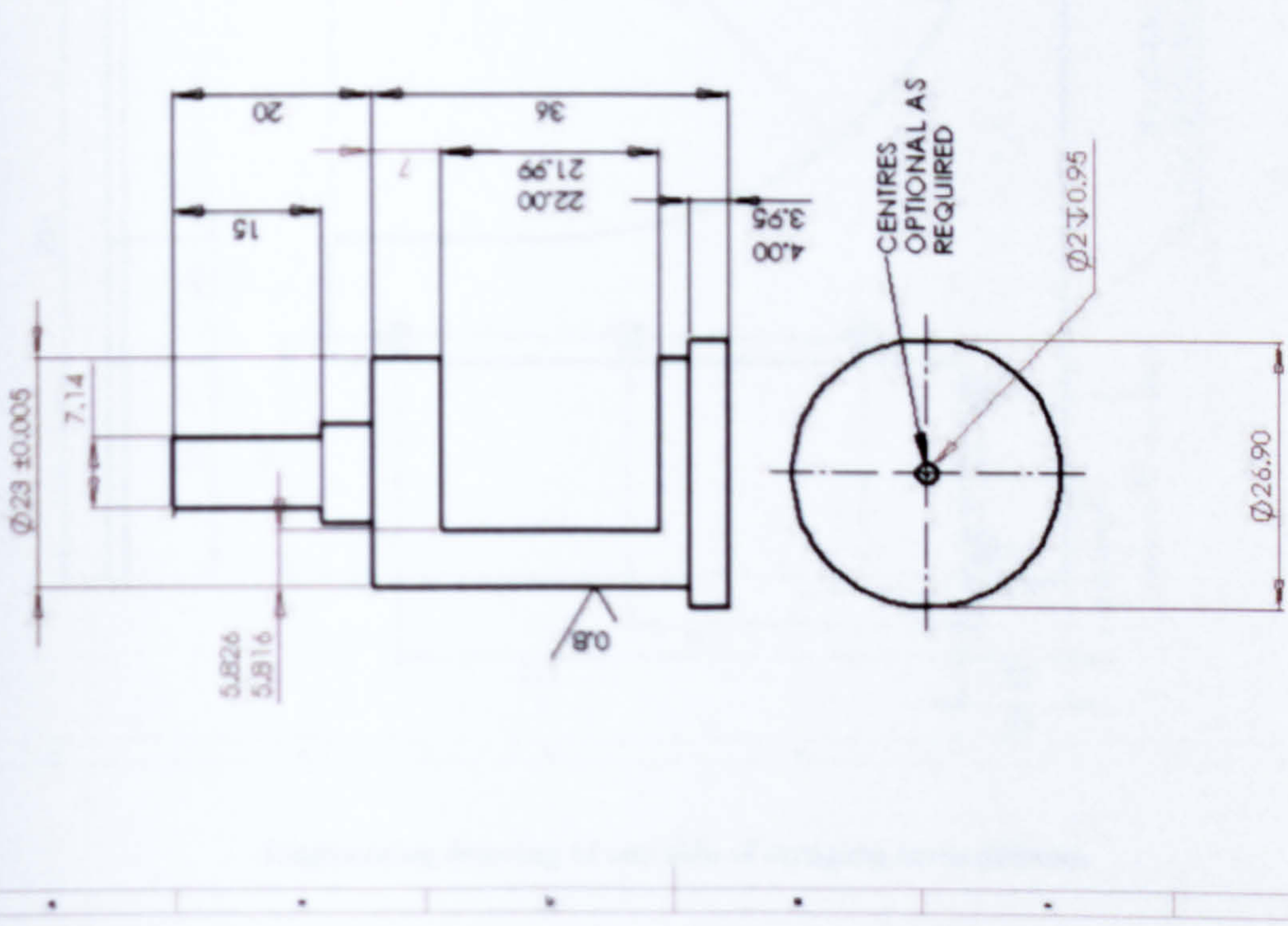

Engineering drawing of pivot valve of Flow Director.

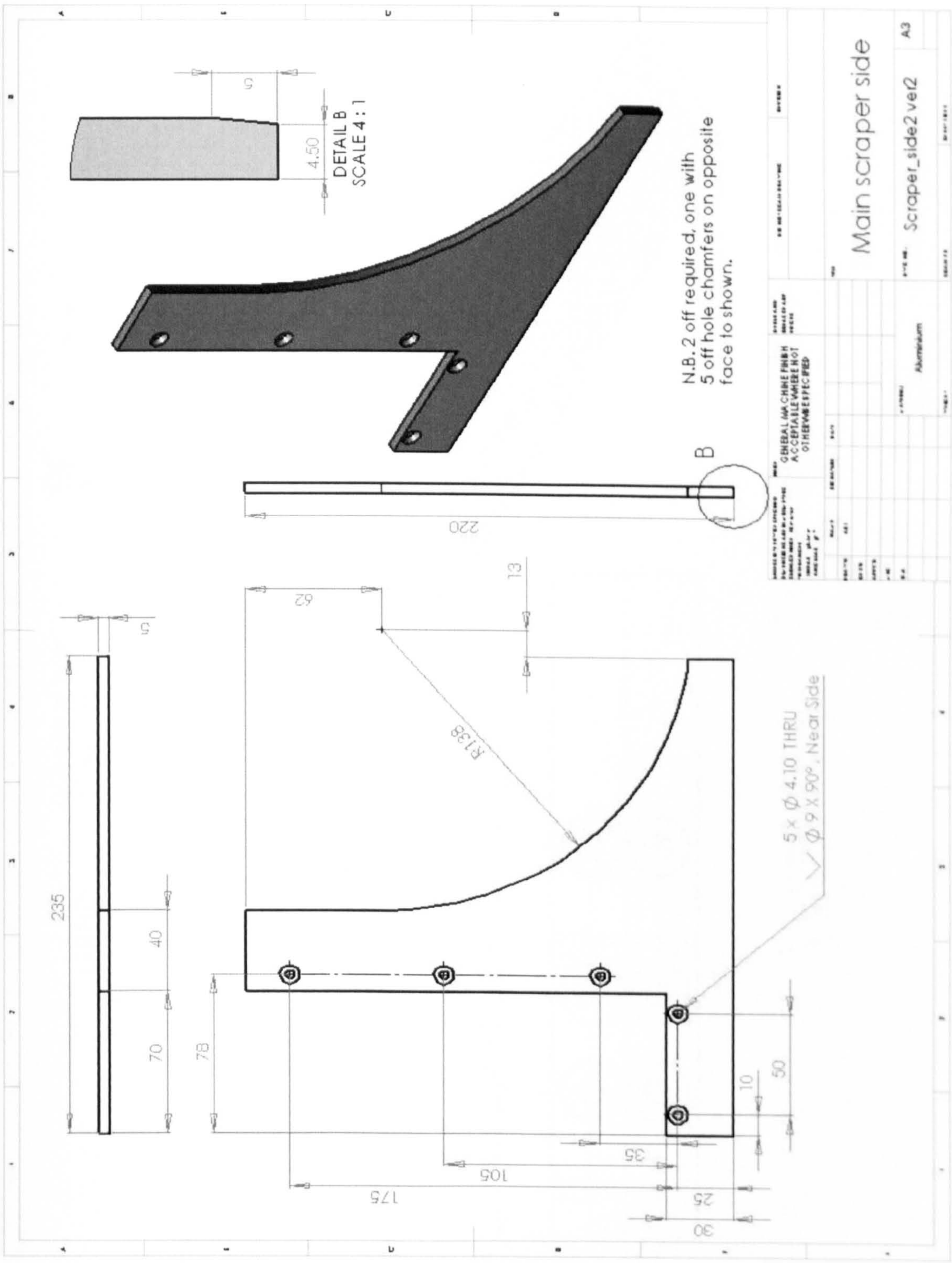

Engineering drawing of one side of scraping arrangement.

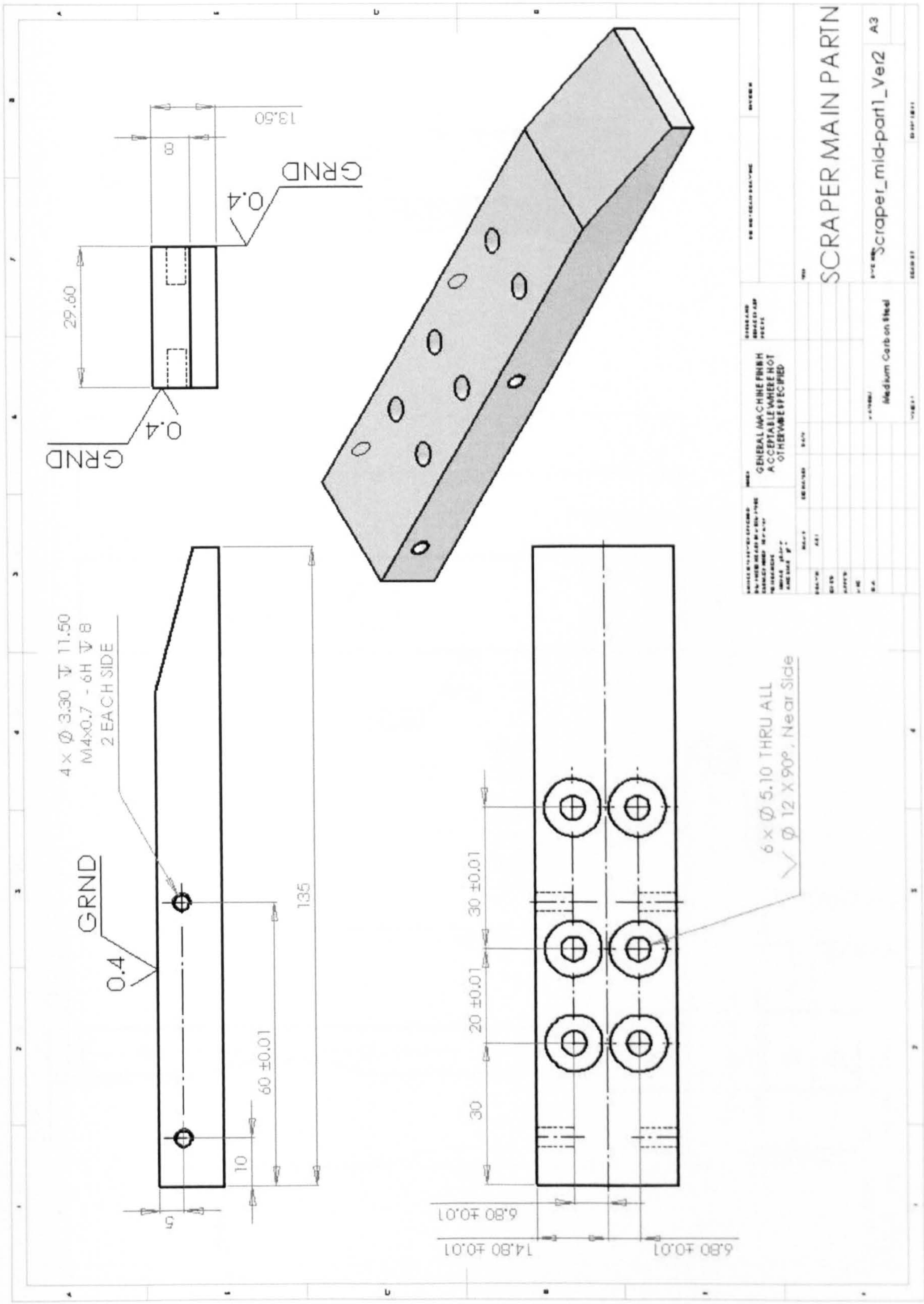

Engineering drawing of Body Section 1 of scraping arrangement.

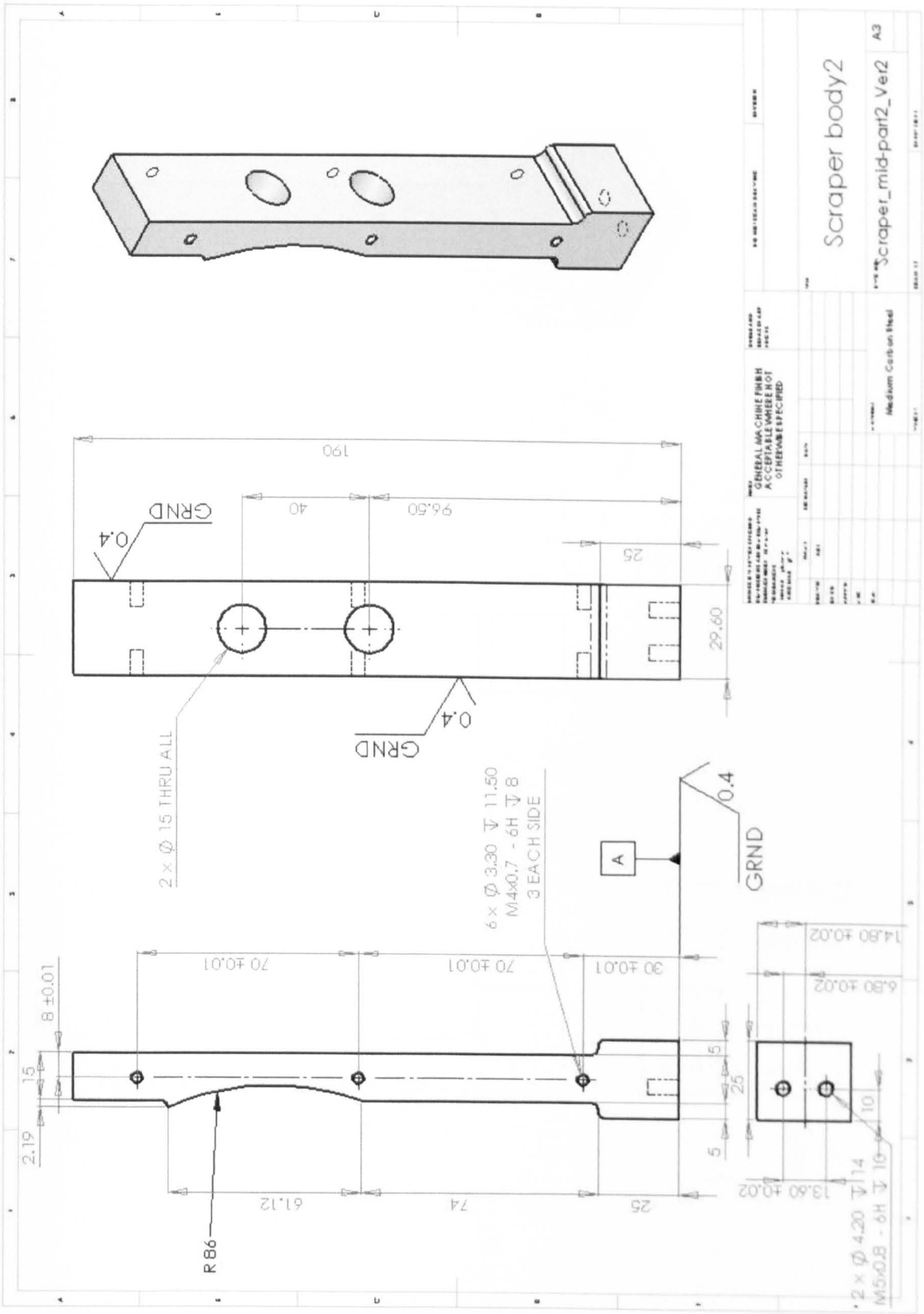

Engineering drawing of Body Section 2 of scraping arrangement.

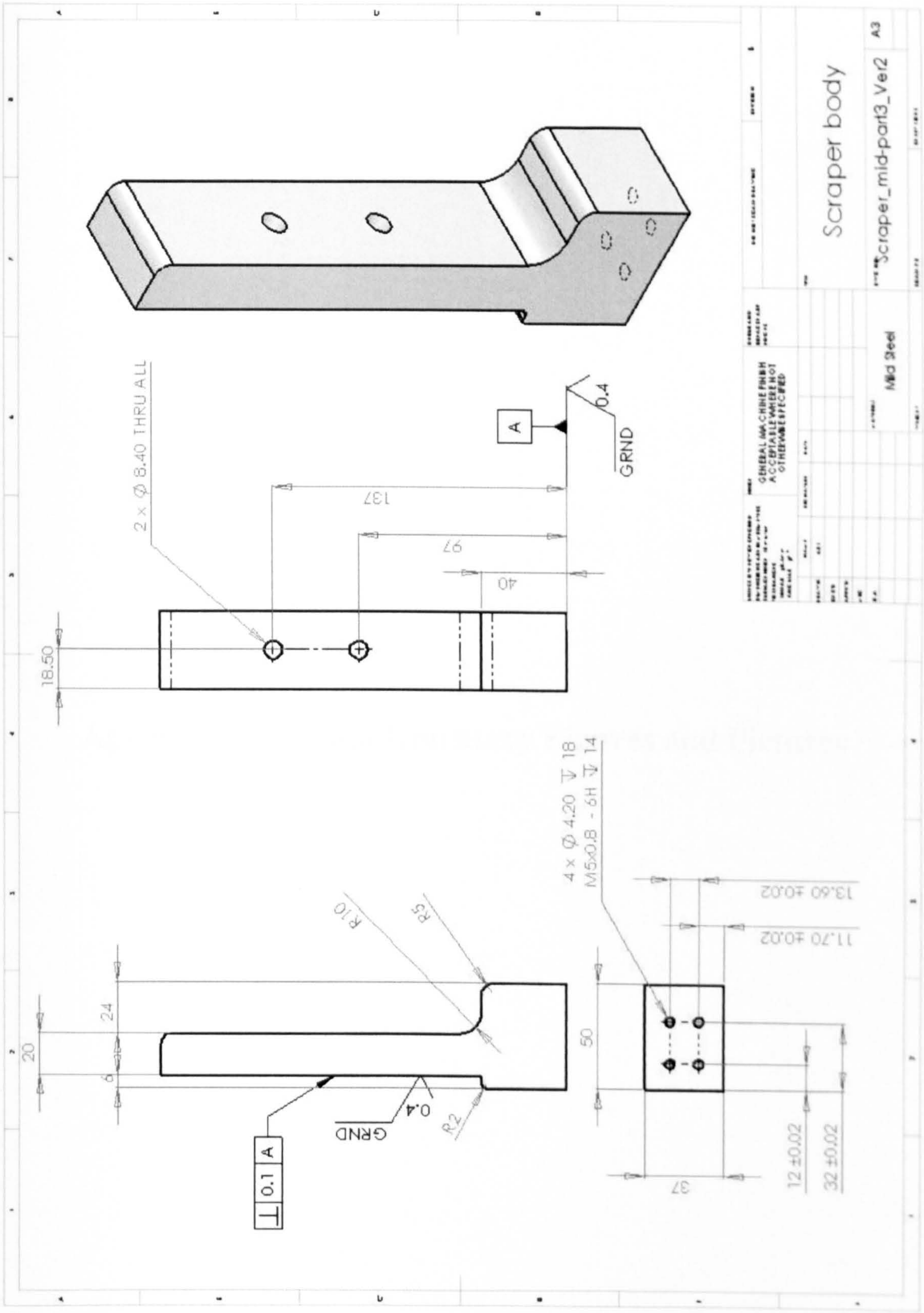

Engineering drawing of Body Section 3 of scraping arrangement.

Appendix C. Supplementary Figures and Pictures

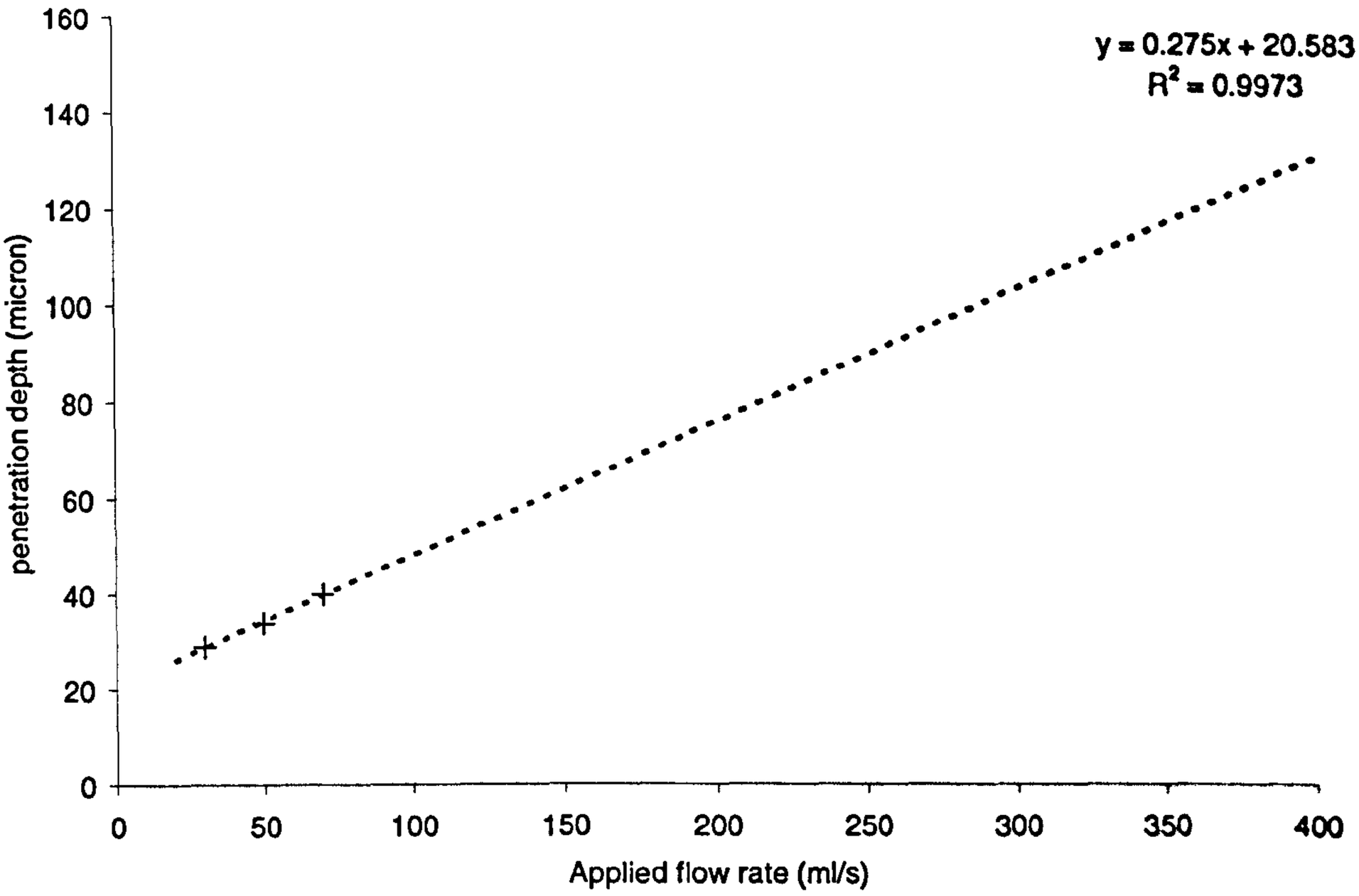

Penetration depth against applied flowrate from the work of Chang (1994)

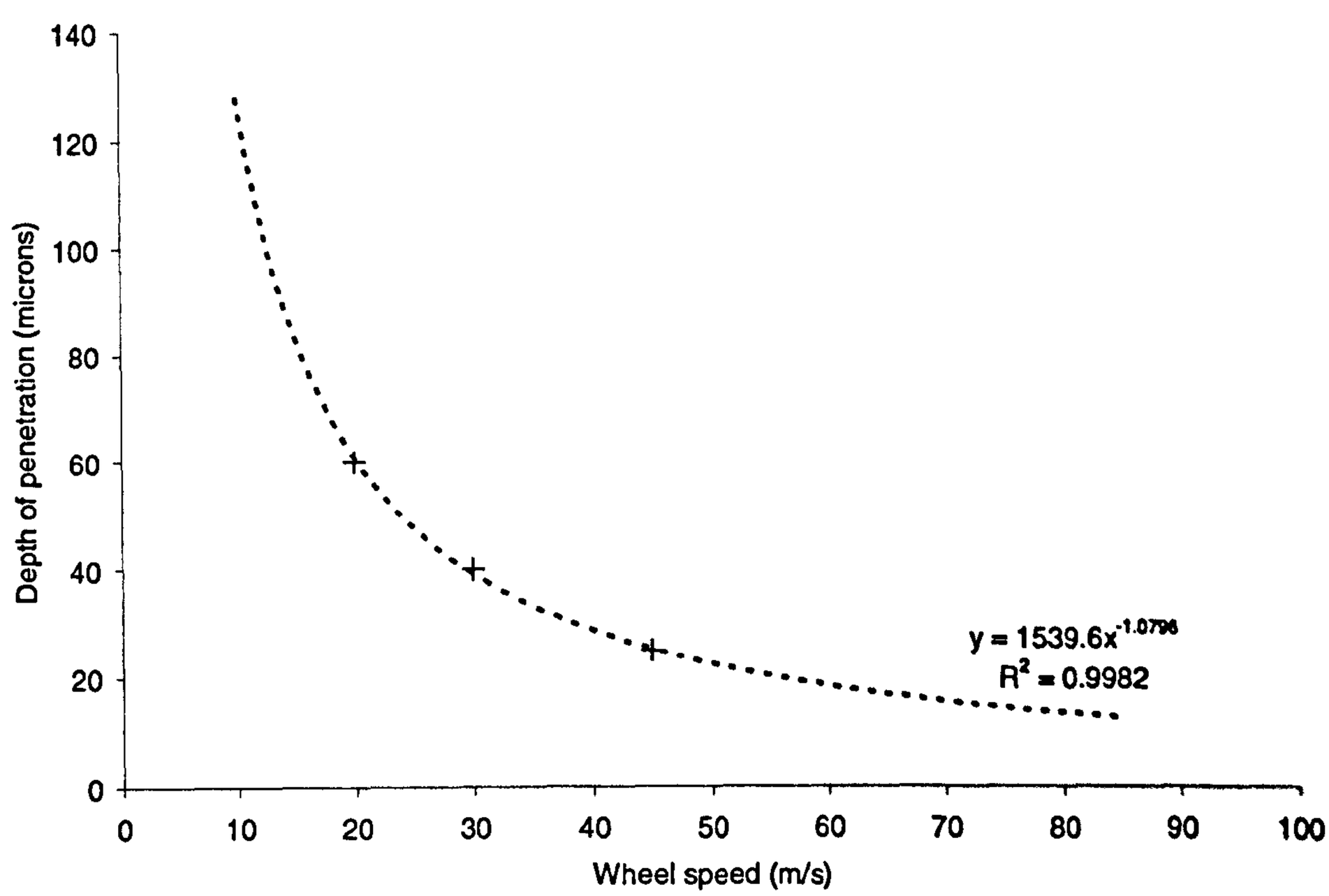

Penetration depth against wheel speed from the work of Chang (1994)

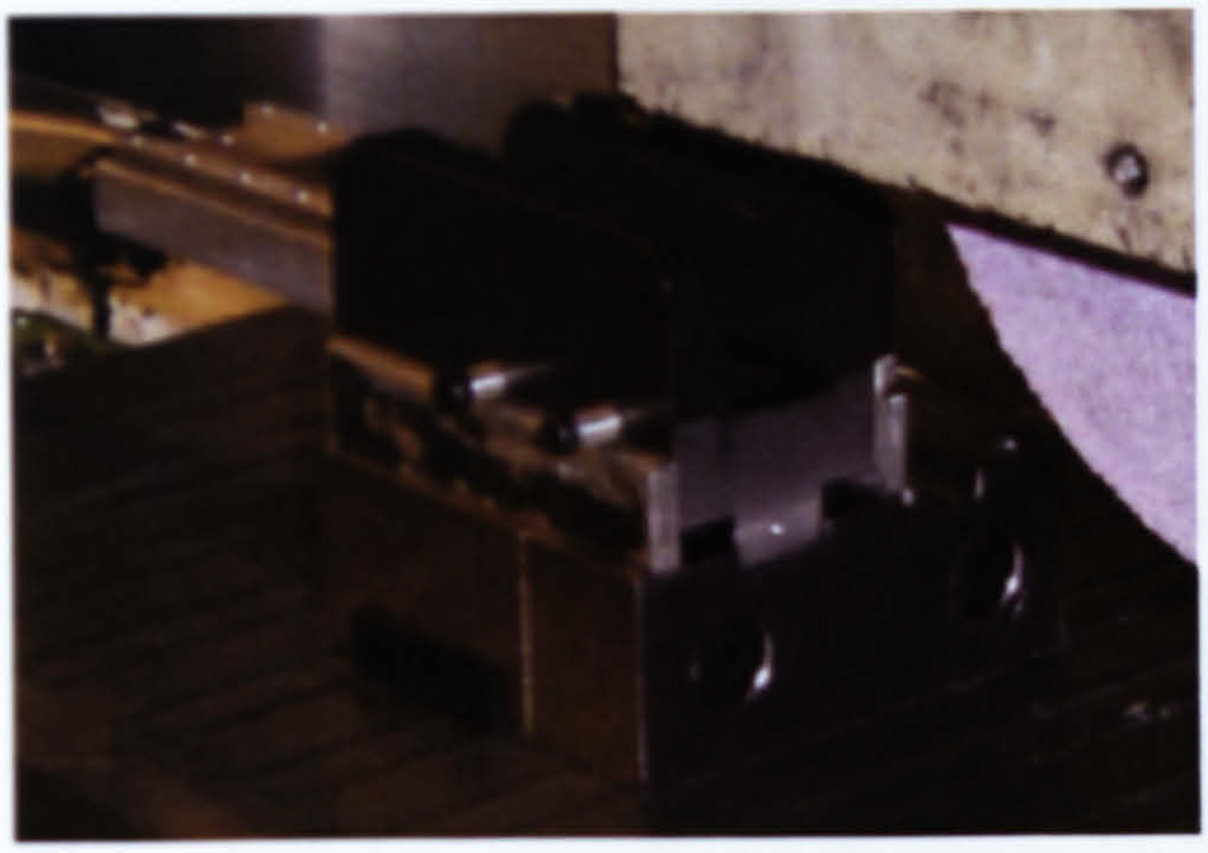

1st generation useful flow collector

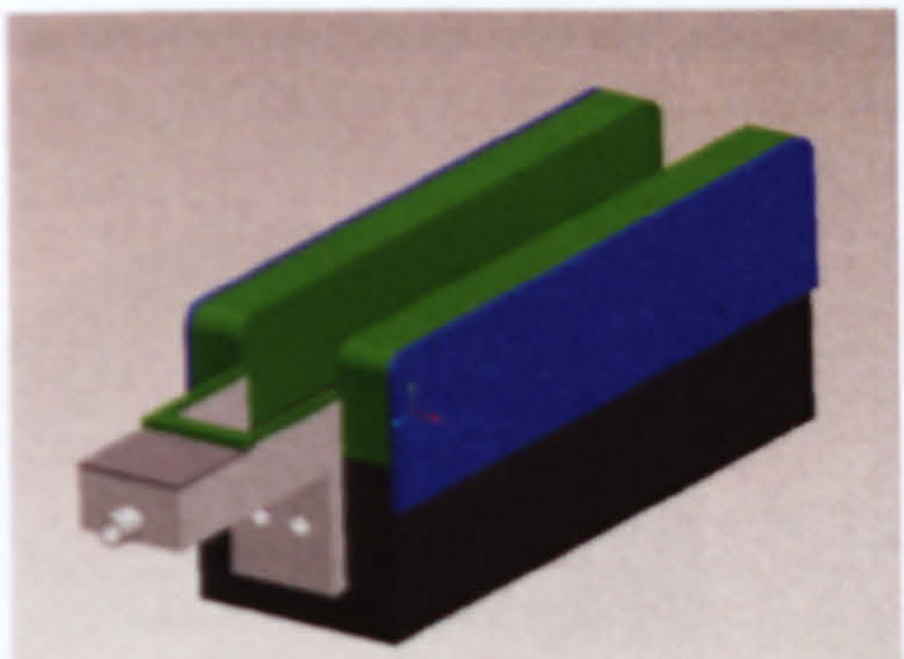

CAD drawing of second generation workpiece and side scraping system

CAD drawing of second generation post-contact zone scraping system

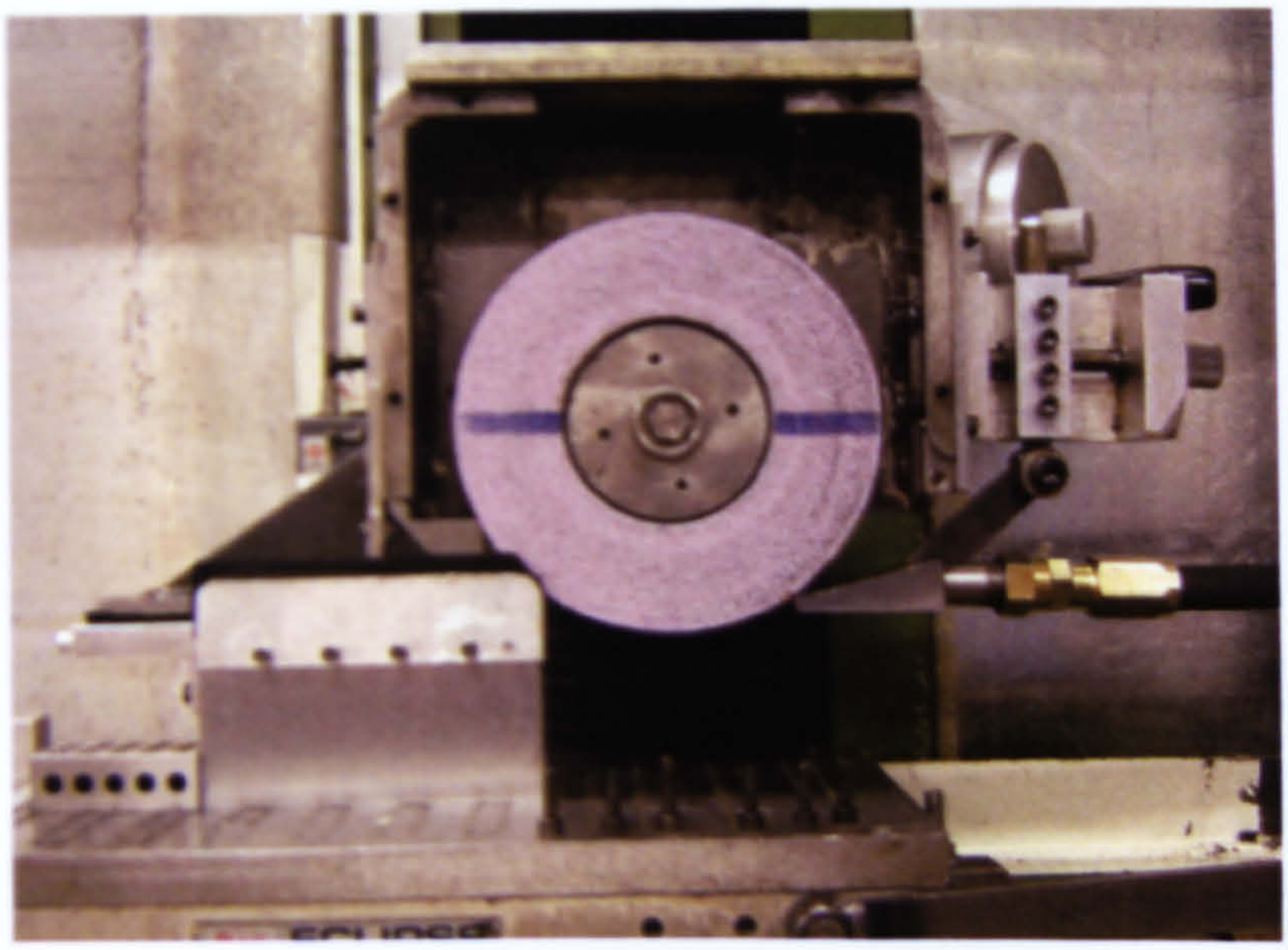

Second generation system on Abwood grinding machine

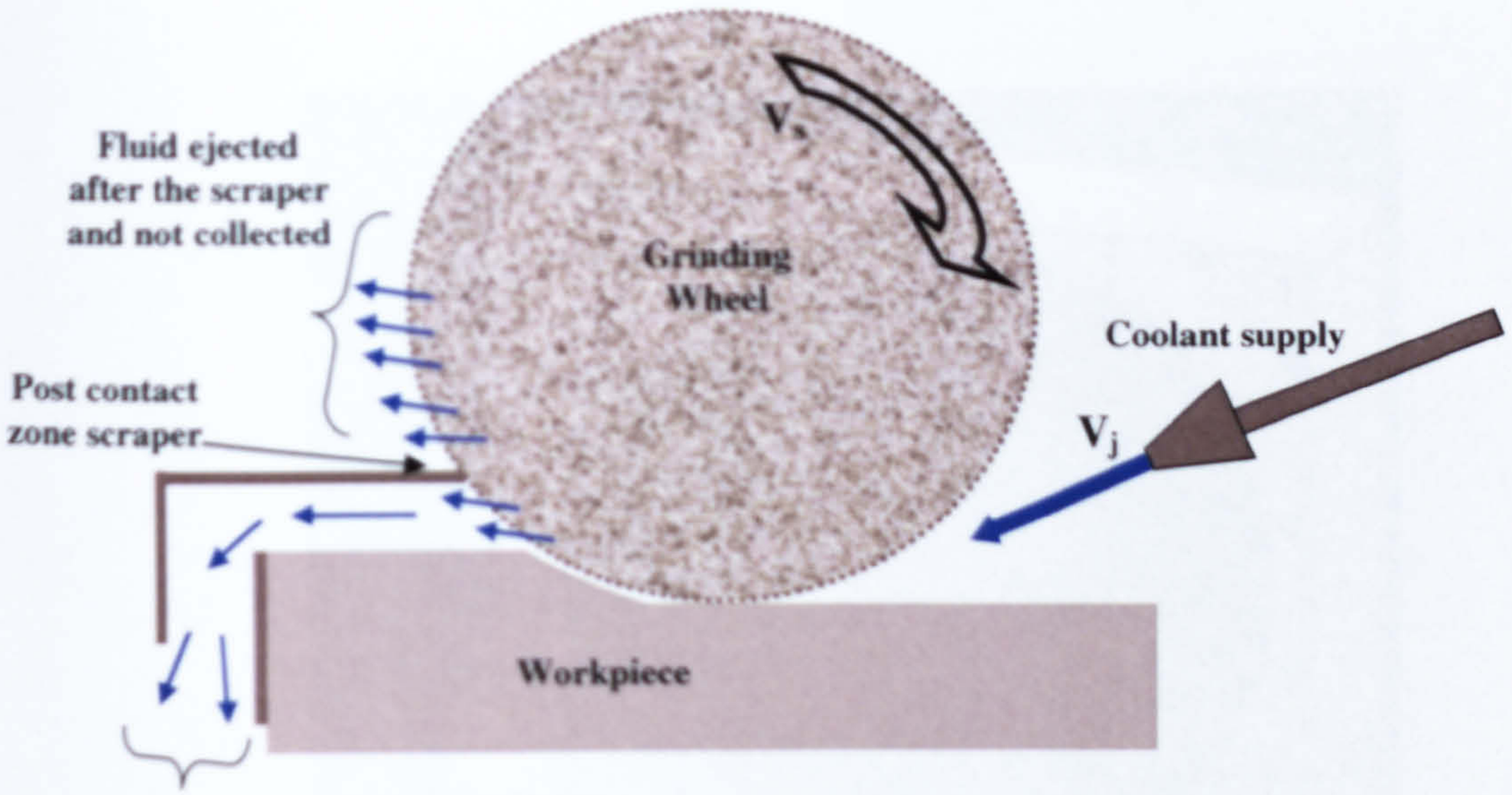

Surface grinding schematic showing fluid ejection from the wheel

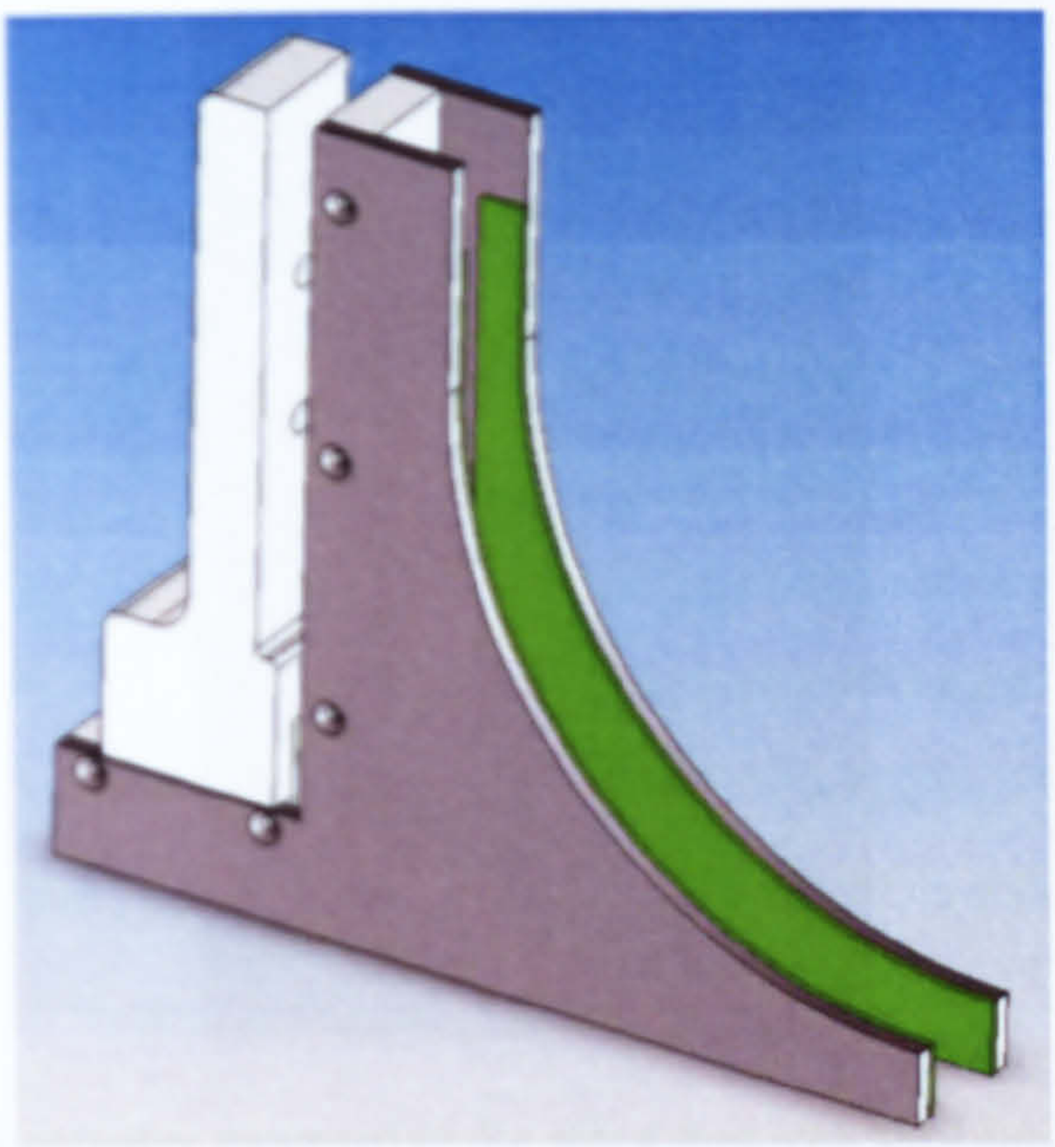

Flow isolation system, showing Aluminium side scrapers in grey, steel infrastructure in white and contact foam in green.

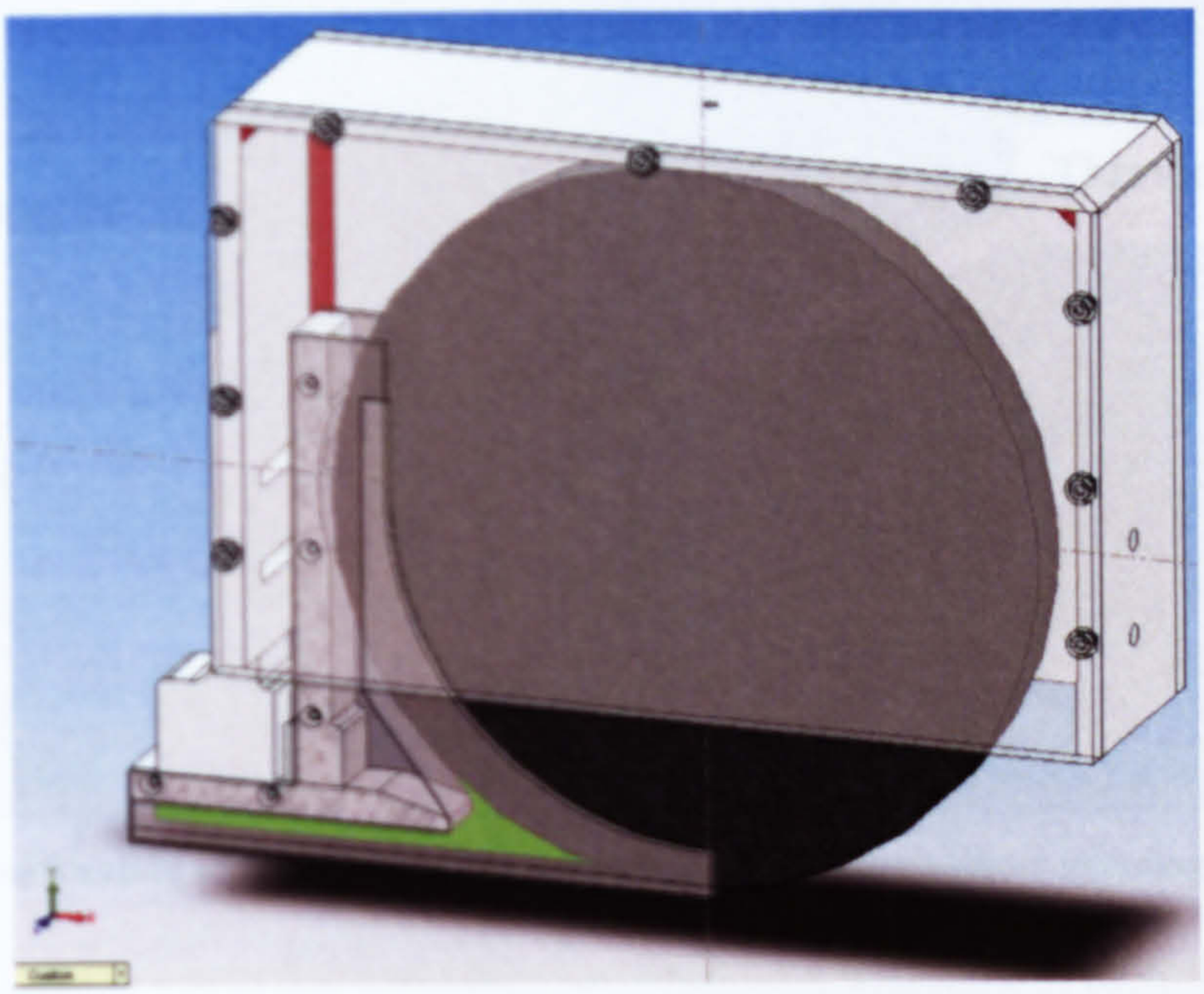

Picture showing flow isolation system (with a transparent front wall) when attached to the Dominator wheel guard.

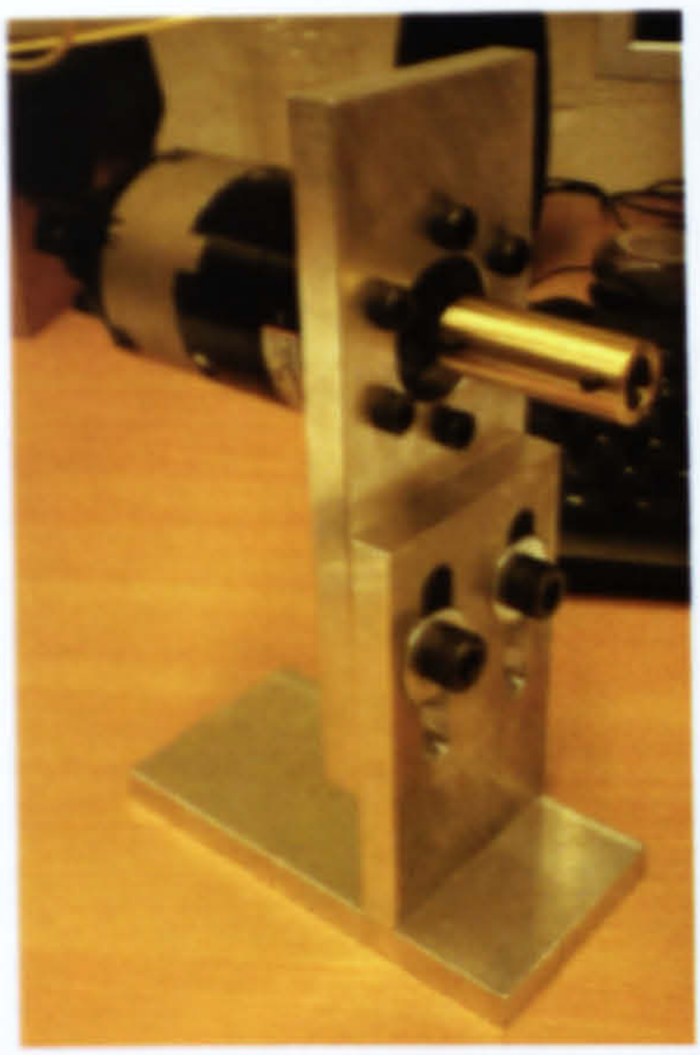

SMC Rotary actuator mounted to the stand and with the coupling attached.

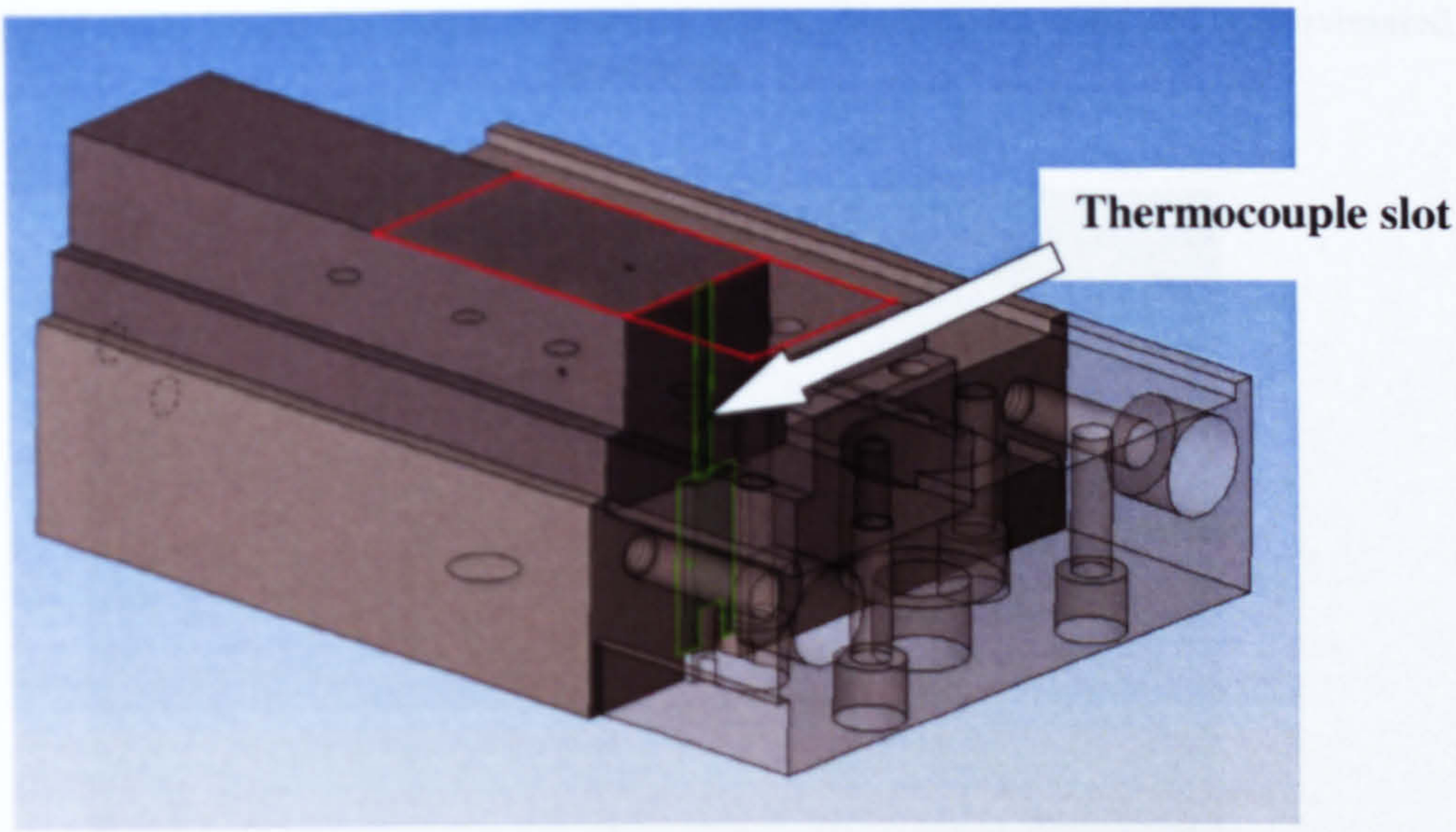

Workpiece showing location of thermocouple slot in green, the red area shows grinding face of workpiece.

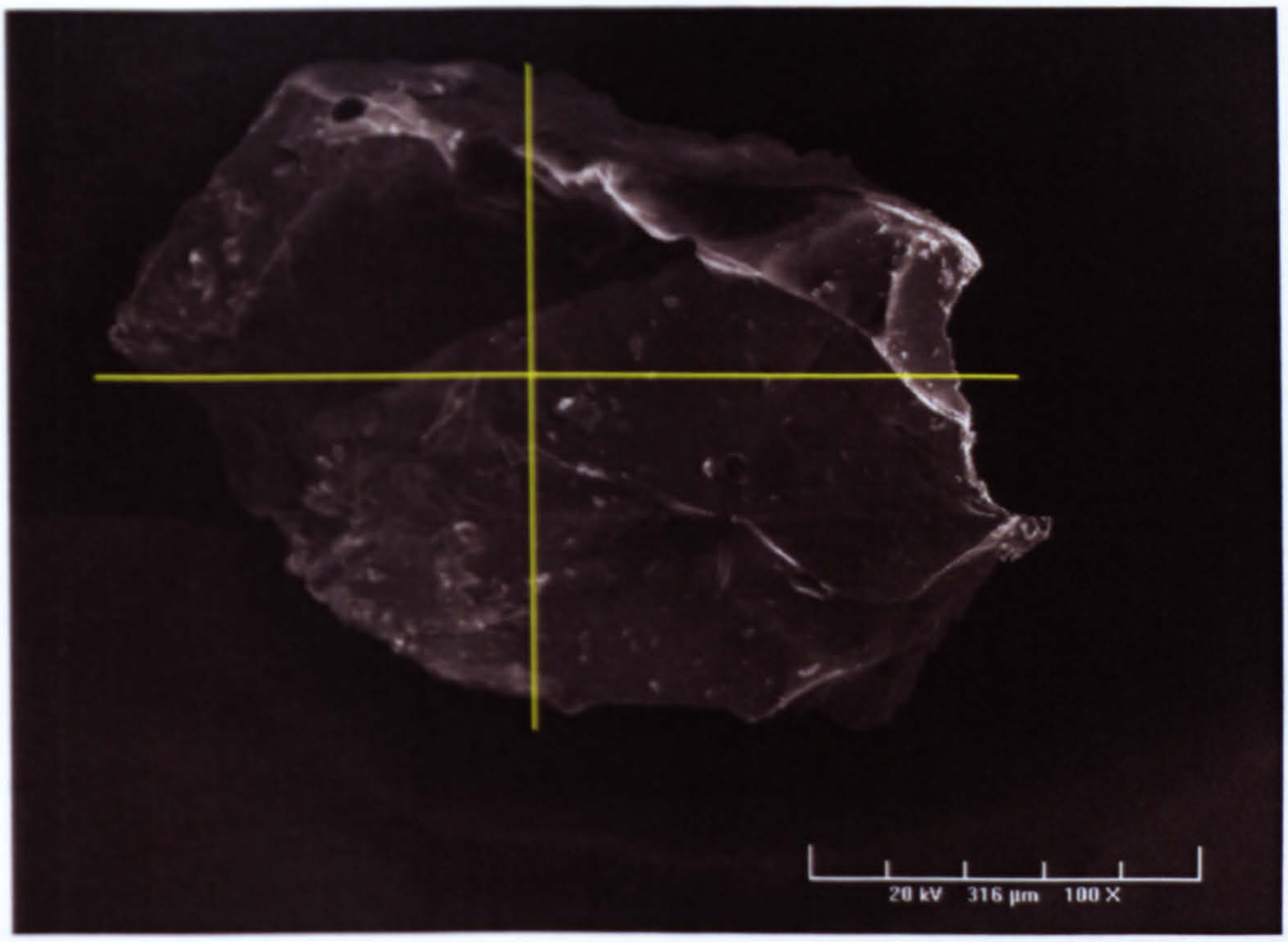

SEM image of grain 1 from the Universal grinding wheel, also showing scale and approximated dimensions.

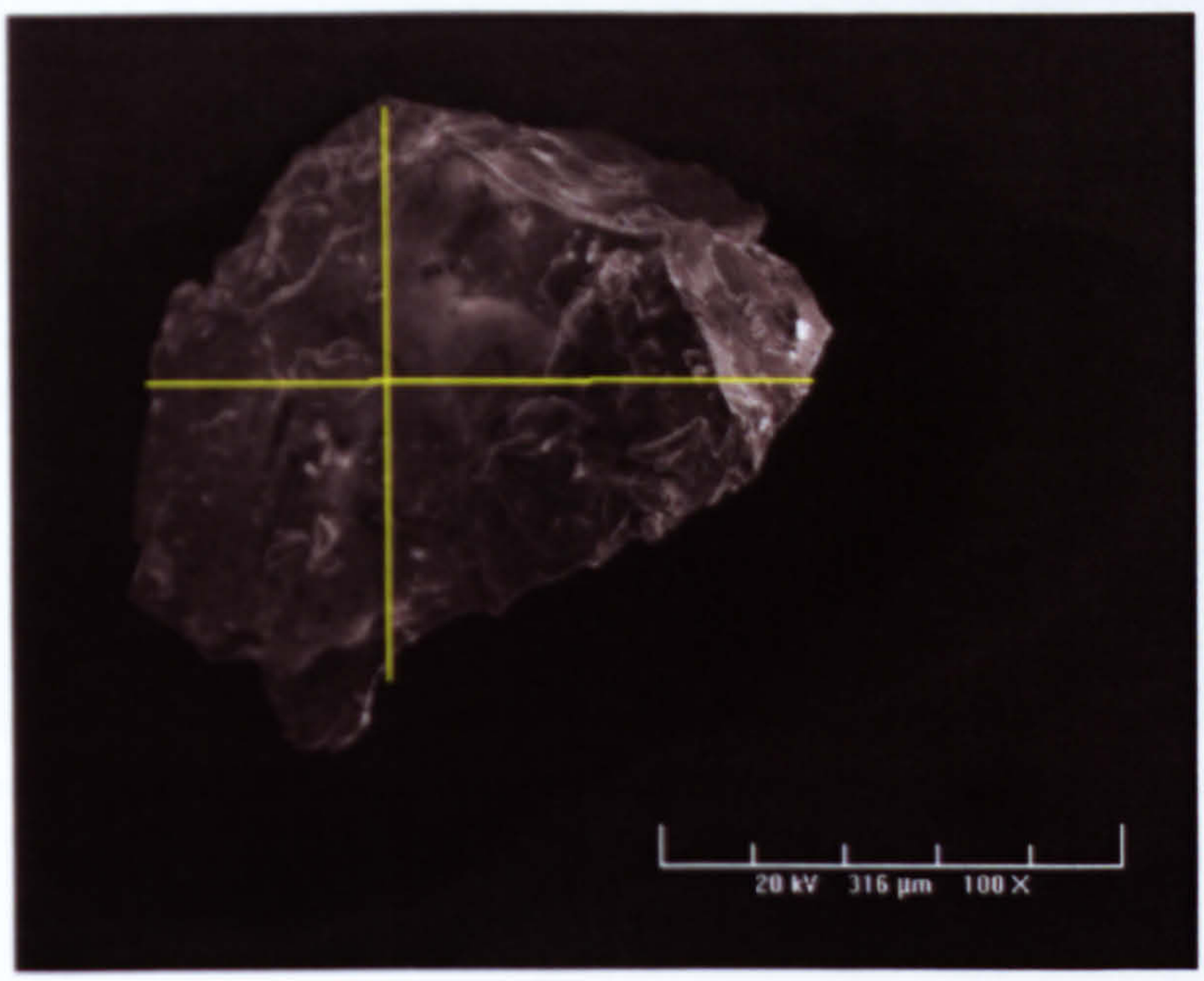

SEM image of grain 2 from the Universal grinding wheel, also showing scale and approximated dimensions.

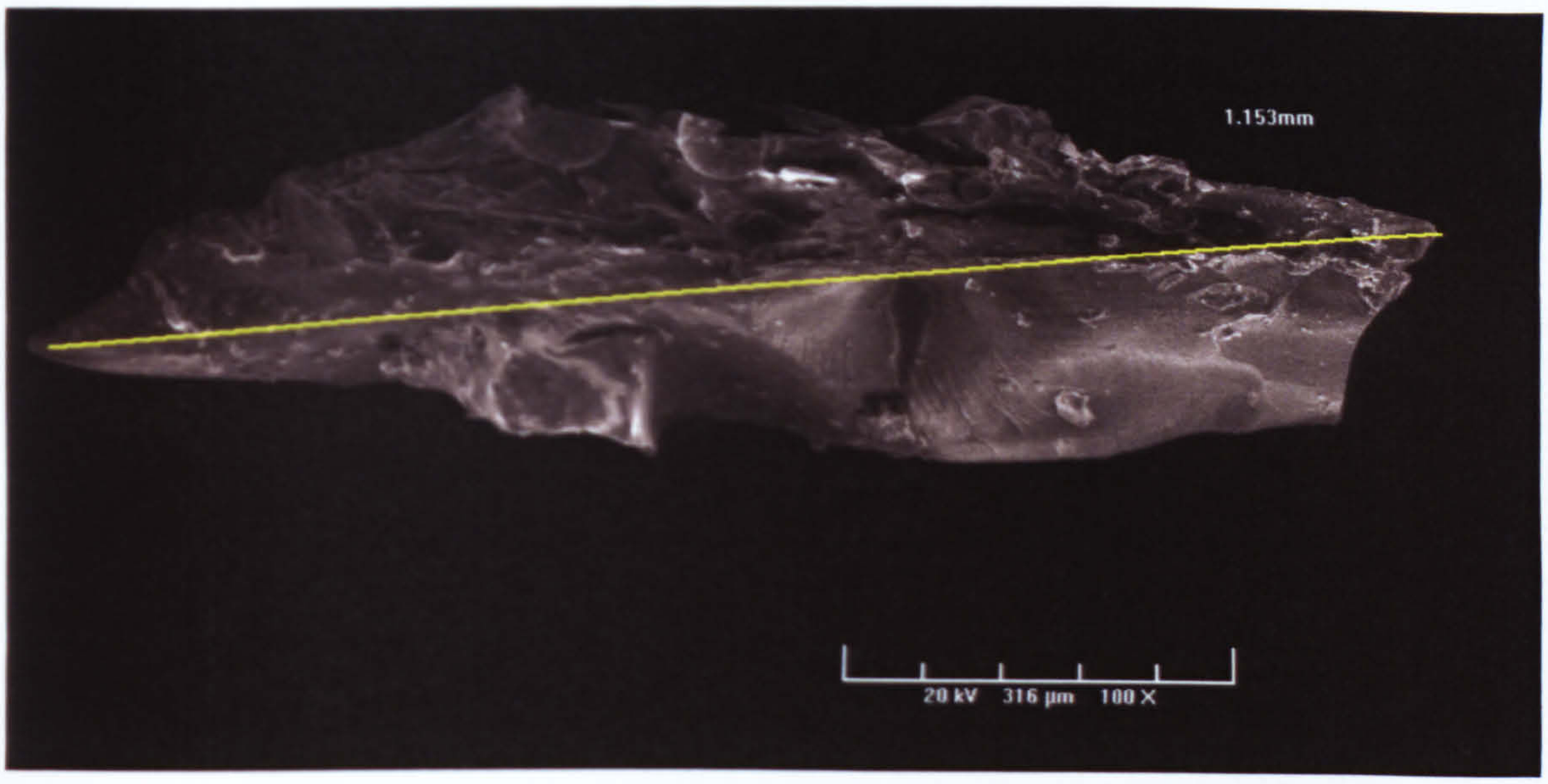

SEM image of grain 1 from the Altos grinding wheel, also showing scale and approximated dimensions.

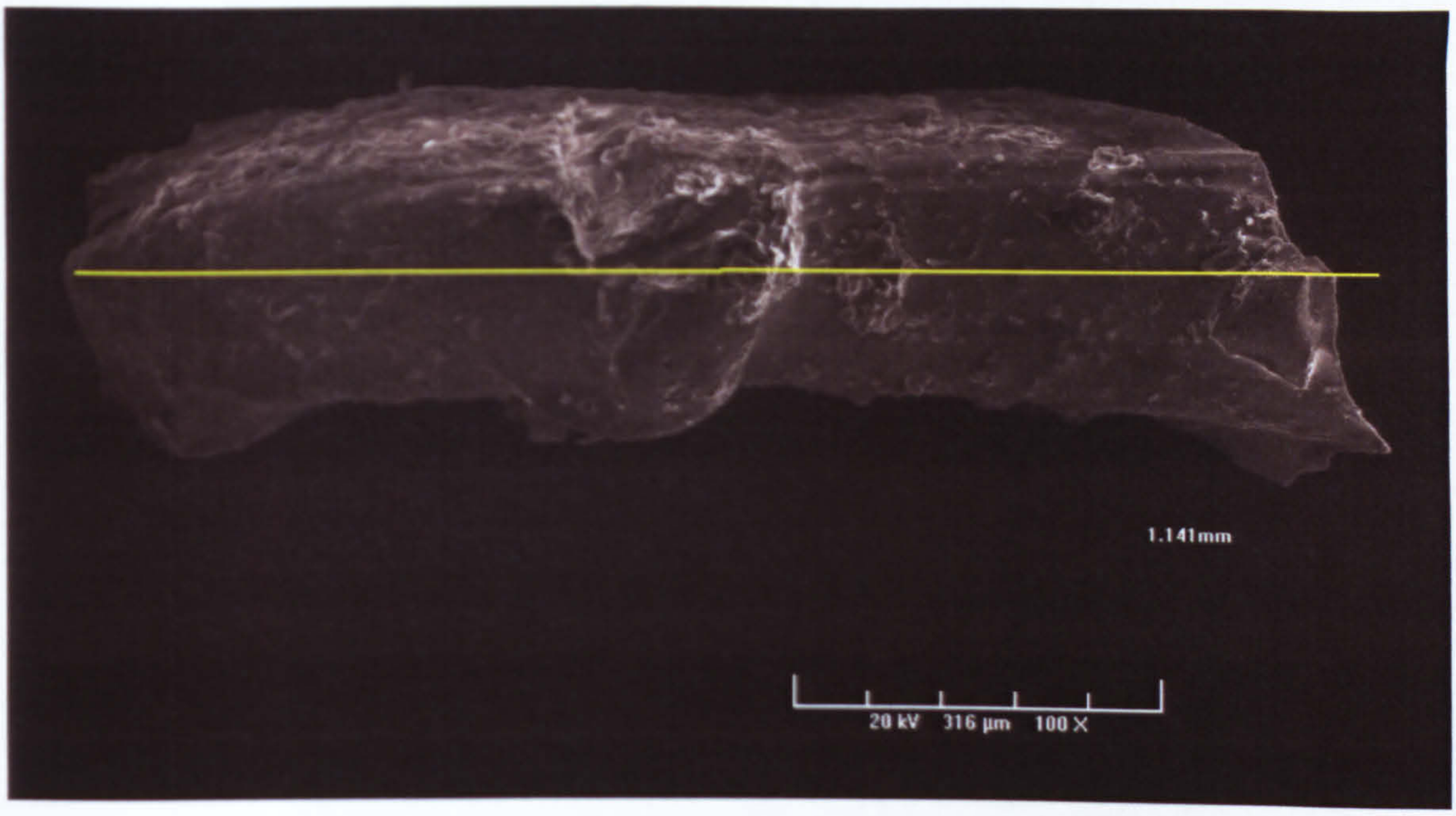

SEM image of grain 2 from the Altos grinding wheel, also showing scale and approximated dimensions.

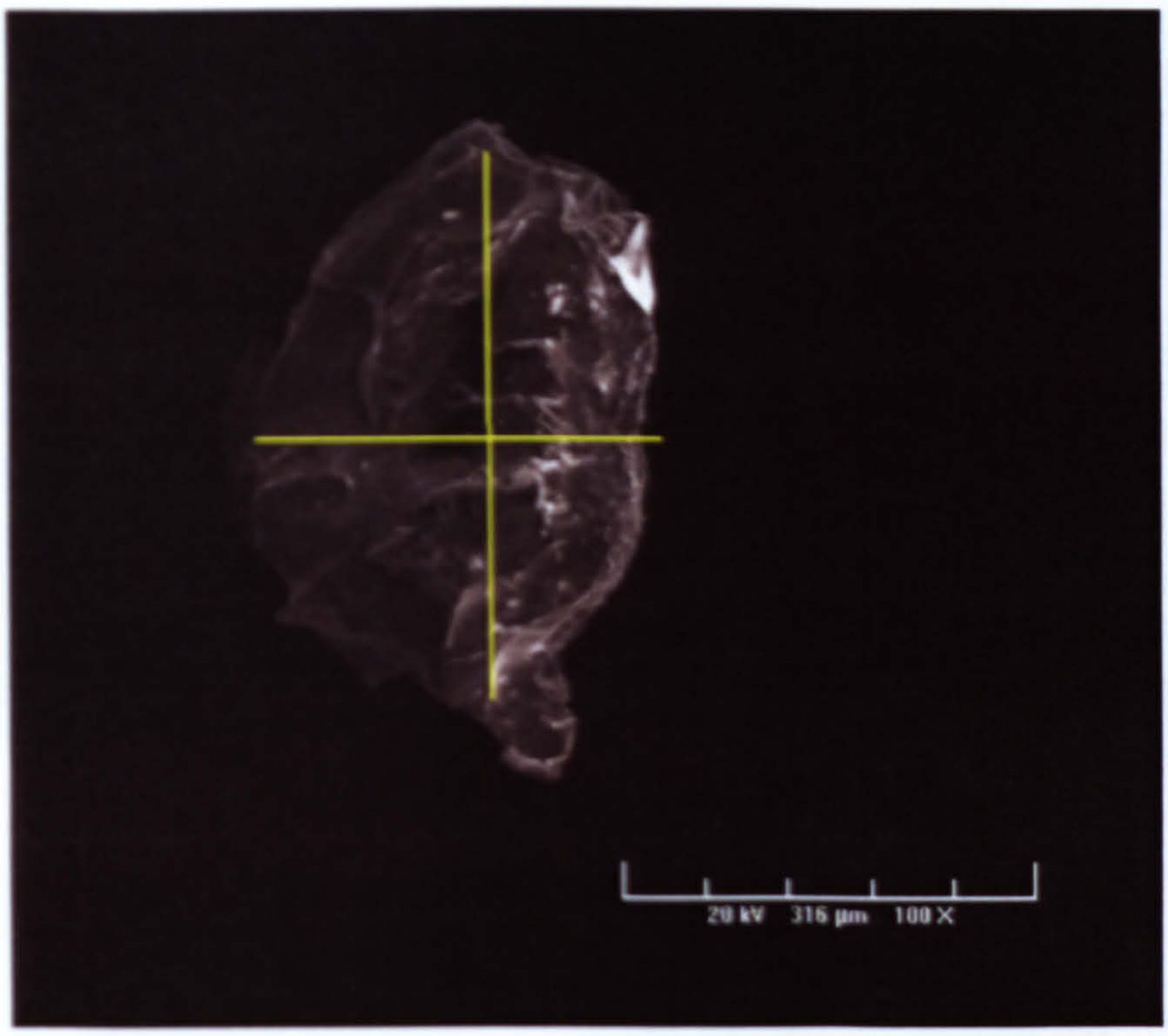

SEM image of grain 1 from the Flexovit grinding wheel, also showing scale.

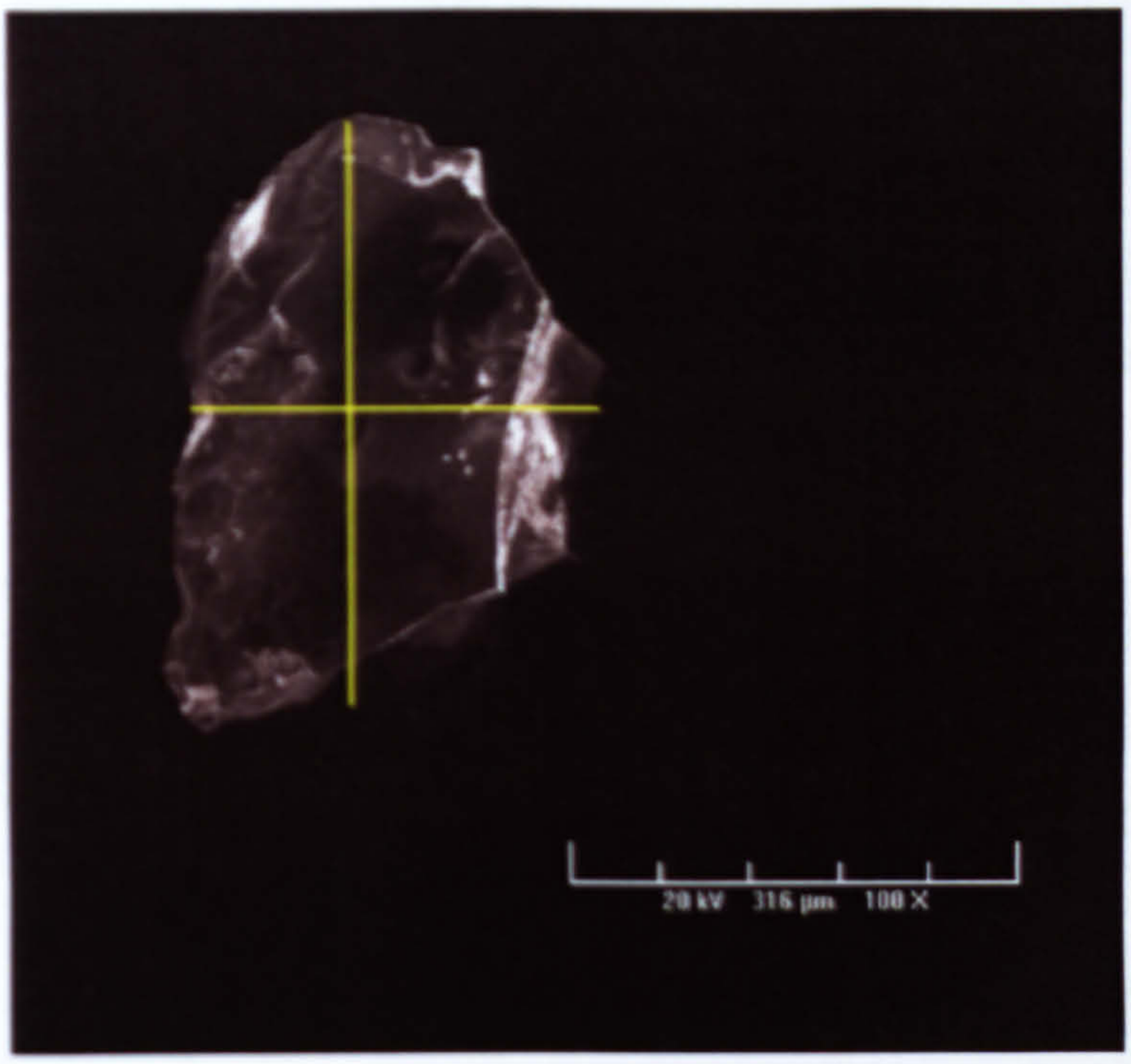

SEM image of grain 2 from the Flexovit grinding wheel, also showing scale.

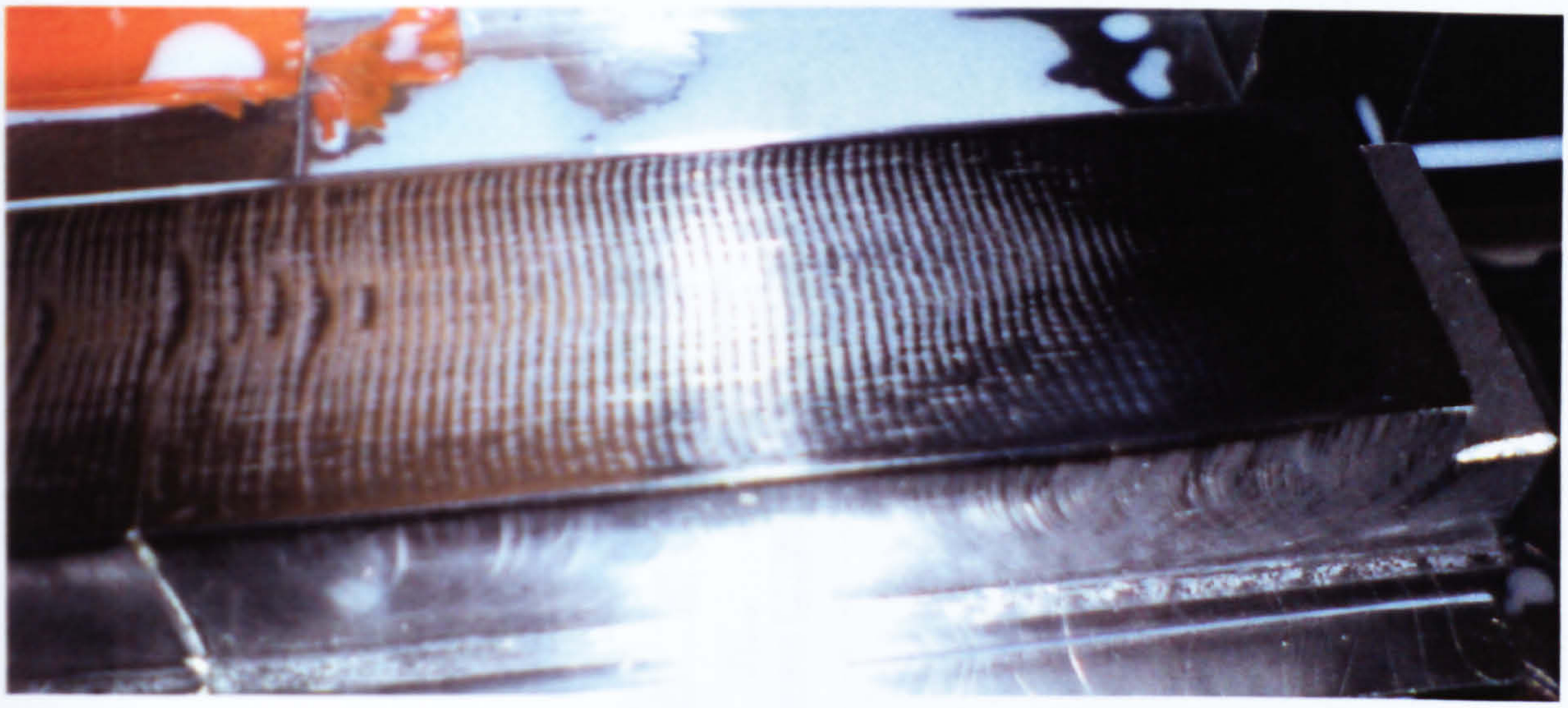

Burn of O1 workpiece during Taguchi tests.

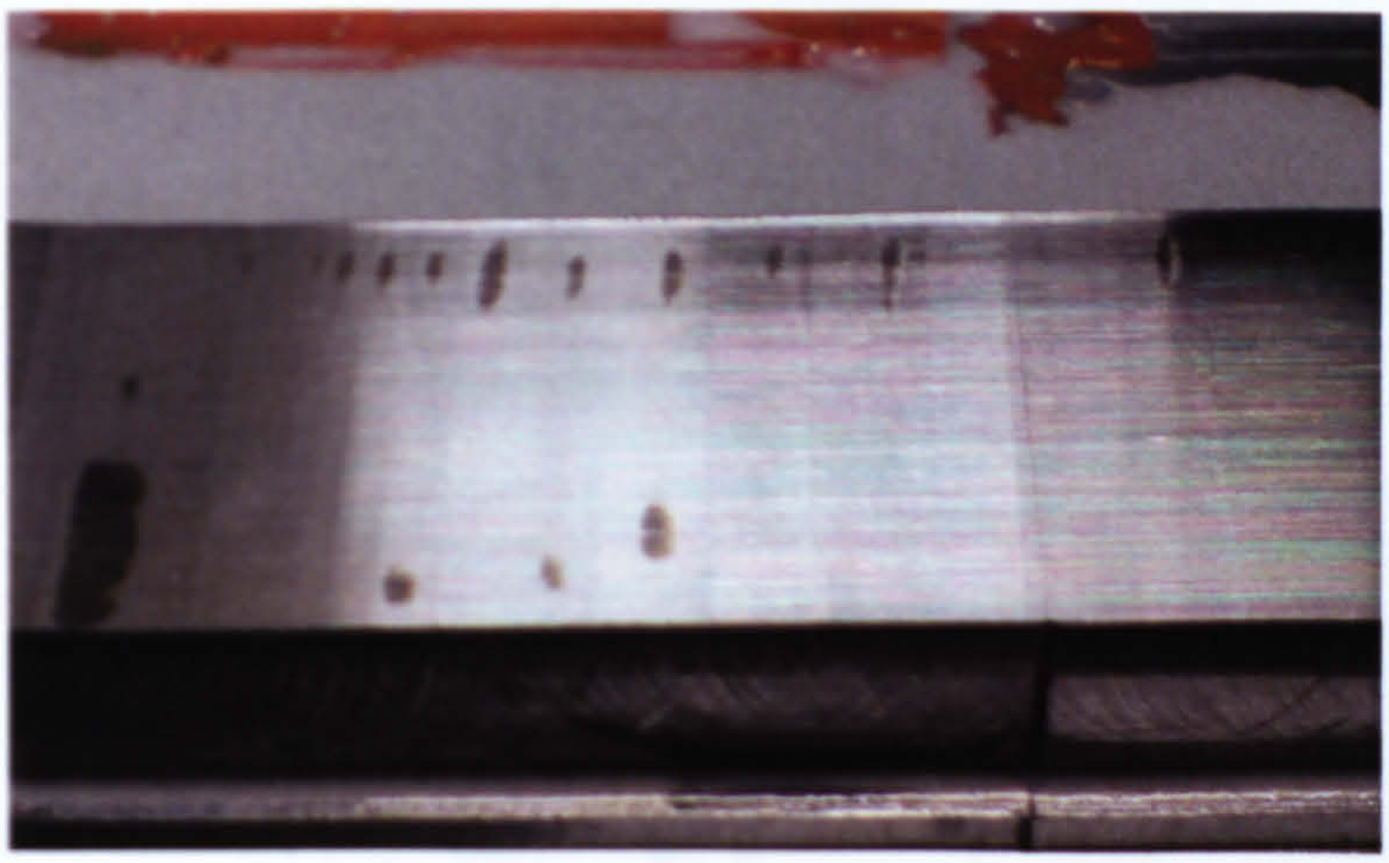

Slight burn of mild steel workpiece during Taguchi test

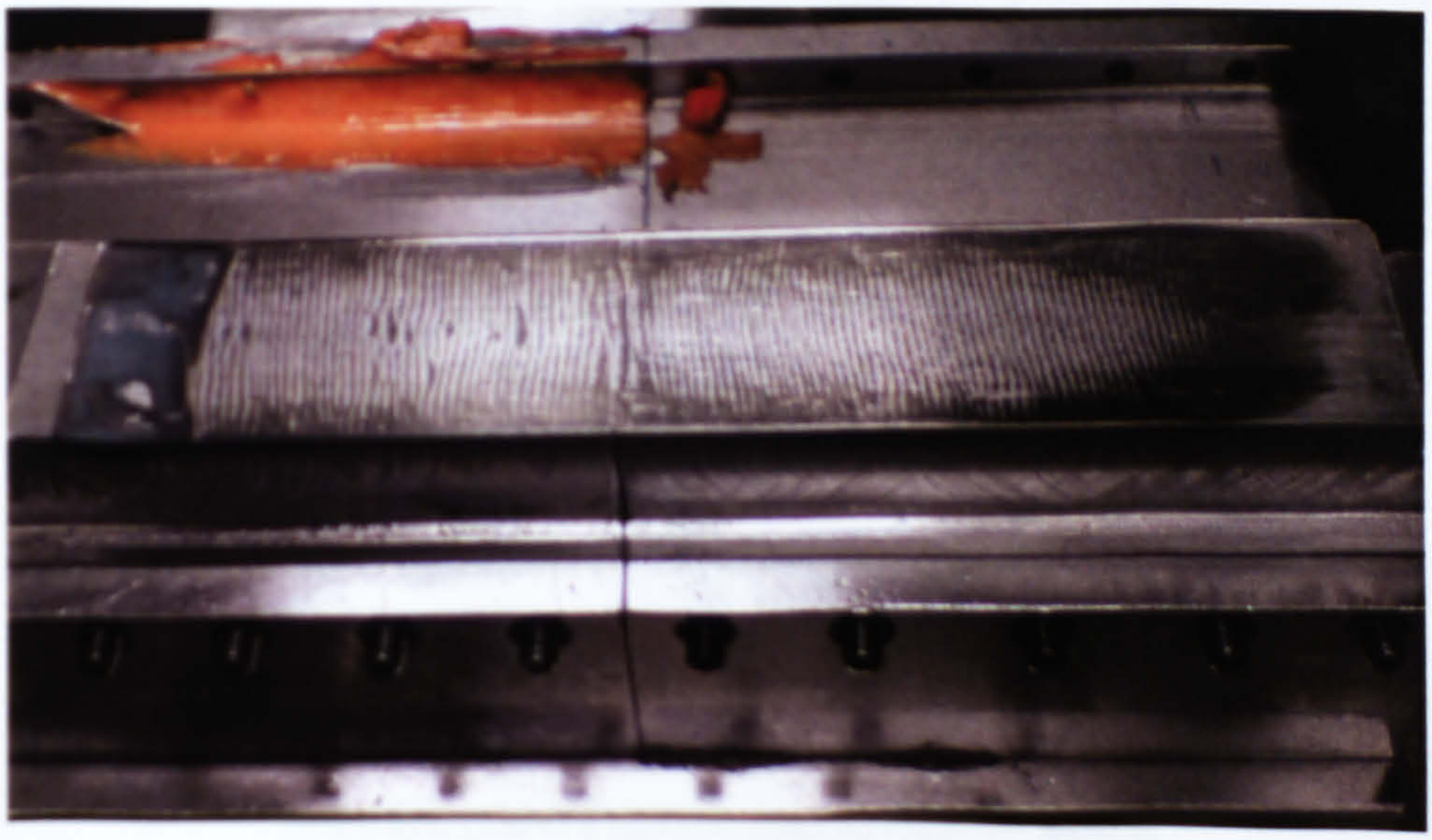

Severe burn of mild steel workpiece during Taguchi test

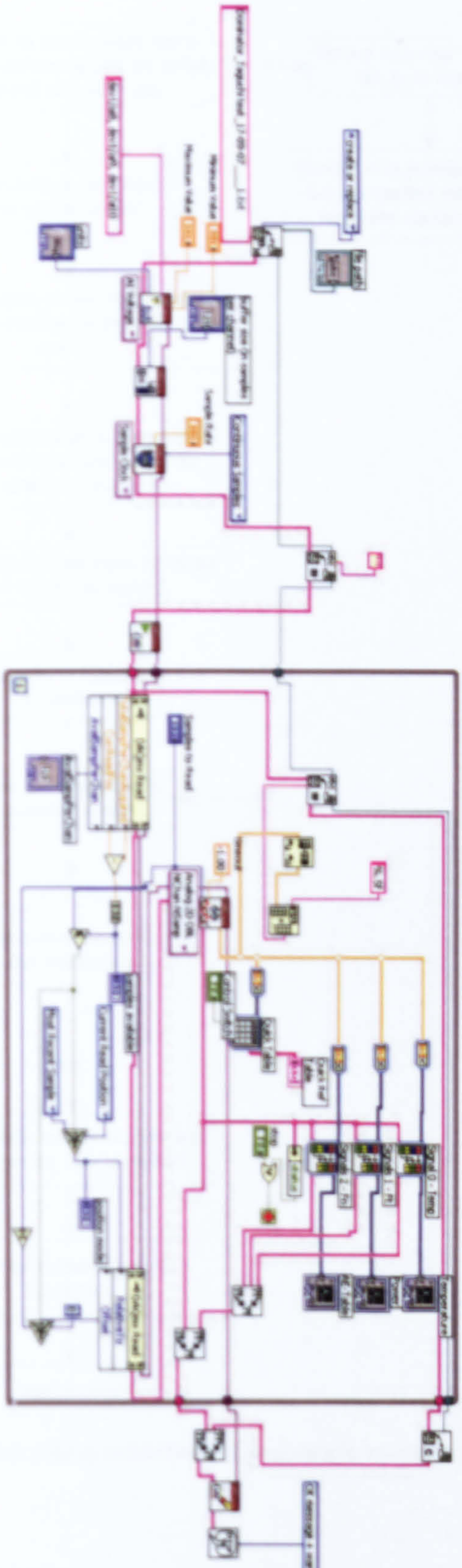

Block diagram of LabView Data Acquisition system

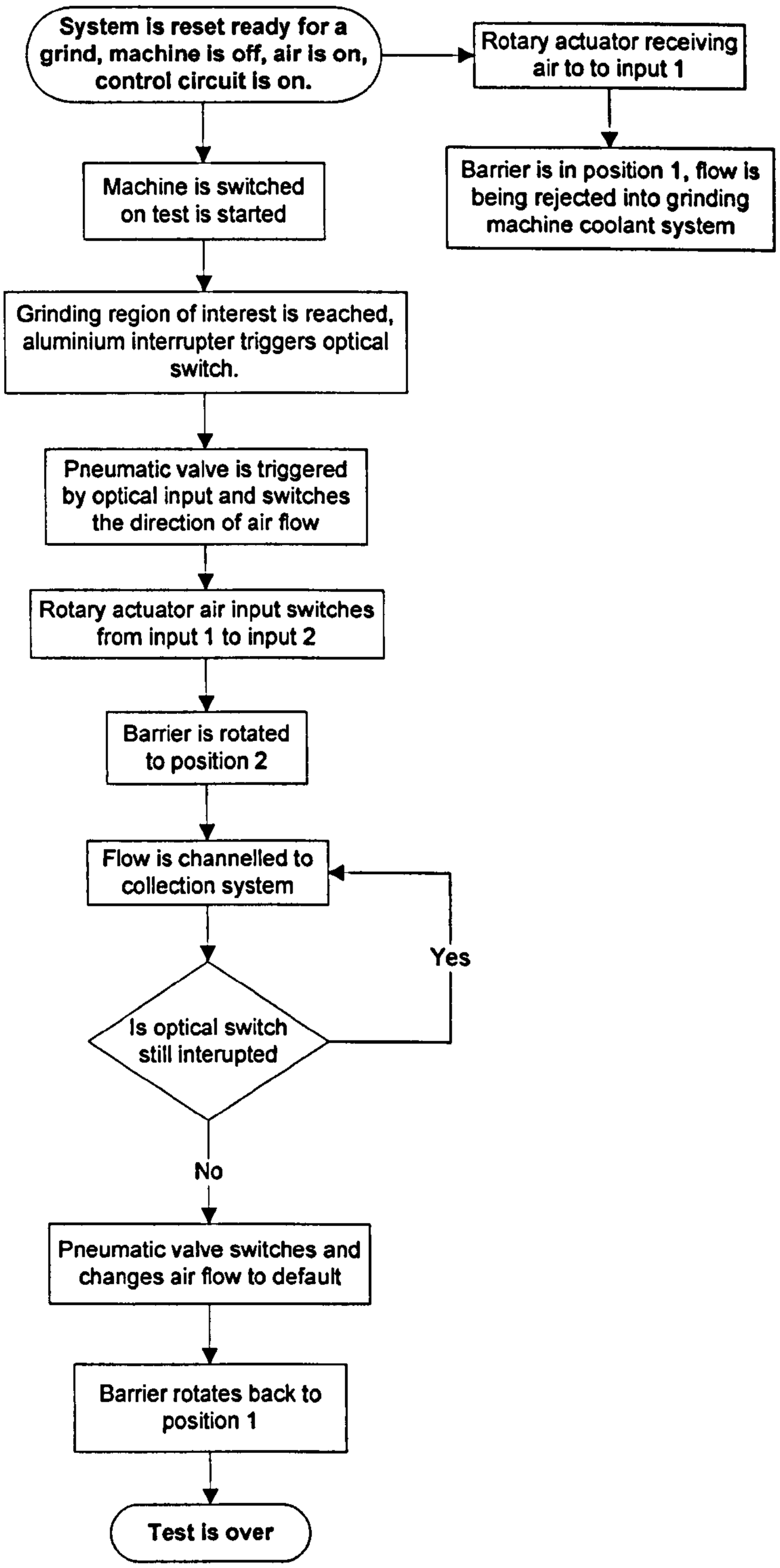

Flow chart describing behaviour of pneumatic valve control circuitry

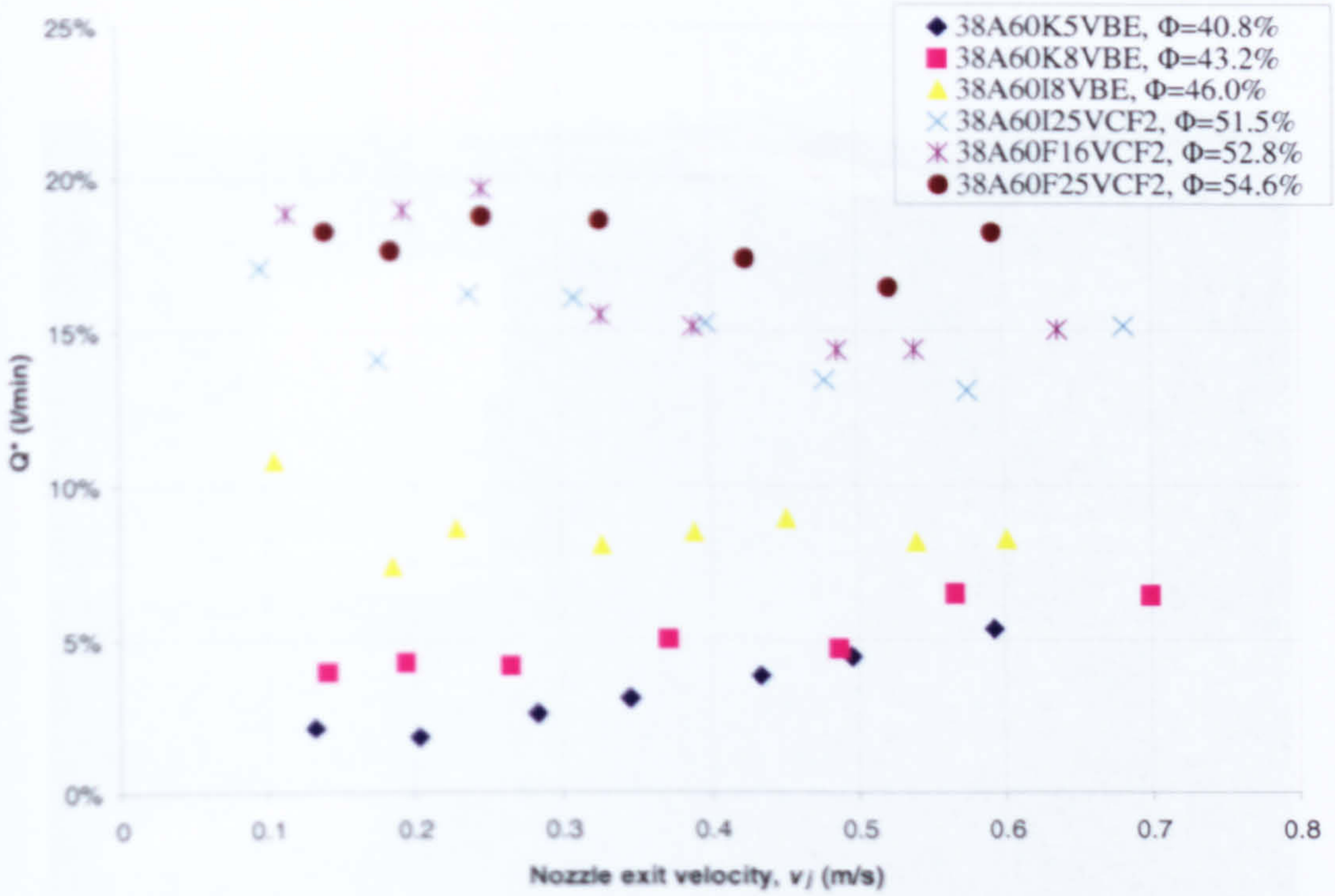

Nozzle exit velocity versus Percentage utilisation for grinding wheels of various bulk porosities Φ, when v_s=30m/s, a=12micron, s_f=160μm, v_w=0.09m/s, b_w=19mm and d_s=250mm. (Engineer *et al*, 1992).

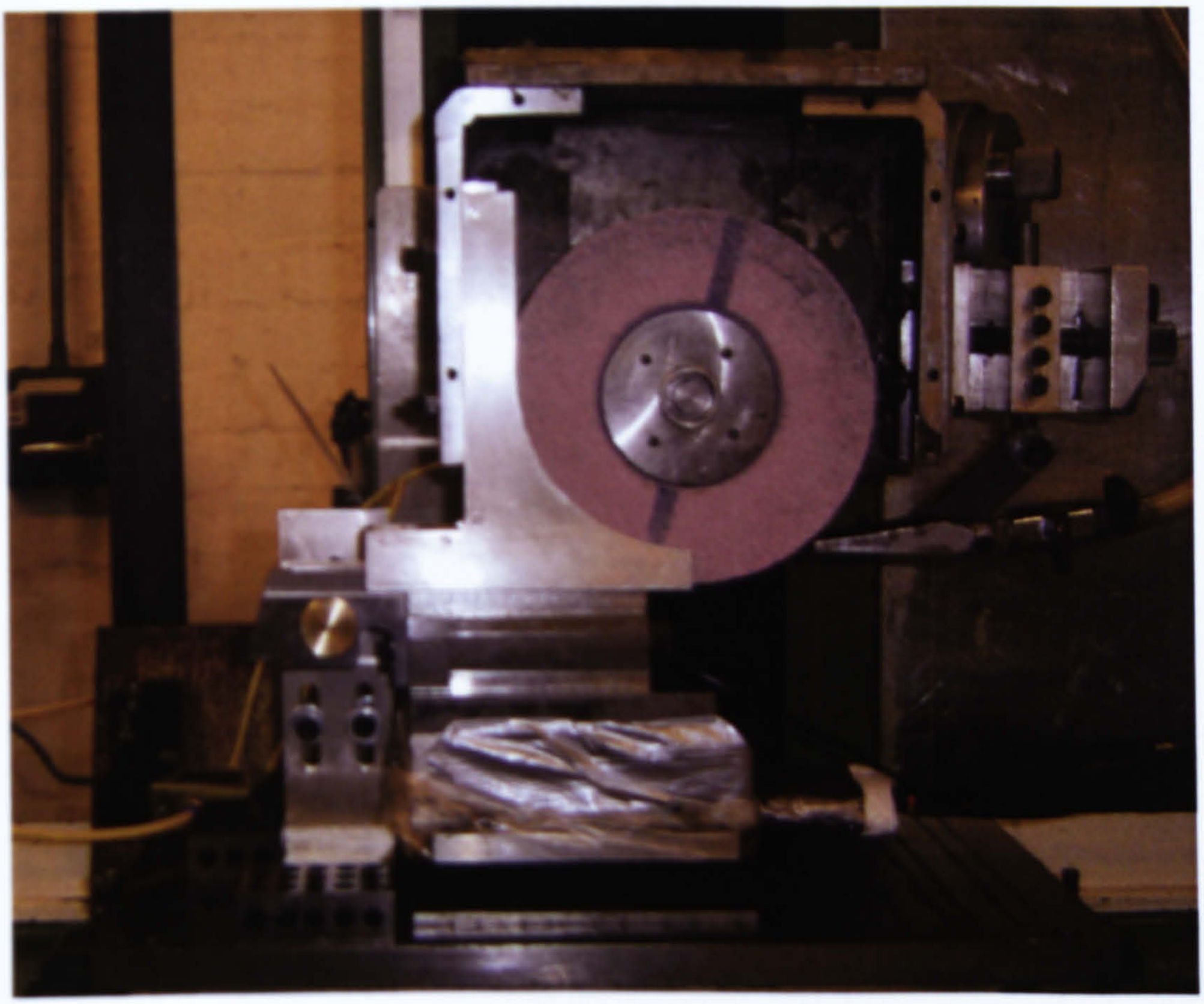

Photograph of experimental rig prior to Abwood speed ratio tests.

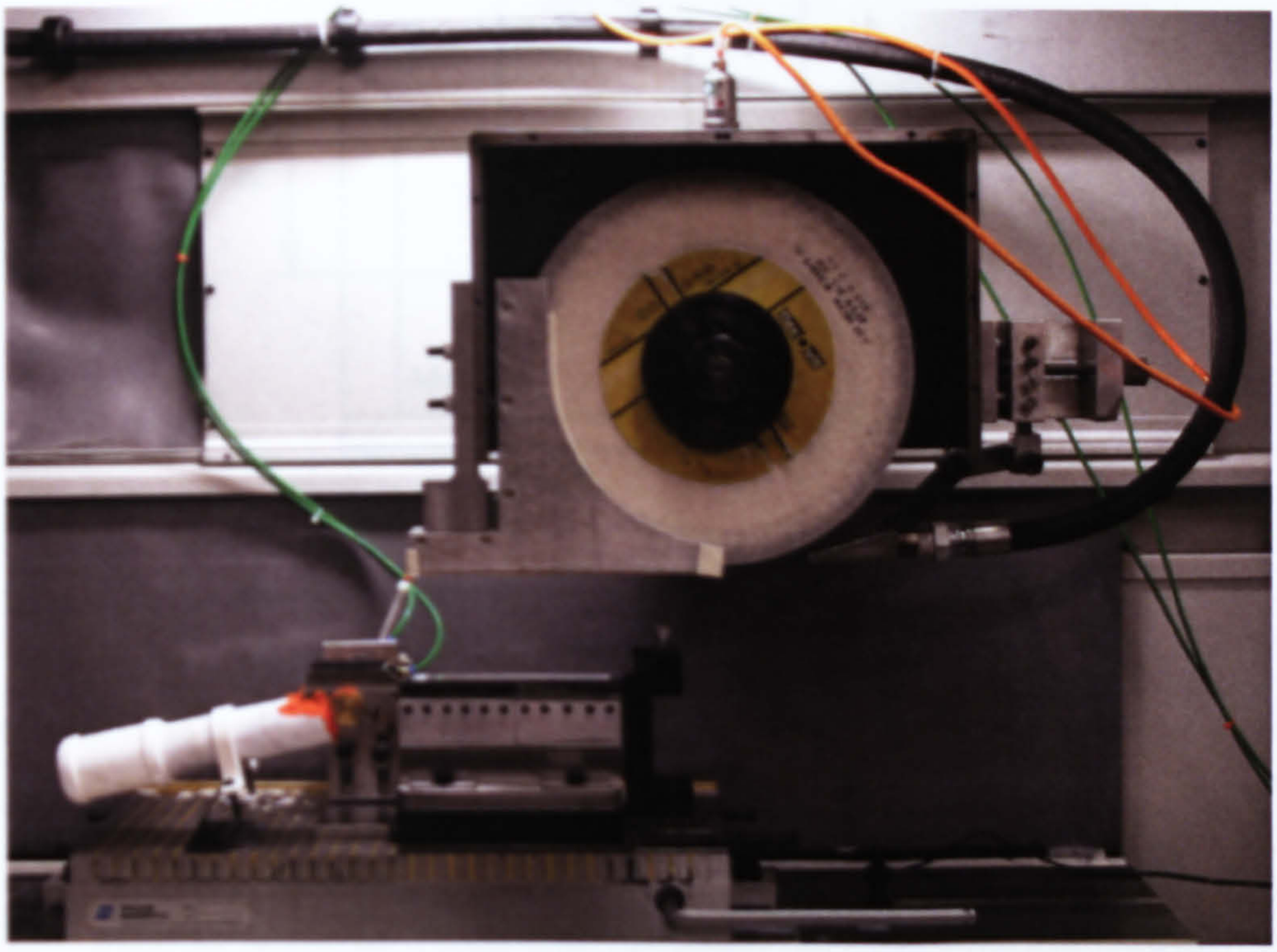

Photograph of experimental rig prior to Dominator speed ratio tests.

Darenth coolant supply unit

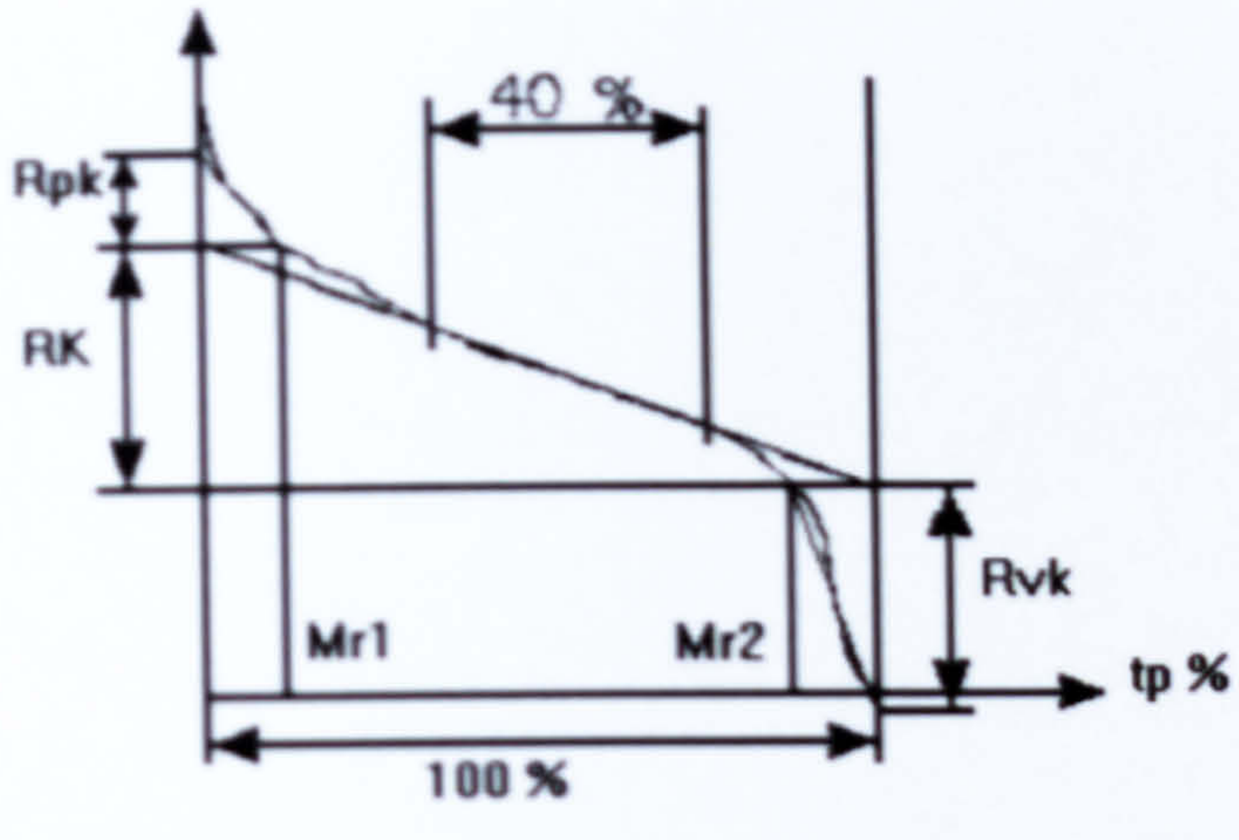

Bearing ratio curve diagram showing important values.

Example of Microset impression of the surface the Altos wheel.

Appendix D. Miscellaneous

Matlab programs

Grinding trials Program

```
%%%%%%%%%%%%%%%%%%%%%%%%%%%%%%%%%%%%%%%%%%%%%%%%%%%%%%%%%%%%%%%%%%%%%%%%%%%%%%%%%%%%%%%
%%%%%%%%%%%%%%%%%%%%%%%%%%%%%%%%%%%%%%%%%%%%%%%%%%%%%%%%%%%%%%%%%%%%%%%%%%%%%%%%%%%%%%%
%%%%%%%%%%%%%%%%%%%%%%%%%                                  %%%%%%%%%%%%%%%%%%%%%%%%%%%%%%%%%%%%%%%
%%%%%%%%%%%%%%%%%%%%%%%%%      Analyse DAQ                 %%%%%%%%%%%%%%%%%%%%%%%%%%%%%%%%%%%%%%%
%%%%%%%%%%%%%%%%%%%%%%%%%      Data and graph              %%%%%%%%%%%%%%%%%%%%%%%%%%%%%%%%%%%%%%%
%%%%%%%%%%%%%%%%%%%%%%%%%                                  %%%%%%%%%%%%%%%%%%%%%%%%%%%%%%%%%%%%%%%
%%%%%%%%%%%%%%%%%%%%%%%%%%%%%%%%%%%%%%%%%%%%%%%%%%%%%%%%%%%%%%%%%%%%%%%%%%%%%%%%%%%%%%%
%%%%%%%%%%%%%%%%%%%%%%%%%%%%%%%%%%%%%%%%%%%%%%%%%%%%%%%%%%%%%%%%%%%%%%%%%%%%%%%%%%%%%%%

clear all; clc; clear

%%%%%%%%%%%%%%%%%%%%%%%%%%%%%%%%%% Initial data %%%%%%%%%%%%%%%%%%%%%%%%%%%%%%%%%%%%%%%%%

Fs = 10000;                              %Input sampling frequency

%%%%%%%%%%%%%%%%%%%%%%%%%% Load, filter and graph data from test %%%%%%%%%%%%%%%%%%%%%%%%%%

load test.txt;                           %file data input
temp = size(test);                       %Finds value of size of matrix
m = (temp(1,1));                         %Creates variable from above for line 8
n = m/Fs;
p = n-(1/Fs);

x1=(0:1/Fs:p);                           %Creates vector for time based on Fs
x = x1';                                 %Column 1 labelled x _Time
y1=(test(1:m,1));                        %Column 1 labelled y _Temp
y2=(test(1:m,2));                        %Column 1 labelled y _AE Table
y3=(test(1:m,3));                        %Column 1 labelled y _Power

%%%%%%%%%%%%%%%%%%%%%%%%%%%%%%%%%%%%%%%%%%%%%%%%%%%%%%%%%%%%%%%%%%%%%%%%%%%%%%%%%%%%%%%

% temp filter
[b,a]=butter(3,0.003,'low');             % best settings 1,0.075  3,0.0075
y1f=filter(b,a,y1);

%Acoustic Emmission filter
[b,a]=butter(3,0.0007,'low');            % best settings 2,0.007
y2f=filter(b,a,y2);

%Power filter
[b,a]=butter(2,0.007,'low');             % best settings 2,0.007
y3f=filter(b,a,y3);

%%%%%%%%%%%%%%%%%%%%%%%%%%%%%%%%%%%%%%%%%%%%%%%%%%%%%%%%%%%%%%%%%%%%%%%%%%%%%%%%%%%%%%%
%%%%%%%%%%%%%%%%%%%%%%%%%        Graphing        %%%%%%%%%%%%%%%%%%%%%%%%%%%%%%%%%%%%%%%%%
%%%%%%%%%%%%%%%%%%%%%%%%%%%%%%%%%%%%%%%%%%%%%%%%%%%%%%%%%%%%%%%%%%%%%%%%%%%%%%%%%%%%%%%

xmin1 = min(x)-(0.2*min(x));
xmax1 = max(x)+(0.2*max(x));

figure (1);

subplot(2,1,1);
plot(x,y1,'--r');
hold on;
plot(x,y1f,'-b');
hold on;
title('Comparison - Both Results Temp');
xlabel('Time (s)');
ylabel('Voltage (V)');
ymin1 = min (y1)-(0.2*(sqrt(min(y1)*min(y1))));
ymax1 = max (y1)+(0.2*max(y1));

if ymin1==ymax1;
   ymin1 = -11;
   ymax1 = 11;
else

end
```

```
axis([xmin1 xmax1 ymin1 ymax1]);
%%%%%%%%%%%%%%%%%%%%%%%%  Temperature scaling  %%%%%%%%%%%%%%%%%%%%%%%%
y1fc=((y1f-0.0054)*(1/0.0088));
%y1fc=(((-3.08190e-4).*(y1f.^8))+((9.39996e-3).*(y1f.^7))-(0.112851.*(y1f.^6))+(0.674855.*(y1f.^5))-
(2.13994.*(y1f.^4))+(3.83305.*(y1f.^3))-(5.35333.*(y1f.^2))+(101.034.*(y1f))-0.0875775);

subplot(2,1,2);
plot(x,y1fc,'-b');
title('Temp');
xlabel('Time (s)');
ylabel('Temp (C)');
ymin1 = 0;
ymax1 = 150;
axis([xmin1 xmax1 ymin1 ymax1]);

%%%%%%%%%%%%%%%%%%%%%%%%%%%%%%%%%%%%%%%%%%%%%%%%%%%%%%%%%%%%%%%%%%%%%%%%%%%

figure (2);

plot(x,y2,'--r');
hold on;
plot(x,y2f,'-b');
hold on;
title('Comparison - Acoustic Emission table');
xlabel('Time (s)');
ylabel('Voltage (V)');
ymin2 = min (y2)-(0.2*(sqrt(min(y2)*min(y2))));
ymax2 = max (y2)+(0.2*max(y2));
axis([xmin1 xmax1 ymin2 ymax2]);

%%%%%%%%%%%%%%%%%%%%%%%%%%%%%%%%%%%%%%%%%%%%%%%%%%%%%%%%%%%%%%%%%%%%%%%%%%%

figure (3);

subplot(2,1,1);
plot(x,y3,'--r');
hold on;
plot(x,y3f,'-b');
hold on;
title('Comparison - Power');
xlabel('Time (s)');
ylabel('Power kW');
ymin3 = min (y3)-(0.2*(sqrt(min(y3)*min(y3))));
ymax3 = max (y3)+(0.2*max(y3));
axis([xmin1 xmax1 ymin3 ymax3]);

%%%%%%%%%%%%%%%%%%%%%%%%  Force-Normal scaling  %%%%%%%%%%%%%%%%%%%%%%%%
y3fc=((y3f/100)*7.5);

subplot(2,1,2);
plot(x,y3fc,'-b');
title('Power');
xlabel('Time (s)');
ylabel('Power (kW))');
ymin3 = min (y3fc)-(0.2*(sqrt(min(y3fc)*min(y3fc))));
ymax3 = max (y3fc)+(0.2*max(y3fc));
axis([xmin1 xmax1 ymin3 ymax3]);

figure (4);
H3 = plot(x,y3fc,'-.b');                    %Change this (to y3fc1)if an offset is needed for
                                            NORMAL force
hold on;

[AX,H1,H2] = plotyy(x,y2f,x,y1fc,'plot');   % change to y2fc1 if inversion is needed
set(get(AX(1),'Ylabel'),'String','Power (kW)');
set(get(AX(2),'Ylabel'),'String','Temperature (C)');

title('Test-');
xlabel('Time (s)');

set(H1,'LineStyle','--');   % tangential
set(H1,'color','r');
set(H2,'LineStyle','-');    % temp
set(H2,'color','g');
```

```
[legh, objh] = legend([H1 H2 H3], 'AE Table', 'Temp', 'Power');

set(AX(1),'box','off');
set(AX(1),'YLim',[-0.25 2.25]);
set(AX(1),'YTick',[-0.25 0 0.25 0.5 0.75 1 1.25 1.5 1.75 2 2.25]);
set(AX(2),'YLim',[0 200]);
set(AX(2),'YTick',[0 20 40 60 80 100 120 140 160 180 200]);
set(AX(2),'YColor','g');

saveas(4,'Dominator Taguchi Test_figure4.jpg')

%%%%%%%%%%%%%%%%%%%%%%%%%%%%%%%%%%%%%%%%%%%%%%%%%%%%%%%%%%%%%%%%%%%%%%%%%%%
%%%%%%%%%%%%%%%%%%          Post processing          %%%%%%%%%%%%%%%%%%%%%%%%
%%%%%%%%%%%%%%%%%%%%%%%%%%%%%%%%%%%%%%%%%%%%%%%%%%%%%%%%%%%%%%%%%%%%%%%%%%%

%%%%%%%%%%%%%%%%%% Create Vector for maximum power %%%%%%%%%%%%%%%%%%%%%%%%

power_dif=0.5;
interval=1;

Load_start_time=5;
Load_sample_period=10;
Load_end_time=Load_start_time+Load_sample_period;
no_load_sample_end=2;
no_load_sample_period=1;

end_p =0.9*temp(1,1);
load_vect=[];
no_load_vect=[];
s_time=[];
s_end=[];
sub_s_time=[];
z=0;
z1=0;
a=0;
b=0;

j0=[];
j1=[];
j2=[];
j3=1;
j4=1;
.
i=1;
i1=1;
i2=1;

t0=no_load_sample_period*Fs;
thalf=no_load_sample_end*Fs;
t1=interval*Fs;
t2=Load_start_time*Fs;
t3=Load_end_time*Fs;

%%%%%%%%%%%%%%%%%% Create vector of load power %%%%%%%%%%%%%%%%%%%%%%%%%%%%

while i<=end_p;
   a=test(i,3);
   b=test(i+t1,3);

   if b-a>power_dif;
   j1=i;
   j2=i+t2;
   j3=i+t3;
   s_time=j2/Fs;
   s_end=j3/Fs;

   for j=(j2:1:j3);

      z=test(j,3);
      load_vect(i1,1)=z;
      i1=i1+1;

   end

i=end_p;
```

```
   else

   end
i=i+1;

end

%%%%%%%%%%%%%%%% Create vector of no load power %%%%%%%%%%%%%%%%%%%%%%%%%%%%

jhalf=j1-thalf;
j0=j1-thalf-t0;
sub_s_time=j0/Fs;
sub_e_time=jhalf/Fs;

disp(['No Load Start time, (s) =']), disp(sub_s_time)
disp(['No Load End time, (s) =']), disp(sub_e_time)
disp(['Full Load Start time, (s) =']), disp(s_time)
disp(['Full Load End time, (s) =']), disp(s_end)

for j=(j0:1:jhalf);
   z1=test(j,3);
   no_load_vect(i2,1)=z1;
   i2=i2+1;

end

Load_vect_adj=((load_vect./100).*7.5);
No_load_vect_adj=((no_load_vect./100).*7.5);

%%%%%%%%%%%%%%%% Calculate grinding power %%%%%%%%%%%%%%%%%%%%%%%%%%%%%%%%%%%%

ave_load_power=mean(Load_vect_adj);
max_load_power=max(Load_vect_adj);
ave_no_load_power=mean(No_load_vect_adj);
max_no_load_power=max(No_load_vect_adj);
grinding_power=ave_load_power-ave_no_load_power;
disp(['Mean Full Load Power, (kW) =']), disp(ave_load_power)
disp(['Max Full Load Power, (kW) =']), disp(max_load_power)
disp(['Mean No Load Power, (kW) =']), disp(ave_no_load_power)
disp(['Max No Load Power, (kW) =']), disp(max_no_load_power)
disp(['Grinding Power, (kW) =']), disp(grinding_power)

%%%%%%%%%%%%%%%% Display and save data %%%%%%%%%%%%%%%%%%%%%%%%%%%%%%%%%%%%

Test.Name = 'Data_09-2007';
Test.Max_Temp = max(y1fc);
Test.Median_Temp = median(y1fc);
Test.Min_AE_Table = min(y2f);                    %% change to y2fc1 if inversion is needed
Test.Max_AE_Table = max(y2f);
Test.Median_AE_Table = median(y2f);
Test.Grinding_Power = grinding_power;
Test.No_Load_Power = ave_no_load_power;

Test

%%%%%%%%%%%%%%%%%%%%%%%%%%%%%%%%%%%%%%%%%%%%%%%%%%%%%%%%%%%%%%%%%%%%%%%%%%%%
%%%%%%%%%%%%%%%%%%%%%%%%%%%%%%%%%%%%%%%%%%%%%%%%%%%%%%%%%%%%%%%%%%%%%%%%%%%%
%%%%%%%%%%%%%%%%%%%%%%%%%%%%%%%%%%%%%%%%%%%%%%%%%%%%%%%%%%%%%%%%%%%%%%%%%%%%
```

Topography program 1

```
%%%%%%%%%%%%%%%%%%%%%%%%%%%%%%%%%%%%%%%%%%%%%%%%%%%%%%%%%%%%%%%%%%%%%%%%%%%%%%%%%%%%%%%%%%%%%%%%%%%%%%%%%%%%%%%%%%%%%%%%%%%%%%%%%%%%%%%%%%%%%%%%%%%%%%%%%%%%%%%%%%%%%%%%%%%
%%%%%%%%%%%%%%%%%%%%%%%%%%%%%%%%%%%%%%%%%%%%%%%%%%%%%%%%%%%%%%%%%%%%%%%%%%%%%%%%%%%%%%%%%%%%%%%%%%%%%%%%%%%%%%%%%%%%%%%%%%%%%%%%%%%%%%%%%%%%%%%%%%%%%%%%%%%%%%%%%%%%%%%%%%%
%%%%%%%%%%%%%%%%%%%%%%%%%%%%%%%%%                                       %%%%%%%%%%%%%%%%%%%%%%%%%%%%%%%%%%%%%%%%%%%%%%%%%%%%%%%%%%%%%%%%%%%
%%%%%%%%%%%%%%%%%%%%%%%%%%%%%%%%%   PROGRAM FOR SMALL                   %%%%%%%%%%%%%%%%%%%%%%%%%%%%%%%%%%%%%%%%%%%%%%%%%%%%%%%%%%%%%%%%%%%
%%%%%%%%%%%%%%%%%%%%%%%%%%%%%%%%%   SAMPLE SIZE                         %%%%%%%%%%%%%%%%%%%%%%%%%%%%%%%%%%%%%%%%%%%%%%%%%%%%%%%%%%%%%%%%%%%
%%%%%%%%%%%%%%%%%%%%%%%%%%%%%%%%%   5.3mm x 7mm                         %%%%%%%%%%%%%%%%%%%%%%%%%%%%%%%%%%%%%%%%%%%%%%%%%%%%%%%%%%%%%%%%%%%
%%%%%%%%%%%%%%%%%%%%%%%%%%%%%%%%%   5mm x 3.8mm                         %%%%%%%%%%%%%%%%%%%%%%%%%%%%%%%%%%%%%%%%%%%%%%%%%%%%%%%%%%%%%%%%%%%
%%%%%%%%%%%%%%%%%%%%%%%%%%%%%%%%%                                       %%%%%%%%%%%%%%%%%%%%%%%%%%%%%%%%%%%%%%%%%%%%%%%%%%%%%%%%%%%%%%%%%%%
%%%%%%%%%%%%%%%%%%%%%%%%%%%%%%%%%%%%%%%%%%%%%%%%%%%%%%%%%%%%%%%%%%%%%%%%%%%%%%%%%%%%%%%%%%%%%%%%%%%%%%%%%%%%%%%%%%%%%%%%%%%%%%%%%%%%%%%%%%%%%%%%%%%%%%%%%%%%%%%%%%%%%%%%%%%
%%%%%%%%%%%%%%%%%%%%%%%%%%%%%%%%%%%%%%%%%%%%%%%%%%%%%%%%%%%%%%%%%%%%%%%%%%%%%%%%%%%%%%%%%%%%%%%%%%%%%%%%%%%%%%%%%%%%%%%%%%%%%%%%%%%%%%%%%%%%%%%%%%%%%%%%%%%%%%%%%%%%%%%%%%%

clear all, clc, clear

%load aj_3_5.txt                              % BEDDING IN TESTS
load 2bf3.txt                                 % CONVENIENT FLOW TESTS
%load 1bf5.txt                                % CONVENIENT FLOW TESTS

%file1=aj_3_5;                                % BEDDING IN TESTS
file1=X2bf3;                                  % CONVENIENT FLOW TESTS
%file1=X1bf5;                                 % CONVENIENT FLOW TESTS

temp=(size(file1));
endl1= temp(1,2);                             % establish side 2
endl2= temp(1,1);                             % establish side 1

%%%%%%%%%%%%%%%%%%%%%%%%%%%%%%%%%%%%%%%%%%%%%%%%%%%%%%%%%%%%%%%%%%%%%%%%%%%%%%%%%%%%%%%%%%%%%%%%%%%%%%%%%%%%%%%%%%%%%%%%%%%%%%%%%%%%%%%%%%%%%%%%%%%%%%%%%%%%%%%%%%%%%%%%%%%
%%%%%%%%%%%%%%%%%%%%%%%%%%%%%%%%%%%%%   Input Analysis parameters   %%%%%%%%%%%%%%%%%%%%%%%%%%%%%%%%%%%%%%%%%%%%%%%%%%%%%%%%%%%%%%%%%%%%%%%
%%%%%%%%%%%%%%%%%%%%%%%%%%%%%%%%%%%%%%%%%%%%%%%%%%%%%%%%%%%%%%%%%%%%%%%%%%%%%%%%%%%%%%%%%%%%%%%%%%%%%%%%%%%%%%%%%%%%%%%%%%%%%%%%%%%%%%%%%%%%%%%%%%%%%%%%%%%%%%%%%%%%%%%%%%%

vs=30;                                        % wheel speed in m/s
bs_mm=25;                                     % wheel width in mm
bs=0.025;                                     % wheel width in m
%wheel_porosity=0.54;                         % Pink wheel (1) 54%
wheel_porosity=0.44;                          % white wheel (2) 44%
wheel_porosity_perc=wheel_porosity*100;

%%%%%%%%%%%%%%%%%%%%%%%%%%%%%%%%%%%%%%%%%%%%%%%%%%%%%%%%%%%%%%%%%%%%%%%%%%%%%%%%%%%%%%%%%%%%%%%%%%%%%%%%%%%%%%%%%%%%%%%%%%%%%%%%%%%%%%%%%%%%%%%%%%%%%%%%%%%%%%%%%%%%%%%%%%%%
%%%%%%%%%%%%%%%%%%%%%%%%%%%%%%%%%%%%%%%   Setup parameters for loops   %%%%%%%%%%%%%%%%%%%%%%%%%%%%%%%%%%%%%%%%%%%%%%%%%%%%%%%%%%%%%%%%%
%%%%%%%%%%%%%%%%%%%%%%%%%%%%%%%%%%%%%%%%%%%%%%%%%%%%%%%%%%%%%%%%%%%%%%%%%%%%%%%%%%%%%%%%%%%%%%%%%%%%%%%%%%%%%%%%%%%%%%%%%%%%%%%%%%%%%%%%%%%%%%%%%%%%%%%%%%%%%%%%%%%%%%%%%%%%

j=1;
i=1;
b=[];

%%%%%%%%%%%%%%%%%%%%%%%%%%%%%%%%%%%%%%%%%%%%%%%%%%%%%%%%%%%%%%%%%%%%%%%%%%%%%%%%%%%%%%%%%%%%%%%%%%%%%%%%%%%%%%%%%%%%%%%%%%%%%%%%%%%%%%%%%%%%%%%%%%%%%%%%%%%%%%%%%%%%%%%%%%%%
%%%%%%%%%%%%%%%%%%%%%%%%%%%%%%%%%   Analysis of initial profiles   %%%%%%%%%%%%%%%%%%%%%%%%%%%%%%%%%%%%%%%%%%%%%%%%%%%%%%%%%%%%%%%%%%%%%%%%%%
%%%%%%%%%%%%%%%%%%%%%%%%%%%%%%%%%%%%%%%%%%%%%%%%%%%%%%%%%%%%%%%%%%%%%%%%%%%%%%%%%%%%%%%%%%%%%%%%%%%%%%%%%%%%%%%%%%%%%%%%%%%%%%%%%%%%%%%%%%%%%%%%%%%%%%%%%%%%%%%%%%%%%%%%%%%%

l1=5.3;
l2=7;

%l1=5;
%l2=3.8;

l1_inc=l1/endl1;
l2_inc=l2/endl2;

l1_vect=(0+l1_inc:l1_inc:l1);
l2_vect=(0+l2_inc:l2_inc:l2);

%%%%%%%%%%%%%%%%%%%%%%%%%%%%%%%%%%%%%%%%%%%%%%%%%%%%%%%%%%%%%%%%%%%%%%%%%%%%%%%%%%%%%%%%%%%%%%%%%%%%%%%%%%%%%%%%%%%%%%%%%%%%%%%%%%%%%%%%%%%%%%%%%%%%%%%%%%%%%%%%%%%%%%%%%%%%
%%%%%%%%%%%%%%%%%%%%%%%%%%%   Evaluate area for subtraction of integrals   %%%%%%%%%%%%%%%%%%%%%%%%%%%%%%%%%%%%%%%%%%%%%%%%%%%%%%%%%%%%%%%
%%%%%%%%%%%%%%%%%%%%%%%%%%%%%%%%%%%%%%%%%%%%%%%%%%%%%%%%%%%%%%%%%%%%%%%%%%%%%%%%%%%%%%%%%%%%%%%%%%%%%%%%%%%%%%%%%%%%%%%%%%%%%%%%%%%%%%%%%%%%%%%%%%%%%%%%%%%%%%%%%%%%%%%%%%%%
%%%%%%%%%%%%%%%%%%%%%%%%%               Find trough value            %%%%%%%%%%%%%%%%%%%%%%%%%%%%%%%%%%%%%%%%%%%%%%%%%%%%%%%%%%%%%%
%%%%%%%%%%%%%%%%%%%%%%%%%%%%%%%%%%%%%%%%%%%%%%%%%%%%%%%%%%%%%%%%%%%%%%%%%%%%%%%%%%%%%%%%%%%%%%%%%%%%%%%%%%%%%%%%%%%%%%%%%%%%%%%%%%%%%%%%%%%%%%%%%%%%%%%%%%%%%%%%%%%%%%%%%%%%

z1=min(file1);                                % Create vector of minimum points
z2=min(z1);                                   % Create vector of minimum points
z2_mean_min_vector=mean(z1);                  % find mean of vector of minimums
z3=z2_mean_min_vector;                        % Create lower limit for use in fluid calculations
```

```
z3_mm=z3/1000;                                    % Convert low point to milimetres

%%%%%%%%%%%%%%%%%%%%%%%%%%%%%%%%%%%%%%%%%%%%%%%%%%%%%%%%%%%%%%%%%
%%%%%%%%%%%%%%           Find Peak value         %%%%%%%%%%%%%%%%%%%%%
%%%%%%%%%%%%%%%%%%%%%%%%%%%%%%%%%%%%%%%%%%%%%%%%%%%%%%%%%%%%%%%%%

w1=max(file1);                                    % Create vector of maximum points
w2=max(w1);
w2_mean_max_vector=mean(w1);                      % find mean of vector of maximums
w3=w2_mean_max_vector;                            % Create upper limit for use in fluid
                                                  calculations using mean of mean

w3_mm=w3/1000;                                    % Convert high point to milimetres

%%%%%%%%%%%%%%%%%%%%%%%%%%%%%%%%%%%%%%%%%%%%%%%%%%%%%%%%%%%%%%%%%

Rt=w3-z2;                                         % Calculate height of maximum area
area_1=Rt*endl2;                                  % Calculate maximum UNIT area
                                                        for row all rows
Rt_mm=Rt/1000;                                    % convert Rt to millimetres
tot_area_mm2=Rt_mm*bs_mm;                         % Calculate maximum area in mm2
                                                        for all rows
Rt1=w2-z2;                                        % Calculate height of maximum area
Rt1_mm=Rt1/1000;                                  % convert Rt1 to millimetres

%%%%%%%%%%%%%%%%%%%%%%%%%%%%%%%%%%%%%%%%%%%%%%%%%%%%%%%%%%%%%%%%%
%%%%%%%%%%%%%%%%%      Initiate scanning of profiles      %%%%%%%%%%%%%%%%%%
%%%%%%%%%%%%%%%%%%%%%%%%%%%%%%%%%%%%%%%%%%%%%%%%%%%%%%%%%%%%%%%%%

for i=(1:1:endl1);                                % Select row to analyse
  k=0;
  vol=[];
  y=[];                                           % clear 'y' for next increment
  e=[];
  c=file1(:,i);                                   % create row vector at row 'i'

  for j=(1:1:endl2);                              % Pass through row
    d=file1(j,i);                                 % pick point to analyse
    a=d+abs(z2);                                  % offset data against lowest
                                                  point so all values are positive
    w4=w3+abs(z2);                                % crate a maximum point for sampling

    if a>=0 & a<=w4;                              % is point greater than value and
                                                  less than the adjusted height
      k=k+1;                                      % Increment along vector y
      y(1,k)=a;                                   % add point to vector 'y'
      j=j+1;                                      % Increment along row

    elseif a>=0 & a>=w4;                          % is point greater than value and
                                                  greater than the adjusted height
      k=k+1;                                      % Increment along vector y
      y(1,k)=w4;                                  % add point to vector represensted
                                                  by maximum height w3
      j=j+1;                                      % Increment along row

    else
      j=j+1;

    end

  end

  %%%%%%%%%%%%%% calculate area occupied by +ve values %%%%%%%%%%%%%%%%%%

  b_temp=trapz(y);                                % integrate altered row
  b(1,i)=b_temp;                                  % add integrant to new vector 'b'

  %%%%%%%%%%%%%%%%%%%%%%%%%%%%%%%%%%%%%%%%%%%%%%%%%%%%%%%%%%%%%%%%%


  if i==50;
    prof1=(file1(:,i))./1000;
    prof1_alt=(c+abs(z3))./1000;
  end
```

```
if i==100;
   prof2=(file1(:,i))./1000;
   prof2_alt=(c+abs(z3))./1000;
end

if i==150;
   prof3=(file1(:,i))./1000;
   prof3_alt=(c+abs(z3))./1000;
end

%%%%%%%%%%%% calculate values of open space from row vector %%%%%%%%%%%%%%%%
vol=area_1-b_temp;                                          % calculate space vol for each row by
                                                            subtracting integrant from total area
vol_space_vect(1,i)=vol;                                    % add calculated area to a vector to
                                                            store value

   area_perc=((vol)/(area_1))*100;                          % create pecentage (as a %) value for
                                                            each integrate over possible max
   area_perc_dec=(vol)/(area_1);                            % create pecentage (in decimal form)
                                                            value for each integrate over possible max
   vol_space_perc_vector(1,i)=area_perc;                    % create vector store data of percentage
                                                            free space per row i
   tot_area_space_mm_vect(1,i)=area_perc_dec*tot_area_mm2;  % create true volume available for fluid
                                                            in each row

   %%%%%%%%%%%%%%%%%%%%%%%%%%%%%%%%%%%%%%%%%%%%%%%%%%%%%%%%%%%%%%%%%%%%%%%%%%%

   i=i+1 ;                                                  % Increment to next row

end

%%%%%%%%%%%%%%%%%%%%%%%%%%%%%%%%%%%%%%%%%%%%%%%%%%%%%%%%%%%%%%%%%%%%%%%%%%%
%%%%%%%%%%%%%%%%%%%%  Calculate output values  %%%%%%%%%%%%%%%%%%%%%%%%%%%%
%%%%%%%%%%%%%%%%%%%%%%%%%%%%%%%%%%%%%%%%%%%%%%%%%%%%%%%%%%%%%%%%%%%%%%%%%%%

max_peak_mm=w2/1000;                                        % find highest point in analysis
min_peak_mm=z2/1000;                                        % find lowest point in analysis

Total_space_area=sum(tot_area_space_mm_vect);               % calculate total volume available in
                                                            sample
ave_area_space_mm2=Total_space_area/endl1;                  % calculate average area available in
                                                            contact zone [mm2]
ave_area_space_m2=ave_area_space_mm2/(1e6);                 % calculate average area available in
                                                            contact zone [m2]

vol_space_perc=mean(vol_space_perc_vector);                 % Calculate average surface porosity [%]

vol_flowrate_m3s=ave_area_space_m2*vs;                      % calculate flow rate [m3/s]
vol_flowrate_lmin=vol_flowrate_m3s*(1e3)*60;                % convert flow rate [l/min]
vol_flowrate2_lmin=vol_flowrate_lmin*wheel_porosity;        % use bulk wheel prosity to factor
                                                            uniform flowrate value

max_area_space_m2=tot_area_mm2/(1e6);                       % calculate average are available in
                                                            contact zone [m2]
max_vol_flowrate_m3s=max_area_space_m2*vs;                  % calculate flow rate [m3/s]
max_vol_flowrate_lmin=max_vol_flowrate_m3s*(1e3)*60;        % convert flow rate [l/min]

%%%%%%%%%%%%%%%%%%  Display all relevant data  %%%%%%%%%%%%%%%%%%%%%%%%%%%%%
disp(['Wheelspeed, vs (m/s) =']), disp(vs)
disp(['Wheel width, bs (mm) =']), disp(bs_mm)
disp(['Bulk wheel porosity, phi (%) =']), disp(wheel_porosity_perc)
disp('  ')
disp(['Average surface porosity, (%) =']), disp(vol_space_perc)
disp(['Average area available for fluid, (mm2) =']), disp(ave_area_space_mm2)
disp(['Possible Volumetric Flowrate, Qu (l/min)=']), disp(vol_flowrate_lmin)
disp(['Realistic Volumetric Flowrate, Qu (l/min)=']), disp(vol_flowrate2_lmin)
disp('  ')
disp(['Highest point on topography (mm) =']), disp(max_peak_mm)
disp(['Highest point of analysis (mm) =']), disp(w3_mm)
disp('  ')
disp(['Lowest point on topography (mm) =']), disp(min_peak_mm)
disp(['Lowest point of analysis (mm) =']), disp(z3_mm)
```

```
disp(['Equivalent Rt (mm) =']), disp(Rt_mm)
disp(['Rt (mm) =']), disp(Rt1_mm)

%%%%%%%%%%%%%%%%%%%%%%%%%   Plot relevant graphs   %%%%%%%%%%%%%%%%%%%%%%%%%%%%%%%%%%%%%

set(0,'Units','pixels')
scn_pos1=get(0,'ScreenSize');
scn_pos=scn_pos1.*0.9;
scn_pos(1,1)=5;
scn_pos(1,2)=10;
scn_pos(1,3)=scn_pos1(1,3);

figure(1)
plot(l1_vect,vol_space_perc_vector)
title('Showing percentage of free space under each row');
xlabel('Distance through sample (mm)');
ylabel('Percentage free space (%)');
saveas(1,'Percentage free space versus row for large sample size','bmp')

figure('Position',scn_pos)
figure(2)
title('Showing comparison of true profile to offset only profile');

subplot(3,1,1);
plot(l2_vect,prof1,'--r');
hold on;
plot(l2_vect,prof1_alt,'-b');
ylabel('Height (mm)');
xlabel('Distance through sample (mm)');

subplot(3,1,2);
plot(l2_vect,prof2,'--r');
hold on;
plot(l2_vect,prof2_alt,'-b');
ylabel('Height (mm)');
xlabel('Distance through sample (mm)');

subplot(3,1,3);
plot(l2_vect,prof3,'--r');
hold on;
plot(l2_vect,prof3_alt,'-b');
ylabel('Height (mm)');
xlabel('Distance through sample (mm)');
saveas(2,'Example of three profiles through the sample','bmp')

%%%%%%%%%%%%%%%%%%%%%%%%%%%%%%%%%%%%%%%%%%%%%%%%%%%%%%%%%%%%%%%%%%%%%%%%
%%%%%%%%%%%%%%%%%%%%%%%%%    END    %%%%%%%%%%%%%%%%%%%%%%%%%%%%%%%%%%%%%%%%%%
%%%%%%%%%%%%%%%%%%%%%%%%%%%%%%%%%%%%%%%%%%%%%%%%%%%%%%%%%%%%%%%%%%%%%%%%
```

Topography program 2

```
%%%%%%%%%%%%%%%%%%%%%%%%%%%%%%%%%%%%%%%%%%%%%%%%%%%%%%%%%%%%%%%%
%%%%%%%%%%%%%%%%%%%%%%%%%%%%%%%%%%%%%%%%%%%%%%%%%%%%%%%%%%%%%%%%
%%%%%%%%%%%%%%%%%%%%                                %%%%%%%%%%%%%%%%%%%%
%%%%%%%%%%%%%%%%%%%%  PROGRAM FOR LARGE             %%%%%%%%%%%%%%%%%%%%%
%%%%%%%%%%%%%%%%%%%%  SAMPLE SIZE                   %%%%%%%%%%%%%%%%%%%%%
%%%%%%%%%%%%%%%%%%%%  19mm x 25mm                   %%%%%%%%%%%%%%%%%%%%%
%%%%%%%%%%%%%%%%%%%%  15mm x 20mm                   %%%%%%%%%%%%%%%%%%%%%
%%%%%%%%%%%%%%%%%%%%                                %%%%%%%%%%%%%%%%%%%%%
%%%%%%%%%%%%%%%%%%%%%%%%%%%%%%%%%%%%%%%%%%%%%%%%%%%%%%%%%%%%%%%%
%%%%%%%%%%%%%%%%%%%%%%%%%%%%%%%%%%%%%%%%%%%%%%%%%%%%%%%%%%%%%%%%

clear all, clc, clear

%load aj_3_20.txt                       % BEDDING IN TESTS
%load 1f5.txt                           % DRESSING TESTS
%load 1af5.txt                          % CONVENIENT FLOW TESTS
load 2af3.txt                           % CONVENIENT FLOW TESTS

%file1=aj_3_20;                         % BEDDING IN TESTS
%file1=X1f5;                            % DRESSING TESTS
%file1=X1af5;                           % CONVENIENT FLOW TESTS
file1=X2af3;                            % CONVENIENT FLOW TESTS

temp=(size(file1));
endl1= temp(1,2);                       % establish side 2
endl2= temp(1,1);                       % establish side 1

%%%%%%%%%%%%%%%%%%%%%%%%%%%%%%%%%%%%%%%%%%%%%%%%%%%%%%%%%%%%%%%%
%%%%%%%%%%%%%%%  Input Analysis parameters  %%%%%%%%%%%%%%%%%%%%%%%%%%
%%%%%%%%%%%%%%%%%%%%%%%%%%%%%%%%%%%%%%%%%%%%%%%%%%%%%%%%%%%%%%%%

vs=30;                                  % wheel speed in m/s
bs_mm=25;                               % wheel width in mm
bs=0.025;                               % wheel width in m
%wheel_porosity=0.54;                   % Pink wheel (1) 54%
wheel_porosity=0.44;                    % white wheel (2) 44%
wheel_porosity_perc=wheel_porosity*100;

%%%%%%%%%%%%%%%%%%%%%%%%%%%%%%%%%%%%%%%%%%%%%%%%%%%%%%%%%%%%%%%%
%%%%%%%%%%%%%%%%  Setup parameters for loops  %%%%%%%%%%%%%%%%%%%%%
%%%%%%%%%%%%%%%%%%%%%%%%%%%%%%%%%%%%%%%%%%%%%%%%%%%%%%%%%%%%%%%%

j=1;
i=1;
b=[];

%%%%%%%%%%%%%%%%%%%%%%%%%%%%%%%%%%%%%%%%%%%%%%%%%%%%%%%%%%%%%%%%
%%%%%%%%%%%%%%%  Analysis of initial profiles  %%%%%%%%%%%%%%%%%%%%%%%%%%
%%%%%%%%%%%%%%%%%%%%%%%%%%%%%%%%%%%%%%%%%%%%%%%%%%%%%%%%%%%%%%%%

%l1=15;                                 % BEDDING IN TESTS
%l2=20;

%l1=5;                                  % DRESSING TESTS
%l2=5;

l1=19;                                  % CONVENIENT FLOW TESTS
l2=25;

l1_inc=l1/endl1;
l2_inc=l2/endl2;

l1_vect=(0+l1_inc:l1_inc:l1);
l2_vect=(0+l2_inc:l2_inc:l2);

%%%%%%%%%%%%%%%%%%%%%%%%%%%%%%%%%%%%%%%%%%%%%%%%%%%%%%%%%%%%%%%%
%%%%%%%%%%%%%%%  Evaluate area for subtraction of integrals  %%%%%%%%%%%%%%%%%%%%
%%%%%%%%%%%%%%%%%%%%%%%%%%%%%%%%%%%%%%%%%%%%%%%%%%%%%%%%%%%%%%%%
%%%%%%%%%%%%%%%%%%%%          Find trough value       %%%%%%%%%%%%%%%%%%%%
%%%%%%%%%%%%%%%%%%%%%%%%%%%%%%%%%%%%%%%%%%%%%%%%%%%%%%%%%%%%%%%%
```

```
z1=min(file1);                              % Create vector of minimum points
z2=min(z1);                                 % Create vector of minimum points
z2_mean_min_vector=mean(z1);                % find mean of vector of minimums
z3=z2_mean_min_vector;                      % Create lower limit for use in fluid calculations

z3_mm=z3/1000;                              % Convert low point to millimetres

%%%%%%%%%%%%%%%%%%%%%%%%%%%%%%%%%%%%%%%%%%%%%%%%%%%%%%%%
%%%%%%%%%%%%%%%%%%         Find Peak value          %%%%%%%%%%%%%%%%%%
%%%%%%%%%%%%%%%%%%%%%%%%%%%%%%%%%%%%%%%%%%%%%%%%%%%%%%%%

w1=max(file1);                              % Create vector of maximum points
w2=max(w1);
w2_mean_max_vector=mean(w1);                % find mean of vector of maximums
w3=w2_mean_max_vector;                      % Create upper limit for use in fluid
                                            calculations using mean of mean

w3_mm=w3/1000;                              % Convert high point to milimetres

%%%%%%%%%%%%%%%%%%%%%%%%%%%%%%%%%%%%%%%%%%%%%%%%%%%%%%%%

Rt=w3-z2;                                   % Calculate height of maximum area
area_1=Rt*endl2;                            % Calculate maximum UNIT area for row all rows
Rt_mm=Rt/1000;                              % convert Rt to millimetres
tot_area_mm2=Rt_mm*bs_mm;                   % Calculate maximum area in mm2 for all rows
Rt1=w2-z2;                                  % Calculate height of maximum area
Rt1_mm=Rt1/1000;                            % convert Rt1 to millimetres

%%%%%%%%%%%%%%%%%%%%%%%%%%%%%%%%%%%%%%%%%%%%%%%%%%%%%%%%
%%%%%%%%%%%%%%%%%%      Initiate scanning of profiles      %%%%%%%%%%%%%%%%%%
%%%%%%%%%%%%%%%%%%%%%%%%%%%%%%%%%%%%%%%%%%%%%%%%%%%%%%%%

for i=(1:1:endl1);                          % Select row to analyse
  k=0;
  vol=[];
  y=[];                                     % clear 'y' for next increment
  e=[];
  c=file1(:,i);                             % create row vector at row 'i'

  for j=(1:1:endl2);                        % Pass through row
    d=file1(j,i);                           % pick point to analyse
    a=d+abs(z2);                            % offset data against lowest point so all
                                            values are positive
    w4=w3+abs(z2);                          % crate a maximum point for sampling

    if a>=0 & a<=w4;                        % is point greater than value and less than
                                            the adjusted height
      k=k+1;                                % Increment along vector y
      y(1,k)=a;                             % add point to vector 'y'
      j=j+1;                                % Increment along row

    elseif a>=0 & a>=w4;                    % is point greater than value and greater
                                            than the adjusted height
      k=k+1;                                % Increment along vector y
      y(1,k)=w4;                            % add point to vector represented by
                                            maximum height w3
      j=j+1;                                % Increment along row

    else
      j=j+1;

    end

  end

  %%%%%%%%%   calculate area occupied by +ve values    %%%%%%%%%%%%%%

  b_temp=trapz(y);                          % integrate altered row
  b(1,i)=b_temp;                            % add integrant to new vector 'b'

  %%%%%%%%%%%%%%%%%%%%%%%%%%%%%%%%%%%%%%%%%%%%%%%%%%%%%%%%

  if i==50;
```

```
    prof1=(file1(:,i))./1000;
    prof1_alt=(c+abs(z3))./1000;
  end

  if i==100;
    prof2=(file1(:,i))./1000;
    prof2_alt=(c+abs(z3))./1000;
  end

  if i==150;
    prof3=(file1(:,i))./1000;
    prof3_alt=(c+abs(z3))./1000;
  end

  %%%%%%%%    calculate values of open space from row vector   %%%%%%%%
  vol=area_1-b_temp;                                    % calculate space vol for each row by
                                                        subtracting integrant from total area
  vol_space_vect(1,i)=vol;                              % add calculated area to a vector to store value

  area_perc=((vol)/(area_1))*100;                       % create pecentage (as a %) value for each
                                                        integrate over possible max
  area_perc_dec=(vol)/(area_1);                         % create pecentage (in decimal form) value for
                                                        each integrate over possible max
  vol_space_perc_vector(1,i)=area_perc;                 % create vector store data of percentage free
                                                        space per row i
  tot_area_space_mm_vect(1,i)=area_perc_dec*tot_area_mm2;   % create true volume available for fluid in
                                                        each row

  %%%%%%%%%%%%%%%%%%%%%%%%%%%%%%%%%%%%%%%%%%%%%%%%%%%%%%%%%%%%%%%%%%%%%


  i=i+1  ;                          % Increment to next row

end

%%%%%%%%%%%%%%%%%%%%%%%%%%%%%%%%%%%%%%%%%%%%%%%%%%%%%%%%%%%%%%%%%%%%%
%%%%%%%%%%%%%%%%%%%%%%    Calculate output values    %%%%%%%%%%%%%%%%%%%%%%%%
%%%%%%%%%%%%%%%%%%%%%%%%%%%%%%%%%%%%%%%%%%%%%%%%%%%%%%%%%%%%%%%%%%%%%

max_peak_mm=w2/1000;                                    % find highest point in analysis
min_peak_mm=z2/1000;                                    % find lowest point in analysis

Total_space_area=sum(tot_area_space_mm_vect);           % calculate total volume available in sample
ave_area_space_mm2=Total_space_area/endl1;              % calculate average area available in
                                                        contact zone[mm2]
ave_area_space_m2=ave_area_space_mm2/(1e6);              % calculate average area available in
                                                        contact zone [m2]

vol_space_perc=mean(vol_space_perc_vector);             % Calculate average surface porosity [%]

vol_flowrate_m3s=ave_area_space_m2*vs;                  % calculate flow rate [m3/s]
vol_flowrate_lmin=vol_flowrate_m3s*(1e3)*60;            % convert flow rate [l/min]
vol_flowrate2_lmin=vol_flowrate_lmin*wheel_porosity;    % use bulk wheel prosity to factor uniform
                                                        flowrate value

max_area_space_m2=tot_area_mm2/(1e6);                   % calculate average are available in
                                                        contact zone [m2]
max_vol_flowrate_m3s=max_area_space_m2*vs;              % calculate flow rate [m3/s]
max_vol_flowrate_lmin=max_vol_flowrate_m3s*(1e3)*60;      % convert flow rate [l/min]

%%%%%%%%%%%%%%%%%%%%    Display all relevant data   %%%%%%%%%%%%%%%%%%%%%%%%%%%%%

disp(['Wheelspeed, vs (m/s) =']), disp(vs)
disp(['Wheel width, bs (mm) =']), disp(bs_mm)
disp(['Bulk wheel porosity, phi (%) =']), disp(wheel_porosity_perc)
disp('  ')
disp(['Average surface porosity, (%) =']), disp(vol_space_perc)
disp(['Average area available for fluid, (mm2) =']), disp(ave_area_space_mm2)
disp(['Maximum Volumetric Flowrate, Qu (l/min)=']), disp(max_vol_flowrate_lmin)
disp(['Possible Volumetric Flowrate, Qu (l/min)=']), disp(vol_flowrate_lmin)
disp(['Realistic Volumetric Flowrate, Qu (l/min)=']), disp(vol_flowrate2_lmin)
disp('  ')
disp(['Highest point on topography (mm) =']), disp(max_peak_mm)
disp(['Highest point of analysis (mm) =']), disp(w3_mm)
disp('  ')
```

```
disp(['Lowest point on topography (mm) =']), disp(min_peak_mm)
disp(['Lowest point of analysis (mm) =']), disp(z3_mm)
disp(['Equivalent Rt (mm) =']), disp(Rt_mm)
disp(['Rt (mm) =']), disp(Rt1_mm)

%%%%%%%%%%%%%%%%%%%%%%%%   Plot relevant graphs   %%%%%%%%%%%%%%%%%%%%%%%%%%%%%%%%

set(0,'Units','pixels')
scn_pos1=get(0,'ScreenSize');
scn_pos=scn_pos1.*0.9;
scn_pos(1,1)=5;
scn_pos(1,2)=10;
scn_pos(1,3)=scn_pos1(1,3);

figure(1)
plot(l1_vect,vol_space_perc_vector)
title('Showing percentage of free space under each row');
xlabel('Distance through sample (mm)');
ylabel('Percentage free space (%)');
saveas(1,'Percentage free space versus row for large sample size','bmp')

figure('Position',scn_pos)
figure(2)
title('Showing comparison of true profile to offset only profile');

subplot(3,1,1);
plot(l2_vect,prof1,'--r');
hold on;
plot(l2_vect,prof1_alt,'-b');
ylabel('Height (mm)');
xlabel('Distance through sample (mm)');

subplot(3,1,2);
plot(l2_vect,prof2,'--r');
hold on;
plot(l2_vect,prof2_alt,'-b');
ylabel('Height (mm)');
xlabel('Distance through sample (mm)');

subplot(3,1,3);
plot(l2_vect,prof3,'--r');
hold on;
plot(l2_vect,prof3_alt,'-b');
ylabel('Height (mm)');
xlabel('Distance through sample (mm)');
saveas(2,'Example of three profiles through the sample','bmp')

%%%%%%%%%%%%%%%%%%%%%%%%%%%%%%%%%%%%%%%%%%%%%%%%%%%%%%%%%%%%%%%%%%
%%%%%%%%%%%%%%%%%%%%%%%%   END   %%%%%%%%%%%%%%%%%%%%%%%%%%%%%%%%%%
%%%%%%%%%%%%%%%%%%%%%%%%%%%%%%%%%%%%%%%%%%%%%%%%%%%%%%%%%%%%%%%%%%
```